University of Glasgow

McQuaker, Stephen (2013) *Functional molecules to test the free radical theory of ageing.* PhD thesis.

https://theses.gla.ac.uk/4211/

Copyright and moral rights for this work are retained by the author

A copy can be downloaded for personal non-commercial research or study, without prior permission or charge

This work cannot be reproduced or quoted extensively from without first obtaining permission in writing from the author

The content must not be changed in any way or sold commercially in any format or medium without the formal permission of the author

When referring to this work, full bibliographic details including the author, title, awarding institution and date of the thesis must be given

Enlighten: Theses
https://theses.gla.ac.uk/
research-enlighten@glasgow.ac.uk

Functional Molecules to Test the Free Radical Theory of Ageing

Stephen McQuaker

Supervisor : Dr Richard Hartley

Thesis submitted in part fulfilment of the requirements for the degree of Doctor of Philosophy in chemistry

UNIVERSITY
of
GLASGOW

School of Chemistry
University of Glasgow
September 2012

Abstract

Oxidative stress at a cellular level resulting from reactive oxygen species (ROS) has been implicated as a key factor in the ageing process and the development of age-related diseases. Mitochondria are the primary source of endogenously generated ROS through the leakage of electrons from the respiratory chain to molecular oxygen. Therefore there is a lot of interest in investigating ROS production and their biological impacts on both a cellular level and whole organism level.

A mitochondria-targeted hydrogen peroxide (H_2O_2) probe (MitoB) **i** and a mitochondria-targeted nitric oxide ($^{\bullet}NO$) probe (MitoDA) **iii** have been prepared to allow the detection and quantification of mitochondrial concentrations of these species *in vitro* and *in vivo*. These utilise the selective reactivity of boronic acids with H_2O_2 and 1,2-dianilines with the combination of $^{\bullet}NO$ and oxygen respectively to afford specific reaction products. These conversions are readily detectable by ESI-MS and quantified using deuterated internal standards.

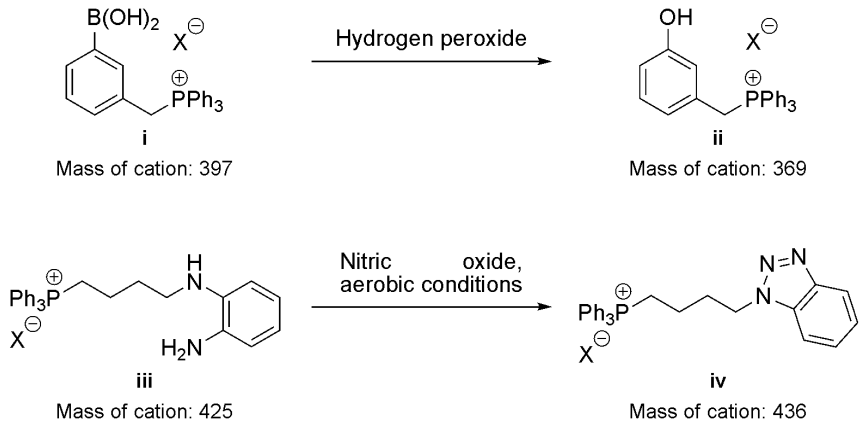

The mitochondrial membrane potential ($\Delta\Psi_m$) is directly linked to levels of ROS production, with an elevated $\Delta\Psi_m$ resulting in increased ROS production. Mitochondrial membrane potential moderators that release uncoupling molecules from caged precursors selectively in the presence of H_2O_2 were developed. Two untargeted analogues, DNP-SUM **v** and FCCP-SUM **viii** were prepared to release 2,4-dinitrophenoxyl anions (DNP^-, **vi**) or carbonyl cyanide-*p*-trifluoromethoxyphenylhydrazonyl anions ($FCCP^-$, **ix**) respectively and their *pseudo*-first order kinetics assessed.

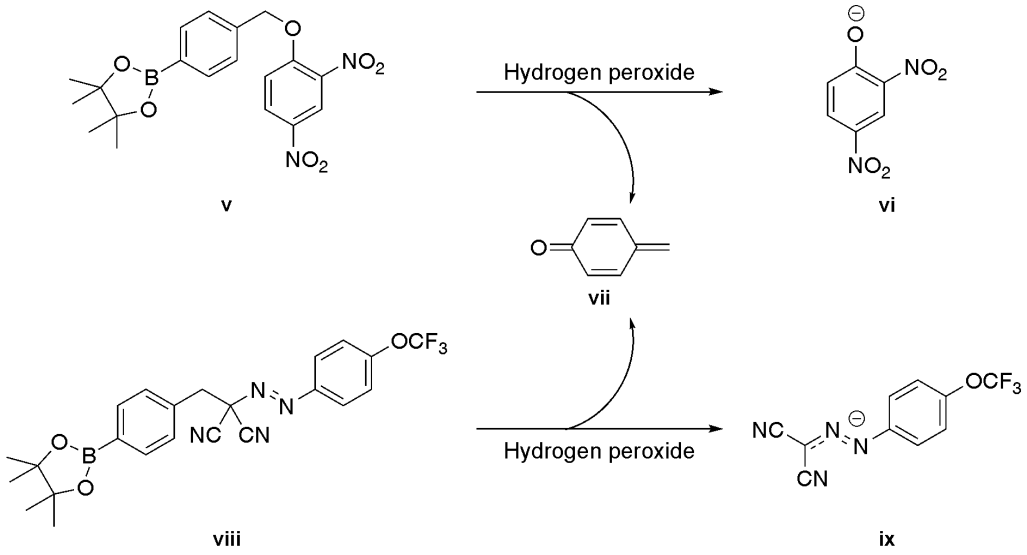

Two mitochondria-targeted analogues, MitoDNP-SUM(1) **x** and MitoDNP-SUM(2) **xi** designed to release DNP^- **vi** inside the mitochondrial matrix were prepared. Their abilities to lower the $\Delta\Psi_m$ and therefore the ROS producing capabilities in isolated rat skeletal muscle mitochondria in response to endogenously generated H_2O_2 were assessed.

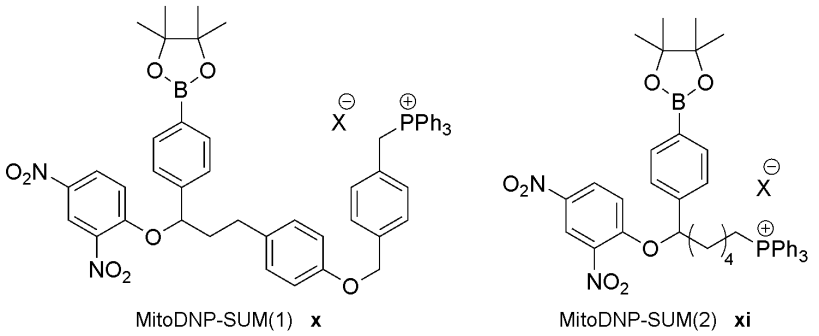

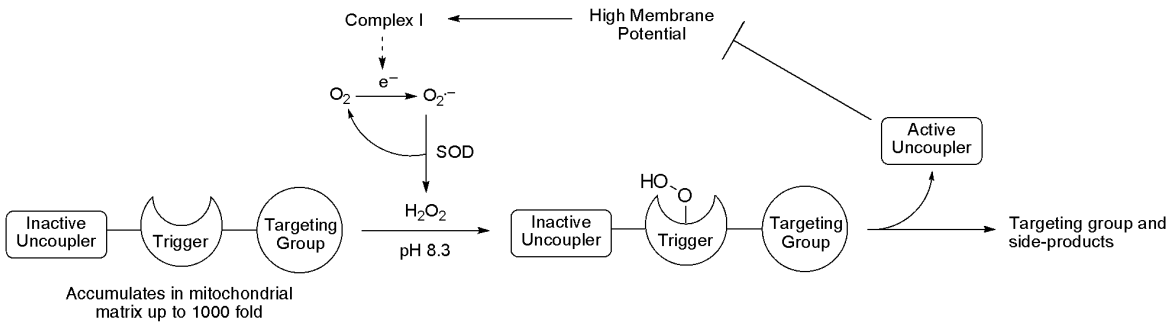

Work was also conducted towards the development of mitochondria-targeted photo-activatable probes that could potentially release small functional bioactive compounds from caged precursors inside individual mitochondria upon selective irradiation.

Declaration

This thesis represents the original work of Stephen John McQuaker unless explicitly stated otherwise in the text. No part of this thesis has previously been submitted for a degree at the University of Glasgow or any other university. The research was predominantly carried out at the University of Glasgow (UK) in the Loudon laboratory under the supervision of Dr Richard C. Hartley during the period of October 2008 to May 2012. During this time, further contributions were carried out at the Buck Institute for Research on Aging (CA, USA) under the supervision of Professor Martin Brand.

Acknowledgements

Firstly I would like to thank my principle supervisor Dr Richard Hartley for his invaluable guidance and support throughout my PhD studies.

I would also like to thank all members of the Hartley research group and Loudon lab, past and present for making the research laboratory and office such a pleasant place to work and for putting up with my wonderful singing talent, general prattle and occasional chemistry rage.

I wish to thank all those whom have helped me during my placements at the Buck Institute for Research on Aging (CA, USA) and at the New York State University at Stony Brook (NY, USA) with settling in, experimental guidance, driving me around and generally making my visits unforgettable experiences. A special thanks goes to Professors Martin Brand (CA) and Iwao Ojima (NY) for welcoming me into their respective research laboratories.

I would also like to thank all those whom have collaborated with me on these research projects or given technical support throughout my time conducting research at the University of Glasgow.

Finally I want to thank my girlfriend, family and friends for their unwavering and much appreciated support throughout my time at the University of Glasgow. Without you all, things would never be the same.

Abbreviations

(g)	gas
(l)	liquid
$\Delta\Psi_m$	mitochondrial membrane potential
$\Delta\Psi_p$	plasma membrane potential
λ_{abs}	absorption wavelength
λ_{em}	emission wavelength
λ_{ex}	excitation wavelength
ϕ	quantum yield
°C	degrees Celsius
µg	microgram(s)
µL	microlitre(s)
µM	micromole(s) per litre
µmol	micromole(s)
Å	angstrom
Ac	acetate
ADP	adenosine diphosphate
ANT	adenosine nucleotide translocase
Ar	aromatic
ATP	adenosine triphosphate
ATPase	adenosine triphosphate synthase
ATR	attenuated total reflectance
Ax	axial
BHA	butylated hydroxyanisole
BHT	butylated hydroxytoluene
Bn	benzyl
Boc	*tert*-butyloxycarbonyl
BODIPY	boron-dipyrromethene
BSA	bovine serum albumin
Bu	butyl
C	coulomb
CACT	carnitine/acyl carnitine translocase
CAT	catalase
CI	chemical ionisation

CK	creatine kinase
cm^{-1}	wavenumber
COSY	correlation spectroscopy
CP	creatine phosphate
CsA	cyclosporin A
CyP	cyclophilin
Cyt C	cytochrome C
d	day(s)
DAF	diaminofluorescein
DAR	diaminorhodamine
DCF	dichlorofluorescein
DCFH	dichlorodihydrofluorescein
DCFH-DA	dichlorodihydrofluorescein diacetate
DCM	dichloromethane
Decomp	decomposition
DEPT	distortionless enhancement by polarization transfer
DHLA	dihydrolipoic acid
DHP	dihydropyran
DIBALH	diisobutylaluminium hydride
DIPEA	*N*,*N*-diisopropylethylamine
DLC	delocalised lipophilic cation
DMAP	4-dimethylaminopyridine
DMF	dimethylformamide
DMSO	dimethylsulfoxide
Dmt	dimethyltyrosine
DNA	deoxyribonucleic acid
DNB	dinitrobenzene
DNP	dinitrophenol
dppf	1,1'-bis(diphenylphosphino)ferrocene
DR	dietary restriction
E	energy
e	electron
E.C.	enzyme commission
E2	bimolecular elimination
EDC	*N*-(3-dimethylaminopropyl)-*N*′-ethylcarbodiimide
EGTA	ethylene glycol tetraacetic acid

EI	electron impact
eNOS	endothelial NOS
EPR	electroparamagnetic resonance
Eq	equatorial
eq	equivalence(s)
ESI	electrospray ionisation
Et	ethyl
F	Faraday constant
$F_{###}$	fluorescence (at wavelength ###)
FA	fatty acid
FAB	fast atom bombardment
FCCP	carbonyl cyanide-*p*-trifluoromethoxyphenylhydrazone
Fig	figure
FMN	flavin mononucleotide
FRET	fluorescence resonance energy transfer
FRTA	free radical theory of ageing
g	gram(s)
g	relative centrifugal force
GADPH	glyceraldehyde-3-phosphate dehydrogenase
GFP	green fluorescent protein
GPDH-M	mitochondrial glycerol phosphate dehydrogenase
GPx	glutathione peroxidase
Grx	glutaredoxin
GSH	glutathione
GSR	glutathione reductase
GSSG	glutathione dimer
h	hour(s)
HE	hydroethidium
HEPES	4-(2'-hydroxyethyl)-1-piperazineethanesulfonic acid
HMBC	heteronuclear multiple-bond correlation spectroscopy
HPLC	high performance liquid chromatography
HRMS	high resolution mass spectroscopy
HSQC	heteronuclear single-quantum correlation spectroscopy
Hz	hertz
I/R	ischemia-reperfusion
IAM	iodoacetamide

IMS	intermembrane space
iNOS	inducible NOS
iPr	*iso*-propyl
IR	infra-red
IRA	ion exchange resin anionic
J	joule(s)
K	Kelvin
LA	lipoic acid
LC	liquid chromatography
Lit	literature reference
LRMS	low resolution mass spectroscopy
Lys	lysine
M	mole(s) per litre
m/z	mass/charge
m-	meta
Me	methyl
mg	milligram(s)
MHz	megahertz
MIM	mitochondrial inner membrane
min	minute(s)
Mito	mitochondria-targeted
mL	millilitre(s)
mM	millimole(s) per litre
mmol	millimole(s)
Mol	mole(s)
MOM	mitochondrial outer membrane
MOM	methoxymethyl ether
MOMP	mitochondrial outer membrane permeability
Mp	melting point
Ms	mesyl
MS	mass spectrometry
mtNOS	mitochondrial NOS
MTPP	methyltriphenylphosphonium
mV	millivolt(s)
NB	nitrobenzyl
NBS	*N*-bromosuccinamide

nm	nanometre
NMO	*N*-methylmorpholine-*N*-oxide
nmol	nanomole(s)
NMPO	*N*-methylpyrolidinone
NMR	nuclear magnetic resonance
nNOS	neuronal NOS
NOS	nitric oxide synthase
NOESY	nuclear Overhauser effect spectroscopy
NPA	3-nitropropionic acid
Nu	nucleophile
o-	ortho
OCR	oxygen consumption rate
p-	para
Pd/C	palladium on carbon
PDT	photodynamic therapy
PET	photon-electron transfer
Ph	phenyl
Phe	phenylalanine
Pi	phosphate
Pin	pinacol
pM	picomole(s) per litre
PT	permeability transition
Q	quinone
R	gas constant
R_f	retention factor
RNA	ribonucleic acid
RNS	reactive nitrogen species
ROS	reactive oxygen species
RT	room temperature
s	second(s)
SET	single electron transfer
S_N2	bimolecular nucleophilic substitution
S_NAr	nucleophilic aromatic substitution
SOD	superoxide dismutase
SS	Schiller-Szeto
SUM	selective uncoupling molecule

T	Temperature
^{t}Bu	*tert*-butyl
TC	time course
TEMPOL	4-hydroxy-2,2,6,6-tetramethylpiperidin-1-oxyl
Tf	triflyl
THF	tetrahydrofuran
THP	tetrahydropyran
TMS	trimethylsilyl
TPMP	As MTPP
TPP	triphenylphosphonium
$Trx(SH)_2$	thioredoxin
TrxR	thioredoxin reductase
Ts	tosyl
U	units
UCP	uncoupling protein
UV	ultraviolet
V	volt(s)
Vis	visible
w/v	weight/volume
wt	weight
XDH	xanthine dehydrogenase
XO	xanthine oxidase
XOR	xanthine oxidoreductase

Table of Contents

Chapter 1: The free radical theory of ageing

1.1 Mitochondria and the electron transport chain

Mitochondria (Fig.1) are organelles found in the majority of eukaryotic cells (including human cells) inside which an array of biosynthetic reactions occur central to many biological processes. Mitochondria play a number of key biological roles including the harnessing of dietary energy from fats and sugars, maintaining calcium and redox homeostasis as well as being critically involved in apoptotic and necrotic cell death. These organelles comprise two semi-permeable phospholipid bilayer membranes, the mitochondrial outer membrane (MOM) enclosing the entire organelle and the mitochondrial inner membrane (MIM). Embedded in the MIM are a number of specialised proteins that perform the various redox reactions of the respiratory chain (electron transport chain).[1,2] The primary function of mitochondria uses the respiratory chain to produce the cellular "energy currency" adenosine triphosphate (ATP) by ATP synthase (ATPase, E.C. 3.6.3.14) inside the mitochondrial matrix. A number of MIM infolds (cristae) maximise the surface area to maximise the number of potential reaction sites and hence maximise the efficiency of the energy generation process.

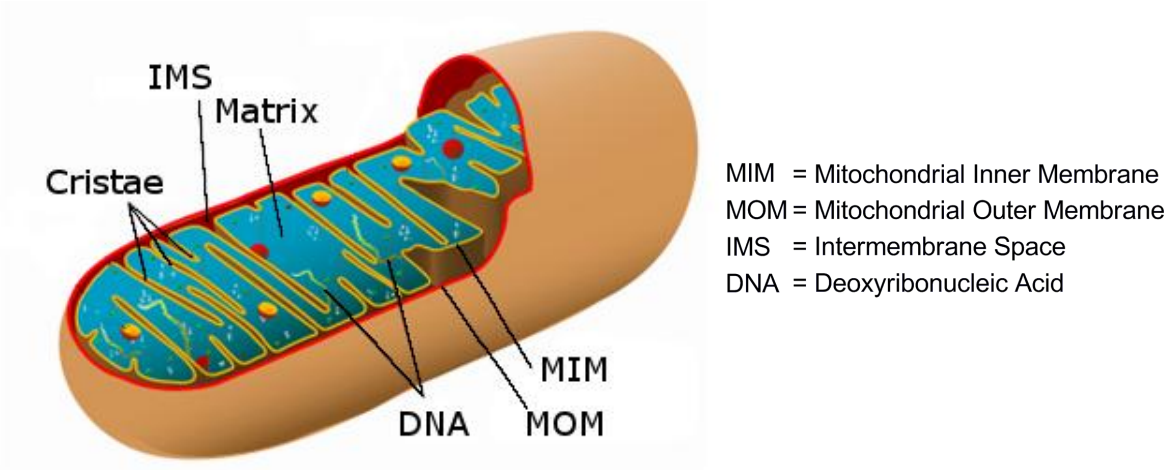

Fig.1: Mitochondrion structure[3]

The energy released from the oxidation of dietary energy sources such as sugars and fatty acids, leads to the flow of electrons along the four discrete, sequential protein complexes of the respiratory chain with concomitant pumping of protons out of the mitochondrial matrix (Fig.2).

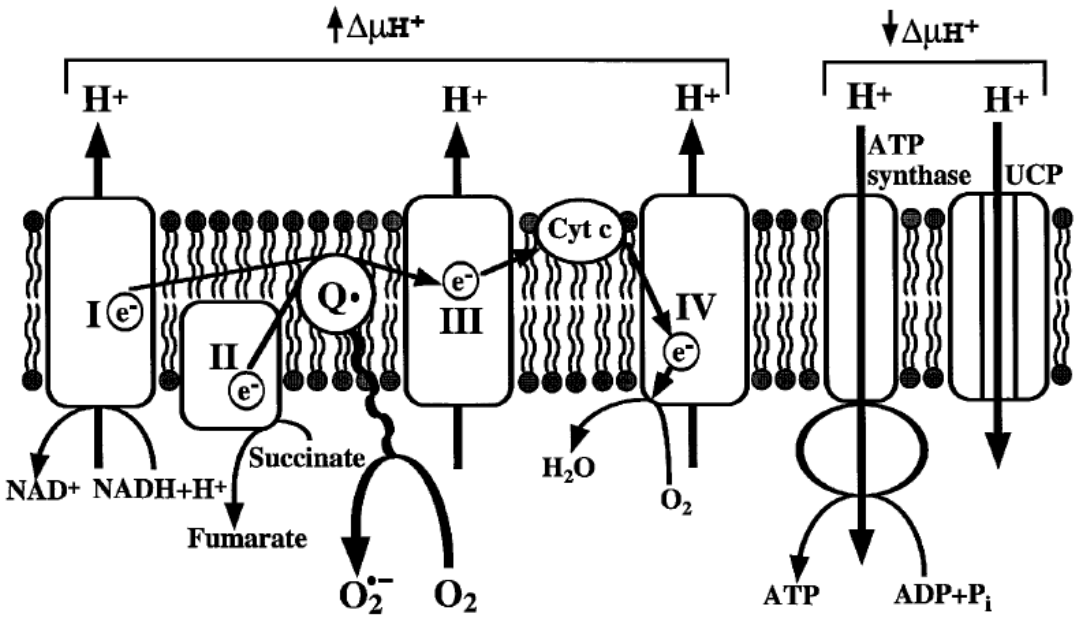

Fig.2: MIM supported electron transport chain proteins and electron carriers[1,4]

Electrons can enter the electron transport chain *via* a number of points depending on the specific energy source. NADH dehydrogenase (complex I, E.C. 1.6.5.3) or succinate dehydrogenase (complex II, E.C. 1.3.5.1) where NADH and succinate are converted into NAD^+ and fumarate respectively are two of the key electron entry points although others exist such as mitochondrial glycerol phosphate dehydrogenase (GPDH-M, E.C. 1.1.5.3).

The oxidation of NADH at complex I occurs in a single two electron transfer process which reduces flavin mononucleotide (FMN) into $FMNH_2$.[1] Two subsequent single electron transfers (SET) to Fe-S centres in complex I occur before the electrons are passed on to reduce the lipid-soluble electron-carrier ubiquinone **1** (coenzyme Q) into ubiquinol **3** (QH_2) *via* a semiquinone intermediate **2**.

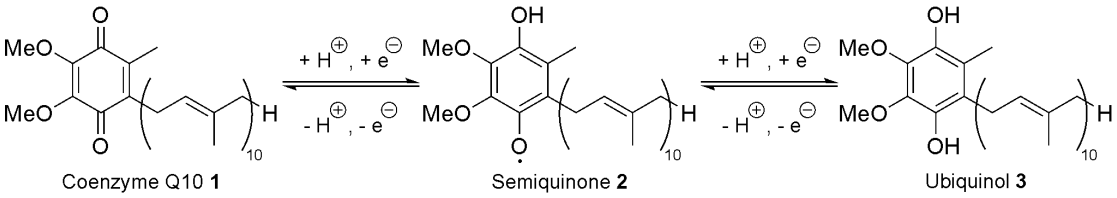

Scheme 1: Reduction/oxidation of coenzyme Q/ubiquinol

L to R – Q_i site : R to L – Q_o site

Complex I translocates four protons from the matrix into the intermembrane space (with a further two protons entering the Q-pool), helping to establish the MIM membrane protomotive force which comprises electrochemical potential ($\Delta\Psi_m$) and pH gradient components.

Succinate dehydrogenase (complex II, E.C. 1.3.5.1) obtains electrons following the reduction of flavin adenine dinucleotide (FAD) to $FADH_2$ by succinate (which itself is oxidised to fumarate) before being passed to coenzyme Q *via* three Fe-S centres. Minor contributors of electrons to the Q-pool such as fatty acid metabolism (acyl-CoA-dehydrogenase, E.C. 1.3.99.3) or from GPDH-M are also passed to co-enzyme Q *via* FAD/ $FADH_2$ co-factors. Complex II is not involved in proton pumping across the MIM.

In the cytochrome bc_1 complex (complex III, E.C. 1.10.2.2), cytochrome b sequentially binds two molecules of QH_2 from the quinone pool (Q-pool) which are then divergently oxidised (Fig.3) at the Q_o site.[1] One electron from each of the two QH_2 molecules is passed sequentially to water-soluble electron-carrier cytochrome c in the intermembrane space (IMS) *via* a Rieske iron-sulphur centre with four protons being released into the IMS. The other electron from each QH_2 molecule is passed to the Q_i site (*via* the cytochrome b_L and cytochrome b_H hemes) where one molecule of coenzyme Q is reduced to QH_2 taking two protons from the mitochondrial matrix. In total four protons enter the IMS from the Q-pool, with two protons from the mitochondrial matrix partially replenishing the Q-pool in each cycle. All processes in complex III are single electron transfer processes.

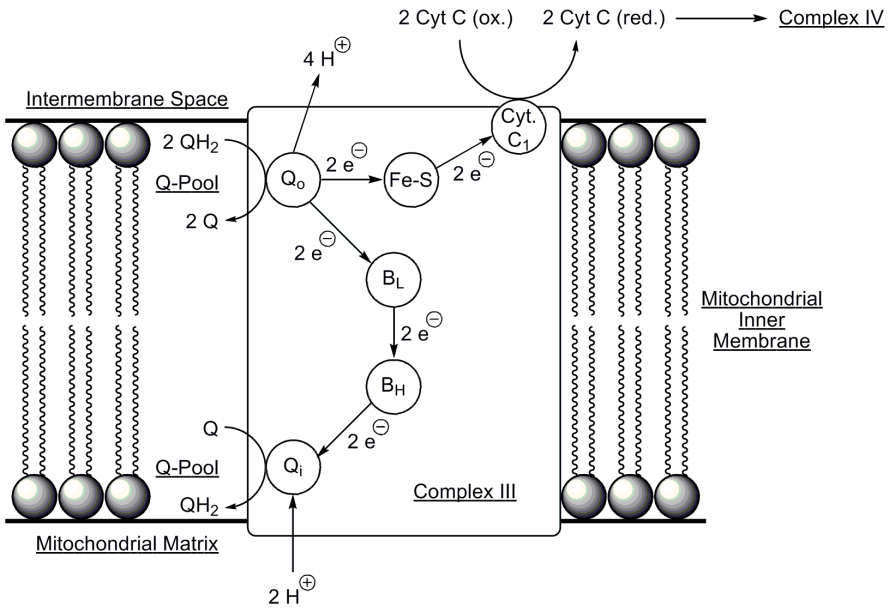

Fig.3: Overall cytochrome bc_1 complex cycle (complex III)[1]

Cytochrome c oxidase (complex IV, E.C. 1.9.3.1) transfers one electron each from four molecules of cytochrome c to molecular oxygen generating two molecules of water in the mitochondrial matrix.[1] Eight protons are removed from the matrix with four forming water and four protons entering the IMS per O_2 molecule fully reduced.

MIM supported transmembrane protein ATPase harnesses the energy of $\Delta\Psi_m$ established by complexes I, III and IV by allowing protons to flow back down the gradient into the mitochondrial matrix.[1] ATPase uses this energy to convert adenosine diphosphate **4** (ADP) into the high energy molecule ATP **5** through oxidative phosphorylation with the stepwise reduction of oxygen to water as a by-product (Scheme 2). ATPase comprises a membrane pore with a rotating head group of subunits on the matrix side which is where ADP **4** is converted into ATP **5**. For each full head group rotation of mitochondrial ATPase, nine protons are taken from the IMS and three molecules of ATP **5** are produced. ATP **5** is then transported around the body and used as the energy source to power a plethora of biochemical reactions before being transported back to a mitochondrial matrix as ADP **4** to once again be converted into ATP **5**. Signalling molecule guanosine-5'-triphosphate produced in the citric acid (Krebs) cycle can also be converted into ATP **5** by nucleoside-diphosphate kinases, however this is generally not a major contributing factor to overall ATP **5** levels.

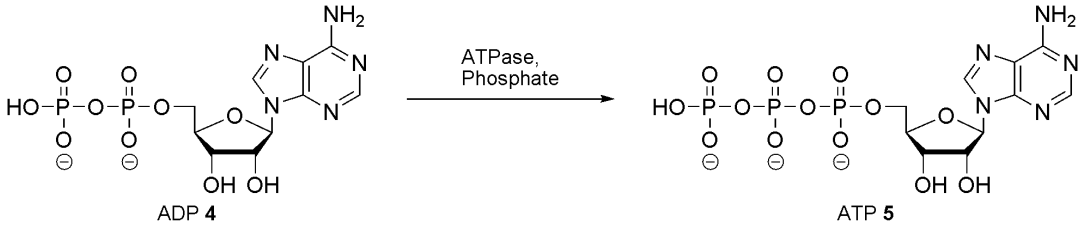

Scheme 2: Synthesis of ATP **5** from ADP **4** by ATPase

A number of MIM uncoupling proteins that regulate the controlled dissipation of $\Delta\Psi_m$ have been identified. The first known as thermogenin or uncoupling protein 1 (UCP1) was discovered by Nicholls *et al* in 1978.[5] Since then a further four uncoupling proteins have been confirmed. This energy-dissipation mechanism serves a number of functions including thermogenesis, maintaining redox homeostasis and the reduction of reactive oxygen species (ROS) production. The concept of mitochondrial uncoupling and in particular its impact on ROS levels will be discussed in further detail in chapter 6.

1.2 Oxidative stress, ROS production

The term oxidative stress describes an imbalance between a biological systems production of ROS and its ability to readily detoxify the species produced or to repair the resulting damage.[6] Alterations to the normal redox state of cells can lead to toxic effects through the production of free radicals and peroxides that can damage all components of the cell, including proteins, lipids and DNA.

Molecular oxygen (O_2) exists predominantly as a diradical or "triplet" state but also as the much shorter lived electron-paired or "singlet" state resulting from spin flipping of one electron in the highest occupied molecular orbital (Fig.4). Oxygen availability is highly controlled in the body and is transported tightly bound to iron-based metalloproteins hemoglobin in the blood and myoglobin in muscle tissue. These give the body a high level of control ensuring that oxygen is delivered when and where it is needed by the body. Perhaps more importantly, although necessary for the vast majority of life, oxygen can be toxic and so highly efficient sequestering of oxygen within an organism is vital to prevent cytotoxicity. If triplet oxygen gains an electron it becomes the superoxide radical anion ($O_2^{\bullet-}$). If a second electron is gained the oxygen-oxygen bond order is reduced to one with a peroxide dianion (O_2^{2-}) formed. In an aqueous medium this will pick up one or two protons depending on the pH to form hydroperoxide anions (HO_2^-) or hydrogen peroxide (H_2O_2, pKa = 11.62 at 25 °C). Addition of a further electron causes oxygen-oxygen bond cleavage giving a hydroxide anion (HO^-) and a hydroxyl radical ($HO^{\bullet}$).[7]

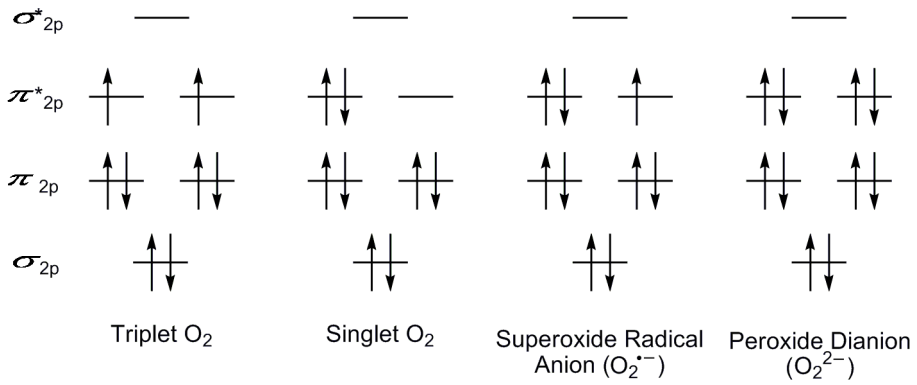

Fig.4: Oxygen orbital filling – In all diagrams, the lower energy σ_{1s}, σ_{1s}*, σ_{2s} and σ_{2s}* molecular orbitals are all fully occupied

Despite the electron transport chain being a highly efficient process, during its many redox reactions, occasionally electrons are prematurely leaked to molecular oxygen from complexes I and III of the respiratory chain or directly from the Q-pool to produce $O_2^{\bullet-}$, particularly if normal cellular redox states have been altered. Evidence from studies in isolated mitochondria suggest that approximately 0.1-2% of electrons are leaked from the electron transport chain.[8]

Although mitochondria are thought to be the main endogenous source of ROS, other biological sources have been identified including xanthine oxidoreductase (XOR). XOR exists as one of two interconvertable enzymatic forms, xanthine oxidase (XO, E.C. 1.17.3.2) and xanthine dehydrogenase (XDH, E.C. 1.17.3.4). XO catalyses the two step catabolism of purine residues such as the oxidation of hypoxanthine **6** to uric acid **8** (Scheme 3) and is often reported as a producer of superoxide. However under physiological conditions hydrogen peroxide has recently been reported to be the major form of ROS produced by XO in an approximate 4:1 ratio (H_2O_2:$O_2^{\bullet-}$).[9,10]

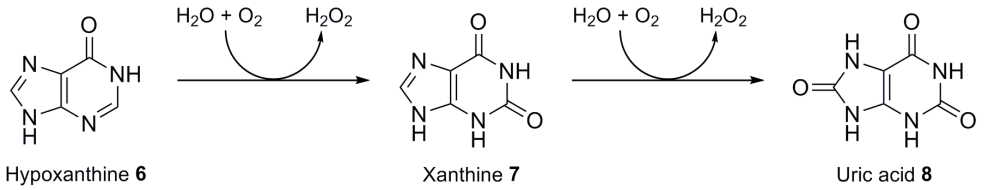

Scheme 3: Xanthine oxidase oxidation of purine residues produce ROS

Additional ROS sources include the body's immune system which uses ROS such as hypochlorous acid (HOCl) generated by neutrophils to eradicate bacterial infections and background ionising radiation that can lead to ROS formation through homolytic cleavage of oxygen-hydrogen bonds in water.

1.3 ROS proliferation and biological defence mechanisms

The human body has developed a range of defence mechanisms to protect against oxidative stress. Superoxide dismutase (SOD, E.C. 1.15.1.1) rapidly converts superoxide into H_2O_2 and O_2 in the mitochondrial matrix *via* a disproportionation reaction mechanism (Scheme 4). In eukaryotic cells, SOD predominantly use Cu/Zn co-factors. Prokaryotes and protists utilise Mn or Fe co-factors while prokaryotic cells may also use Ni as a co-factor.

Half Reaction : M^{n+}−SOD + $O_2^{\bullet-}$ + $2H^+$ → $M^{(n+1)+}$−SOD + H_2O_2

Half Reaction : $M^{(n+1)+}$−SOD + $O_2^{\bullet-}$ → M^{n+}−SOD + O_2

Overall SOD Disproportionation Reaction : $2O_2^{\bullet-} + 2H^+ \rightarrow H_2O_2 + O_2$

where M = Cu (n=1) ; Mn, Fe or Ni (n=2)

Scheme 4: SOD disproportionation reaction

Catalase enzymes (CAT, E.C. 1.11.1.6) catalyse the disproportionation reaction that converts H_2O_2 into O_2 and water (Scheme 5) without the formation of radical by-products and are found in the cells of almost all living organisms that utilise aerobic respiration as well as certain anaerobic organisms.[11] CAT is present to minimise ROS damage resulting from H_2O_2 generated by SOD. Human CAT targeted to the mitochondrion of transgenic mice can lead to a significant increase in both maximum and average murine lifespan by approximately 20% and can also reduce markers of oxidative damage.[12]

Proposed Half Reaction : H_2O_2 + Fe(III)−CAT → H_2O + O=Fe(IV)−CAT(˙+)

Proposed Half Reaction : H_2O_2 + O=Fe(IV)−CAT(˙+) → H_2O + Fe(III)−CAT + O_2

Overall CAT Disproportionation Reaction : $2H_2O_2 \rightarrow 2H_2O + O_2$

Scheme 5: Catalase disproportionation Reactions

A family of glutathione peroxidases (GPx, E.C. 1.11.1.9) utilise a selenocysteine residue in their active sites to convert H_2O_2 into water *via* the dimerisation of tripeptide glutathione **9** (GSH) into glutathione disulfide **11** (GSSG, Scheme 6). Glutathione reductase (GSR, E.C. 1.8.1.7) regenerates both molecules of GSH **9** using a stoichiometric NADPH co-factor.

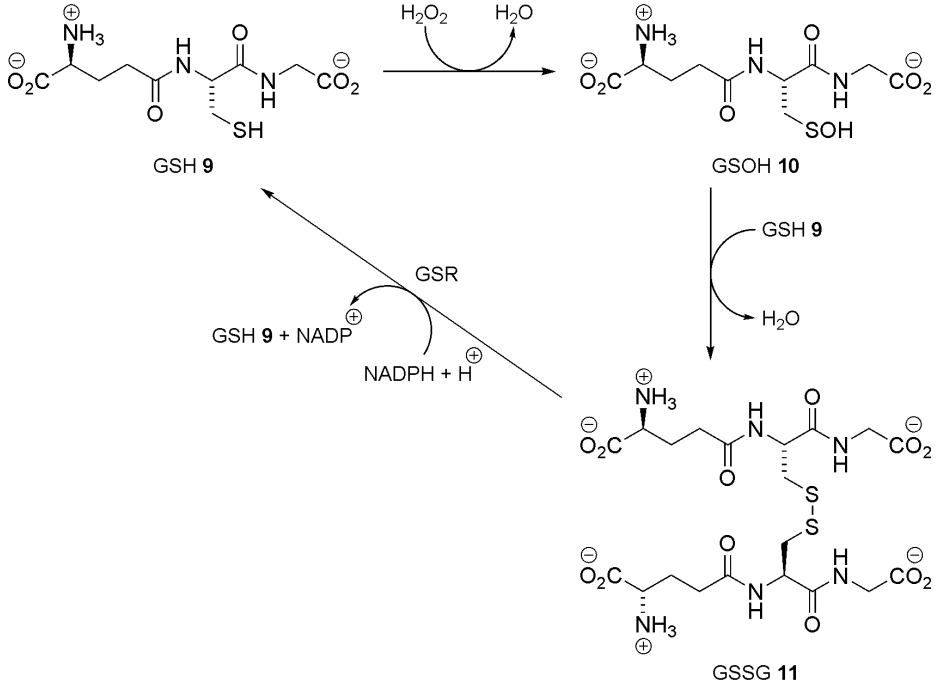

Scheme 6: GPx reaction with H_2O_2 and the reversible dimerisation of GSH **9**

Any H_2O_2 which manages to evade CAT or GPx breakdown exists sufficiently as a neutral molecule at physiological pH to freely diffuse away from the matrix. In contact with redox active metal ions throughout the body, including but not exclusively the first row transition metals [eg. iron(II)] used as enzyme co-factors, H_2O_2 forms highly reactive and damaging hydroxyl radicals ($HO^{\bullet}$). This mechanism was originally reported by Fenton in 1894 as a method for oxidising organic molecules using H_2O_2 in the presence of iron(II) salts (Scheme 7).[13] The toxicity associated with many highly poisonous metals such as cadmium, mercury and lead has been linked in part to their abilities to generate ROS.[14]

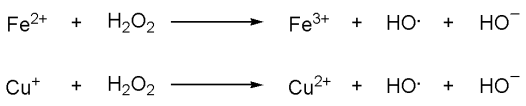

Scheme 7: Reaction of H_2O_2 with biologically important metal ions

Hydroxyl radicals initiate damaging radical cascades, reacting with DNA, lipid membranes, proteins, etc. at rates close to diffusion control. Phospholipids are the major component of lipid membranes comprising polar head groups lined up on the membrane interior and exterior faces with hydrophobic tails embedded within the membrane. The head groups usually comprise a phosphate group and a simple organic molecule such as choline (Fig.5), while tail groups generally contain diglycides which can vary in length and degree of unsaturation.

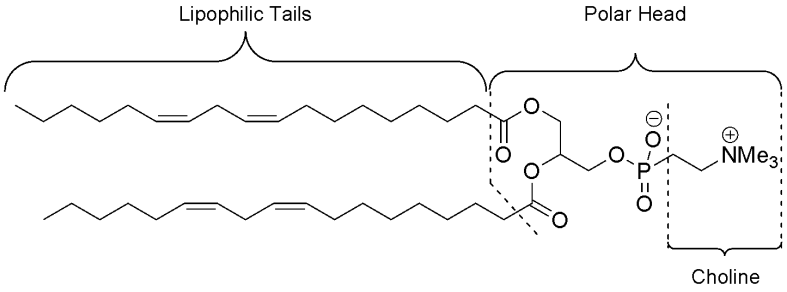

Fig.5: Bis-linoleic acid and choline derived phospholipid

Lipid peroxidation by ROS starts with hydrogen atom abstraction by hydroxyl radicals (Schemes 8 and 9).[15] Polyunsaturated fatty acid tails are more susceptible to oxygen-centred radical induced hydrogen atom abstraction as the lipid radicals generated are more stable. The lipid radicals ($L^{\bullet}$) generated can react with molecular oxygen to give lipid peroxyl radicals ($LOO^{\bullet}$) which can undergo further hydrogen atom abstraction from other fatty acid tails in the membrane, resulting in radical propagation.

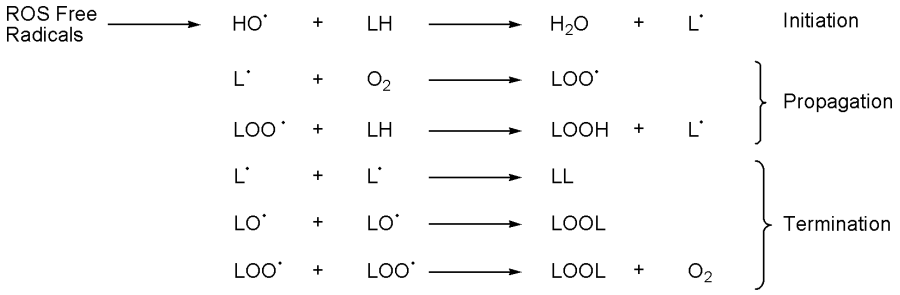

Scheme 8: Lipid (LH) peroxidation radical cascade overview

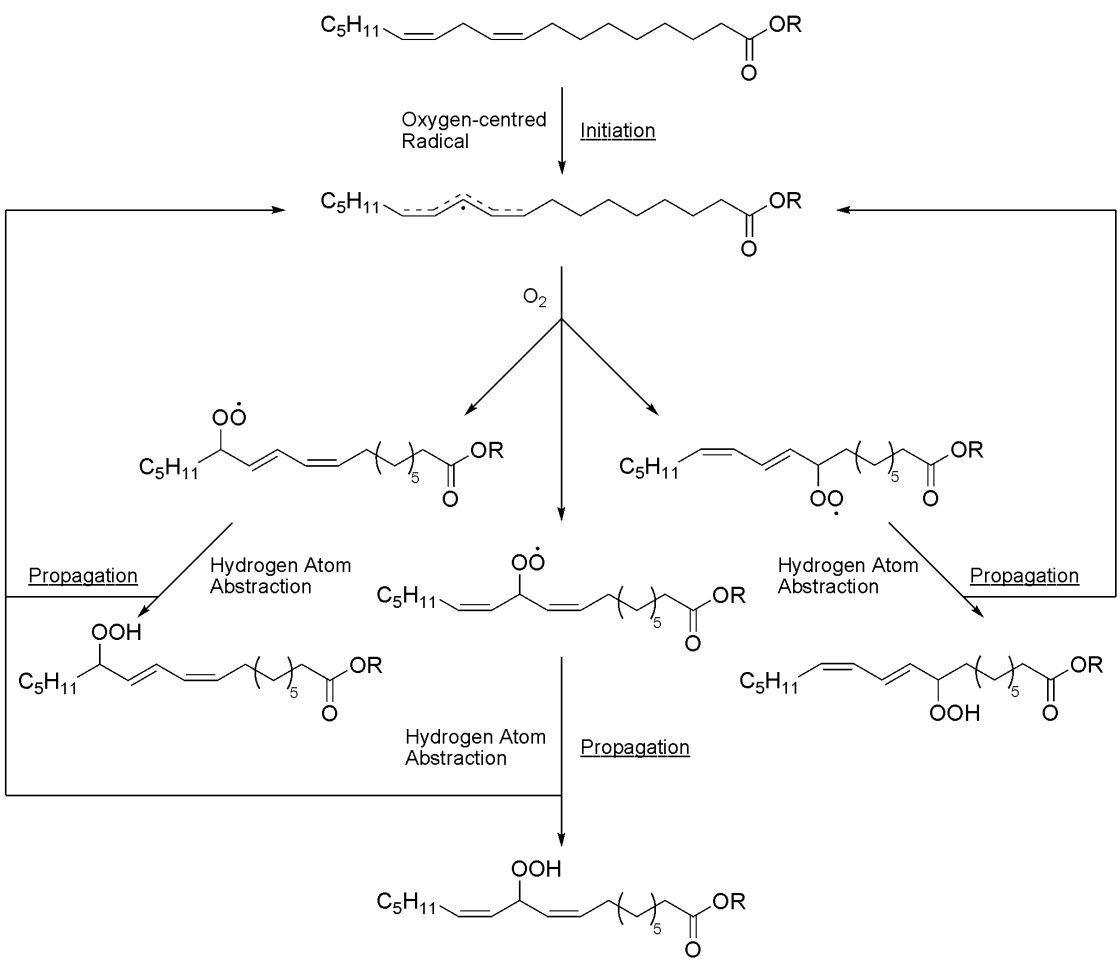

Scheme 9: Lipid peroxidation radical cascade initiation and propagation

Lipid peroxides can further oxidise, cyclise intramolecularly or cross-link with other lipids. These can then fragment by a number of mechanisms including Hock cleavage to give non-radical products including isoprostanes **13**, aldehydes **14** and isofurans (Scheme 10). This leads to lipid membrane instability and potentially cellular or organelle collapse.

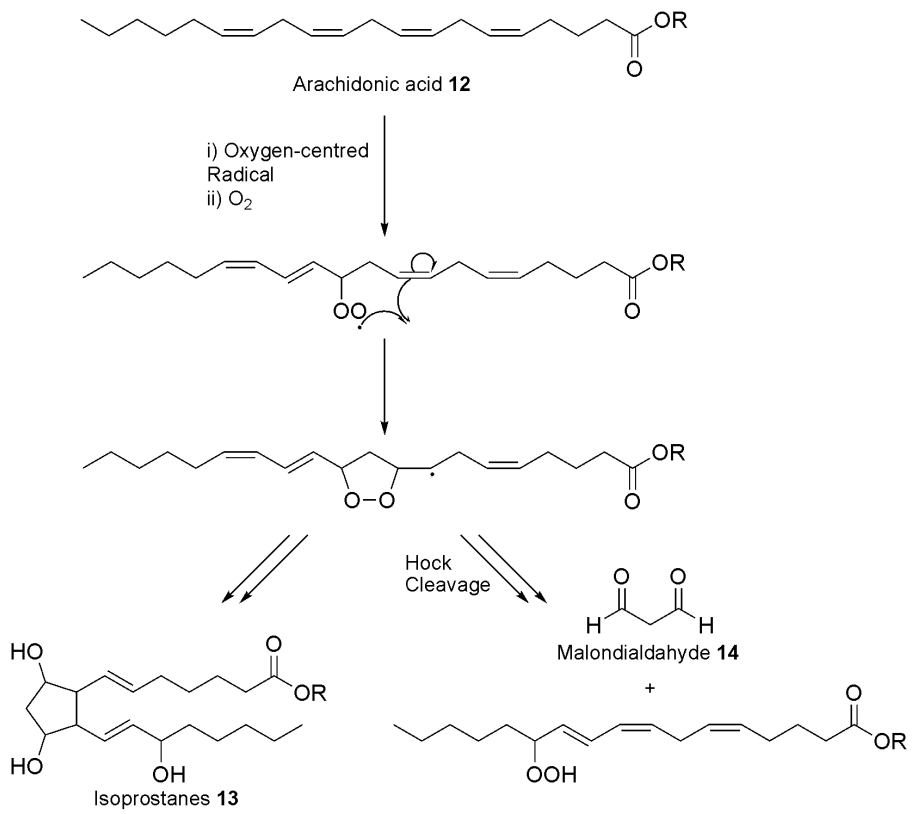

Scheme 10: Radical induced breakdown of arachidonic acid **12**

ROS damage to DNA and RNA occurs predominantly through reaction with hydroxyl radicals or their lipid derived radical products. Superoxide and hydrogen peroxide do not react directly with DNA. A number of potential oxidative modifications to base-pairs can occur which can lead to base-pair mismatches, mutations and DNA strand breakages through the breakdown of the sugar backbone.[16]

Proteins can also be severely damaged by hydroxyl radicals. All amino acids are susceptible to ROS damage with tryptophan, tyrosine, histidine and cysteine noted as particularly vulnerable. ROS damage has been seen to cause significant structural modifications which can impact biological functions and make proteins prone to proteolysis.[17,18,19]

The human body also utilises antioxidants, either endogenously produced or obtained through diet, to inhibit the oxidation of sensitive biomolecules by terminating radical cascades. These may behave in a stoichiometric manner such as melatonin or undergo redox cycling to regenerate the antioxidants, as is the case for ascorbic acid (vitamin C) and the family of tocotrienyls and tocopherols **16** (vitamin E) (Scheme 11). Vitamin E is lipophilic so embeds itself in phospholipid membranes and primarily protects against lipid peroxidation.

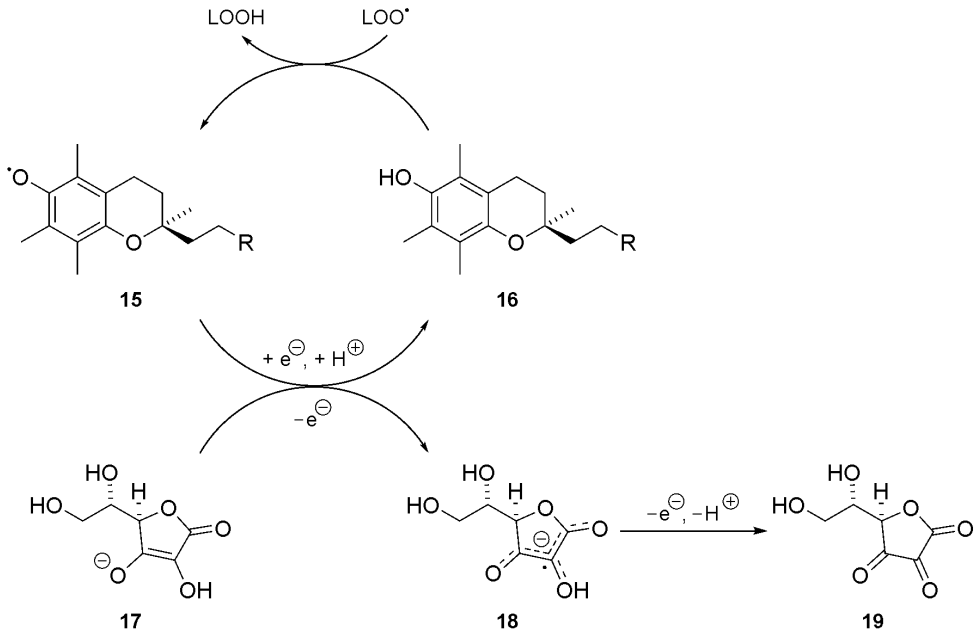

Scheme 11: Vitamin E redox cycling by vitamin C. R = 2,6,10-trimethylundecane

Hydroxyl, lipid peroxyl or carbon-centred radicals can abstract the phenolic hydrogen atom from α-d-tocopherol **16** to generate radical **15**. Ascorbic acid monoanion **17** donates an electron to reform the neutral α-d-tocopherol antioxidant **16**. Unlike vitamin E, vitamin C is water soluble and so this electron transfer must occur at the lipid-water interface. The semihydroascorbate (ascorbyl radical) **18** is a relatively inert radical which loses an electron to form dehydroascorbate **19**. This final electron transfer can paradoxically lead to pro-oxidant behaviour of vitamin C as it may reduce free Fe(III) to Fe(II), which can then participate in the Fenton mechanism of ROS production (Scheme 7). Similarly Cu(II) centres can be reduced to Cu(I).[20]

Endogenous antioxidants GSH **9** and uric acid **8** can react directly with hydroxyl radicals. GSH **9** undergoes hydrogen abstraction followed by dimerisation (Scheme 12) while uric acid **8** (pKa = 3.1, predominantly urate at physiological pHs) donates an electron to give hydroxide and a more stable, longer lived radical **21** which is then quenched by GSH **9** or ascorbic acid (Scheme 13).

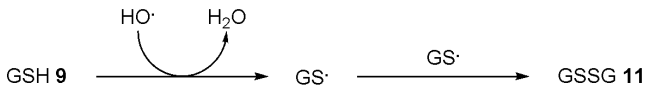

Scheme 12: Glutathione reaction with hydroxyl radicals

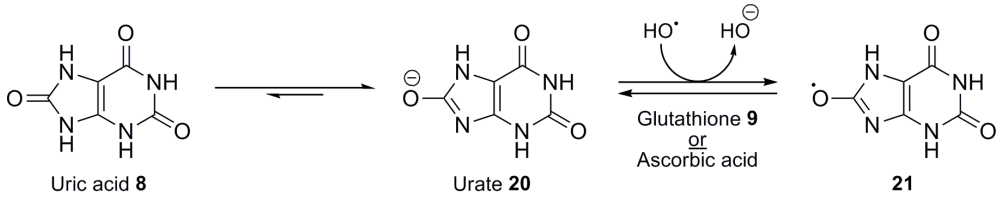

Scheme 13: Uric acid reaction with hydroxyl radicals

Lipoic acid (LA) **23** behaves as an anti-oxidant *in vitro* by rapidly reacting with ROS such as H_2O_2 and hypochlorous acid (HOCl) in its reduced form dihydrolipoic acid **22** (DHLA, Scheme 14). The ability of LA **23** to directly scavenge ROS *in vivo* has been widely debated with much of the antioxidant behaviour of LA **23** potentially coming from DHLA **22** after reduction by the endogenous thioredoxin ($Trx(SH)_2$)/thioredoxin reductase (TrxR, E.C. 1.8.1.9) system or by lipoamide dehydrogenase (E.C. 1.6.4.3).[21,22,23,24]

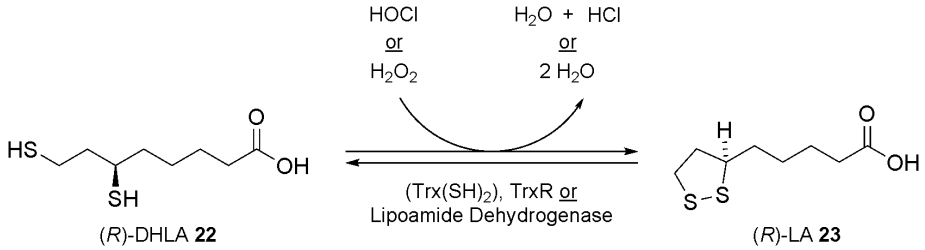

Scheme 14: Lipoic acid reduction/oxidation

(*R*)-Lipoic acid [(*R*)-LA] **23** is a more efficient antioxidant than the unnatural enantiomer (*S*)-LA as the former is enzymatically recycled while the latter appears to reversibly inhibit the enzymes involved in the recycling process.[25] (*R*)-LA **23** and (*S*)-LA will however react with achiral ROS at the same rate. The mechanism for the antioxidant activity of LA **23** may be more complex than simple direct ROS scavenging. Recently the impact of LA **23** on a number of biological processes including modulation of signal transduction and gene transcription was observed. These processes can improve the antioxidant status of the cell (eg. activation of phase II detoxification *via* the transcription factor Nrf2) and it is possible that this is responsible for much of the therapeutic activity possessed by (*R*)-LA **23**.[26]

The ability of antioxidants to protect the body relies heavily on their bioavailabilities and how well they can accumulate in sites of high ROS production. The abilities of other *in vitro* antioxidants (Fig.5) obtained through diet such as polyphenols (eg. quercetin **24** and cathecin **25**) and carotenoids (eg. β-carotene **26**) to protect *in vivo* has been widely debated due to bioavailability issues, rapid metabolism and observed pro-oxidant behaviour.[27,28] Research into the area of antioxidant behaviour and protective mechanisms is ongoing.

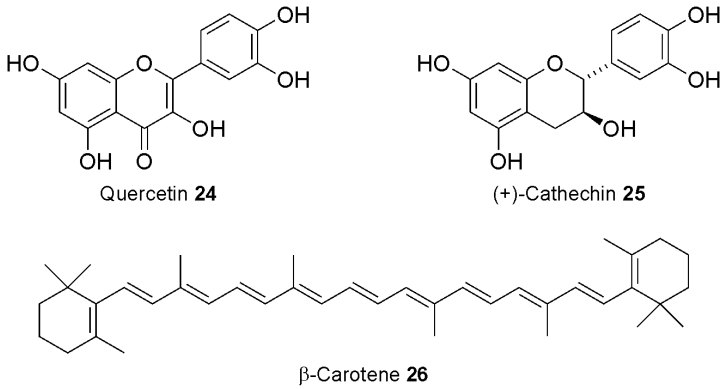

Fig.5: *In vitro* antioxidants may not protect *in vivo*

1.4 Free radical theory of ageing

As an organism ages, oxidative damage accumulates at the cellular level over time. This is the basis for one of the leading theories on ageing and age-related disease known as the free radical theory of ageing (FRTA). First proposed in the mid 1950's by Professor Denham Harman,[29] FRTA describes how the effects of ageing and the resultant diseases can be attributed to the accumulation of lipid, protein and nucleic acid damage from free radicals, leading to a decline in function and ultimately disease with age. The FRTA arose from a number of supporting observations. In particular, exposure to ultraviolet light was known to generate oxygen-centred radical ROS in cells as well as cause signs of premature ageing. This coupled with the knowledge that biological systems generate low levels of oxygen-centred radical ROS under normal conditions led to the basis for the FRTA.

The production of ROS in mitochondria as a by-product of aerobic respiration is the main endogenous source of oxidative stress in the body. It is important to reduce oxidative stress as strong evidence exists implicating it as a contributing factor in the development of a wide range of age-related diseases, including arteriosclerosis, neoplasia, stroke and cataracts as well as neurodegenerative diseases[6,30,31] such as Alzheimer's and Parkinson's. Initially focussed strictly upon free radicals, the FRTA has been expanded to include other ROS and reactive nitrogen species (RNS). Direct evidence for the FRTA was provided by the overexpression of human catalase targeted to murine mitochondria which extended lifespan by 20% and reduce signs of ageing in mice.[12] Furthermore, human $Trx(SH)_2$ expression in transgenic mice showed protection against oxidative stress and extended median lifespan by 35%[32] while overexpression of SOD can extend the lifespan of fruit flies (*Drosophila melanogaster*) by up to 48%.[33]

1.5 RNS Production and proliferation

Reactive nitrogen species (RNS) are a class of compounds including nitric oxide ($^{\bullet}NO$) and products derived thereof such as its reaction products with molecular oxygen (nitrite radical, $^{\bullet}NO_2$), nitrite radicals (dinitrogen trioxide, N_2O_3), superoxide (peroxynitrite, $ONOO^-$)[34] and thiols (*S*-nitrosothiols, RSNO). Nitric oxide is an important intercellular signalling molecule produced by nitric oxide synthases (NOSs, E.C. 1.14.13.39) through the oxidation of L-arginine **27** into L-citrulline **28**, requiring a number of co-factors including hemes, flavins and calmodulins (Scheme 15). Once generated $^{\bullet}NO$ rapidly diffuses (average lifetime ranges from ms to s) from the point of origin and reacts with other biomolecules, often modifying their function.

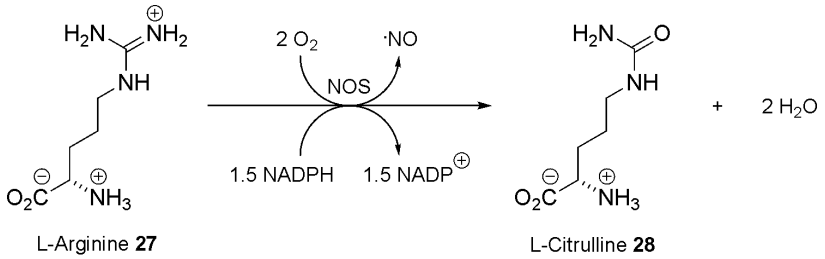

Scheme 15: Nitric oxide production by nitric oxide synthase

In humans, the NOS family includes neuronal NOS (nNOS), a constitutive enzyme found in many different cell types, inducible NOS (iNOS) found in macrophages and endothelial NOS (eNOS) used to modulate vascular tone. A debate as to whether or not mitochondrial NOS (mtNOS) or mitochondrial NOS-like enzymes exist is ongoing. However current evidence suggests this is unlikely as the mitochondrial genome does not contain any NOS-like sequences. If mtNOS was synthesised in the nucleus, import mechanisms for it and all of the necessary co-factors would have to be in place.[35,36] To date no conclusive evidence supporting the existence of mtNOS has been reported.

Nitric oxide plays an important role in a number of biological processes including angiogenesis, insulin secretion, vasodilation, central nervous system development as well as cytotoxic immune responses. Nitric oxide also directly regulates the functions of a whole host of proteins including glyceraldehyde-3-phosphate dehydrogenase (GAPDH, E.C. 1.2.1.12), creatine kinase (CK, E.C. 2.7.3.2), cytoskeletal proteins (tubulin and S-actin), receptors (ryanodine receptor), transcription factors (TF cJun), thioredoxin [$Trx(SH)_2$] and glutaredoxin (Grx).[37] Despite this the entirety of $^{\bullet}NO$ roles in biology has not yet been fully elucidated.

Regardless of whether mtNOS exists or not, and although •NO presence is evidently necessary in mitochondrial biology, it is clear that elevated levels of •NO in mitochondria can produce a number of potentially detrimental biological effects in this organelle and as a result in the organism as a whole.

•NO itself is known to be a potent reversible competitive inhibitor of complexes III and IV as well as mitochondrial actinase at physiological nanomolar concentrations linking it as a potential moderator of physiological respiration.[38] iNOS activated in response to inflammation signals produce sufficient •NO to inhibit not only their own respiration, but also that of surrounding cells. However it is likely that inhibition of the respiratory chain can protect cells *in vivo* under hypoxia conditions by slowing oxygen consumption, preventing anoxia which would cause apoptosis.[39] Reversible inhibition of cytochrome c oxidase occurs when the •NO binds to the reduced copper or iron centres in the catalytic centre leading to the exclusion of oxygen. When •NO binds to the oxidised form, inhibitory nitrite can be produced *via* hydration. Nitrite radicals can oxidise ferrous iron in haemoglobin to ferric iron, preventing it from binding oxygen which combined with the •NO inhibitory effects could potentially sensitise cells to hypoxia. As a result, whether or not •NO has an overall beneficial or detrimental effect on respiration is unclear. It is likely at normal physiological concentrations •NO has a beneficial effect but is detrimental at elevated levels, particularly as this leads to elevated concentrations of secondary RNS species (Scheme 16).

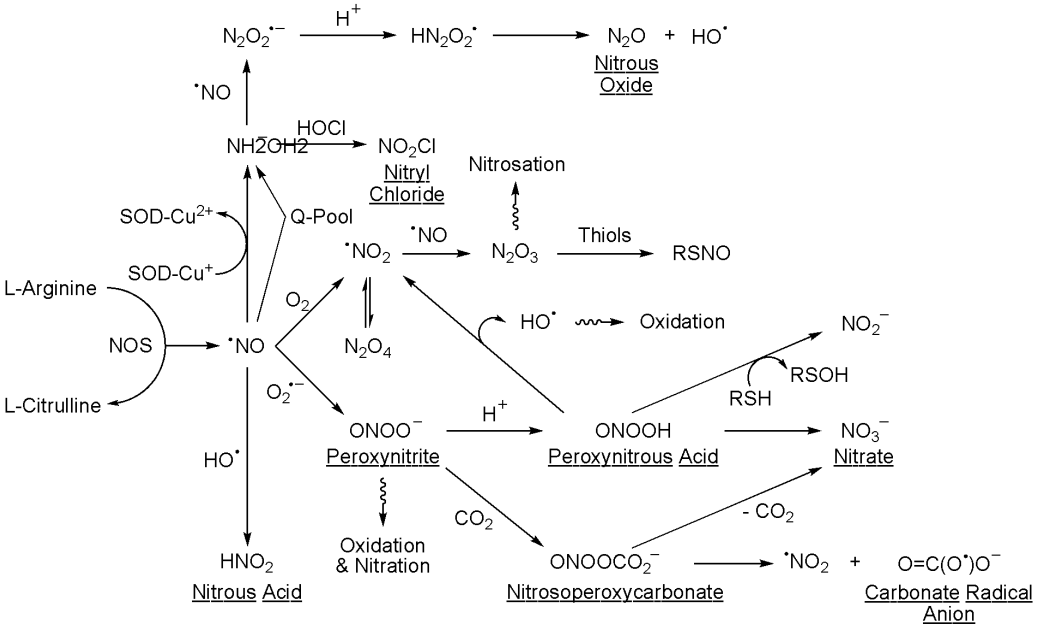

Scheme 16: RNS generation and interconversion cascades[40,41]

Biological RNS can also cause nitration and *S*-nitrosation of proteins leading to direct and indirect changes to function and turnover efficiency. For example it has been observed that nitrosation of complex IV subunit II results in a decline in levels of mitochondrial glutathione (GSH **9**) and its dimer (GSSG **11**).[42,43,44]

Peroxynitrite can inhibit a number of mitochondrial components including complex I, complex II, ATPase, mitochondrial actinase and superoxide dismutase through nitration and/or oxidation.[38,45] $^{\bullet}NO_2$, N_2O_3 and *S*-nitrosothiols have also been seen to cause weak non-selective irreversible inhibition of a number of mitochondrial components.[46,47] Furthermore RNS such as $^{\bullet}NO_2$, N_2O_3, HNO_2 and peroxynitrite can damage DNA through nitration, nitrosation and deamination of DNA bases.[16,48]

Chapter 2: Methods of targeting mitochondria

As mitochondria have been strongly linked as the major cause of oxidative stress in the body, it is important to be able to selectively target potential therapeutic agents to this organelle over other compartments of the cell. A number of methods for the selective delivery of biologically active molecules to mitochondria have been studied and have been recently reviewed.[49] In particular, conjugation of desired payload molecules to delocalised lipophilic cations (DLCs) such as alkyl triphenylphosphonium (TPP)[50] and quaternary ammonium salts,[51] or to short peptide sequences comprising alternating lipophilic and basic side chains (the latter of which are predominantly cationic at physiological pHs) have been utilised.[52,53] The key features of both approaches is to balance the incorporation cationic moieties so as to take advantage of $\Delta\Psi_p$ and the large $\Delta\Psi_m$ established by aerobic respiration to drive compound uptake with the need for sufficient lipophilic character to enable the traversing of the cellular phospholipid membrane, MOM and MIM.

2.1 Delocalised lipophilic cations as a mitochondrial targeting strategy

TPP compounds were originally developed by the groups of Murphy and Smith to investigate $\Delta\Psi_m$, but since have been employed be a number of groups to deliver a plethora of compounds to mitochondria.[49,54] Utilising TPP salts as a mitochondria-targeting group has a number of advantages and disadvantages. Firstly, it is relatively easy to synthetically introduce TPP groups (Chapter 7.4) and if introduced late in the synthesis, it gives a convenient handle for the synthesis of analogues containing radio- or stable deutero-labelled TPP moieties for use in uptake, metabolism or mass spectrometry studies (Chapter 6).

The synthetic disadvantage of TPP moieties is that once incorporated into a molecule, the TPP group often dominates the physical characteristics. If only one TPP species is present this can be advantageous as they can readily be precipitated from ethereal solvents or readily separated by silica column chromatography. However if multiple TPP compounds are present, this can make separation of closely related synthetic products and by-products very difficult. Therefore this limits the reactions that can be easily used after TPP has been introduced as it is vital to obtain high, selective conversion. The scope of available reactions is also narrowed by the possibility of generating undesired phosphonium ylides or oxidation of phosphorous to give diphenylphosphine oxides under certain basic

conditions. The latter is a rapid transformation driven by the formation of the strong phosphorus-oxygen double bond (Scheme 17). This transformation does not occur significantly at physiological pHs.

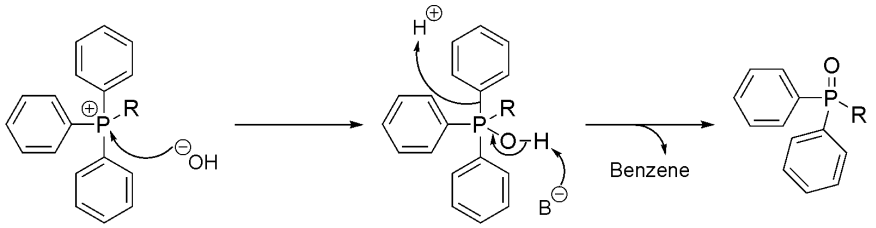

Scheme 17: Undesirable oxidation of TPP compounds to phosphine oxides

The extent to which TPP-conjugates accumulate in the mitochondrial matrix is heavily dependant upon the magnitudes of the potential gradients across the MIM ($\Delta\Psi_m$, 150-180 mV in healthy cells) and to the cellular plasma membrane potential ($\Delta\Psi_p$, 30-60 mV), both of which are negative on the internal membrane face (Fig.6). The Nernst equation (Fig.7) can be used to calculate the concentrations of charged species across these membranes and indicates that singly charged cationic molecules should display a ten-fold increase in accumulation for every 61.5 mV at 37 °C assuming no other significant external factors, such as active molecular transport mechanisms or rapid irreversible binding to cellular components are taking place. TPP compounds generally behave as predicted by the Nernst equation and are known to accumulate in the mitochondrial matrix in concentrations many hundred-fold higher than in the cytosol as a result of the large $\Delta\Psi_m$.[55] Toxicity of TPP compounds is not usually a problem as the compounds are reversibly equilibrated between all intracellular and extracellular regions. For example, a number of mice studies and a year-long phase II trials of MitoQ **29** (Chapter 3.1) in humans have been conducted with no adverse effects observed.[56] As metabolism and excretion occur from circulation, TPP compounds from within the mitochondria diffuse back into the circulation so that the equilibrium is maintained. However, this is not possible if the TPP compound is converted into a cell impermeable compound within the mitochondria or if it forms irreversible covalent attachment to an intracellular macromolecule.

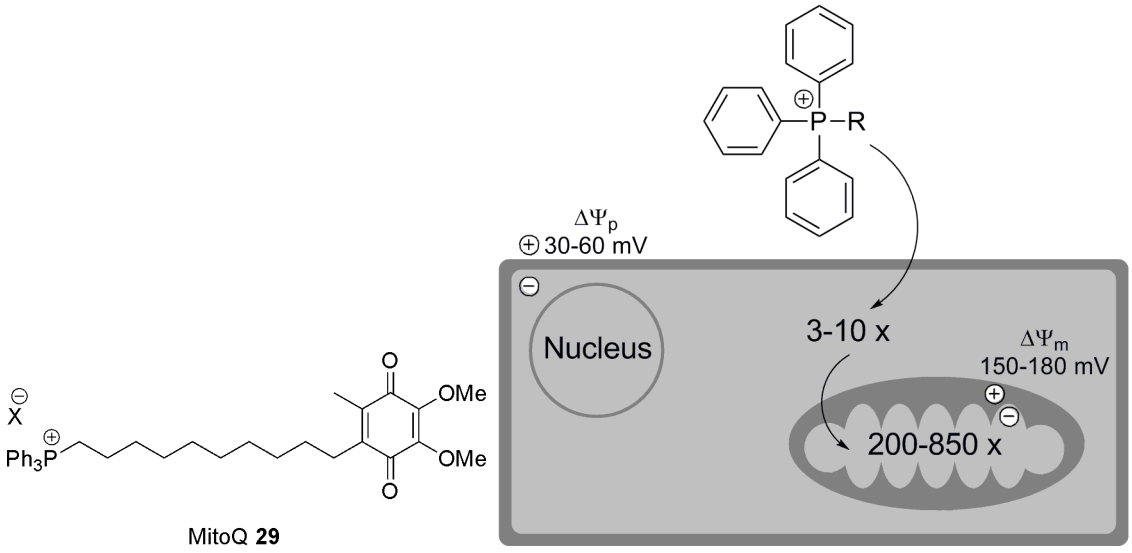

Fig.6: TPP salts such as MitoQ **29** accumulate in mitochondria due to $\Delta\Psi_m$ and $\Delta\Psi_p$[57]

$$E_V = \frac{RT}{zF} \ln \frac{[Ion]_o}{[Ion]_i} \qquad E_{mV} = 61.5 \log \frac{[Ion]_o}{[Ion]_i}$$

Monovalent cation at 37 °C

Fig.7: Nernst equation and its simplified version converted to $\log_{10}$.
Where E_V and $E_{mV} = \Delta\Psi_m$ (in V and mV respectively), R = gas constant (J K^{-1}),
T = temperature (K), z = ion charge, F = Faraday constant (C mol^{-1}),
$[Ion]_o$ and $[Ion]_i$ = ion concentration outside and inside of the membrane respectively.

Studies to assess the uptake by TPP dications found that although uptake was higher than the analogous TPP monocations, the uptake levels predicted by the Nernst equation (10-fold increase for each ~30 mV) were not reached. The exact reasons for this are currently unclear but it was understandably found that the lipophilic character had to be higher for dication uptake across phospholipid membranes.[58]

It is not sufficient that TPP-conjugates accumulate in mitochondria; they must also not disrupt the cellular or mitochondrial membranes or otherwise adversely affect biological pathways (other than those deliberately targeted by the molecule linked to the TPP group), as this can lead to toxicity and cell death. At low concentrations DLCs have been repeatedly found to be non-toxic, but at elevated concentrations the build up of charge inside the mitochondrial matrix has been seen to inhibit respiration and oxidative phosphorylation and ultimately induce the mitochondrial permeability transition, a trigger of apoptosis. However it must be noted that the concentrations in question are usually significantly higher than therapeutic doses. Incubating cells with micromolar

concentrations of TPP compounds allows for millimolar concentrations to be achieved in the mitochondrial matrix, levels at which no disruption of membranes or inhibition of respiration is generally seen.[59]

TPP compounds are rapidly taken up (within 5 min) by energised mitochondria after intravenus administration[60] and clearance profiles fit well to the Nernstian distribution of cationic compounds. TPP compounds are also readily distributed throughout the body through oral administration as long as they can withstand the high acidity of the stomach and first pass effects. As compounds are metabolised and excreted *via* liver and kidneys, redistribution from high concentrations to circulation maintains equilibrium with half lives for clearance ranging between 2 and 15 h.[61]

Extensive work has been conducted on TPP compound uptake by isolated energised mitochondria. However when studying intact cell systems it is more difficult to clearly illustrate TPP-derivatives have successfully accumulated in mitochondria over other cellular compartments as mitochondria depolarise and as a result release lipophilic cations during cell subfractionation. Iodoacetamide-TPP **30** (IAM-TPP, Fig.8) has been used to label mitochondrial thiols such as membrane protein cysteine residues. IAM-TPP **30** accumulates in the mitochondrial matrix in the standard TPP manner but the reactive iodoacetamide moiety undergoes S_N2 displacement of iodide by protein thiols in the matrix to form stable thioethers that cannot be cleared. Localisation of IAM-TPP **30** can subsequently be confirmed using anti-TPP antibodies and immunocytochemistry.[61,62]

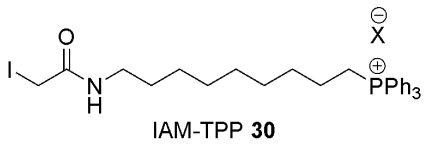

IAM-TPP **30**

Fig.8: IAM-TPP **30** alkylates mitochondrial protein thiols

2.2 Mitochondria-penetrating peptides

An alternative approach for the selective delivery of molecules to mitochondria is through the use of mitochondria-targeted peptides. These are comprised of a short peptide chains of alternating lipophilic and basic (protonated at physiological pH) side-chains.[52] Initial studies by Schiller, Szeto and co-workers indicated that uptake of tetra-peptides (SS-peptides) into cells followed by localisation to mitochondria was largely independent of $\Delta\Psi_m$, although other studies suggest a significant $\Delta\Psi_m$ dependence.[63] One such example is

SS-31 **31** (Fig.9) which is comprised of D-Arg–Dmt (dimethyltyrosine)–Lys–Phe–NH_2. A number of analogues have been made with similar side chains with alternating arrangements and the *C*-terminus is often amidated to improve stability. Observations during fluorescence tagging studies indicated that SS-peptides may selectively bind to the MIM, however the exact nature of any such interactions remain unclear.

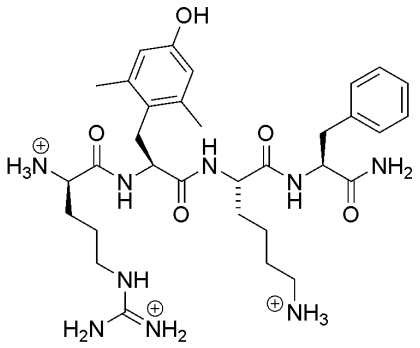

SS-31 **31**

Fig.9: Mitochondria-targeting by peptides with lipophilic and cationic side chains

To date no comprehensive *in vivo* studies have been reported that look at potential metabolism issues which arise from using a peptide targeting system, however incorporation of unnatural D-amino acids and unnatural side chains like Dmt should slow metabolism due to mismatching with enzymatic binding sites.

This concept has been developed further by Kelley and co-workers who have looked to optimise peptide chain properties through the adaption of peptide length, side-chain type and ordering of amino acids to deliver of bioactives to mitochondria.[53,63,64] Mitochondria-targeting of chemotherapy drug chlorambucil **32** led to a significant increase in potency resulting from targeted cross-linking of mitochondrial DNA by the nitrogen mustard (Fig.10). The therapeutic window was maintained through elevated uptake by chronic lymphocytic leukaemia cells compared to normal healthy cells as the mitochondria of cancer cells often have elevated $\Delta\Psi_m$. Combined with the reduced uptake to HL60 cells in the presence of mitochondrial uncoupler carbonyl cyanide-*p*-trifluoromethoxyphenylhydrazone (FCCP **33**, Fig.11), $\Delta\Psi_m$ appears to play a role in compound uptake. A thiazole orange fluorophore was incorporated to enable compound monitoring by confocal microscopy. Despite thiazole orange being a lipophilic cation itself, no comment was made as to the effect that this unit had on uptake but it is highly likely that this would have assisted uptake in this study. However, it has since been reported that anionic fluorophores can also be delivered by this approach due to the

molecule maintaining a net positive charge, something not possible for singly cationic TPP molecules.[65] As in SS-peptides, unnatural amino acid residues are incorporated to slow metabolism.

This study is one of many that highlights the fact that mitochondria-targeting of therapeutics is a realistic strategy for improving both new and existing disease treatments including chemotherapy agents.[63,66]

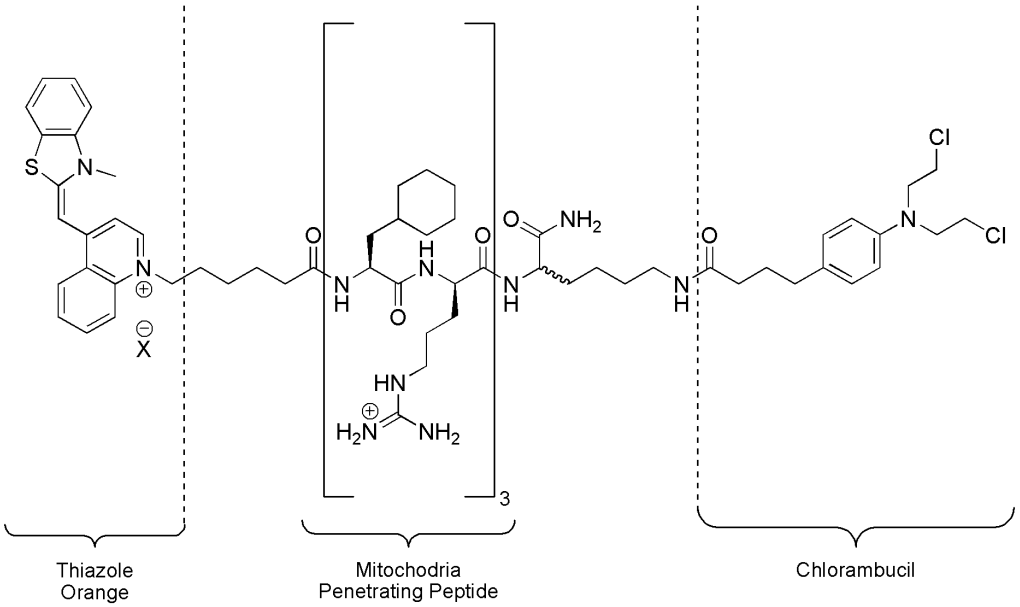

Fig.10: Mitochondria-targeted chlorambucil **32**

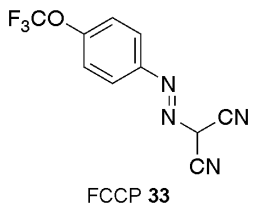

Fig.11: Mitochondrial uncoupler FCCP **33** (Chapter 7 for further discussion)

2.3 Alternative mitochondria-targeting approaches

Alternative approaches for targeting materials to mitochondria to date have found limited usage but are in principle viable targeting mechanisms. Harnessing some of the mitochondrial active transport machinery is one potential route that may be explored further in time. Recently a patent has been granted related to the use of the carnitine-acylcarnitine translocase (CACT) system for the mitochondria-targeted delivery of cis-platin anti-cancer agents.[67] The molecule L-carnitine **34** is used by the body to recognise

and actively transport fatty acids into the mitochondrial matrix for catabolism. Incorporating an L-carnitine **34** like moiety into a prodrug molecule could potentially allow delivery of molecules by the CACT system with prodrug release by carnitine palmitoyltransferase II (E.C. 2.3.1.21) embedded on the inside wall of the MIM. The Hartley group recently published work towards a mitochondria-targeted spin-trap CarnDOD-7C **35**, designed to utilise this delivery mechanism (Fig.12).[68]

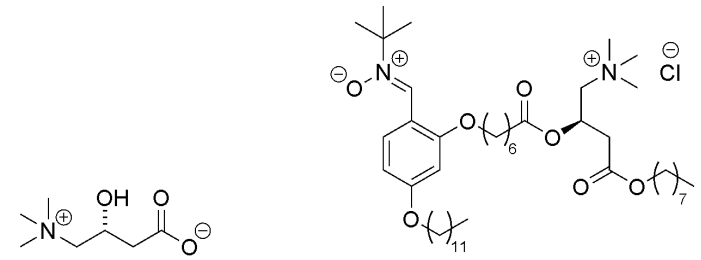

Fig.12: L-Carnitine **34** derivatives are potential mitochondria-targeting agents

This method may be particularly suited to targeting cancerous cells as these rapidly dividing cells require an elevated uptake of raw materials including fatty acids. Thus harnessing the up-regulated CACT system may allow some degree of selectivity to be achieved. However to exploit active transport machinery the compounds used must retain binding properties to enzymatic active sites which in certain cases may not be accessible to molecules of substantially altered size, lipophilicity, number of rotatable bonds, etc.

Targeting to mitochondria-specific binding sites has also been considered. It has been suggested that the accumulation of 10-*N*-nonylacridine orange **36** (Fig.13) results from binding mitochondria-specific phospholipid cardiolipins.[69] However this molecule is itself a lipophilic cation and therefore some (if not a large) degree of uptake would be expected to result *via* the same passive mechanism as other DLC compounds.

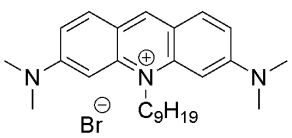

Fig.13: $\Delta\Psi_m$ independent uptake mechanisms have been proposed

Chapter 3: Small molecules targeted to mitochondria

3.1 Mitochondria-targeted antioxidants

A wide range of antioxidants, dyes, molecular probes and sensors have been made to accumulate in mitochondria utilising lipophilic TPP cations. Conventional antioxidants are ineffective as they lack the ability to accumulate in sufficient concentrations where ROS are produced and most lack the ability to penetrate mitochondria. Therefore mitochondria-targeted antioxidants have been designed to protect against all components of intramitochondrial ROS cascades and many are known to protect against markers of oxidative stress *in vitro* and *in vivo* (Figs.14 and 15).[49] In the literature discussion that follows the anionic counterion is arbitrary as this will rapidly exchange *in vitro* or *in vivo*.

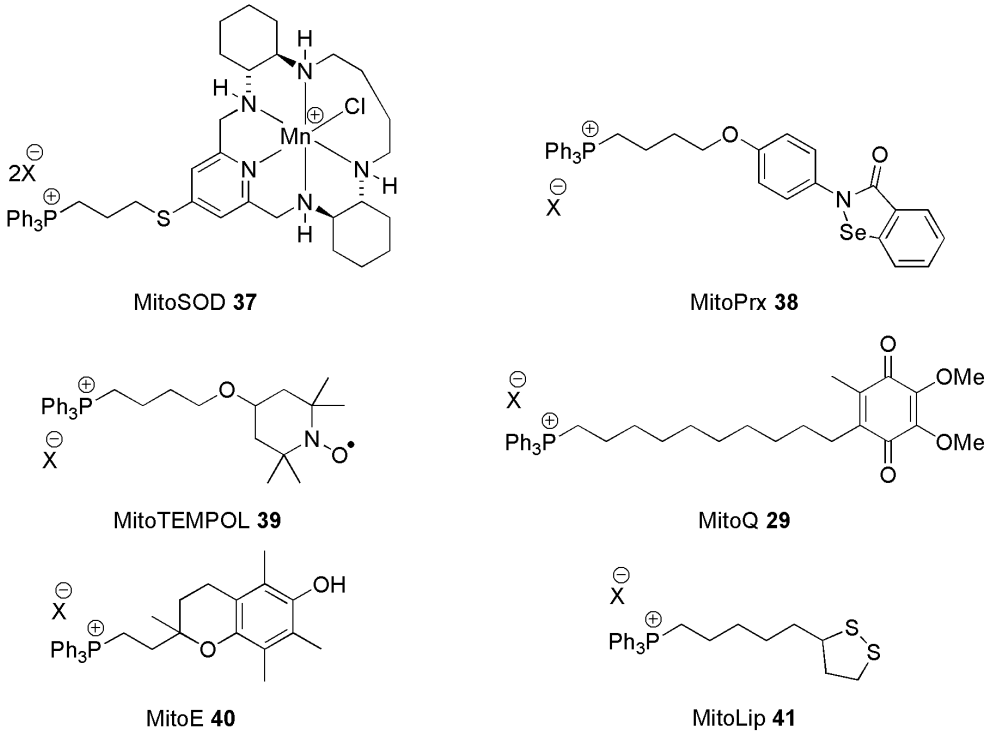

Fig.14: Mitochondria-targeted antioxidants

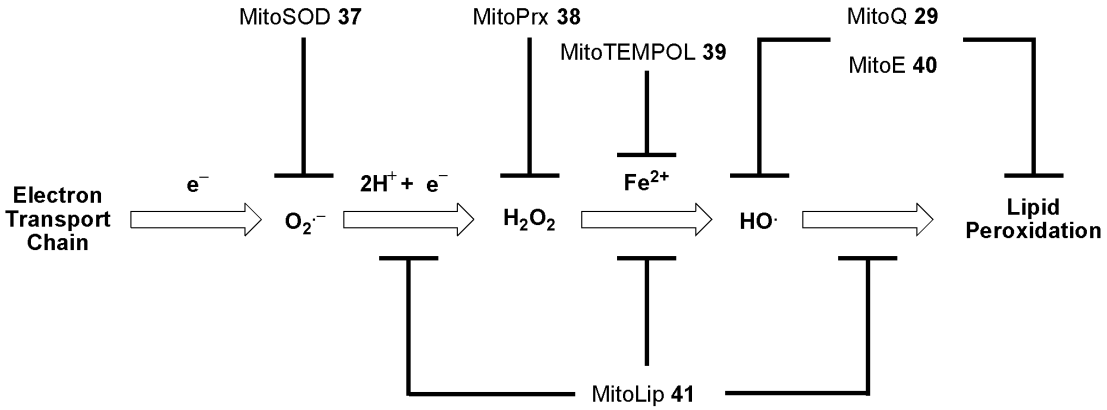

Fig.15: Mitochondria-targeted antioxidants can target all aspects of mitochondrial ROS[57]

By far the most extensively studied TPP antioxidant is MitoQuinone **29** (MitoQ). It was studied *in vivo* to assess the distribution properties of the TPP compounds throughout an organism depending on the route of administration.[61] [^{3}H] Radiolabelled MitoQ **29** and controls were administered *via* either oral or intravenous (IV) tail vein injections in mice and concentrations in various organ tissues assessed at differing time points. It was found that blood concentrations fell rapidly with a substantial uptake by kidney and liver tissues within 5 min of IV administration. A lesser uptake to heart tissue and very little uptake by brain or adipose tissue were seen. MitoQ **29** clearance from liver, kidneys and heart were 2, 4 and 15 h respectively with almost complete loss of MitoQ **29** after 48 h. Due to the lipophilicity of MitoQ **29** it is predominantly found adsorbed to the mitochondrial membranes and as a result has been found effective at reducing lipid peroxidation.[60]

When the quinol form of MitoQ **29** acts as an antioxidant it is oxidized to the quinone form, which is then rapidly reduced by complex II back to the quinol, restoring its antioxidant efficacy. Using a reverse driven ATPase system to establish $\Delta\Psi_m$ (Chapter 8.2.2) enables MitoQ **29** uptake but lacks the ability for the respiratory chain to reduce MitoQ **29** and so efficacy is lost. Furthermore it was found that the reduced form MitoQ **29** is not oxidized by complex III and therefore cannot act as an electron carrier to restore respiration in mitochondria deficient in coenzyme Q. Quinols have been seen to undergo redox cycling *in vitro* under certain conditions which can lead to $O_2^{\bullet-}$ formation however no pro-oxidation effects of MitoQ **29** have been observed *in vivo* at therapeutic doses.[70]

MitoPeroxidase **38** (MitoPrx, Fig.14) is a mitochondria-targeted version of the isoselenazole derivative ebselen **43**, which is a mimetic of glutathione peroxidase (E.C. 1.11.1.9, Scheme 18). Ebselen **43** uses a selenium atom to reduce H_2O_2 to water and converts lipid hydroperoxides into the corresponding alcohols.[71,72] Selenol **46** is the catalytically active species which can be formed from ebselen **43** by reaction with two equivalents of glutathione or by reduction by either thioredoxin [$Trx(SH)_2$] or thioredoxin reductase (TrxR). Oxidation of selenol **46** by hydroperoxides regenerates ebselen **43** *via* selenenic acid **47**, which rapidly undergoes an intramolecular condensation reaction.

Ebselen **43** itself can be directly oxidised slowly by hydroperoxides or rapidly by peroxynitrite to selenoxide **42**. However this is readily re-reduced by GSH **9** or TrxR. Diselenide **44** is also readily reduced to the active selenol **46** by TrxR or $Trx(SH)_2$ and slowly by GSH.

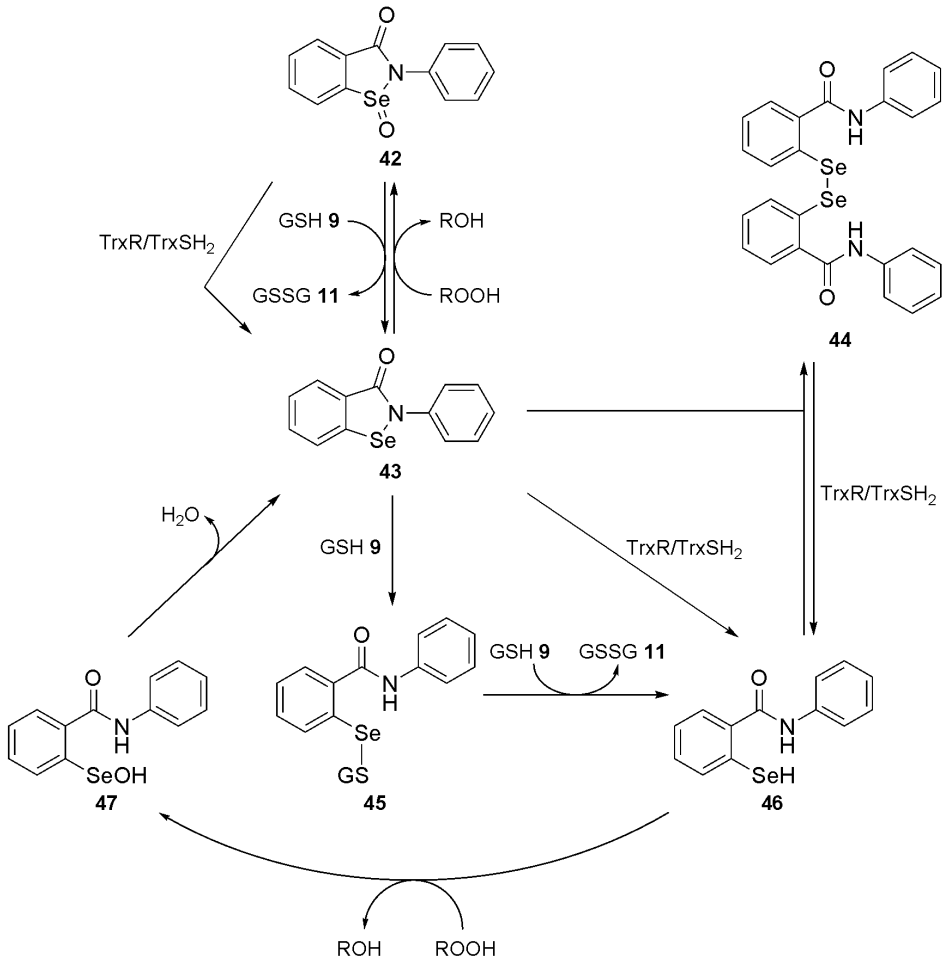

Scheme 18: Ebselen mimetic catalyses the detoxification of peroxides. R = H or lipid.

MitoPrx **38** uptake into energised, isolated mitochondria was confirmed as well as its activation in cells by intracellular GSH **9** and thioredoxin systems. Additionally it was successful in reducing oxidative damage by hydroperoxides in cells. However, unlike MitoQ **29** and MitoE **40**, no significant improvement in efficacy over ebselen **43** itself through TPP conjugation was found. The reason for this is currently unclear.

MitoE **40** is a mitochondria-targeted version of α-d-tocopherol (the main component of vitamin E) found to accumulate rapidly in mitochondria, approximately 80-fold greater than endogenous vitamin E.[59] As a result of elevated mitochondrial concentrations, MitoE **40** was found to protect against oxidative stress, reducing lipid peroxidation and protein damage significantly better than the natural antioxidant. MitoE **40** protects against oxidative stress by exactly the same mechanism as vitamin E (Chapter 1.3, Scheme 11), involving redox cycling by ascorbic acid. Like vitamin E, MitoE **40** is lipophilic so embeds itself in phospholipid membranes and primarily protects against lipid peroxidation.

Mitochondria-targeted lipoic acid **41** (MitoLip) was synthesised and assessed for its ability to protect against oxidative stress by the groups of Murphy and Smith.[24] It was found that although uptake by energised mitochondria occurred, no protection against ROS was observed. This was due to the minimal reduction (5-10%) of MitoLip **41** to the active reduced form, dithiol MitoLipH_2 compared to endogenous (*R*)-lipoic acid **23**. In particular TrxR was unable to reduce MitoLA **41** *in vitro*.

A mitochondria-targeted version of the superoxide dismutase mimetic (M40403) developed by Salvemini *et al*[73] has also been developed by the group of Smith (MitoSOD **37**) with results appearing in abstracts but currently unpublished.

Stable piperidine and pyrrolidine nitroxides 4-hydroxy-2,2,6,6-tetramethylpiperidin-1-oxyl (TEMPO) and the analogous 3-carboxy proxyl (CP) can scavenge radicals *in vitro* and *in vivo* and mitochondria-targeted analogues MitoTEMPO **48** and MitoCP **49** have been developed (Fig.16).[74,75,76] These can directly scavenge radicals, act as SOD mimetics (Scheme 19) and oxidise Fe(II) to Fe(III) preventing radical formation *via* the Fenton mechanism (Chapter 1.3, Scheme 7).

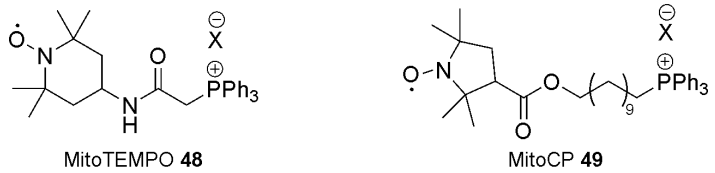

Fig.16: Mitochondria-targeted radical scavengers act as SOD mimetics

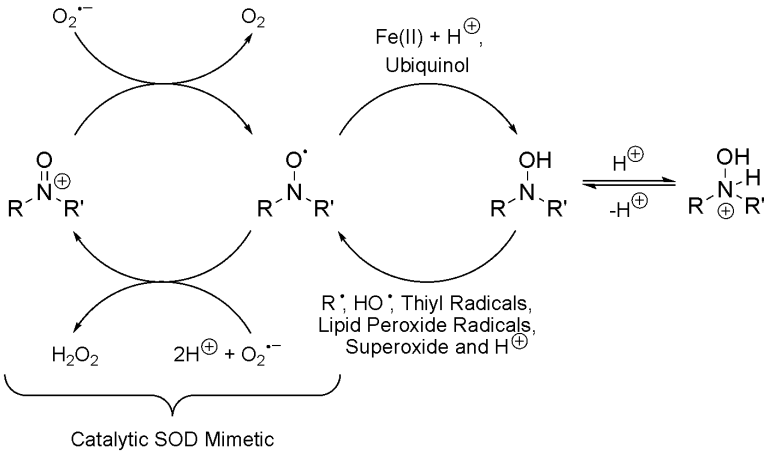

Scheme 19: Nitroxides as SOD mimetics and direct radical scavengers

Nitroxides behave as SOD mimetics through redox cycling between the nitroxide radical and the oxidised oxoammonium cation forms. Nitroxide redox potentials are tuneable by modification of ring sizes and substituent effects.[77] For each complete redox cycle two molecules of superoxide are disproportionated into one molecule of molecular oxygen and one molecule of hydrogen peroxide.

A potential limitation of nitroxide usage as antioxidants in biological systems is that they are rapidly reduced to hydroxylamines by species such as ubiquinol in the MIM. However in studies of MitoTEMPOL **48** and MitoCP **49**, protection against oxidative stress was maintained even in the hydroxylamine forms.[78,79] Hydroxylamines protect against radicals through hydrogen atom abstraction to reform a nitroxide radical species in a stoichiometric manner. Murphy and co-workers found hydroxylamines to be significantly better at protecting against lipid peroxidation and DNA damage than the parent nitroxide.

The above examples show that targeting materials to mitochondria can yield improved selectivity and/or efficacy (MitoQ **29**, MitoE **40**, MitoTEMPOL **48**) demonstrating the viability of mitochondria as a potential therapeutic target. However, in dealing with complex biological systems in which many pathways and their interactions are still not fully understood, success is not guaranteed (MitoLip **41**). Nonetheless, targeting by TPP provides a robust and reliable approach to deliver materials to mitochondria, allowing the roles of ROS/RNS and various bioactive molecules to be probed and understanding of their effects to be developed.

3.2 Mitochondria-targeted bioactives

A number of biologically active molecules other than antioxidants have been targeted to mitochondria using DLCs as a targeting mechanism. These can be broadly split into two classes. The first class like the antioxidants previously discussed retain a covalent attachment to their TPP moiety throughout usage while a second class undergo specific fragmentations to release active molecules *in situ*.

Mitochondria-targeted *S*-nitrosothiol **50** (MitoSNO) selectively delivers $^{\bullet}$NO to the mitochondrial matrix (Scheme 20).[43] $^{\bullet}$NO release from MitoSNO **50** by reaction with glutathione (or other mitochondrial thiols) was found to reversibly inhibit complex III, cause vasodilation and protect against heart ischemia-reperfusion (I/R) injury (through *S*-nitrosation of mitochondrial proteins), consistent with the known behaviour of

endogenously produced •NO (Chapter 1.5). Thus MitoSNO **50** can be used to study the reversible modulation of respiration and protection against I/R by •NO. The *S*-nitrosation occurred in approximately 1% of mitochondrial protein thiols despite the presence of a fully reduced GSH **9** pool. Therefore it is possible that certain thiols are particularly susceptible to *S*-nitrosation and the biological relevance of this may be investigated using MitoSNO **50**.

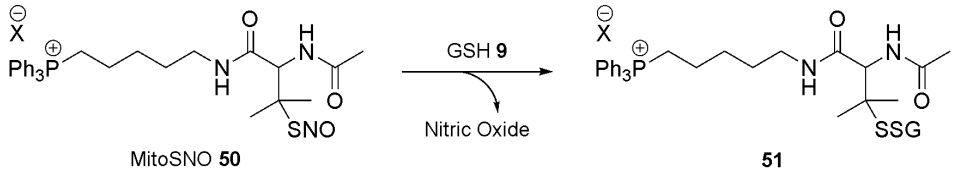

MitoSNO **50** **51**

Scheme 20: MitoSNO **50** delivers nitric oxide to mitochondria

Spin traps react selectively with free radicals such as HO• to give longer-lived radicals that can then be detected using electroparamagnetic resonance (EPR) spectroscopy (Scheme 21). The high selectivity of spin traps overcomes a number of problems inherent with using the commonly used fluorescent sensors for identifying ROS in biological systems (discussed further in Chapter 4). However, despite being longer-lived species than the highly reactive free radicals, the spin trap adducts formed are themselves often decomposed or metabolised relatively quickly to EPR silent products, limiting their use as an identification and quantification tool.[80] Furthermore reactions of free radicals with nitrone spin traps are often slow, leading to elevated concentrations of the probes being required which increases the chance of cytotoxicity issues. Mitochondria-targeted spin traps MitoSpin **52**[81], MitoPBN **53**[82], MitoBMPO **54**[83] and MitoDEPMPO **55**[80,84] have been developed but due to low sensitivities of these probes combined with adduct decomposition, none have been successfully used to quantify ROS *in vivo*. Spin traps may be developed in the future with improved stability and reactivity but until then a better approach to quantifying ROS and RNS is to develop mass spectrometry based probes (Chapter 6).

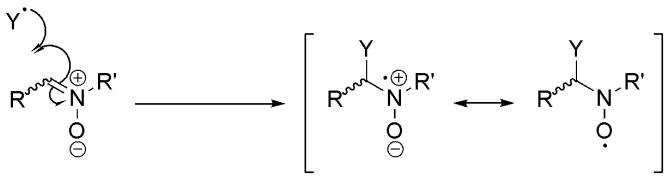

Scheme 21: Radical trapping by nitrone spin traps

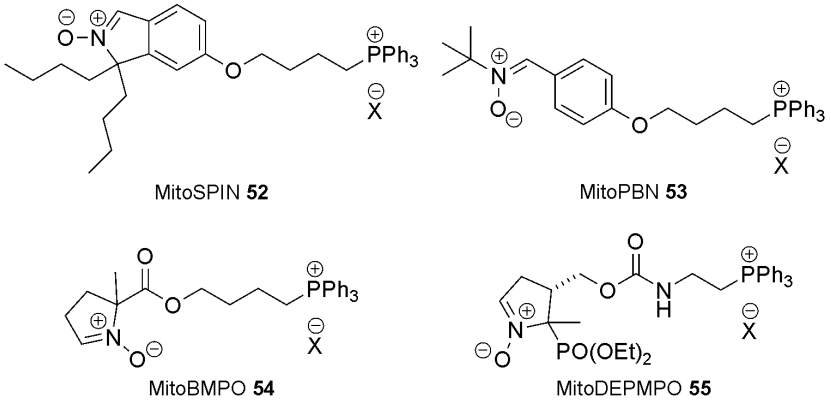

Fig.17: Mitochondria-targeted spin traps

A range of photosensitisers such as MitoPorphyrin **56** have been targeted to mitochondria using DLCs with the view to developing photodynamic therapy (PDT) agents to treat cancer (Fig.18).[85,86,87] PDT uses photoreactions mediated by photosensitisers activated by light to produce bursts of ROS such as singlet oxygen in specific cells or cellular compartments. The localised ROS generated damage the cell sufficiently so that apoptosis occurs. As mitochondria are key regulators of damage signalling and apoptosis through the activation of the mitochondria outer membrane permeability (MOMP) transition pores, triggering mitochondria-induced apoptosis is seen as a promising route to killing cancerous cells selectively.

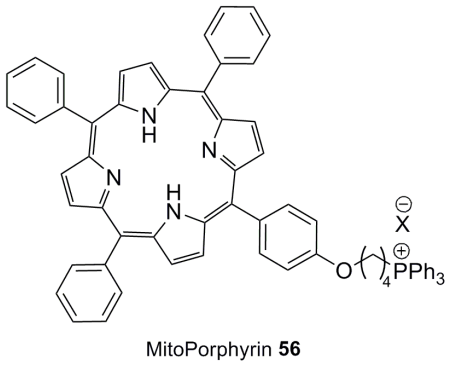

Fig.18: Mitochondria-targeted photosensitisers are potential PDT agents

Cyclosporin A (CsA) is a lipophilic undecapeptide inhibitor of cyclophilins (CyPs), a family of peptidylprolyl *cis-trans* isomerases.[88] CyP-D localised in mitochondria facilitates MOMP through the formation of permeability transition (PT) pores. Inhibition of CyP-D by CsA can protect against much of the mitochondrial damage caused by I/R injury and subsequent necrosis by preventing PT pore formation. In targeting CsA to mitochondria (Fig.19), although binding affinity was partially reduced, its selectivity towards CyP-D over cytosolic CyP-A was markedly increased leading to an improvement

in cytoprotection against I/R induced necrosis. In contrast to the many small functional molecules previously discussed, this study displays the abilities of TPP targeting to deliver relatively large, complex molecules to mitochondria and the possibilities of modulating function through selective inhibition of mitochondrial enzymes.

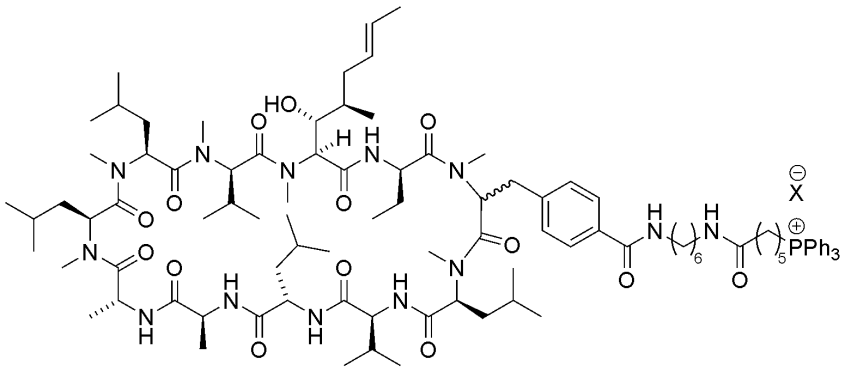

Fig.19: Mitochondria-targeted cyclosporine A

3.3 Mitochondria staining

Although TPP targeting has been extensively studied, other non-phosphorus based lipophilic cations can also accumulate selectively in mitochondria. For example, rhodamine, rosamine and carbocyanine cationic fluorescent dyes such as the MitoTracker series have been widely used to stain energised mitochondria *in vitro* (Fig.20). These not only allow the position and quantity of mitochondria present to be observed, but also can allow the effects that various stimuli such as UV or oxidative bursts have on the respiratory chain to be monitored.

All of the probes in the MitoTracker series (**58** to **64**, Fig.20) use non-phosphorus based DLCs to drive accumulation in mitochondria with modifications to fluorophore substituents and spacers optimising fluorescence properties. Rosamine-type probes **61** and **63** require oxidation into lipophilic cations **62** and **64** inside the cell before mitochondrial uptake can occur which can give information regarding the redox state of cells under study. Once in the mitochondrial matrix, the benzylic chloride moieties react with membrane-bound protein thiols giving covalent attachment through stable thioether linkages. The concentrated localisation of fluorescence allows mitochondria to be imaged. One problem with the MitoTracker series (Invitrogen) beyond inherent fluorescence limitations (Chapter 4.5), is that they are known to photosensitize cells which can lead to depolarisation of $\Delta\Psi_m$, mitochondrial swelling and apoptosis.[89] Covalently binding to cysteine residues also

prevents clearance from cells increasing toxicity profiles and can potentially impact protein function by modifying structure or by blocking either active or co-factor binding sites.

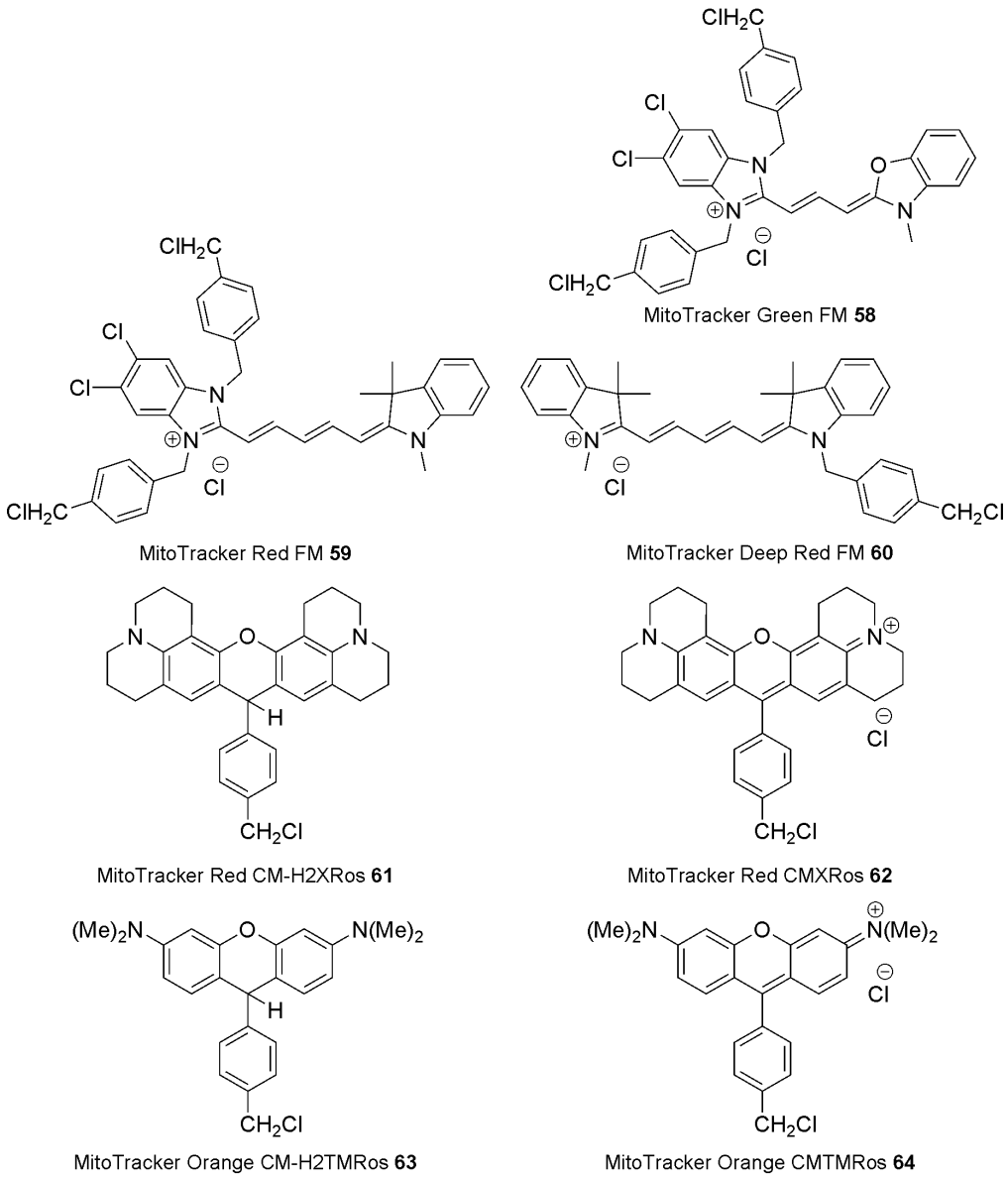

Fig.20: MitoTracker dye series used to stain energised mitochondria

Carbocyanine dye **65** (JC-1, Invitrogen) is a fluorescent dye that allows the $\Delta\Psi_m$ status of individual mitochondrion to be monitored (Fig.21). As a lipophilic cation, JC-1 **65** accumulates in energised mitochondria as previously discussed. Mitochondria with elevated $\Delta\Psi_m$ will uptake higher concentrations of JC-1 **65**, as defined by the Nernst equation. Under these conditions JC-1 **65** forms aggregates within the mitochondrial matrix which modify its fluorescent properties. Above a critical concentration, J-aggregates form. This stains mitochondria red-fluorescent with λ_{em} maximum at 590 nm. If $\Delta\Psi_m$ collapses (a key sign of apoptosis), monomeric JC-1 **65** is released into the cytoplasm where it is green-fluorescent with λ_{em} maximum at 527 nm. Thus clear

differentiation between mitochondria of varying $\Delta\Psi_m$ can be made, in particular in the study of apoptotic or necrotic cell death in which $\Delta\Psi_m$ becomes dissipated. Furthermore, JC-1 **65** monomers and J-aggregates both can be visualised simultaneously by fluorescence microscopy using a wide band-pass filter exciting at 488 nm.

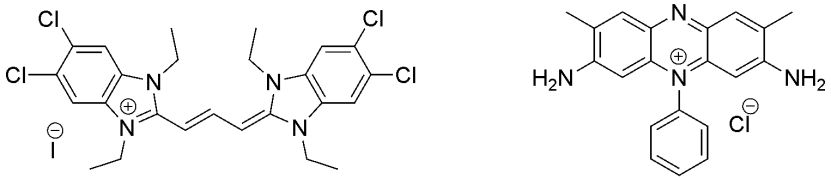

JC-1 **65** Safranin O **66**

Fig.21: $\Delta\Psi_m$ sensitive fluorescent probes

The fluorescent dye Safranin O **66** (Fig.21) can also be used to monitor $\Delta\Psi_m$ of isolated mitochondria. Safranin O **66** fluoresces when used in dilute solutions but upon uptake into the small volume of the mitochondrial matrix, the elevated concentration causes self-quenching to occur. Thus $\Delta\Psi_m$ and perturbations thereof can be monitored. However, Safranin O **66** is not suited for studying mitochondria in intact cells as it will readily stain cell nuclei and can also be used to stain cartilage, mucins and mast cell granules.

An alternative approach to mitochondrial staining is to employ mitochondria-targeted photoproteins such as aequorin or green fluorescent proteins (GFPs). GFPs refer to a number of natural and artificially modified proteins obtained from marine organisms, traditionally from the jellyfish *aequorea victoria*. These have been expressed in a number of transgenic organisms and cell lines with mitochondria-targeted versions expressed in plants.[90] However modification of gene expression is not a robust, versatile tool for studying mitochondria and altering gene expression can lead to many unpredicted modifications to other biological systems.

Chapter 4: Fluorescent ROS and RNS sensors

ROS and RNS are central to pathological oxidative stress, cellular redox signalling pathways and a host of other metabolic functions ranging from stimulating cell growth to defence. As previously discussed (Chapter 1) the exact biological roles of the individual ROS and RNS are poorly understood due to difficulties in measuring their individual concentrations *in vivo*. Thus it is vital to develop techniques that allow the selective and accurate measurement of these dynamic species and to be able to make these measurements with confidence.

In recent years a vast array of small molecule sensors have been developed to detect and quantify ROS and RNS as well as probe many other biological systems including calcium and protein binding.[91] Chemical sensors designed to probe biological ROS or RNS must display high sensitivity and selectivity towards specific ROS/RNS, give a measureable response and ideally in a ratiometric manner (ie. the unreacted and reacted probes can both be detected so that a ratio of these can be determined and quantification of the ROS/RNS is not distorted by the concentration of the probe). All reaction products must be clearly distinguishable from both the starting probe molecules and any by-products/breakdown products. The probes must also be stable to the environments under study, be non-toxic and ideally cell permeable.

The majority of sensors have been developed to detect changes in fluorescence resulting from direct reaction between the probe and ROS/RNS. These are extensively used as they are generally simple, user-friendly assays that can be monitored with a range of fluorescence-based techniques such as confocal microscopy and flow cytometry.

Sensors can be categorised as reversible or irreversible. The output signal of a reversible sensor is directly related to the concentration of the species being detected at any given time and can go down if the concentration of that species drops. Ion sensors are generally reversible and use ligands to bind an ion of interest. The resulting complex has different fluorescent properties from the free sensor that can be detected. An increase or decrease in the ion concentration leads to an increase or decrease in the complex concentration and so leads to a corresponding amplification or drop in the emission signal of the complex. On the other hand, the output signal of irreversible sensors (or detectors) always increases as the sensor is irreversibly converted into another compound by the species being detected.

The concentration of the species being detected affects the rate of this conversion and therefore the rate of the output signal change. As the incubation time of the sensor affects the magnitude of the signal, the sensor outputs are determined as the total change in output after a given period of time. Almost all ROS/RNS sensors are irreversible sensors.

One of the most widely employed sensors to monitor intracellular oxidative stress is dichlorodihydrofluorescein diacetate **67** (DCFH-DA) and its analogues (Scheme 22).[92,93] This cell permeable probe is hydrolysed by intracellular esterases to give DCFH **68** which can be retained by the cell. Two electron oxidation of DCFH **68** gives fluorescent reporter molecule dichlorofluorescein **69** (DCF).

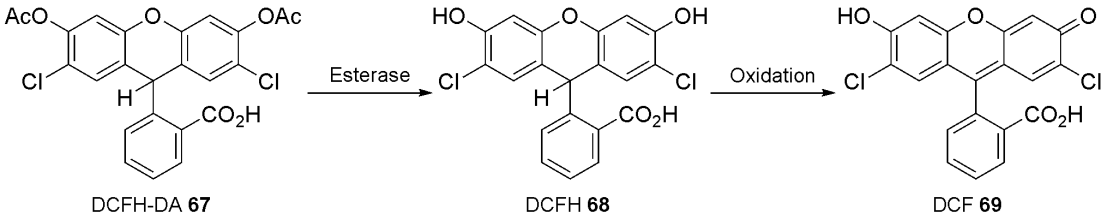

DCFH-DA **67** DCFH **68** DCF **69**

Scheme 22: DCFH-DA **67** hydrolysis and oxidation

Although an extensively used assay, a number of significant limitations exist with DCFH-DA **67** as with many other fluorescence-based assays. Firstly DCFH **68** does not react directly with H_2O_2 (which it is often used to measure), but instead the products of its interactions with peroxidases and hemes (eg. cytochrome c) such as $HO^{\bullet}$ radicals. Furthermore a host of other single-electron oxidising species can oxidise DCFH **68** to DCF **69** such as peroxynitrite, $^{\bullet}NO_2$, HOCl and redox-active metals in the presence of O_2 or H_2O_2.[92,94] The intermediate radical $DCF^{\bullet-}$ also rapidly reacts with O_2 (~10^8 M^{-1} s^{-1}) to give $O_2^{\bullet-}$ which after SOD disproportionation produces H_2O_2, ultimately leading to self-propagating redox cycling and therefore fluorescence signal amplification. In using DCFH-DA **67** a number of reactions are being monitored simultaneously including the rate of acetate hydrolysis by esterase enzymes, which in certain cell lines is insufficient to generate de-acetylated DCFH **68**.[92]

4.1 Hydrogen peroxide detection and boronate caging

One way to overcome the above issues is to detect chemoselective transformations such as the conversion of boronic acids and boronate esters by H_2O_2 under basic conditions to give the corresponding alcohols or phenols (Scheme 23).[95] Initial attack on the vacant *p*-orbital of boron by the hydroperoxide anion is followed by a carbon migration to oxygen displacing a hydroxide anion. This anion then attacks boron atom in an identical manner to the first step and the alkoxy or phenoxy groups (depending on R) are displaced with subsequent protonation from the aqueous environment yielding the desired alcohol or phenol.

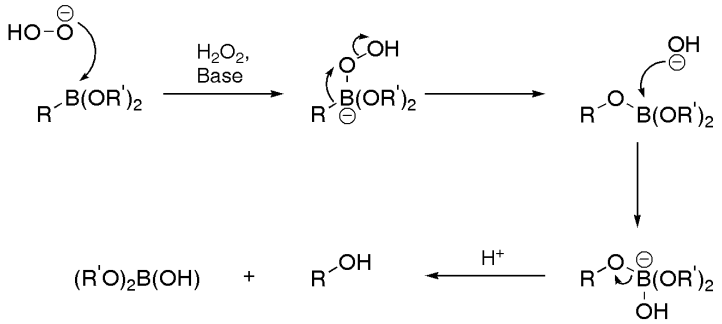

Scheme 23: Reaction of boronic acids/boronate esters with hydrogen peroxide

R = alkyl, aryl or vinyl R' = H, alkyl or aryl

This reaction has been widely employed synthetically in Brown hydroboration-oxidation of alkenes and terminal alkynes to generate anti-Markovnikov alcohols and aldehydes respectively.[96] More recently the mechanism has be used as a trigger in sensors designed to be both sensitive to and selective for H_2O_2 (Scheme 24).[97,98]

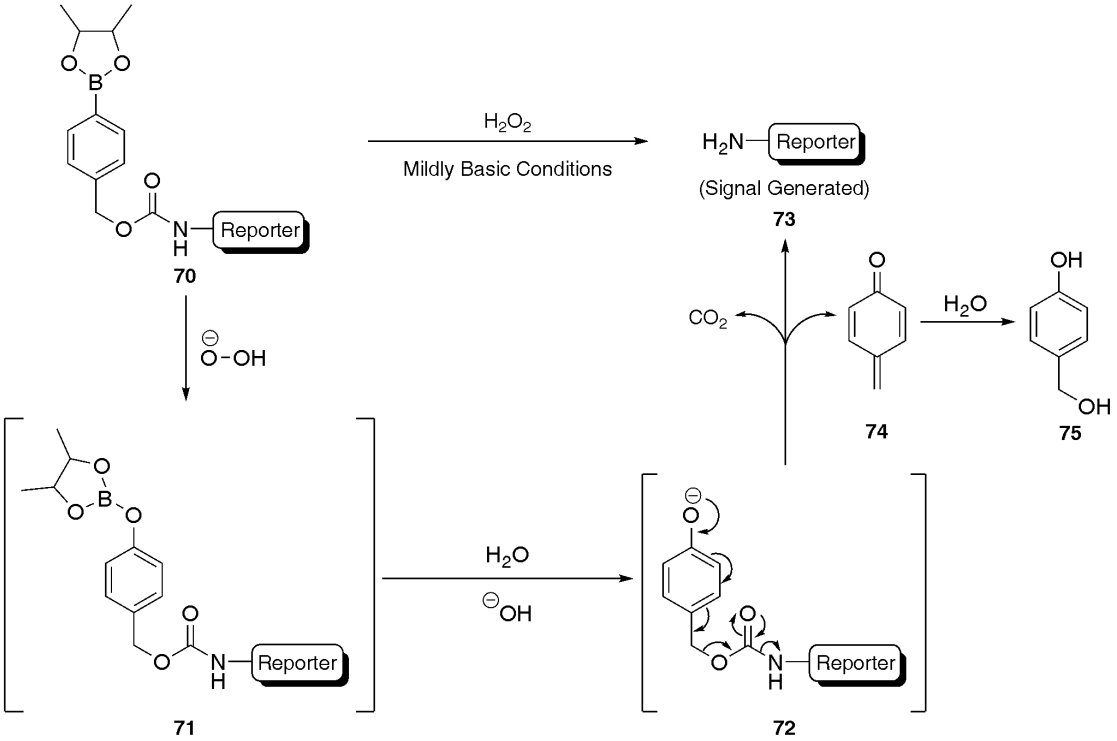

Scheme 24: Arylboronates as H_2O_2-sensitive triggers[97]

Conversion of the electron-withdrawing boronate **70** to an electron-donating phenol/phenoxide **72** allows electron redistribution resulting in fragmentation and release of a reporter molecule such as a fluorophore **73**. Release from the caging linker will modify fluorophore electronics and therefore fluorescence. Thus the presence of H_2O_2 in the system under study acts as a fluorescence "on switch", identifying the presence of this species. The quinone methide by-product **74** will be rapidly trapped by water to form benzylic alcohol **75**.[99]

In 2003, Lu and Chu reported the synthesis of two such boronate-containing H_2O_2 sensors **76** and **77** (Fig.22) that release reporter molecules *p*-nitroaniline or 7-amino-4-methylcoumarin respectively (measured by fluorescence or UV/Vis spectrometry), to be used as diagnostic tools for the presence of H_2O_2.[97] A linear response of reporter molecule release with H_2O_2 addition was observed. Furthermore the potential relevance of this approach towards use in biological systems was demonstrated in the indirect measurement of glucose levels when the substrate was pre-digested with glucose oxidase (E.C. 1.1.3.4) which is known to produce H_2O_2 as a by-product.

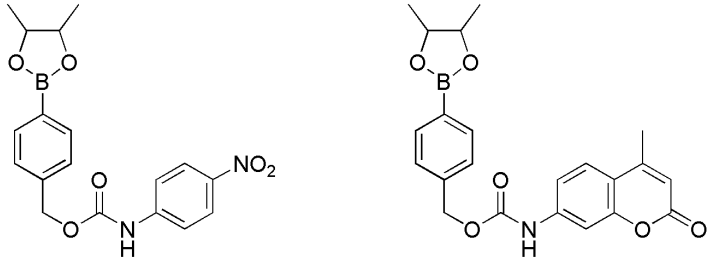

76 **77**

Fig.22: Lo and Chu's H_2O_2 sensitive boronate probes

Chang and co-workers subsequently reported the synthesis of Peroxy Lucifer 1 (PL1) **78** (Fig.23).[100] PL1 reacts with endogenously generated H_2O_2 from macrophages as well as being selective over other ROS tested including superoxide, nitric oxide, hydroxyl radicals and hypochlorite. The probe was cell permeable and ratiometric with a 12-fold increase in the ratio of fluorescence maxima for the released aminonaphthalimide dye after reaction with H_2O_2 over PL1 (F_{540}/F_{475}, λ_{ex} = 410 nm), a blue-fluorescent to green-fluorescent shift. However Lo and Chu's probes, along with PL1 all release cell permeable dyes which results in undesirable background fluorescence due to fluorophore leakage from sites of activation.

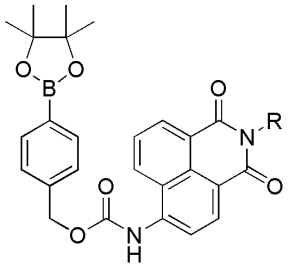

PL1 **78**

Fig.23: PL1 **78** R = $(CH_2)_2O(CH_2)_2OAc$

Thus families of xanthene and phenoxazine based H_2O_2 sensing fluorescent probes have been produced by Chang and co-workers (**79** to **88**, Fig.24, Table 1) with structural modifications used to tune fluorescent properties. The use of a lactone pendant group in fluorescein derivatives (**79** to **85**) is opened after phenol generation forming a caboxylate anion at physiological pHs resulting in the probe becoming trapped inside the cell analogous to DCFH **68**. These probes further differ from the boronate based probes previously discussed as they do not rely upon molecular fragmentation after reaction with H_2O_2. They do however maintain conversion from electron-withdrawing boronates to electron-donating phenols as an "on/off switch" mechanism.[91] Fluorescein analogues have been used in a variety of imaging and labelling studies of biomolecules as they are highly

responsive, generally possess high quantum yields (ϕ) in aqueous environments and are excitable at longer wavelengths (which are convenient for confocal microscopy using Ar/ion lasers and causes less damage to biological components) than many other fluorophores.[101]

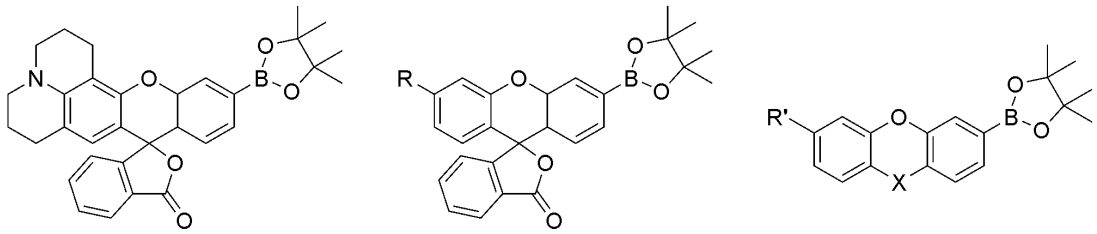

Fig.24 and Table 1: H_2O_2 selective sensors developed by Chang and co-workers

R	R'	X		
B(Pinacol)			PF1	**80**
OMe			PF2	**81**
OH			PF3	**82**
NH_2			PE1	**83**
NEt_2			PY1	**84**
$N(CH_2CH_2)_2N(CH_2)_4PPh_3I$			MitoPY1	**85**
	B(Pinacol)	NH	PR1	**86**
	B(Pinacol)	C(O)	PX1	**87**
	O	N	PC1	**88**

MitoPY1 **79** is a mitochondria-targeted variant which allows mitochondrial H_2O_2 levels to be probed. A further advantage of using arylboronates/arylboronic acids in to study endogenous ROS produced by mitochondria is that the active oxidant is the conjugate base of H_2O_2 (pKa = 11.62 at 25 °C). Consequently the reaction of this trigger mechanism with H_2O_2 is faster in the mitochondrial matrix (pH ~8.0-8.3) compared to the cytosol (pH ~7.2-7.4) resulting in improved selectivity and conversion rates.

A problem with the fluorescent probes discussed above is that fluorescence only occurs after reaction with H_2O_2, while it is often desirable to be able to monitor the probe prior to, as well as after reaction (ie. they are not ratiometric). To this end ratio-peroxyfluor-1 (RPF1 **89**, Scheme 25) was developed by incorporating a fluorescent coumarin marker. RPF1 **89** absorbs and emits predominantly from the coumarin moiety with λ_{abs} and λ_{em} maxima at 420 and 464 nm respectively, consistent with coumarin based emission and

minimal fluorescence resonance energy transfer (FRET) to the closed fluoran acceptor. After reaction with H_2O_2 the major λ_{em} maximum shifted to 517 nm with a minor λ_{em} at 461 nm consistent with the proposed FRET process and emission by the open fluorescein **90**. RPF1 **89** reacts selectively with H_2O_2 over other biologically relevant ROS tested and gave an ~8-fold increase in the ratio of fluorescein-type and coumarin-type emission (F_{517}/F_{464}, λ_{ex} = 420 nm) upon complete conversion of the probe.[102]

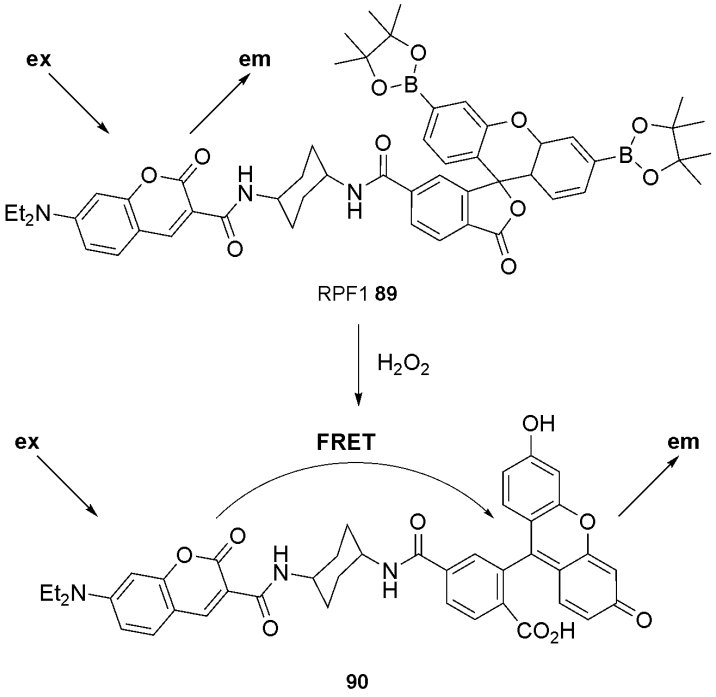

Scheme 25: RPF1 **89** opening allows FRET

RPF1 **89** successfully allowed the detection and ratiometric quantification of H_2O_2 levels in isolated mitochondria from yeast (*Saccharomyces cerevisiae*) inhibited with antimycin A, a complex III inhibitor, to produce endogenous ROS including H_2O_2 after dismutation of $O_2^{\bullet-}$ by SOD.

4.2 Superoxide detection

To date non-fluorescent hydroethidium (HE) **91** and its mitochondria-targeted analogue MitoHE **92** (MitoSOX) are the most widely used probes to detect superoxide ($O_2^{\bullet-}$). In the presence of $O_2^{\bullet-}$, HE **91** and MitoHE **92** are converted into fluorescent products 2-OH-E^+ **101** and 2-OH-MitoE^+ **102** respectively (Scheme 26).[103,104]

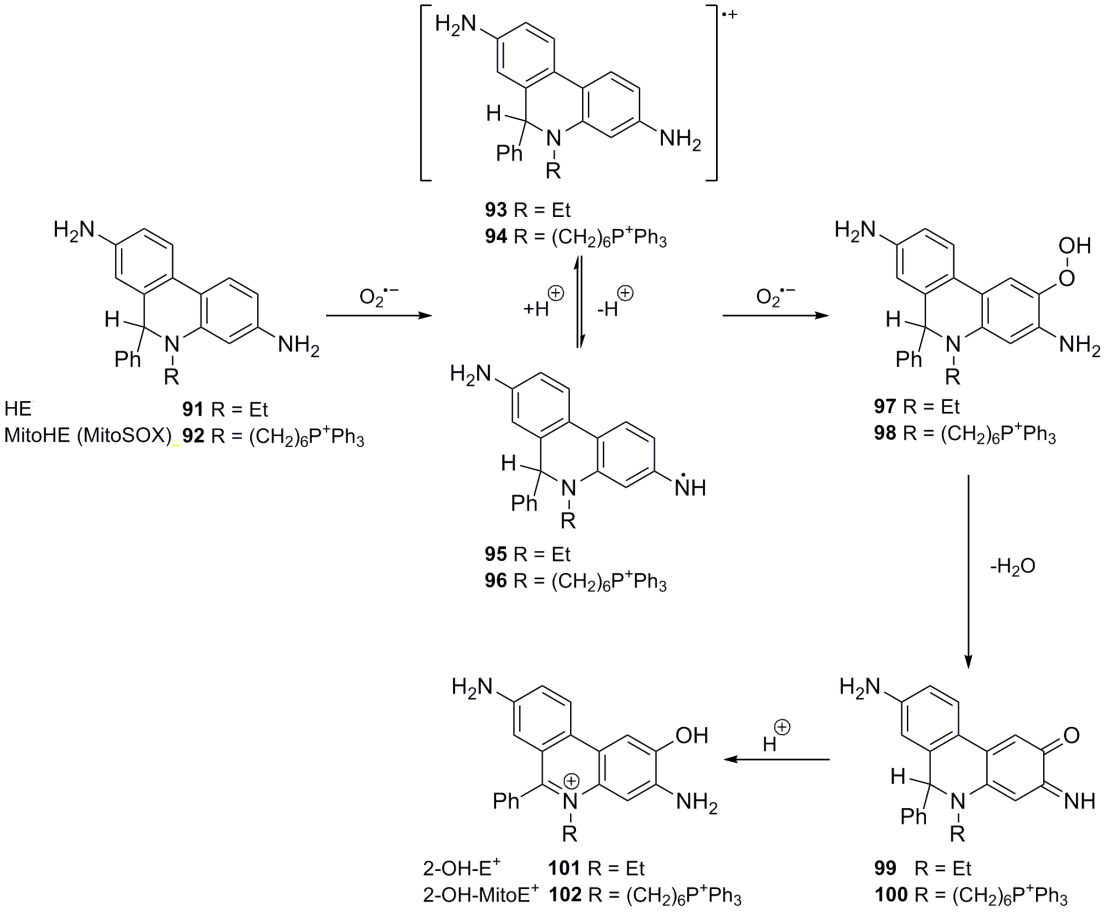

Scheme 26: Proposed reaction of HE **91** or Mito-HE **92** (MitoSOX) with $O_2^{\bullet-}$

A major problem HE **91** and MitoHE **92** is that literature reports indicate that they are susceptible to oxidisation by a variety of biological species other than $O_2^{\bullet-}$ and are oxidised rapidly in air.[103,104,105] For example, non-specific oxidation by $ONOO^-$, $HO^{\bullet}$, heme proteins (cytochrome c, haemoglobin, myoglobin) or manganese porphyrins of HE **91** give E^+ **103** or associated dimers HE-HE **105**, HE-E^+ **107** or E^+-E^+ **109** (Scheme 27). MitoHE **92** undergoes analogous oxidations to give MitoE^+ **104** and dimers MitoHE-MitoHE **106**, MitoHE-MitoE^+ **108** and MitoE^+-MitoE^+ **110**. Furthermore all of these products are known to exhibit very similar fluorescence properties, although the fluorescence of E^+-E^+ **109** (and likely analogue **110**) is significantly lower due to intramolecular quenching. Thus identifying the exact species present and in what ratios in any given mixture by

fluorescence techniques alone is not possible. For a clearer indication of $O_2^{\bullet-}$ presence, HPLC-fluorescence or LC-MS would be required to analyse product distributions.

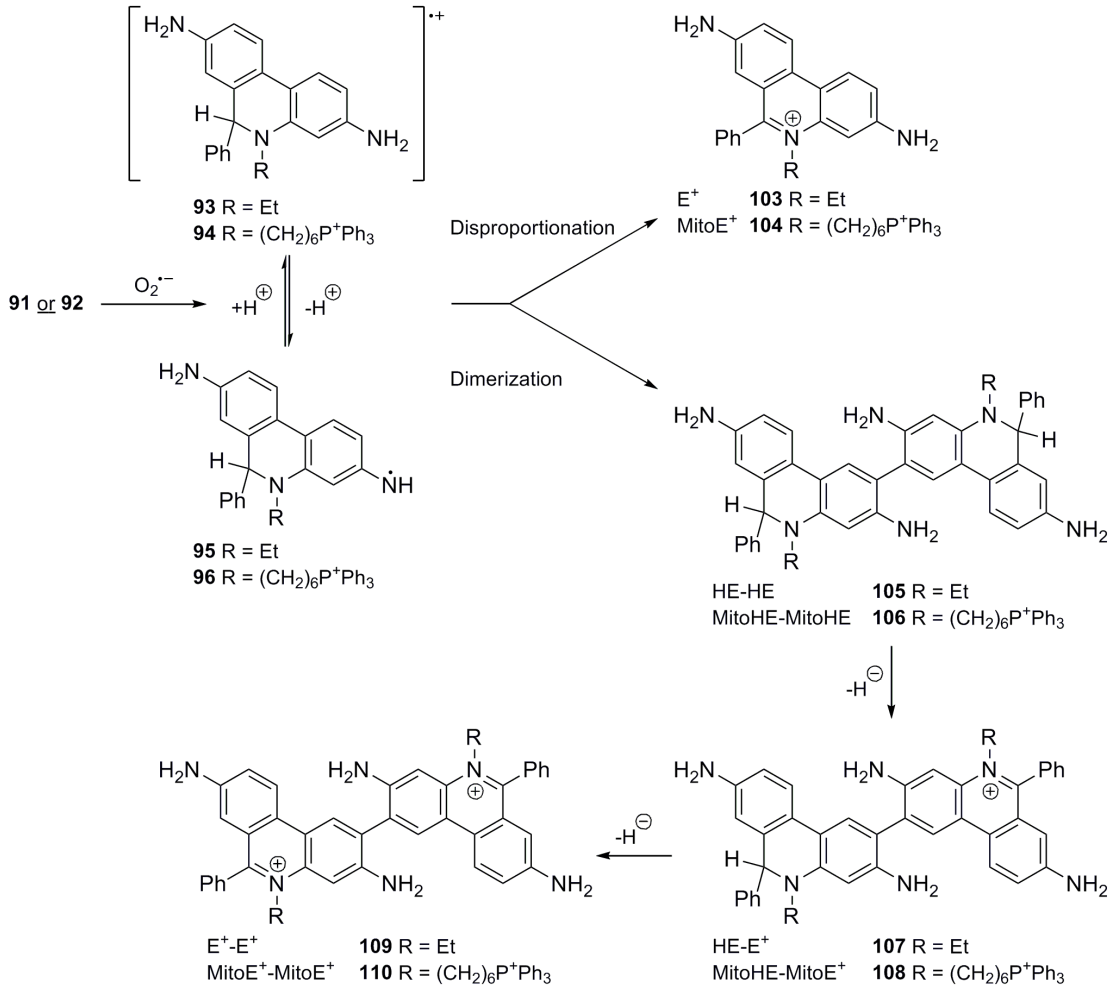

Scheme 27: Non-superoxide specific oxidations of HE **91** and MitoHE **92** (MitoSOX)[103]

The red-fluorescence of the phenanthridinium compounds above are significantly quenched in aqueous environments due to the water molecules in the solvation shell. However upon interchelation to DNA, water molecules are displaced and fluorescence is restored.[106] DNA interchelation raises potential toxicity issues *in vivo* although E^+ **103** has been used as a stain for DNA and RNA *in vitro*.[107] Thus if fluorescence is used as the read out, HE **91** and MitoSOX **92** are inefficient identification or quantitative tools for intracellular $O_2^{\bullet-}$ levels and are instead more suited to assessing the overall redox state of cells. However, to date MitoSOX **92** displays the best selectivity profile for $O_2^{\bullet-}$ and although the above species are indistinguishable from each other *via* fluorescence, using MS techniques should allow each species to be readily identified and quantified.

4.3 Nitric oxide sensors

Molecular probes designed to detect nitric oxide ($^{\bullet}NO$) predominantly use the conversion of 1,2-dianilines **111** into 1,2,3-benzotriazoles **112** by $^{\bullet}NO$ under aerobic conditions.[108] The exact reactive species and mechanism involved has not been confirmed but it is most likely that the reactive species is a nitrosonium (NO^{+}) ion equivalent produced by auto-oxidation of species such as N_2O_3. This can form a diazonium intermediate which closes to give a benzotriazole (Scheme 28). This is a highly selective reaction which gives a single, generally stable product. Although an indirect measurement of $^{\bullet}NO$, the concentrations of any NO^{+} containing species are directly related to the concentrations of precursors molecules $^{\bullet}NO$ as well as O_2 or $O_2^{\bullet-}$.

Scheme 28: Proposed 1,2-diamines react with nitrosonium ions

In recent years Nagano and co-workers have developed families of diaminofluoresceins (DAFs **113-118**, Fig.25, Table 2), diaminorhodamines (DARs, **119-121**, Fig.25, Table 2) as well as BODIPY based systems (Fig.26) to detect $^{\bullet}NO$ as these fluorophores possess high quantum yield (ϕ).[109,110,111,112] In all cases the formation of the electron poor benzotriazole stops photon-electron transfer (PET) and therefore restores fluorescence. This approach behaves as a fluorescence "on/off switch" analogous to the boronate probes designed to detect H_2O_2 developed by Chang and co-workers.[91,102] Several other groups have also used an identical approach to develop $^{\bullet}NO$ fluorescent sensors.[108,113]

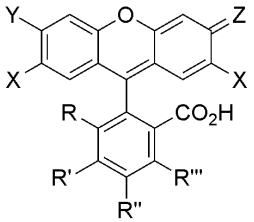

Fig.25 and Table 2: Nitric oxide sensing fluorophores by Nagano

X	Y	Z	R	R’	R’’	R’’’		
H	OH	O	H	H	NH_2	NH_2	DAF-1	**113**
H	OH	O	H	NH_2	NH_2	H	DAF-2	**114**
H	OH	O	NH_2	NH_2	H	H	DAF-3	**115**
Cl	OH	O	H	H	NH_2	NH_2	DAF-4	**116**
Cl	OH	O	H	NH_2	NH_2	H	DAF-5	**117**
Cl	OH	O	NH_2	NH_2	H	H	DAF-6	**118**
H	Et_2N	Et_2N^+	H	H	NH_2	NH_2	DAR-1	**119**
H	Et_2N	Et_2N^+	H	NH_2	NH_2	H	DAR-2	**120**
H	Et_2N	Et_2N^+	H	NH_2	NHMe	H	DAR-M	**121**

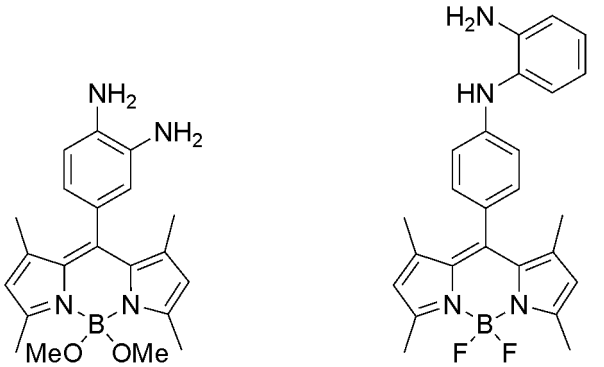

DAMBOO **122** TMAPABODIPY **123**

Fig.26: BODIPY based nitric oxide sensing fluorophores by Nagano

Monosubstitution of the dianiline moiety in DAR-M **121** and TMAPABODIPY **123** will likely improve the selectivity towards $^{\bullet}$NO by preventing 1,2-dicarbonyls found in biological systems (eg. glyoxal) from forming quinoxaline derivatives. In these cases the less favourable, higher energy and likely reversible quinoxalinium derivatives would form.

A number of metal-based fluorescent $^{\bullet}$NO sensors have also been developed which take advantage of the reactions of $^{\bullet}$NO either directly at the metal centre or at ligand sites close to the metal. A number of paramagnetic or heavy metals such as Fe(II), Co(II), Cu(II), Ru(II) and Rh(II) can been used to quench fluorophore fluorescence until reduced and/or

released by reaction with •NO by one of three mechanisms (Scheme 29).[114] Fluorophores ligated to the metal centres can be directly displaced (A) or the metal centre can be reduced with or without fluorophore displacement (B or C) resulting in fluorescence.

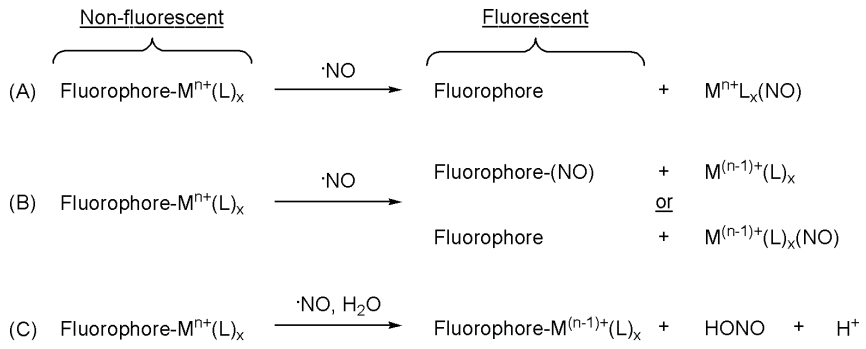

Scheme 29: Metal based nitric oxide probe fluorescence "on/off" mechanisms
L = ligand or metal-metal bond

Although many of these metals are not suitable for biological applications due to toxicity issues, Lippard and co-workers have recently reported the potential for a number of Cu(II) based •NO probes such as CuFL **124** (Scheme 30)[115,116,117,118] as have other groups with probes such as MNIP-Cu **126** (Scheme 31).[119] These probes display excellent selectivity towards •NO over other RNS/ROS and rely on the generation of an *N*-nitrosamine and displacement of a ligated metal ion to moderate fluorophore fluorescence. Incorporating a fluorescein fluorophore, as in CuFL, cell retention can be achieved as previously discussed.

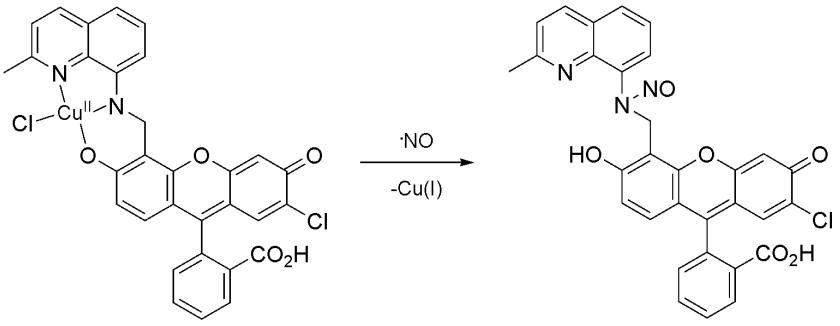

Scheme 30: CuFL **124** reaction with nitric oxide

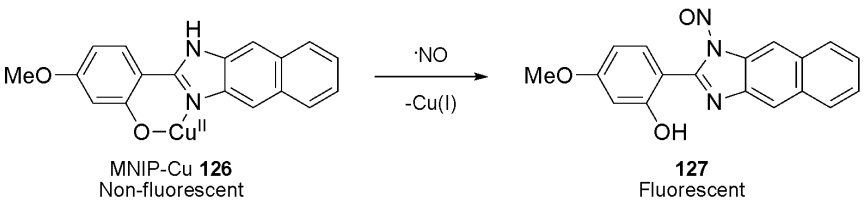

Scheme 31: MNIP **126** reaction with nitric oxide

4.4 Peroxynitrite sensors

Intracellular peroxynitrite ($ONOO^-$) is associated with elevated $^{\bullet}NO$ production and its diffusion to sites of $O_2^{\bullet-}$ formation, where the two react together at close to diffusion rates ($k = 0.4\text{-}1.9 \times 10^{10}\ M^{-1}\ s^{-1}$).[120] The generally low steady state concentrations and high reactivity of this short-lived species make identification and quantification difficult although concentrations are markedly increased under certain circumstances, such as during bacterial infection resulting from elevated $^{\bullet}NO$ production by iNOS. $ONOO^-$ (pKa 6.8) can cause oxidation and nitration and can be converted into other ROS and RNS *via* peroxynitrous acid (ONOOH, ~20% under physiological conditions).[121] This makes obtaining reaction selectivity for $ONOO^-$ over more abundant and longer-lived ROS and RNS which can possess similar reactivity such as H_2O_2, $HO^{\bullet}$ and $^{\bullet}NO_2$ difficult.

A number of groups have used oxidation of dihydrorhodamine-123 **128** (DHR-123, Fig.27) or dichlorodihydrofluorescein (DCDHF) **129** to detect $ONOO^-$ but these molecules suffer from non-peroxynitrite specific oxidation from other ROS and RNS or by light.[121,122] The oxidation of reduced folic acid has also been investigated as a method of detecting $ONOO^-$.[123] Although the photostability is greater and detection limits are lower than for DHR-123 **128** and DCDHF **129**, this approach again suffers from non-peroxynitrite specific oxidations as well as potential metabolism issues.[124]

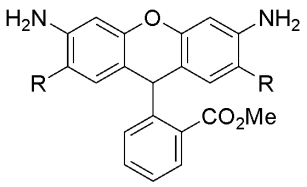

DHR-123 **128** R = H
DCDHF **129** R = Cl

Fig.27: Fluorophores used for $ONOO^-$ detection

To date two notable attempts at developing $ONOO^-$ sensing fluorescent probes have been made. Although both employ a BODIPY fluorophore with modulation of an aromatic pendant acting as an "on/off switch", the approaches look to harness different types of reactivity exhibited by $ONOO^-$.

The group of Nagano have used an analogous approach to their $^{\bullet}NO$ sensors previously discussed to produce dipyrromethenes (NiSPYs) to detect $ONOO^-$.[125] NiSPY-3 **130** relies on nitration of the benzene moiety by peroxynitrite to activate fluorescence (Scheme 32)

by the removal of PET between the aryl and BODIPY moieties. NiSPY-3 **130** showed a linear response towards $ONOO^-$ and high selectivity for this RNS over other ROS and RNS tested (H_2O_2, $HO^•$, superoxide, $^•NO$, singlet oxygen and hypochlorite). The carboxylic acid group is incorporated to improve aqueous solubility and could potentially aid cellular retention, however no studies were reported.

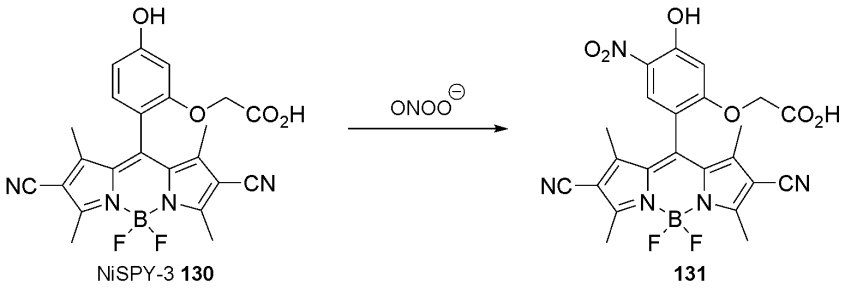

Scheme 32: Nitration of $ONOO^-$ detector NiSPY-3 **130**

Sun *et al* have developed HKGreen-2 **132** to take advantage of the oxidising properties of $ONOO^-$ (Scheme 33).[120] Oxidation of ketone **132** to hemi-acetal **133** gives a large increase in fluorescence through removal of PET. This probe gives a linear response towards $ONOO^-$ and high selectivity for this RNS over other ROS and RNS tested, but showed a lower selectivity (~3 fold) over $HO^•$. *In vitro* studies (murine macrophage cell lines) using lipopolysaccharide, interferon-γ and phorbol myristate acetate to trigger ROS and RNS formation *via* iNOS led to the predicted increase in fluorescence while the use of superoxide scavenger TEMPO led to no fluorescence increase due to the inability to form either $ONOO^-$ or $HO^•$. Reaction of HKGreen-2 **132** with $ONOO^-$ alone was observed in an abiotic system with DMSO suppression of $HO^•$. Unfortunately no reliable routes to *in vitro* suppression of $HO^•$ currently exists without impacting $ONOO^-$ levels. Beyond the potential selectivity issues with endogenous $HO^•$, the probe only fluoresced under artificially high $ONOO^-$ concentration. Therefore monitoring of endogenous $ONOO^-$ levels by HKGreen-2 **132** is likely to be unsuccessful under most circumstances due to insufficient sensitivity.

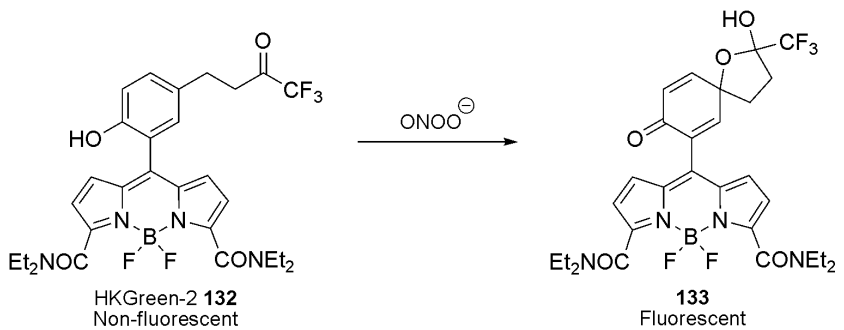

Scheme 33: HKGreen-2 **132** reacts with peroxynitrite to give fluorescent hemi-acetal **133**

4.5 Limitations of existing fluorescence methods

Although improvements to fluorescent ROS and RNS sensors have been made in recent years, a number of underlying problems hinder the usefulness of the field.[105] One major issue regards the selectivity of the probes discussed and the inability to differentiate between the various reaction products as well as metabolism or breakdown products through fluorescence techniques alone. Background fluorescence of the unreacted probes and cell permeability issues reduce measurement sensitivity which is often amplified by slow reactivity of probes with the intended substrates at physiological relevant concentrations.

A number of fluorescent sensors are also not compatible with physiological conditions due to stability or toxicity issues, while those that are suitable are limited to optically accessible environments. These include studies *in vitro*, in outer tissue layers or in transparent organisms such as zebrafish (*Danio rerio*) or nematode worms (*Caenorhabditis elegans*). As a result many desirable areas of *in vivo* study are not accessible and thus it is useful to develop methods that are not optically limited to allow these environments to be probed.

Chapter 5: Research aims

The underlying aim of the following research (Chapters 6-9) is to develop molecular tools to further the understanding of how reactive oxygen species (ROS) and reactive nitrogen species (RNS) are produced and affect biological systems. As the main source of endogenous ROS, this work focuses predominantly on mitochondrially produced ROS/RNS. Accumulation of damage caused by these species may accelerate the ageing process and the onset of age-related disease as defined by the free radical theory of ageing (FRTA).

The results discussed herein are broken into three novel classes of mitochondria-targeted compounds, designed to allow robust testing of the FRTA:

i) Mass spectrometry (MS) probes for identification and quantification of ROS/RNS
ii) Prodrugs to moderate mitochondrial ROS production rates and oxidative stress at a cellular level
iii) Functional molecules to allow for spatially and temporally resolved delivery of biologically active species

Initially these materials will be focused on studying the behaviour and conditions found in mitochondria. However these functional molecules may subsequently be adapted to study a range other cellular or non-cellular compartments through modification of the targeting systems employed.

The first problem in studying mitochondrial ROS/RNS is that it is difficult to accurately identify and quantify these generally short-lived, reactive species that are present in complex biological systems. As a result it is difficult to assess how different chemical, biological or environmental changes affect ROS/RNS production and their subsequent biological roles.

Existing methods of identifying these species *in vitro* predominantly utilise fluorescent techniques, despite a number of limitations (Chapter 4.5). In terms of *in vivo* methods, oxidative stress is studied indirectly (excluding the limited number of systems in which fluorescent techniques are feasible) through oxidative stress markers such as DNA lesions and fatty acid oxidation products. Using markers of oxidative stress can be inaccurate as it

is not possible to study focus solely on a single ROS/RNS of interest and instead must look at the overall oxidative state of the cell. Therefore results of any intervention under study could potentially be affected by changes to a plethora of biological processes such as ROS/RNS production, capture and repair mechanisms as well as a host of other metabolic pathways. Thus a key goal of this research is to develop a small library of probes that will allow for a more accurate identification and quantification of specific ROS/RNS and be broadly applicable *in vitro* and *in vivo* (Chapter 6).

The second goal of this research is to develop a novel class of prodrugs that once administered to an organism will remain inactive until they identify high oxidative stress conditions (Chapters 7-8). These materials will then release biologically active species that will modify the biological processes involved in this elevated ROS production. If the FRTA is correct and the accumulation of ROS/RNS damage is the major cause of ageing, such compounds could extend lifespan and reduce the onset of age-related disease. This class of compounds will initially look at mitochondria-targeted uncoupling molecules, but could easily be adapted to release a wide range of other biologically important species in response to elevated ROS levels.

A further problem that exists in the study of mitochondria is that any compound administered to a system could equally affect any of the mitochondria present. Thus it is impossible to determine if different mitochondrial subpopulations play varying biological roles within a cell and how modifying specific mitochondria may lead to different changes to cellular pathways and behaviour. Therefore the final section of this work will look to develop a new class of photo-activatable compounds to allow temporal and spatial resolution in the delivery of a range of bioactives such as mitochondrial inhibitors (Chapter 9). The intention of this work is to develop a library of such compounds which would allow any molecule of interest to be delivered to mitochondria and selectively released, regardless of its structure so that the effects of localised release can be studied.

Chapter 6: Mitochondria-targeted mass spectrometry probes

I set out to develop a range of mitochondria-targeted ratiometric mass spectrometry probes to allow the identification and quantification of particular mitochondrial ROS/RNS to overcome limitations of fluorescence based probes. Liquid chromatography-tandem mass spectrometry (LC-MS/MS) allows the quantification of ROS/RNS levels present *in vitro* or *in vivo* by analysis of the ion count ratios between the probe and its selective ROS/RNS reaction product, which can be distinguished by differences in mass to charge (*m*/*z*) ratios.

All of the probes retain certain features such as a TPP targeting group to deliver the probes to the mitochondrial matrix. An additional benefit of the TPP moiety is that the inherent positive molecular charge in the starting probe and reaction products facilitates sensitive detection by MS and mild ionisation procedures (electrospray ionisation, ESI) that help to minimise compound fragmentation. Indeed conjugation to TPP groups has been used to augment detection limits in MS[126] and this sensitive technique allows low concentrations (pM) of the compounds to be detected in tissue homogenates. The ratio of compound conversion can be determined through the use of deuterated internal standards to account for any variability in extraction or detection between the probe and its reaction product.

Another major benefit of using a MS based approach is that it allows the study of whole organisms by chemical extraction instead of being limited to studies in cultured cells or tissue surfaces, as is the case for the optical approaches previously discussed (Chapter 4).

6.1 Hydrogen peroxide: MitoB and MitoP

To detect and quantify mitochondrial H_2O_2, the conversion of either an arylboronic acid or arylboronate ester into a phenol, as used in the previously discussed fluorescent H_2O_2 sensors (Chapter 4.1) would be used. To assess levels of mitochondrial H_2O_2, the MS probe MitoBoronic acid (MitoB) **134** and its selective H_2O_2 reaction product, MitoPhenol (MitoP) **136** were designed (Fig.28).[127]

Fig.28: Proposed MS probe and reaction product for mitochondrial H_2O_2

MitoB **134** contains two key moieties. The triphenylphosphonium DLC incorporated targets the probe to mitochondria and is both non-toxic and inert to biological environments while the boronic acid unit is selectively converted by endogenous H_2O_2 into the probes phenolic form (Scheme 34). This conversion leads to a specific change in mass (~28 g mol^{-1}) which allows both species to be identified from a mixture by ESI-MS. Known quantities of deuterated analogues of both MitoB and MitoP (**135** and **137**) would be added prior to extractions as internal standards, so that the unlabelled compounds in the extracts could be readily quantified. Endogenous levels of H_2O_2 could then be calculated from the ratios of the two compounds present.

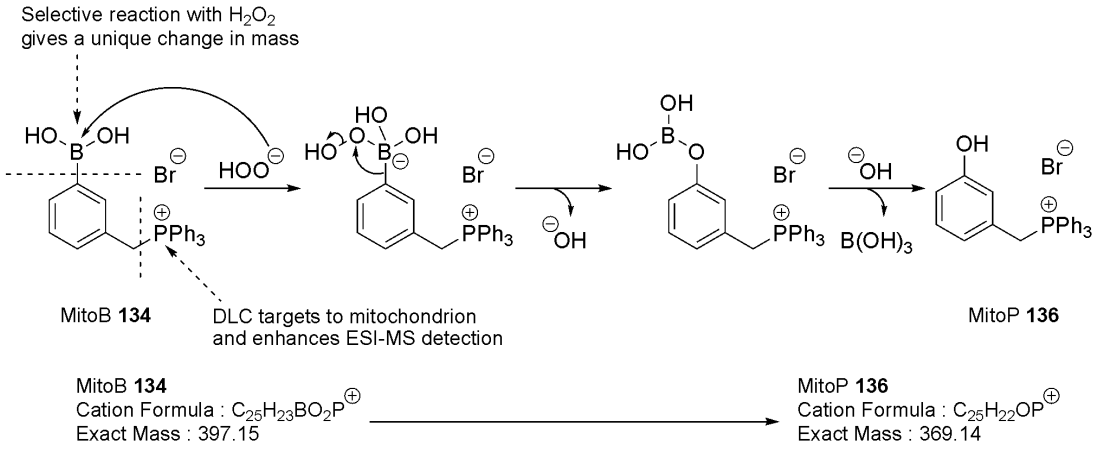

Scheme 34: Proposed structural features and reaction of Mito B **134**

As a result of the probe accumulating in mitochondria, the probe will predominantly be converted by mitochondrial H_2O_2. The probe and its reaction product will distribute throughout an organism and as such will measure the average mitochondrial H_2O_2 levels. Assuming comparable metabolism and excretion rates, the ratio of the two compounds is dependant upon H_2O_2 concentration and incubation time.

6.1.1 Synthesis of MitoB and MitoP

Previous work within the Hartley research group had led to the development of MitoB pinacol ester **141** and MitoP **136** (Scheme **35**) in a moderately yielding three step synthesis with benzylic bromide **140** as the key intermediate for all target compounds.

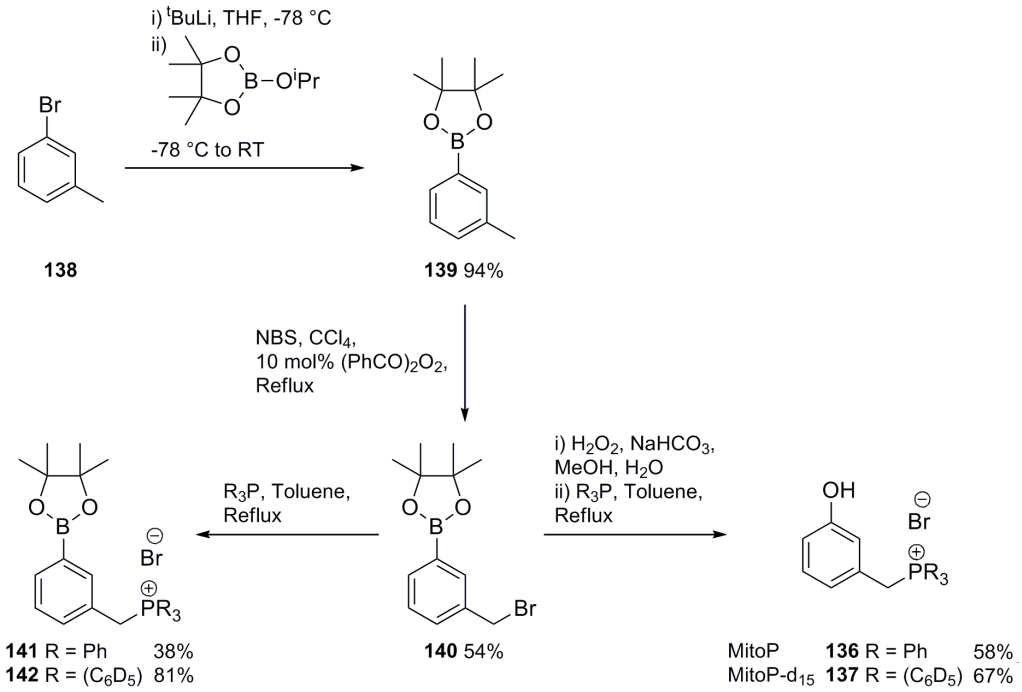

Scheme 35: Previous synthesis of MitoB pinacol ester **141** and MitoP **136**

Although synthetically convenient, an equilibrium between boronate ester **141** and boronic acid **134** is rapidly established in aqueous environments. The position of this equilibrium lies on the side of boronic acid **134**, particularly at the low probe concentrations employed in living cells. Therefore boronic acid **134** was the only detectable species by ESI-MS and as such it was decided to make this compound directly, which simultaneously reduced the length of the synthesis. MitoB **134** solely in the boronic acid form was synthesised in one step from benzylic bromide **143** (Scheme **36**).

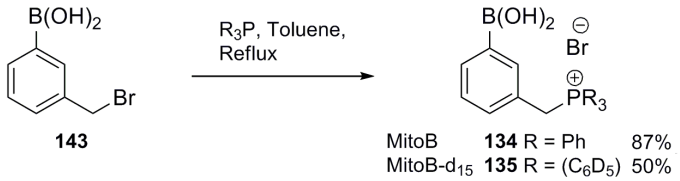

Scheme 36: Synthesis of MitoB **134** and deutero-MitoB **135**

The isolated yield for deutero-MitoB **135** was lower than that of the non-deutero-MitoB **134** for two reasons. Firstly the cost of the deuterated triphenylphosphine prohibits using a large excess of the reagent as can be used in the synthesis of MitoB **134** to drive reaction to completion. Secondly recrystallisation from DMSO/H_2O on a small scale leads to significant material loss which is not as notable on the larger scale reaction of MitoB **134** as recrystallisations can be performed in batches which re-use the same DMSO liquor for every recrystallisation, resulting in less material loss. Recrystallisation from DMSO/H_2O

removed residual traces of toluene and converted small quantities of suspected boroxine trimer **144** (^{1}H NMR) formed in the reaction into the desired monomer **134** (Scheme 37). Subsequent recrystallisation from H_2O removed any residual traces of DMSO.

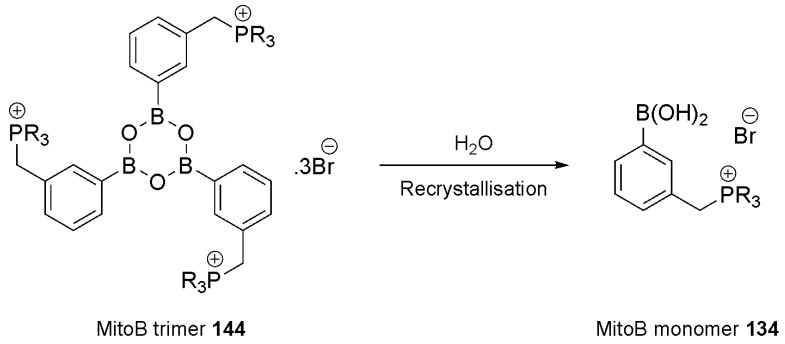

Scheme 37: Traces of MitoB trimer **144** are converted into the desired monomer **134**

R = Ph or C_6D_5

MitoP **136** and its deuterated analogue **137** were initially synthesised in moderate yield from phenol **145** (Scheme **38**) (Chapter 7.7, Scheme 84 for starting material isolation). The instability of the starting material and its tendency to polymerise (from the observed formation of a completely insoluble brown gum) reduced reaction yields.

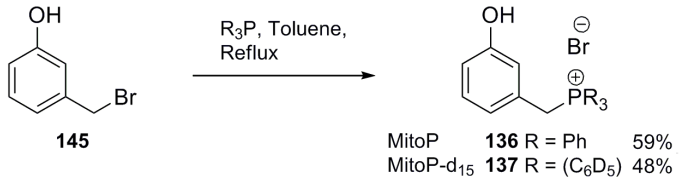

Scheme 38: Synthesis of MitoP **136** and deutero-MitoP **137**

Adapting the procedure of Dawson *et al*,[128] MitoP **136** was also synthesised directly from commercially available diol **146** in moderate yield (Scheme 39). This is a faster, more reliable route towards MitoP **136** and is scalable.

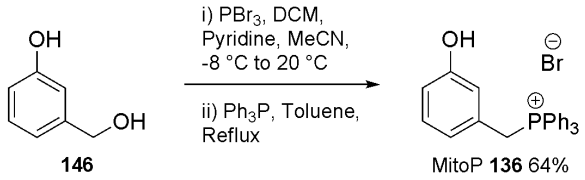

Scheme 39: Alternative MitoP **136** synthesis

As MitoB **134** was recrystallised from water and contains both TPP and boronic acid moieties, it was necessary to assess whether or not the crystalline materials existed as

hydrates. This information is essential to ensure that accurate concentrations of the probes could be used in biological tests. Microanalysis confirmed that neither sets of compounds contained any co-ordinated water molecules and this was further confirmed with the crystal structure of MitoB **134** (Fig.29) obtained by Dr Louis Farrugia (University of Glasgow).

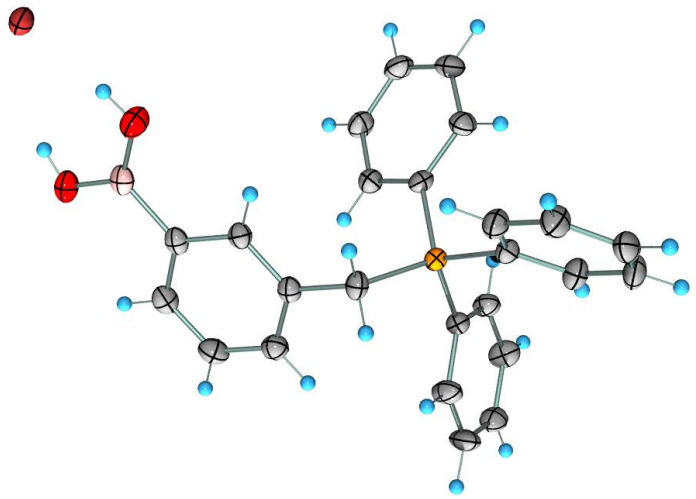

Fig.29: Crystal Structure of MitoB **134**[CCDC 900923]

C = Grey, H = Blue, B = Pink, Br = Red (not covalently bound to structure),

O = Red (covalently bound to structure), P = Yellow

6.1.2 Biological results

In vivo testing in fruit flies was conducted at University College London (UK) and MS analysis, kinetic studies and *in vitro* tests were carried out at the medical research council (MRC) mitochondrial biology unit (Cambridge, UK) by the groups of Partridge and Murphy by lead researcher Dr Helena Cochemé.[127,129] The rates of MitoB **134** to MitoP **136** conversion by H_2O_2 were measured by monitoring the rate of change in absorption at 285 nm. Determined second order rate constants of 9 M^{-1} s^{-1} and 3.8 M^{-1} s^{-1} at 37 °C and 25 °C respectively at pH 8.0 are well below that of the dominant mitochondrial peroxidase (peroxiredoxin III) which has a rate constant of 2×10^7 M^{-1} s^{-1} at physiological temperatures.[130] Therefore MitoB **134** does not affect the overall physiological H_2O_2 levels. This is vital as if MitoB **134** consumed significant amounts of H_2O_2 this would perturb the cellular steady state and affect the signalling processes and other biochemistry, resulting in studies being conducted on systems away from their natural states. Selectivity towards mitochondrial H_2O_2 is achieved due the mitochondria-targeting ability of the

probes and is further enhanced as the reaction with MitoB **134** was found to be ~4-fold slower at cytosolic pH 7.2 compared to mitochondrial matrix pH 8.0, which is consistent with the increased reactivity of the hydroperoxide anion at elevated pH.

MitoB **134** can be given to an organism *via* either oral or IV administration and is rapidly distributed throughout the organism by the circulation. MitoB **134** equilibrates throughout all cellular compartments with predominant accumulation in cell mitochondria (Fig.30) as it contains a DLC and gives information about the average mitochondrial H_2O_2 levels.

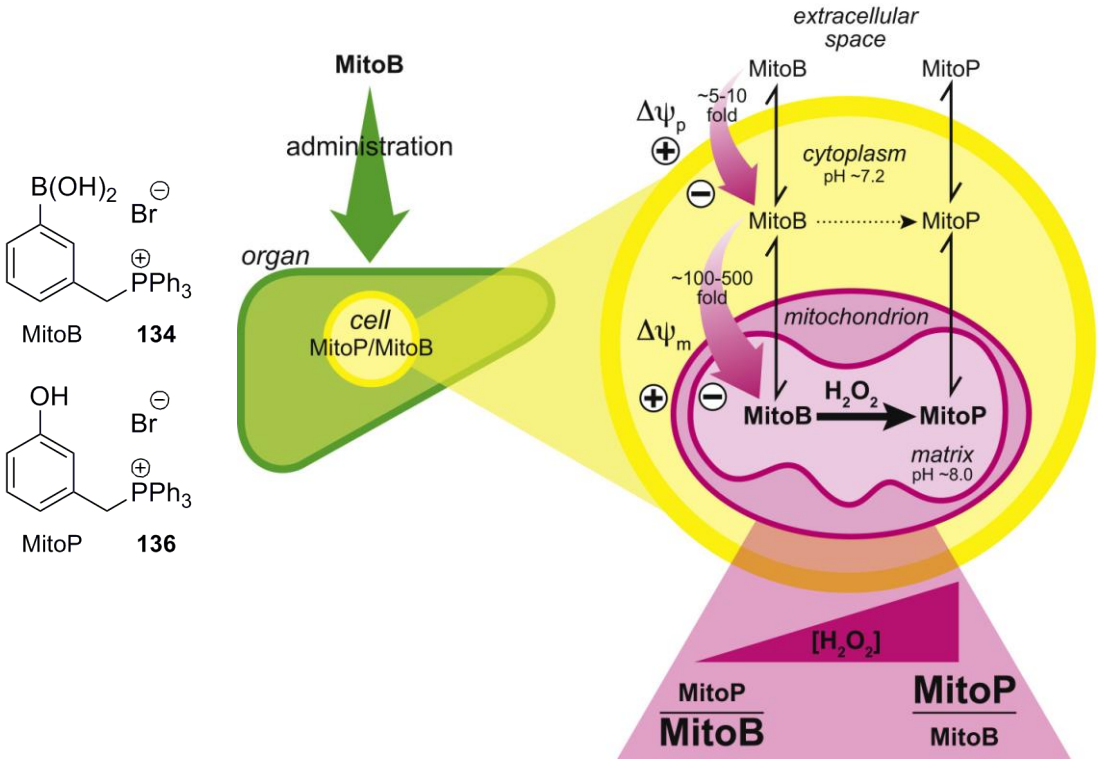

Fig.30: MitoB **134** mode of action and conversion to MitoP **136**

MitoB **134** displayed a high selectivity for reaction with H_2O_2 over *tert*-butylhydroperoxide and cumene hydroperoxide and it was not converted into MitoP **136** by $O_2^{\bullet-}$, $^{\bullet}NO$, linoleic acid peroxide or peroxidase enzymes tested. However, $ONOO^-$ does convert MitoB **134** into MitoP **136**, consistent with rapid rate constants reported for $ONOO^-$ with analogous arylboronates (~1.6 × 10^6 M^{-1} s^{-1}, Scheme 40).[131] Although acutely sensitive to $ONOO^-$, biological concentrations of this species are predicted to be very low compared to H_2O_2 and as such probe conversion will predominantly occur in response to H_2O_2. This was confirmed during *in vitro* studies in which NOS inhibitor *N*-nitro-L-arginine methyl ester was administered along with MitoB **134** and this showed no significant change to MitoP **136**/MitoB **134** ratios under a range of test conditions.[127]

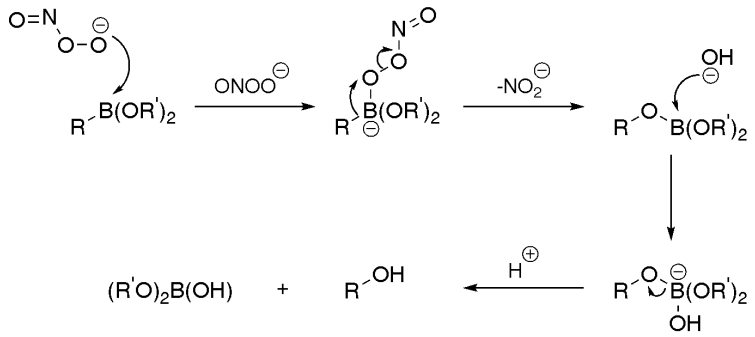

Scheme 40: Boronic acids and boronate esters rapidly react with peroxynitrite

R = alkyl, aryl or vinyl R' = H, alkyl or aryl

Initial tests assessed whether or not MitoB **134** would accumulate in isolated rat liver mitochondria (Fig.**31**) using electrodes sensitive to the TPP cation in a KCl medium (pH 7.2). Aliquots of MitoB **134** (5 × 1 µM) were added to establish a calibration curve and subsequent addition of de-energized mitochondria leads to a small amount of unspecific lipophilic uptake. Upon addition of succinate the electron transport chain has a substrate with which to generate a $\Delta\Psi_m$ through succinate dehydrogenase (complex II). As expected a rapid uptake of MitoB **134** by energised mitochondria was observed and de-energizing the mitochondria (dissipating $\Delta\Psi_m$) with known mitochondrial uncoupler FCCP **33** triggered the release of MitoB **134** back into solution. Similar results are observed for MitoP **136** and the deuterated analogues of both compounds (**135** and **137**). Uptake levels measured in intact Jurkat cells were consistent with uptake of other known TPP conjugates.[132]

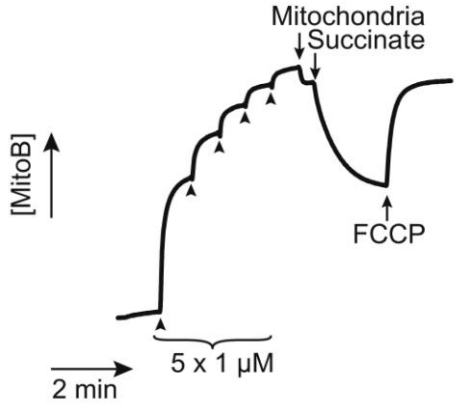

Fig.31: MitoB **134** uptake by energised isolated rat liver mitochondria

In vivo studies discussed herein were conducted in fruit flies (*Drosophila melanogaster*), although similar proof-of-principle studies were successfully conducted in mice and nematode *Caenorhabditis elegans* worms. MitoB **134** was found to accumulate in higher

concentrations in the thorax compared to the head or the abdomen of the fly which is consistent with the knowledge that thoracic muscle cells contain larger numbers of mitochondria. MitoB **134** and MitoP **136** underwent the same first-order elimination kinetics meaning differences in the MitoP **136**/MitoB **134** ratio were due to MitoB **134** oxidation and not differential excretion rates. Furthermore no signs of toxicity were observed for either of the compounds.

Assessing the MitoP **136**/MitoB **134** ratios measured 6 h after injection into female flies and 3 h after injection into male flies of varying ages confirmed that *in vivo* mitochondrial H_2O_2 levels significantly increase with age (Fig.32).

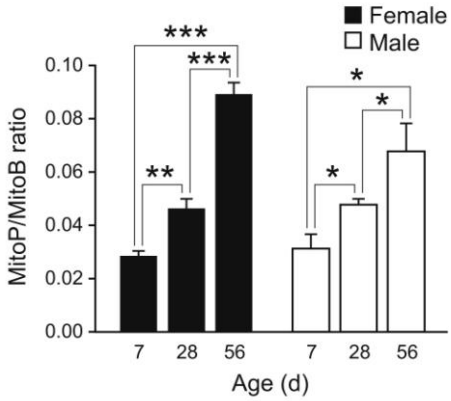

Fig.32: H_2O_2 concentrations increase with age[127]

To determine whether or not the observed increase in average H_2O_2 concentrations play a role in increased mortality, two well-studied and robust interventions that are known to increase the lifespan of *Drosophila* were studied along with their effects on mitochondrial H_2O_2 concentrations. Dietary restriction (DR) is a strongly reproducible effect that increases lifespan in a number of organisms while reducing female fecundity (Fig.33). Cohorts of *Drosophila* were given standard, increased or decreased calorie diets. It was previously widely hypothesised that reducing the calorific intake of an organism extended lifespan by reducing ROS production. Intuitively, it might seem that less food would lead to less metabolism and therefore less ROS. However, the experiments with MitoB **134** showed that although average mitochondrial H_2O_2 levels increase with age, DR in fact has no impact on these levels (Fig.34). Thus the reason for DR extending lifespan must result from an alternative mechanism such as having an impact on an organism's ability to scavenge ROS and/or repair oxidative damage.

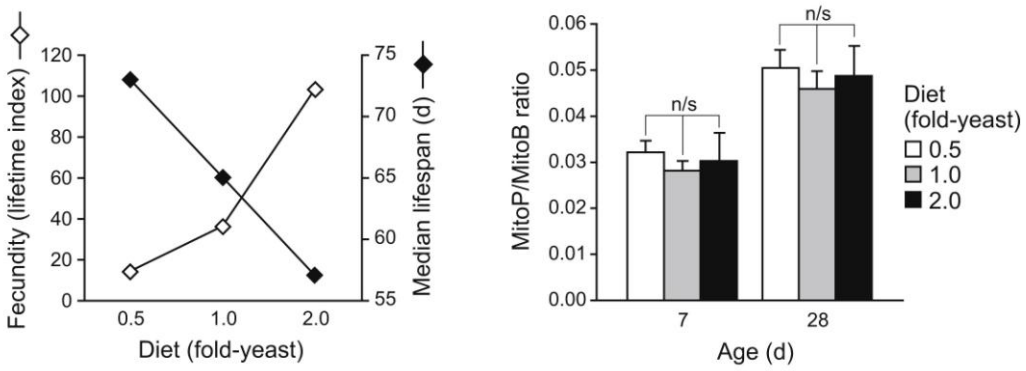

Figs.33 and 34: DR extends lifespan and reduces fecundity but does not impact average mitochondrial H_2O_2 levels[127]

Restricting the physical activity of *Drosophila* is known to extend lifespan by up to a third.[133] This is achieved by restricting the space inside which the flies are kept such that the "inactive" cohorts have no space to fly around and may only walk. In young flies significant differences were found in MitoP **136**/MitoB **134** ratios between active and inactive cohorts while none were found in older flies consistent with a general decline of physical activity with age (Fig.35). The fact that inactive young flies show higher H_2O_2 levels can be explained by these flies not using up their stores of ATP **5**. As a result $\Delta\Psi_m$ is not dissipated by ATPase and a high $\Delta\Psi_m$ is known to cause increased ROS production.[6]

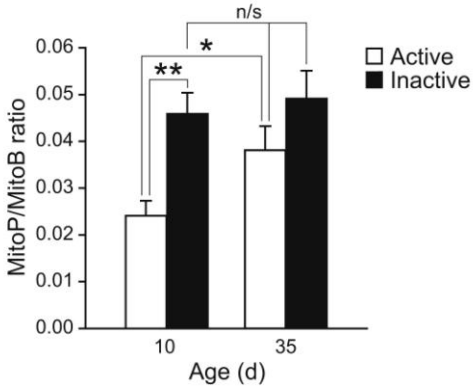

Fig.35: Physical activity impacts mitochondrial H_2O_2 levels[127]

Further studies were conducted in flies to assess the effects on MitoP **136**/MitoB **134** ratios under a number of conditions known to lead to increased ROS production. For example hyperoxia is known to increase H_2O_2 levels as the precursor mitochondrial $O_2^{\bullet-}$ concentrations are directly dependent on the O_2 concentration. As expected, hyperoxia as well as other interventions such as treatment with redox cycler paraquat, increased MitoP **136**/MitoB **134** ratios.

To date MitoB **134** has successfully demonstrated the validity of using a MS approach to measure and quantify the average mitochondrial H_2O_2 levels in cultured cells, flies, worms and mice as well as the ability to monitor changes in H_2O_2 levels in response to a range of interventions or environmental changes. These methods require tissue samples to be taken but preliminary mice studies have revealed that MitoB **134** and MitoP **136** are readily detectable in urine, raising the possibility of non-invasive measurements of *in vivo* ROS levels in mammals.

6.2 Hydrogen peroxide: ExoCellB

The concept of exocellular boronic acid (ExoCellB) **147** is directly analogous to that of MitoB **134** except by existing in an anionic form instead of a cationic form, ExoCellB **147** would be actively excluded from cells (due to $\Delta\Psi_p$) and mitochondria in particular (due to $\Delta\Psi_m$), therefore allowing ratiometric detection of extracellular H_2O_2 levels. In this case negative mode ESI-MS would be used to quantify ExoCellP **149**/ExoCellB **147** ratios (Fig.36).

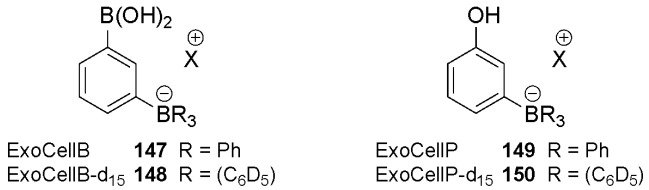

Fig.36: Proposed MS probe and reaction product for extracellular H_2O_2

The *meta*-substituted boronate **152** was synthesised (Scheme 41) using the conditions of Knochel (Chapter 7.8 for further discussion),[134,135] as was the *para*-substituted boronate **155** (Scheme 42) which was used as an intermediate in the synthesis of mitochondria-targeted uncoupling molecules (Chapters 7.8-7.10). Although the yields for the *para*-analogue **155** (88-98% depending on scale) were consistent with those reported by Baron and Knochel,[134] the yields for the *meta*-analogue **152** were consistently lower (32-36%) than in the literature and the reason for this is unclear.

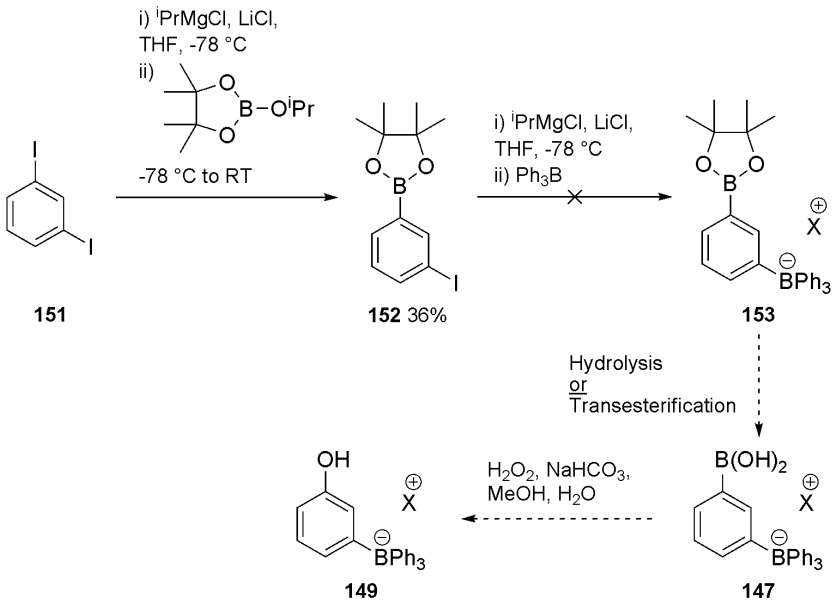

Scheme 41: Proposed synthesis of ExoCellB **147** and ExoCellP **149**

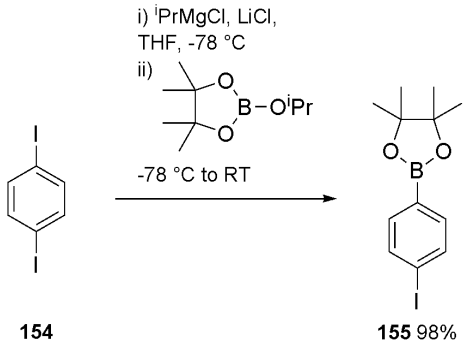

Scheme 42: Synthesis of boronate isomer **155** from 1,4-diiodobenzene **154**

Magnesiation of aryl iodide **152** followed by reaction with triphenylborane failed to yield boronate **153**. This was possibly a result of instability to the mildly acidic work-up conditions. Attempts to synthesise model compound lithium tetraphenylborate from triphenylborate and phenyllithium in THF was similarly unsuccessful and it was subsequently found that commercially available sodium tetraphenylborane rapidly decomposed under acidic conditions through proto-deborylation. Modifying the electronics of the aromatic units to be electron-withdrawing by replacing the phenyl groups with pentafluorophenyl or di-/tri-(trifluoromethyl)phenyl groups could slow, or even prevent this decomposition. Further work on developing an extracellular ratiometric MS probe to quantify H_2O_2 is currently ongoing within the Hartley research group.

6.3 Nitric oxide: MitoDA and MitoBT

To quantify mitochondrial •NO levels, the selective conversion of mitochondria-targeted 1,2-dianiline derivatives **111** under aerobic conditions would be used to give stable 1,2,3-benzotriazole products **112** (Scheme 43), as used in the •NO fluorescent sensors previously discussed (Chapter 4.3, Scheme 28).

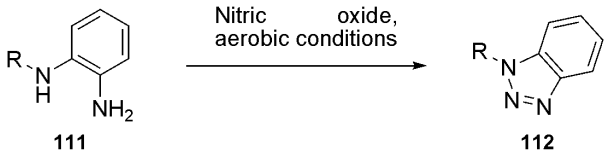

Scheme 43: Conversion of diamines to benzotriazoles

6.3.1 Synthesis of MitoDA and MitoBT

With the knowledge that monoalkylation of a single amine moiety as seen in DAR-M **121** should reduce side reactions with 1,2-dicarbonyls such as glyoxal that could otherwise form quinoxaline derivatives, MitoDiamine (MitoDA **156**) and MitoBenzotriazole (MitoBT **158**) structures were proposed (Fig.37).

Fig.37: Proposed MS probe and reaction product for mitochondrial •NO

The original synthesis of MitoDA **156** and its deuterated analogue **157** began with mono-TPP salt formation from diiodobutane **160** followed by functional group interconversion to give azides **163** and **164** in excellent yields (Scheme 44).

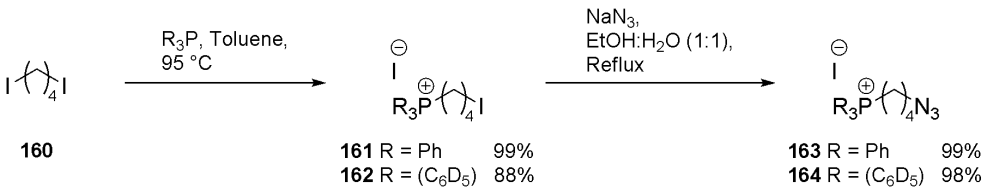

Scheme 44: Synthesis of intermediate azides **163** and **164**

A number of routes to intermediate amine **165** were attempted (Scheme 45). Standard Staudinger reduction conditions were successful at reducing azide **163** but purification from the triphenylphosphine oxide and an unknown TPP containing by-product was unsuccessful. Palladium on carbon reduction conditions using ammonium formate as a hydrogen source gave no conversion to product while using hydrogen gas itself gave good conversion to amine **165** but again led to the formation of an unidentified, inseparable side product [~5-10% by ^{1}H NMR spectroscopy: triplet at 2.71 ppm, J = 6.8 Hz (400 MHz spectrometer) plus a corresponding over-integration of other signals] believed to be some form of compound dimer linked through a central nitrogen-bearing unit.

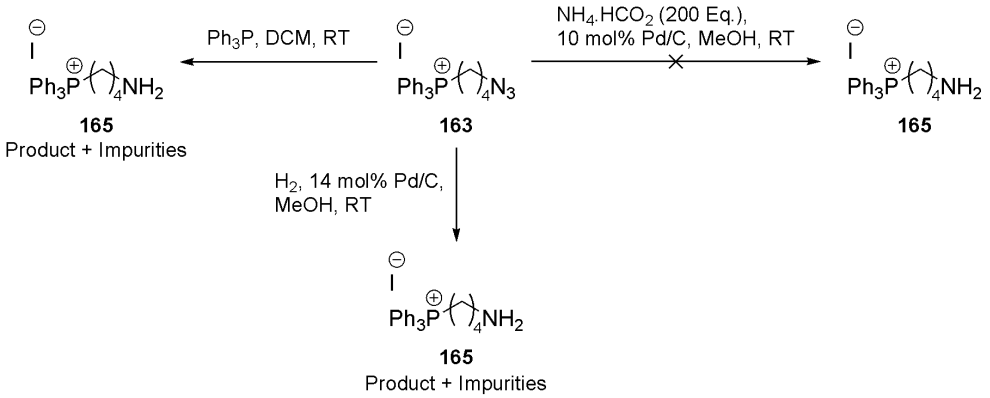

Scheme 45: Attempted synthesis of amine **165**

Attempts to synthesise amine **165** directly from alkyl iodide **160** using ammonia[136] were partially successful although complete conversion was never achieved and prolonged exposure resulted in the formation of small amounts of secondary amine (resulting from amine **165** reacting with alkyl iodide **160**) which could not be readily separated from the desired primary amine **165** (Scheme **46**). Optimisation of this procedure by slowing the addition of alkyl iodide **160** to the ammonia saturated methanol solution in which the concentrations of alkyl iodide **160** and amine **165** are kept low would likely allow this approach to yield the desired product.

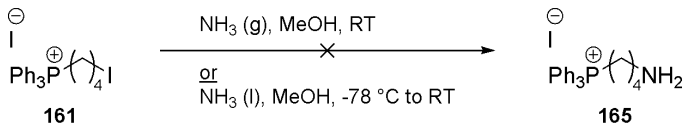

Scheme 46: Attempted synthesis of amine **165**

The first synthesis of MitoDA **156** was completed using amine **165** obtained from hydrogenation (H_2 gas) conditions (Scheme 45). Carrying forward ~5% of an unknown TPP containing impurity through an S_NAr reaction to give aniline derivative **166**, followed by the reduction of the nitro group using sodium dithionite and anion exchange (Appendix 1) to give the desired diamine **156** in moderate yield over the four steps (Scheme 47).

Purification was achieved using column chromatography on silica after the final step. The methylsulfonate anion was chosen as unlike many other common counter ions (eg. halides, triflate, tetrafluoroborate, etc.), it is readily identifiable and quantifiable using ^1H NMR spectroscopy due to the presence of its methyl group.

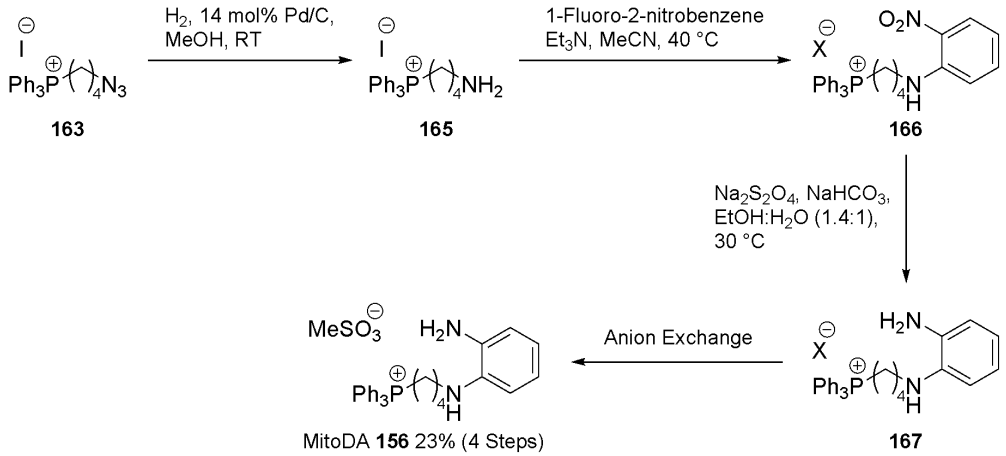

Scheme 47: First synthesis of MitoDA **156**

Initial attempts at reducing the nitro group of aniline derivative **166** using standard iron and tin reagents were unsuccessful (Scheme 48, Table **3**) with no conversion observed under any of the test conditions. Unlike the more common procedures tested, sodium dithionite reduction is rapid (complete in under 45 min), conducted at RT and under mildly basic conditions making it particularly suited to acid-sensitive or thermally-sensitive molecules. Reduction occurs through a series of SET and protonation steps with a number of products possible including nitroso and hydroxylamine compounds due to incomplete reduction if fewer than 3 equivalences of the reagent are used (Scheme 49).

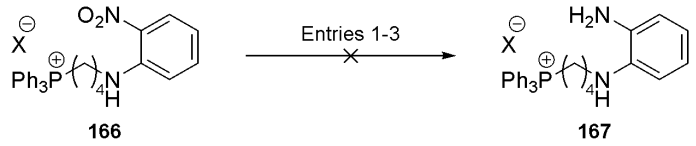

166 167

Scheme 48 and Table 3: Attempted nitro-group reduction conditions

Entry	Conditions	Time (h)	Temp. (°C)	Conversion (%)
1	Fe (4 Eq), NH_4Cl (5 Eq), EtOH	48	Reflux	0
2	Fe (8 Eq), EtOH, AcOH	48	Reflux	0
3	$SnCl_2.2H_2O$ (4 Eq), EtOH	24	Reflux	0

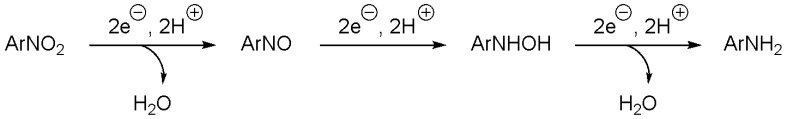

Scheme 49: Sodium dithionite reduction of aryl nitro groups

A modified approach was also employed to synthesise MitoDA **156** and deutero-MitoDA **157** starting from alkyl bromide **168** (Scheme 50). TPP formation, followed by phthalimide removal by hydrazine yielded amines **171** and **172** after which the route follows that of the original synthesis (Scheme 47). This approach prevents the formation of TPP-containing impurities during the synthesis of intermediate amines **171** and **172** which are difficult to separate from the desired TPP compounds.

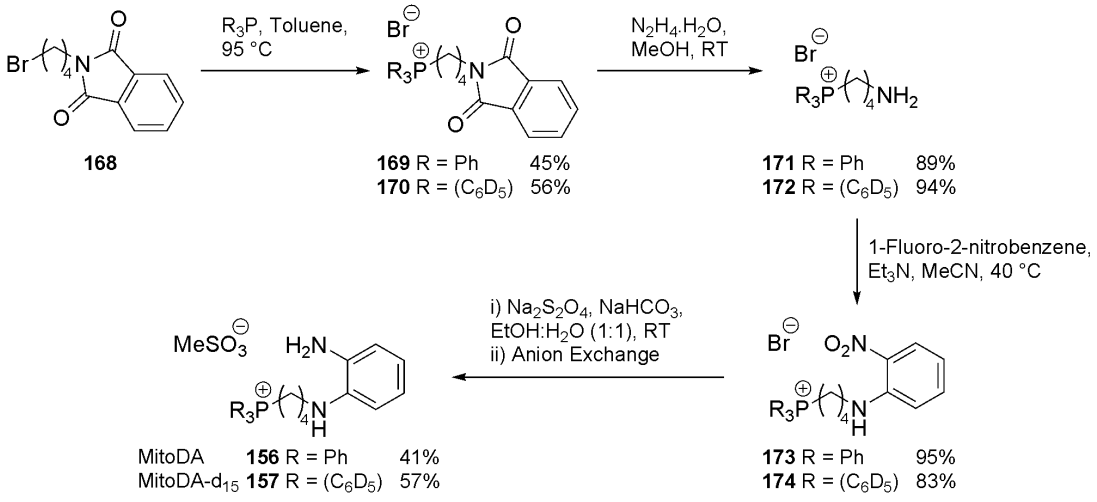

Scheme 50: Alternative synthesis of MitoDA **156** and deutero-MitoDA **157**

A further attempt to synthesise MitoDA **156** designed to prevent the need to carry phosphonium salts through the entire synthesis started with the S_NAr reaction between amine **175** and 2-fluoronitrobenzene (Scheme 51) to give alcohol **177** in high yield. Subsequent Appel reaction gave iodide **177** and cyclised product **178** in an approximate 1:1 ratio after purification by column chromatography on silica despite little cyclisation product being observed in the crude reaction mixture, indicating that cyclisation occurred predominantly during purification. TPP formation could have been carried out on the crude mixture (before or after chromatography) as only alkyl iodide **177** could generate a phosphonium salt product which would be readily separable from the cyclised by-product **178**. However this was not conducted due to the more promising results towards MitoDA **156** previously discussed (Scheme 50).

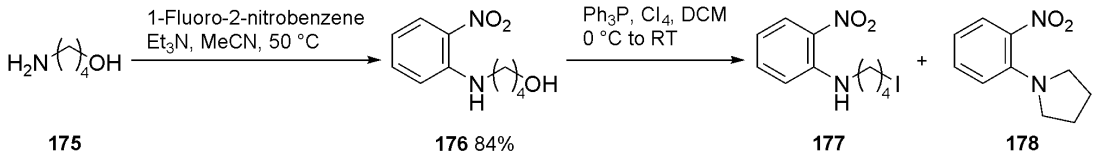

Scheme 51: Alternative attempted synthesis of MitoDA **156**

The first attempted synthesis of MitoBT **158** and deutero-MitoBT **159** began with the alkylation of 1,2,3-benzotriazole **179** using the procedure of Cho *et al.*[137] This was unsuccessful as the sodium salt of the deprotonated benzotriazole is completely insoluble in MeCN (or DCM), although the starting materials were readily recovered. Switching the solvent to DMF allowed the reaction to proceed but despite using an excess of alkyl diiodide **160** a number of by-products were generated (Scheme 52). Reaction products include mainly single alkylation products **180** and **181**, but also not insignificant quantities of double alkylation products **182**-**184** (as well as some other minor products including iodide elimination which generated terminal alkenes) the distribution of which indicates that the reactivity of the three nitrogen atoms are comparable to each other (~2:1 *N*1:*N*2 alkylation components observed in crude ^{1}H NMR). Assessing the composition of crude reaction mixtures was initially difficult as the ^{1}H NMR spectra of each *N*1-alkylation aryl component (**180**, **182** and **183**) are almost identical and the same is the case for each *N*2-alkylation aryl component (**181**, **183** and **184**). To make matters worse, alkyl chain proton signals from both monoalkylated products (**180** and **181**) overlap while all dialkylated products (**182**-**184**) similarly overlap with each other.

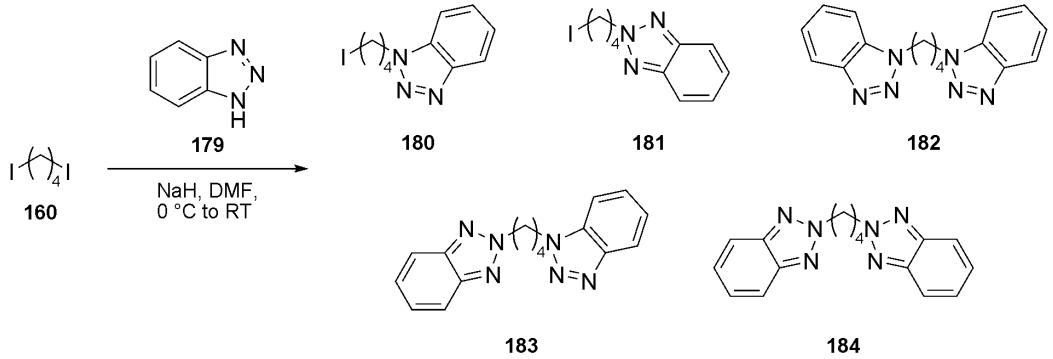

Scheme 52: Selected products of benzotriazole alkylation

Purification can be achieved by column chromatography on silica although significant overlap in product elution is observed. Compounds containing *N*1-alkylation have a stronger retention on silica than the *N*2-alkylated analogues with order of elution: *N*2-alkylated product **181**, *N*1-alkylated product **180**, *N*2-*N*2-double alkylation product **184**, *N*1-*N*2-double alkylation product **183** and *N*1-*N*1-double alkylation product **182** in petroleum ether:EtOAc (1:1). This is likely to be due to the greater dipole moment in the unsymmetrical triazole generated by *N*1-alkylation **180** compared to the symmetrical triazole generated by *N*2-alkylation **181** and where the free nitrogen lone pairs are less likely to interact with silica simultaneously.

An alternative route to alkyl iodide **180** was also assessed (Scheme 53, Table 4). The first attempt to alkylate 1,2,3-benzotriazole **179** using sodium carbonate as a base in MeCN was promising in that using only a slight excess (1.2 eq.) of diiodobutane **160** gave only monoalkylated products **180** and **181** as well as trace amounts of bis-alkylation product **185** along with unreacted starting materials (Entry 1). Increasing the equivalence of the alkylating reagent and the reaction temperature (50 °C to reflux), led to a greater number of unidentified impurities forming including alkenes generated through iodide elimination, with the majority of identifiable material in the bis-alkylated form **185** (Entry 2). Reducing the reaction temperature back to 50 °C and extending the reaction time gave improved isolated yields of the desired compound. The predicted 2:1 ratio of the *N*1-alkylation **180**:*N*2-alkylation **179** was reduced as the *N*1-alkylation product **179** is free to undergo a second alkylation to give the *N*1-*N*3-alkylation product **185**. Other minor unidentified reaction products and unreacted benzotriazole **179** were observable in the ^{1}H NMR spectrum of the crude reaction mixture (Entry 3).

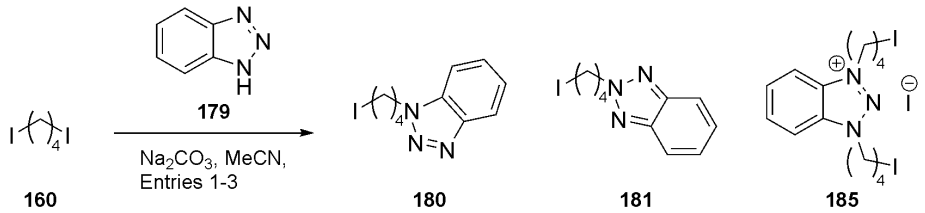

Scheme 53 and Table 4: Optimisation of 1,2,3-benzotriazole alkylation

Entry	Reaction Conditions			Conversion/Yield (%)		
	Temp. (°C)	Time (h)	Diiodobutane **160**	*N*1 **180**	*N*2 **181**	*N*1 and *N*3 **185**
1	50	18	1.2 eq.	26	13	Trace
2*	Reflux	20	4 eq.	Minor	Minor	Major
3	50	48	4 eq.	47	32	12

* Reaction not purified due multiple unidentified reaction products

Alkyl iodide **180** was readily converted into MitoBT **158** and deutero-MitoBT **159** in excellent yields using triphenylphosphine and its deuterated analogue respectively (Scheme 54). Prolonged reaction times at relatively low temperatures compared to standard TPP formation conditions were employed to prevent any unwanted iodide elimination or other side-products.

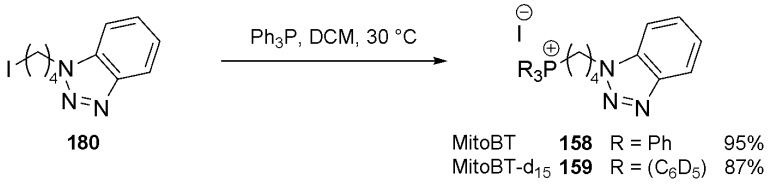

Scheme 54: Synthesis of MitoBT **158** and deutero-MitoBT **159**

MitoBT **158** may also be synthesised from the reaction of azide **163** using a benzyne generating reagent (Scheme 55). Due to its high reactivity, benzyne must be produced *in situ* and can be generated from a number of benzyne precursors including under mild conditions from TMS-triflate **186**.[138]

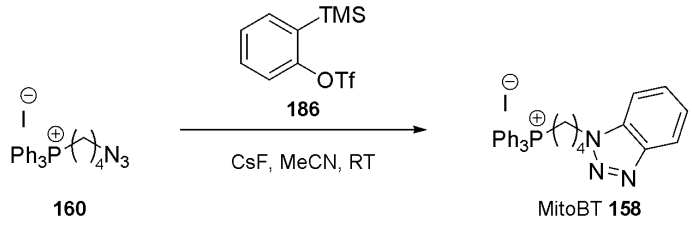

Scheme 55: MitoBT **158** synthesis using benzyne chemistry

Activation of the silyl group by fluoride leads to displacement of the *ortho*-triflate leaving group to generate highly reactive benzyne **187**, which undergoes a click-type reaction analogous to azide-alkyne Huisgen cycloaddition to generate benzotriazoles (Scheme 56). A key factor in benzyne chemistry is to ensure that concentrations of the benzyne species is kept low as dimers **188** and trimers **189** will rapidly form if concentrations are too high. Although no product was isolated *via* this route, conversion to benzotriazole **158** is clean (as determined by ^{1}H NMR spectroscopy) with benzyne derived impurities (eg. **188** and **189**) readily washed out with diethyl ether.

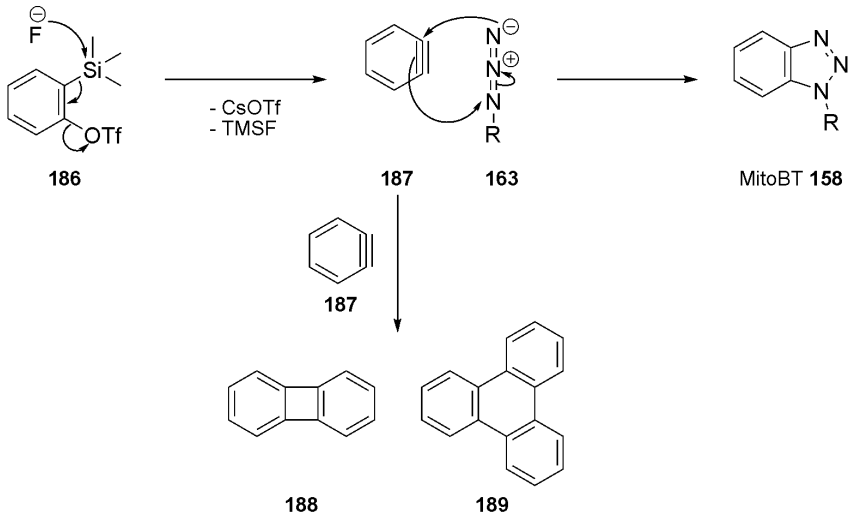

Scheme 56: Benzyne formation and pericyclic reactions R = $I^{-}Ph_3P^{+}(CH_2)_4$

Although the benzyne precursor **186** was added slowly in two batches, the presence of a full equivalence of a fluoride source (cesium fluoride) in the reaction mixture may have led to benzyne formation occurring too quickly. It is strongly believed that with slower addition of fluoride and benzyne precursor, with elevated equivalences of the latter, MitoBT **158** could be accessible using this approach. No attempts at optimising this route were made as by this point MitoBT **158** and its deuterated analogue had been successfully synthesised by the previously discussed route (Schemes 53-54).

Alternative methods of benzyne **187** formation involve harsher conditions such as the decomposition of anthranilic acid **190** derived diazonium salt **191** (Scheme 57).[138] This approach liberates large quantities of carbon dioxide and nitrogen and therefore is potentially explosive. Lithium-halogen exchange of an aryl *ortho*-dihalides or aryl *ortho*-halide-triflate **193** or *ortho*-lithiation of an aryl fluoride **192**, followed by release of the *ortho*-substituent can also be used to generate benzyne, but the necessary lithiation reagents are not compatible with TPP-azides **163** or **164** (Scheme 57).[138]

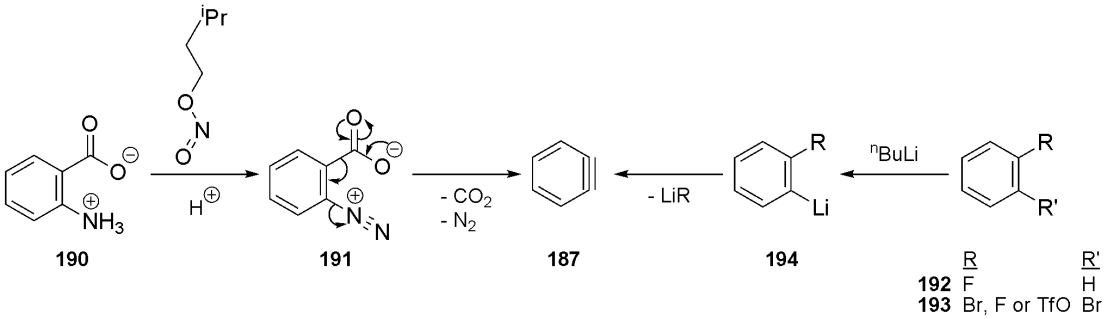

Scheme 57: Alternative methods of benzyne formation

To assess if MitoDA **156** could be converted into MitoBT **158** by the proposed reaction mechanism (Schemes 28 and 43), •NO was released *in situ* by the thermal decomposition of NONOate sodium salt **194** under *pseudo*-physiological [KHE buffer (Appendix **2**), pH 7.4, 37 °C] aerobic conditions (Scheme 58). The crude mixture was subsequently analysed by positive mode ESI-MS with the only observed cations corresponding to MitoDA **156** and MitoBT **158**. Therefore this strongly supports the concept of MitoDA **156** as a potential biological •NO quantification tool by its clean conversion into MitoBT **158**. Biological testing is currently underway at the MRC mitochondrial biology unit (Cambridge, UK) by the group of Murphy.

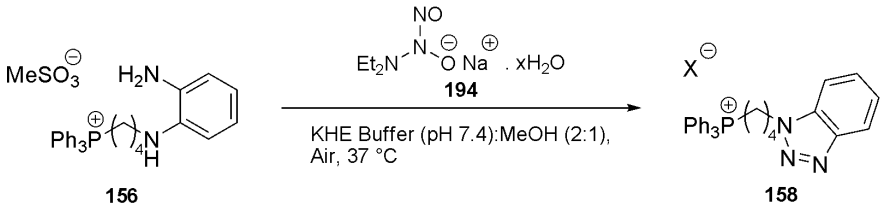

Scheme 58: Conversion of MitoDA **156** into MitoBT **158**

6.4 Superoxide: MitoSOX

The aim of this project was to develop a ratiometric mitochondria-targeted $O_2^{\bullet-}$ probe to allow the accurate determination of endogenous $O_2^{\bullet-}$ levels inside mitochondria. The proposed probe design was based on mitochondria-targeted superoxide fluorescent sensor MitoSOX **92** (Chapter 4.2) as to date this molecule displays the best reaction selectivity for $O_2^{\bullet-}$ over other ROS/RNS. Initial synthetic targets included MitoSOX$^+$ **104**, deutero-MitoSOX$^+$ **195** along with their respective $O_2^{\bullet-}$ reaction products 2-OH-MitoSOX **102** and deuterated analogue **197** (Scheme 59). The phenanthridinium probes **104** and **195** will be reduced using sodium borohydride immediately prior to use so that they are responsive to

$O_2^{\bullet-}$ (or may be reduced in advance if stored under anaerobic conditions) as the tertiary amines **92** and **196** will rapidly re-oxidise in air to phenanthridiniums **104** and **195**.

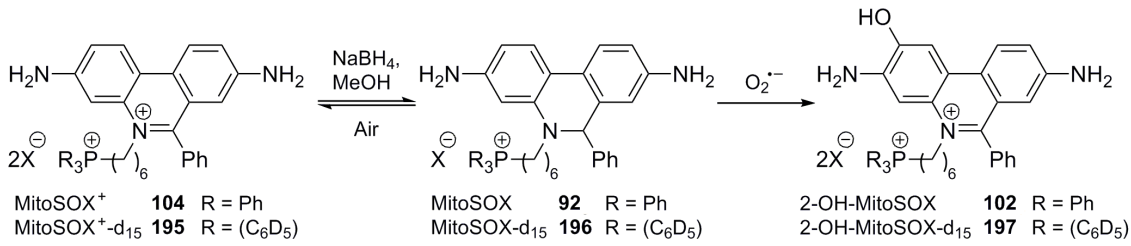

Scheme 59: Proposed MS probe and reaction product for mitochondrial $O_2^{\bullet-}$

Although MitoSOX **92** is commercially available, no complete synthesis has been reported in the literature. To enable the subsequent selective alkylation of the phenanthridine core nitrogen atom, both amine moieties of diaminophenanthridine **198** were Boc protected. This was initially achieved in a low yield similar to that obtained by Ross *et al*,[139] using a comparable method and purification by column chromatography on silica (Scheme 60, Table 5, Entry 1). Conversion in this reaction was very high, although a significant amount of material was lost during purification. Changing the procedure to enable product precipitation from a THF:H_2O co-solvent system gave a significantly improved yield (Entry 2).

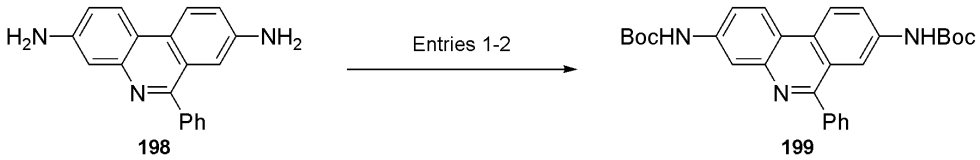

Scheme 60 and Table 5: Bis-amine protection conditions to give dicarbamate **199**

Entry	Conditions	Temp. (°C)	Time (h)	Isolated Yield (%)
1	Boc_2O, $CHCl_3$	RT	66	20
2	Boc_2O, THF:H_2O (10:1), K_2CO_3	RT	96	85

Alkylation of phenanthridines using alkyl halides has previously been reported by a number of groups but none of the alkylation conditions tested gave any signs of alkylation product (Scheme 61, Table 6).[140,141] It is possible that reversible alkylation was occurring, with the liberated iodide quickly displacing the phenanthridine to regenerate starting materials. $AgNO_3$ was used as an additive to trap any iodide generated as AgI which would precipitate out of solution and drive the reaction to completion, but again no signs of alkylation were observed.

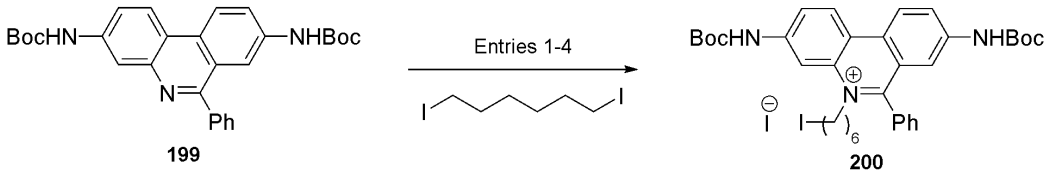

Scheme 60 and Table 6: Attempted alkylation to give alkyl iodide **200**

Entry	Solvent	$AgNO_3$	Temp. (°C)	Time (d)	Yield (%)
1	THF	N/A	Reflux	10	0
2	THF	1 eq.	Reflux	7	0
3	$PhNO_2$	N/A	RT	5	0
4	$PhNO_2$	1 eq.	Reflux	3	0

Triflates have also been employed to alkylate phenanthridines[139,142] and to date have been employed within the Hartley research group with limited success due to purification issues. Ongoing work on this project is focussed on synthesising the complete phenanthridinium core, pre-alkylated from mono-aryl precursor fragments which will allow a family of related mitochondria-targeted species to be developed.

Chapter 7: Mitochondrial uncoupling

7.1 Mitochondrial uncoupling molecules

In mitochondrial biology, uncoupling refers to the process of detaching the workings of the respiratory chain from the oxidative phosphorylation of ATPase, principally as a result of dissipating $\Delta\Psi_m$. The electron transport chain responds to uncoupling by upregulating protein turnover (complexes I to IV) in an attempt to maintain the protomotive force while ATP **5** synthesis is slowed. In strongly uncoupling conditions ATPase can reverse, with the energy released from the conversion of ATP **5** back into ADP **4** being used to pump protons into the IMS to maintain $\Delta\Psi_m$.

An increase in $\Delta\Psi_m$ leads to an increase in ROS production[6] and mild mitochondrial uncoupling can reduce the markers of oxidative stress through the lowering of this potential gradient[143,144] as this reduces ROS production, allowing the organism's natural defences such as anti-oxidants to regain control of the system. To date five transmembrane uncoupling proteins (UCPs) have been identified. These have evolved to protect an organism from excessive ROS production in times of elevated $\Delta\Psi_m$. Dissipation of $\Delta\Psi_m$ through uncoupling processes leads to thermogenesis which is used by a number of animals to maintain body temperature during hibernation.

Small molecule mitochondrial uncouplers[145,146] predominantly act as proton translocators (protonophores) that catalytically cycle protons from the IMS into the mitochondrial matrix (Figs.38 and 39), although a few can uncouple through interactions with certain transmembrane protein pores. As the $\Delta\Psi_m$ is reduced, there is no way to power ATPase and so the mitochondria stop producing ATP **5** as well as lowering ROS production. Uncoupling molecules must be lipophilic enough to diffuse passively through lipid bilayers in both the neutral and anionic forms as well as possess a suitable pKa so as to be sufficiently protonated in the IMS and deprotonated in the mitochondrial matrix. The most commonly used uncoupling molecules are 2,4-dinitrophenol (DNP) **201** and carbonyl cyanide-*p*-trifluoromethoxyphenylhydrazone (FCCP) **33** with pKa values of 4.1[147] and 5.8[148] respectively. Both possess suitable lipophilicity, pKa, and stability for biological testing and also possess characteristic UV/VIS spectra making them extremely simple to identify in solution.

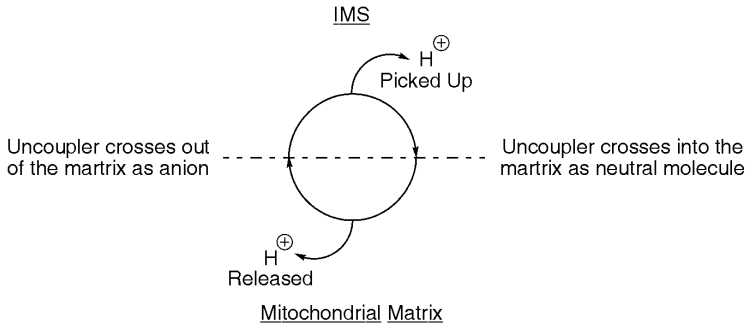

Fig.38: Mitochondrial uncoupling mechanism *via* proton translocation

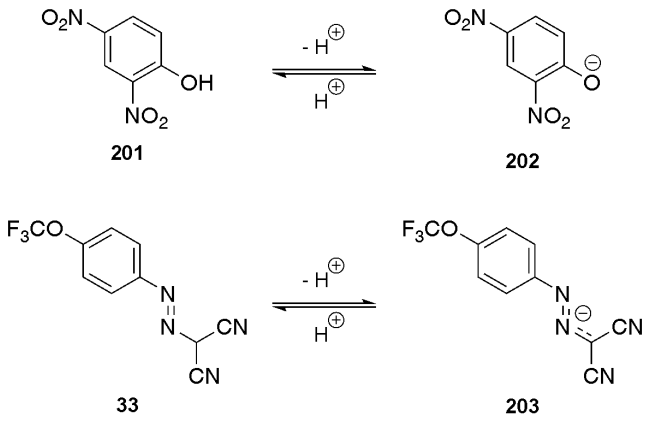

Fig.39: DNP **201** and FCCP **33** with corresponding DNP$^-$ **202** and FCCP$^-$ **203**

DNP **201** was successfully used in the 1930's to treat obesity as it uncouples mitochondrial ATP **5** production from the energy obtained from oxidation of fuel sources such as fatty acids and sugars. Mitochondria respond to the reduced efficiency of ATP **5** production by increasing the rate at which they metabolise fatty acids stored in adipose tissue in order to maintain a sufficient energy supply for the organism. However, as calories are dissipated as heat the differences in therapeutic and toxic doses proved insufficient for DNP **201** (and many other uncoupling molecules) to continue to be used in the treatment of obesity with extreme cases of mitochondrial uncoupling leading to hyperthermia, cell necrosis and death.[149] The second issue with excessive uncoupling is that at a $\Delta\Psi_m$ of below ~120 mV, ATP **5** synthesis stops and reversal of ATPase attenuates any further drop in $\Delta\Psi_m$. This diminishes ATP **5** stores by conversion into ADP **4**, which can result in insufficient energy stores to maintain cellular functions (eg. heart muscle contraction). Thus, uncoupling molecules delivered unselectively have severe limitations.

Many molecules have been examined for their abilities to uncouple mitochondria and have been found to uncouple to different extents (Fig.40).[145,146,149] Such molecules can act as mitochondrial uncouplers behaving as proton translocators as previously discussed, or by

interacting with mitochondrial membrane proteins such as adenosine nucleotide translocase (ANT) (ie. benzoic acid **204**), or a combination of both [ie. butylated hydroxytoluene (BHT) **205**]. ANT is a common MIM protein that facilitates the import of ADP **4** and the export of ATP **5** during oxidative phosphorylation. Interactions with ANT have been seen to increase the uncoupling ability of several uncoupling molecules including DNP **201**. The mode of action for certain molecules which possess some (albeit low) degree of uncoupling ability such as fatty acids is not fully understood,[150] and research in the field is ongoing.

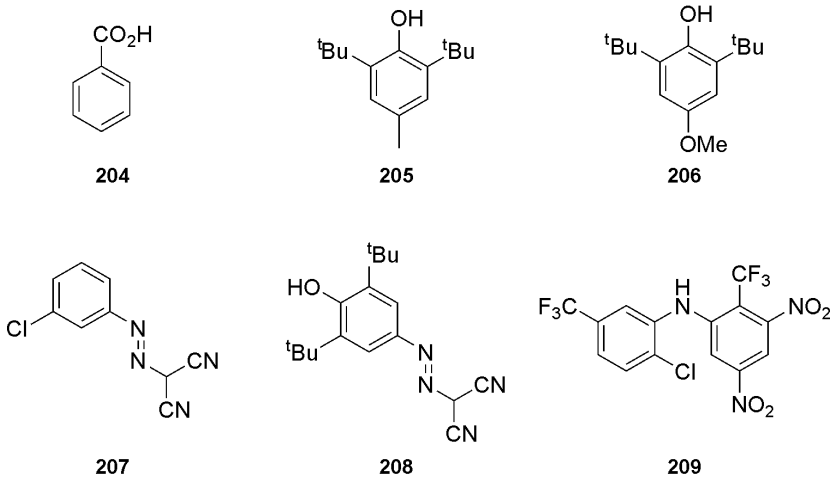

204 **205** **206**

207 **208** **209**

Fig.40: Examples of small molecule mitochondrial uncouplers

Benzoic acid **24** is a weak uncoupler as it displays only limited interactions with ANT and cannot behave as a proton translocator as its anionic form (pKa 4.2) is insufficiently lipophilic to cross the MIM.[149] Carbonylcyanide *m*-chlorophenylhydrazone (CCCP) **207** is a stronger uncoupler than FCCP **33** with the former known to be a proton translocator as well as acting on ANT. It is assumed that FCCP **33** would similarly interact with ANT although confirmation of this has not been reported to date. Malonoben **208** acts as an uncoupler directly analogous to CCCP **207** but is a more potent.[146] Diarylamines with suitably electron withdrawing and lipophilic substituents such as fentrifanil **209** (a more potent uncoupler than CCCP **207**), can behave as weak acids and therefore uncouple mitochondria through a protonophore mechanism.[151] Derivatisations of the carbonylcyanide phenyl hydrazone and BHT **205** backbones have previously been made to modify properties such as pKa, lipophilicity and hydrophilicity, which has led to many variants such as butylated hydroxyanisole **206**. Many molecules such as pentafluorophenol (pKa 5.5)[152] have pKa values between that of DNP **201** and FCCP **33** and would be expected to be sufficiently lipophilic to cross phospholipid membranes. The ability of

pentafluorophenol to uncouple isolated rat skeletal muscle mitochondria was assessed, but no uncoupling behavior was observed (experimental observation, data not shown). It is possible that the physiochemical properties required for mitochondrial uncoupling are more complex than these two characteristics alone or perhaps this molecule was simply too lipophilic, resulting in it becoming membrane bound and therefore unable to cycle protons. Regardless of the reasoning, it was decided that for the following studies, established uncouplers DNP **201** and FCCP **33** would be used.

7.2 Mitochondria-targeted caged selective uncoupling molecules

The primary aim of this project was to produce the first mitochondria-targeted, selective uncoupling molecules (MitoSUMs) that would be able to reduce $\Delta\Psi_m$ and therefore ROS production selectively in response to excess endogenous H_2O_2. The MitoSUMs would accumulate in all mitochondria but only release uncoupling molecules where there was significant oxidative stress, as signalled by high levels of H_2O_2. Rather than working as an antioxidant simply mopping up the oxidant, the uncoupler would shut down the conditions that gave rise to the elevated ROS production.

The advantage of mitochondrial accumulation is that the uncouplers would be released directly at the site of action, maximising effect and reducing dosage requirements to obtain an effective concentration. Concentration of the uncoupler present in the cell as a whole would be low as diffusion away from the mitochondrion in which it was released would lead to significant dilution and because very little of the uncoupler would be released in the cytosol directly due to the low concentration of the MitoSUM in this region. Therefore MitoSUMs would modulate misbehaving mitochondria while well-behaved mitochondria would be unaffected. The MitoSUMs would be used both as a molecular probe to test the free radical theory of ageing and as a prototype drug for combating oxidative stress arising from mitochondria-generated ROS.

The proposed target compounds must be non-toxic and comprise three moieties (Fig.41);

i) A targeting group to allow accumulation inside the mitochondrial matrix to maximise efficiency through a high localised concentration at the site of action.
ii) A H_2O_2-selective trigger mechanism that is stable to *in vivo* conditions ie. pH, temperature, enzymes, etc.
iii) An inactive, caged mitochondrial uncoupler that will become active only after the trigger mechanism is initiated.

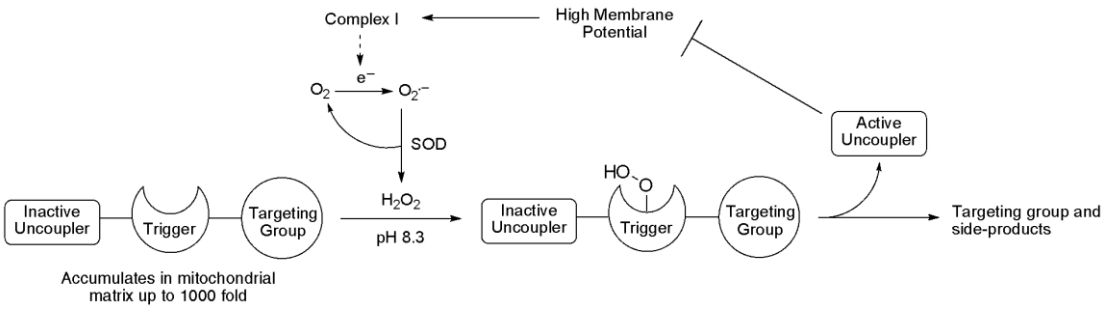

Fig.41: Proposed 3 moiety probes and mode of action

A TPP targeting group was chosen as the probe is designed to reduce ROS produced by mitochondria with elevated $\Delta\Psi_m$. Therefore harnessing the $\Delta\Psi_m$ to drive uptake may provide some degree of selectivity towards high ROS producing mitochondria over healthy mitochondria. Mitochondria-targeting will enable significant reduction in the concentrations required to obtain uncoupling benefits by releasing the uncoupling molecule inside the matrix (ie. at the site of action), reducing any non-mitochondria specific interactions and any effects on mitochondria not producing significant amounts of H_2O_2.

The chosen H_2O_2 selective trigger mechanism will employ a simple boronate ester and will be converted into a phenol by reaction with H_2O_2. The change in the functional group electronics from an electron withdrawing boronate to an electron donating phenol/phenoxide will trigger molecular fragmentation, and hence payload molecule release.

Uncoupling molecules such as DNP **201** are designed to be caged in a manner to prevent their uncoupling function (ie. through the phenol moiety of DNP **201**) prior to release by H_2O_2. This will help reduce their toxicity profile due to excessive uncoupling as only very low concentrations of the free uncoupling molecule will be present in any cell at any time and also only in those cells with elevated ROS levels.

Utilising a carbonate or carbamate linker as used by Chang[100] as well as Lo and Chu[97] introduces an increased driving force for fragmentation with the liberation of a stable carbon dioxide molecule in addition to being entropically favoured (Chapter 4.1, Scheme 24). However, these linkers will likely increase molecule instability due to potential hydrolysis, particularly *in vivo* where these units are potential substrates for esterase enzymes. For this reason, initial studies looked at the viability of using a simplified linker relying on direct release from the triggering unit without carbamate fragmentation.

7.3 Synthesis of DNP-SUM and FCCP-SUM

The initial project aim was to optimise the synthesis of two untargeted SUM molecules, DNP-SUM **210** and FCCP-SUM **211**, developed within the Hartley research group to release DNP^- **202** or $FCCP^-$ **203** respectively in response to H_2O_2 and to assess the viability of their release mechanism and payload molecule attachment (Schemes **60** and **61**).[153]

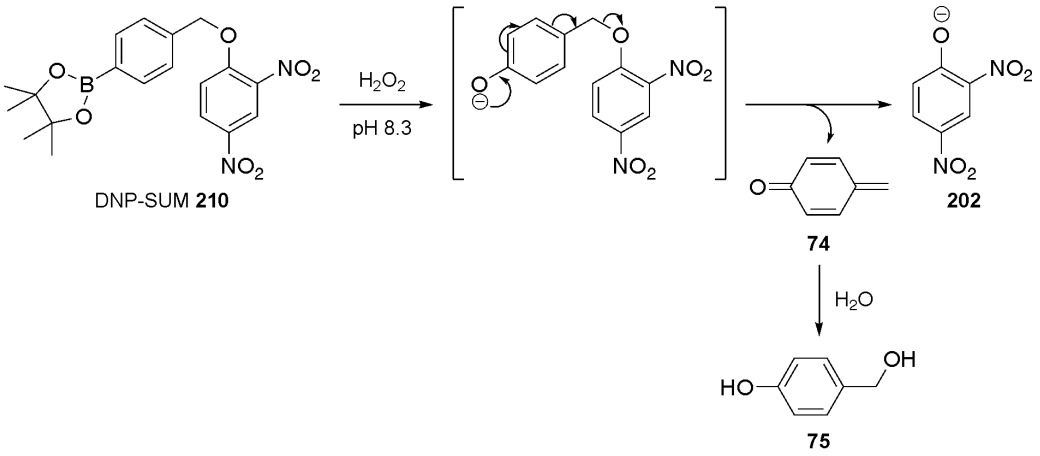

Scheme 60: Release mechanism for H_2O_2 SUMs carrying caged DNP **201**

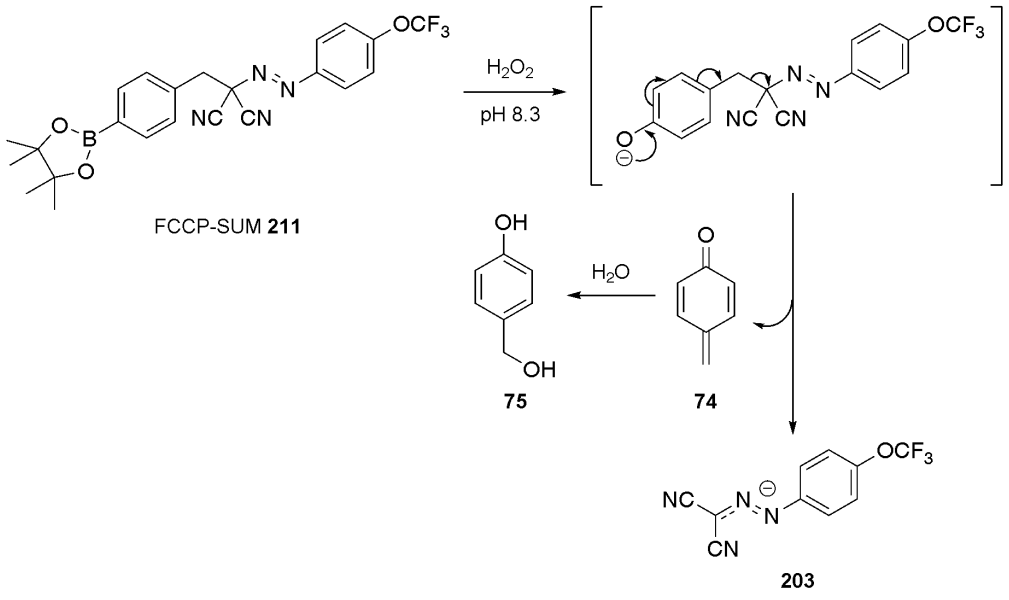

Scheme 61: Release mechanism for H_2O_2 SUMs carrying caged FCCP **33**

The initial synthetic steps towards boronate ester **210** from aryl bromide **212** *via* acetal protection of the benzylic alcohol moiety, lithium-halogen exchange to introduce the boronate group and acid catalysed alcohol deprotection were all achieved in moderate to high yields (Scheme 62).

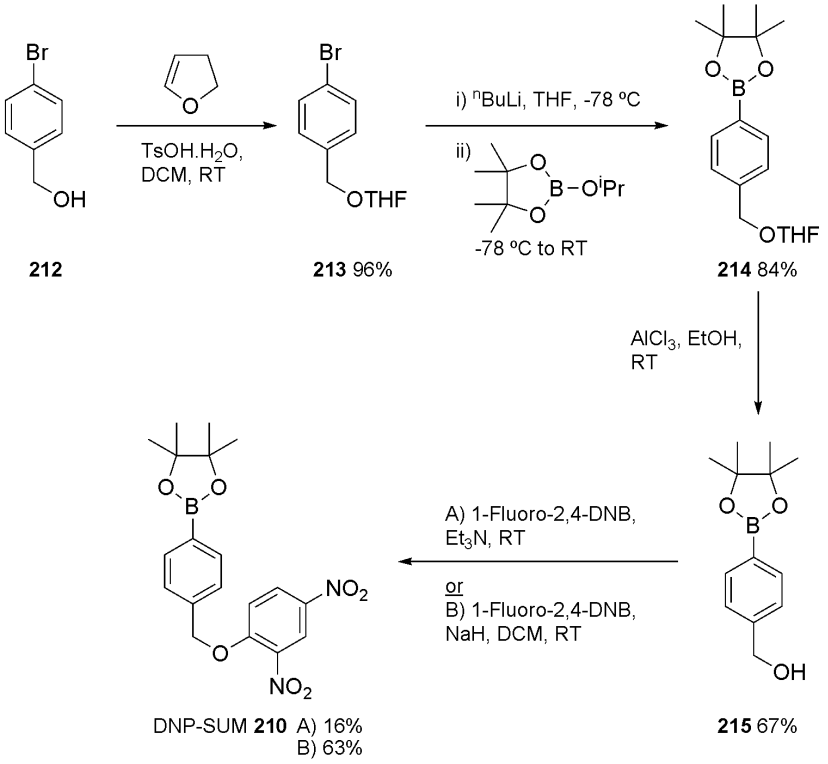

Scheme 62: Synthesis of DNP-SUM **210** (DNB = Dinitrobenzene)

Isolated yields of DNP-SUM **210** using standard S_NAr conditions using triethylamine as a base were repeatedly low due to poor conversion even when neat reagents were used. A number of attempts to optimise this reaction step were made. Attempts to increase the electrophilicity of 1-fluoro-2,4-dinitrophenol by generating an aryl chromium tricarbonyl complex (Scheme 63) were unsuccessful and gave only insoluble material which could not be identified. Mesylation of benzylic alcohol **215** followed by S_N2 displacement by sodium 2,4-dinitrophenoxide (generated from DNP **201** and NaH) was similarly unsuccessful. Switching to sodium hydride as a base to deprotonate benzylic alcohol **215** resulted in an excellent conversion and a significantly increased isolated yield. It is possible that introducing 15-crown-5 to this reaction could allow yields to be increased further through the sequestering of Na^+ ions, resulting in a more nucleophilic aryloxy-anion, although this was not tested.

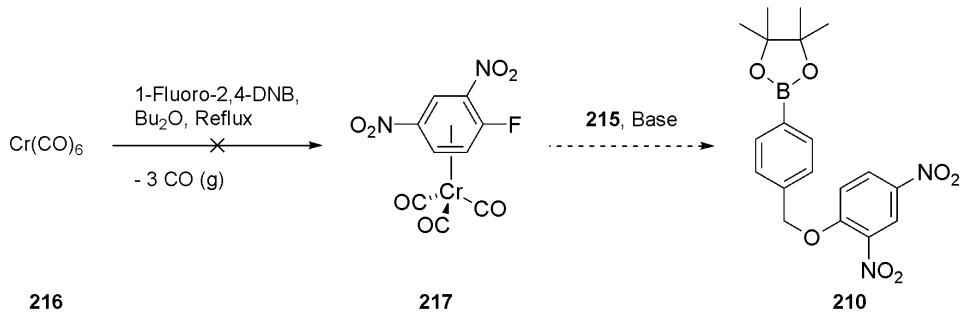

Scheme 63: Attempted synthesis of aryl chromium tricarbonyl complex **217**

To begin the synthesis of FCCP-SUM **211**, the boronate trigger mechanism was introduced to aryl bromide **218** *via* lithium-halogen exchange in excellent yield on a multi-gram scale. Intermediate benzylic bromide **220** had been previously synthesised in the Hartley research group utilising a low yielding (34%) radical bromination of the benzylic carbon atom of boronate **219** (Scheme 64), but isolating the product was unsuccessful during this project.

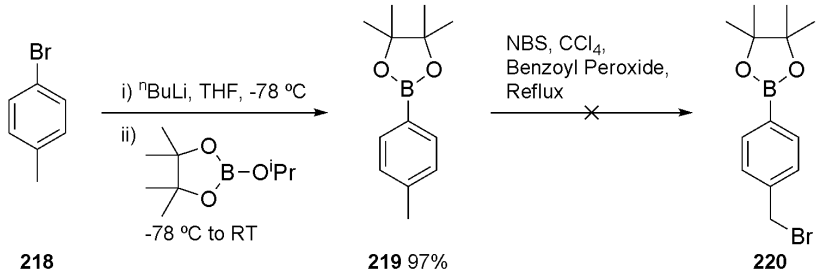

Scheme 64: Attempted synthesis of benzylic bromide **220**

The radical reaction was initiated by the thermal homolytic cleavage of benzoyl peroxide **221** in the presence of *N*-bromosuccinamide **214** but proved difficult to control (Scheme 65).

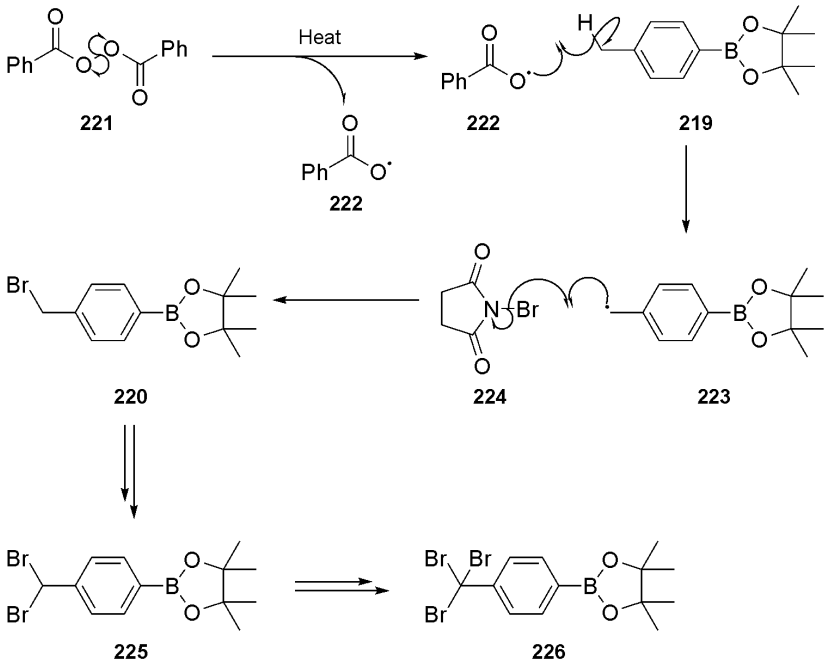

Scheme 65: Benzoyl peroxide initiated radical bromination mechanism

Unreacted starting material **219** and both monobromide **220** and dibromide **225** (Table 7) were identified by ^{1}H NMR spectroscopy. Although tribromide **226** is another potential product of over bromination, no unambiguous confirmation of this species presence was made. The mixtures proved inseparable by column chromatography on silica and recrystallisation was unsuccessful in my hands. Some degree of optimisation was achieved by re-initiating the radical reaction after 24 h (Entry 4), although a previous attempt to restart the reaction (Entry 3) led to over bromination.

Table 7: Radical bromination of dioxaborolane **219**

	Reagent Equivalence					~Product Composition (%) (^{1}H NMR)		
Entry	Boronate Ester **219**	Benzoyl Peroxide	NBS	CCl_4 (mL)	Duration (h)	Starting Material **219**	Monobromo Product **220**	Dibromo Product **225**
1	1	0.02	1.2	6	24	80	20	0
2	1	0.02	1.2	6	48	80	20	0
3*	1	0.02	1.2	6	24	0	56	44
4	1	0.02 + 0.02**	1.2 + 1.2**	6	48	8	84	8

* Entry 3 used crude product mixture from entry 2

** After 24 h

The radical bromination method was discontinued in favour of a more reliable approach to synthesise benzylic bromide **220**. Following the procedure of De Filippis *et al*,[154] benzylic alcohol **215** was readily converted into benzylic bromide **220** (Scheme 66). This step was unoptimised but yielded sufficient material to allow completion of the synthetic route. An Appel reaction (triphenylphosphine and carbon tetrabromide) could also have been employed to achieve this functional group interconversion. Dinitrile **227** was synthesised using an excess of malononitrile to prevent formation of the doubly-reacted product in which deprotonated dinitrile **227** reacts with a second equivalent of benzylic bromide **220**. The diazonium salt prepared from *p*-(trifluoromethoxy)aniline and sodium nitrite under acidic conditions was reacted with dinitrile **227** under basic conditions to complete the synthesis of FCCP-SUM **211** in moderate yield.

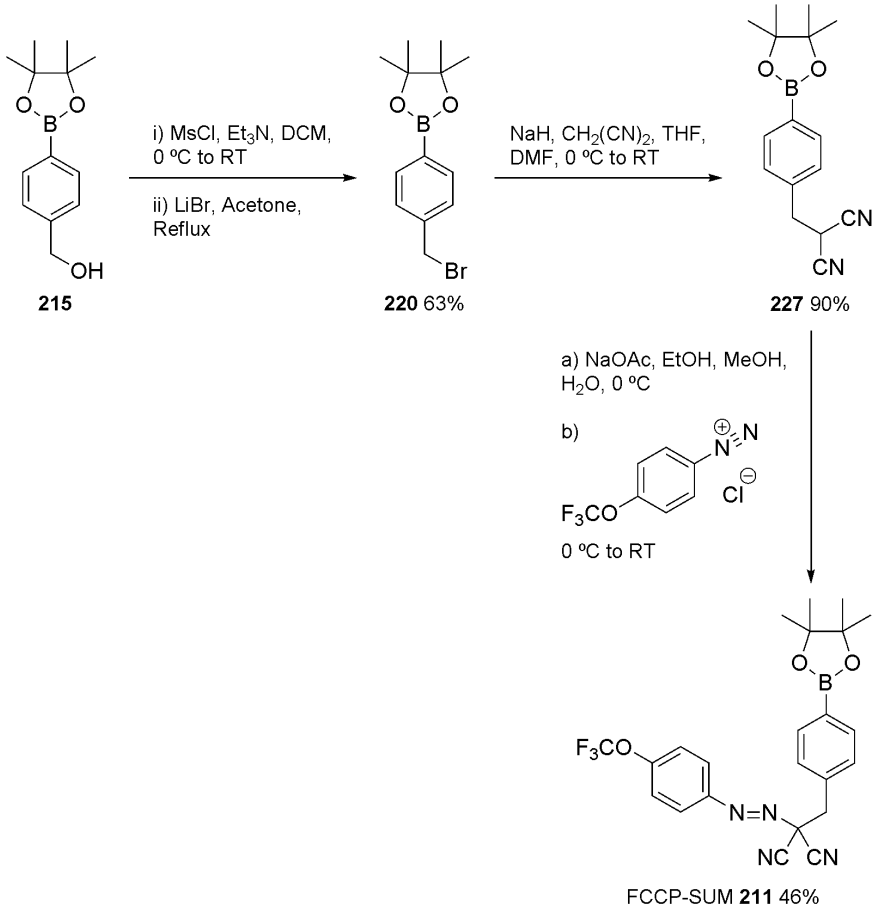

Scheme 66: Synthesis of FCCP-SUM **211**

7.3.1 Kinetic studies of DNP-SUM and FCCP-SUM

Kinetic experiments using DNP-SUM **210** and FCCP-SUM **211** were carried out using a JASCO V-550 UV/VIS spectrophotometer with the assistance of Professor Nicholas Price and Dr Linsey Robertson, University of Glasgow.[153] The expected reaction for each probe (Chapter 7.3, Schemes **60** and **61**) would release one molecule of quinone methide **74** for each molecule of probe reacting in a 1:1 stoichiometry with H_2O_2. This by-product would be rapidly trapped by water to give benzylic alcohol **75**.[99]

The aim of these experiments was to assess the rates of conversion of DNP-SUM **210** and FCCP-SUM **211** into free DNP **201** and FCCP **33** respectively, under *pseudo*-physiological conditions in the presence of known H_2O_2 concentrations to derive the limiting change in A_{410}/A_{385} (ΔA_{lim}) and the *pseudo*-first order rate constants (k_1). Using a 10- or 20-fold excess of SUMs **210** or **211** over the H_2O_2 concentration allow the standard bimolecular second order rate equation (Fig.42) to be simplified to the *pseudo*-first order rate equation (Fig.43) where the concentration of the caged uncoupler is regarded as constant.

$$d[Uncoupler^-]/dt = k_2[Caged\ Uncoupler][H_2O_2]$$

Fig.42: Second order rate equation

$$d[Uncoupler^-]/dt = k_1[H_2O_2]$$

Fig.43: *Pseudo*-first order rate equation

Experiments were conducted at 37 °C in 50% DMF, 50% aqueous solution. Physiological pH 8.3 (mimicking the pH of the mitochondrial matrix) was obtained using a 140 mM $NaHCO_3$ aqueous solution. It was observed that DMF alone caused a slow, steady decomposition of probe DNP-SUM **210** and so this compound was included in both reference and sample cells to account for this spontaneous release of DNP **201**. No such decomposition was observed in 100% water. Kinetic validity is unaffected by this slow decomposition (less than 3% after 2000 s) as the concentration of DNP-SUM **210** (200 μM) was in a large excess compared to H_2O_2 concentrations studied (10 and 20 μM).

Absorption was monitored at 410 nm as free DNP **201** displays a characteristic absorption maximum (λ_{abs}) at this wavelength that does not overlap significantly with the absorption spectrum observed from the caged uncoupler **201**. The λ_{abs} is maintained across the pH range of 7.4 to 8.3 which were assessed. Furthermore pHs outside this range are expected to maintain the maximum λ_{abs} at 410 nm absorption peak across a broad range of pHs above the pKa of DNP **201** (4.1). From earlier studies within the Hartley research group, it was known that the A_{410} of 20 μM DNP **201** in the DMF/buffer mixture was 0.4097. Thus this absorption level would be observed at 100% reaction of 20 μM H_2O_2 based on a 1:1 reaction stoichiometry between H_2O_2 and DNP-SUM **210**.

The reactions were monitored over a 2000 s time course, and results averaged over 3 replicates. For 10 μM H_2O_2, calculated ΔA_{lim} = 0.122 (±0.01), i.e. 5.96 μM DNP **201** was formed or a yield of 60% relative to the H_2O_2 added. The average k_1 is 0.00216 s^{-1}, which when divided by the probe **210** concentration gives a second-order rate of 10.8 M^{-1} s^{-1}.

For 20 μM H_2O_2, calculated ΔA_{lim} = 0.220 (±0.006), i.e. 10.73 μM DNP **201** was formed or a yield of 54% relative to the H_2O_2 added. The average k is 0.00185 s^{-1}, which when divided by the probe **210** concentration gives a second-order rate of 9.3 M^{-1} s^{-1} (Fig.44).

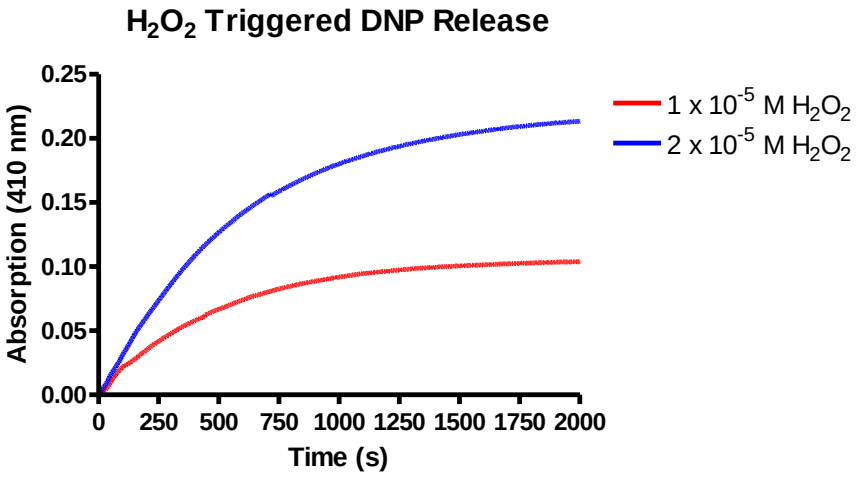

Fig.44: H_2O_2 triggered DNP **201** release from DNP-SUM **210** (Scheme 60)

The overall conversion yields averaged over the 2 sets of runs are 57 (± 3)% and the second-order rate constant is 10 (± 0.8) M^{-1} s^{-1}. The incomplete conversion of the probe may be a result of competing reactions resulting in the consumption of H_2O_2. For example, as the hydroperoxide anion (HOO^-) is the most nucleophilic species present, the quinone methide by-product **74** could react with a second equivalent H_2O_2 molecule, instead of becoming trapped by water to form diol **75**.

The rate of reaction between DNP-SUM **210** and peroxynitrite at pH 7.4 was determined by the group of Kalyanaraman using stopped-flow measurements. The calculated rate constant of (4.5×10^5) M^{-1} s^{-1} is comparable to those observed for peroxynitrite reacting with other arylboronates.[34,131]

These results prove that the boronate ester trigger and subsequent fragmentation mechanisms through a benzylic aryl ether linker can successfully be used to release active uncoupler molecules from inactive precursors, in the presence of H_2O_2. Similarly successful results were obtained by Dr Linsey Robertson for FCCP-SUM **211** (50 μM), measured in the same *pseudo*-physiological conditions over a 1000 s run time (Fig.45). The overall conversion yields averaged over both H_2O_2 concentrations tested (5 and 10 μM) were 58 (± 2)% and the second-order rate constant is 64.8 (± 0.6) M^{-1} s^{-1}. Overall conversion of both probe analogues are comparable suggesting a similar side-reaction may be involved which results in the consumption of similar levels of H_2O_2. The rates of FCCP **33** release from FCCP-SUM **211** by either reaction with H_2O_2 or background probe breakdown were both significantly higher than the rates of DNP **201** release from DNP-SUM **210** due to the former being a better leaving group.

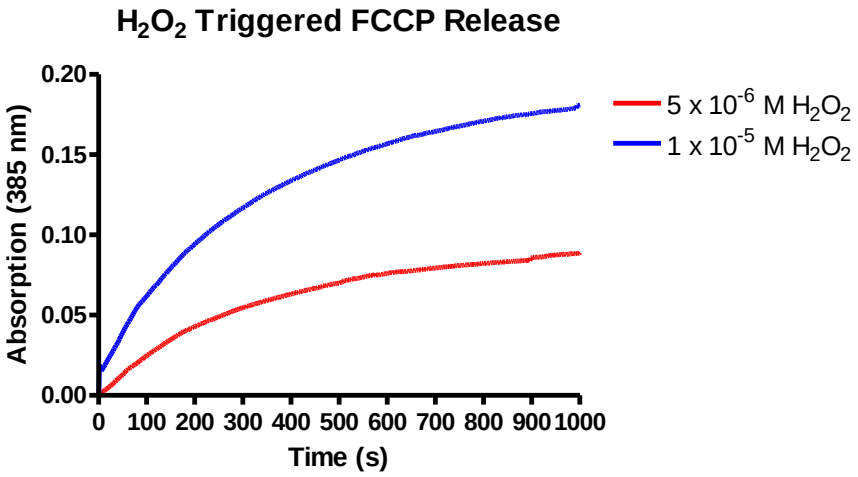

Fig.45: H_2O_2 triggered FCCP **33** release from FCCP-SUM **211** (Scheme 61)

The above results therefore confirm that the proposed mechanism of uncoupling molecule release in response to H_2O_2 works as designed in probes **210** and **211**, with the successful release from benzylic attachment sites without the need for a fragmentable carbonate or carbamate linker.

7.4 Synthesis of TPP salts

Next, targeting of the SUMs to mitochondria was investigated. MitoSUMs were designed to employ the TPP targeting approach previously discussed (Chapter 2.1). Introduction of TPP moieties is generally achieved through S_N2 displacement of a leaving group such as a halide, triflate or mesylate. Using this approach a number of TPP compounds with ready-to-attach linkers were synthesised (Schemes 67-70). TPP formation from short linear chain (n = 1-4; where n = number of methylene units) dihaloalkanes in toluene allows rapid synthesis and straight-forward isolation by collection of the precipitated product (Scheme 67). Increasing alkyl chain lengths above n = 4 results in partial solubility and so mixtures of mono-TPP **228** and di-TPP **229** compounds are produced which are difficult to separate from each other. Similar mono- and di-TPP compound mixtures arise regardless of the choice of halide leaving group (Cl, Br or I).

Switching solvents to diethyl ether slows reaction rates due to the reduction in maximum obtainable temperatures, but allows the straight-forward synthesis of TPP-alkyl halides up to at least n = 6 **228** (Scheme 67) due to the poor solubility profile of TPP compounds in ethereal solvents. When n = 10, partial solubility returns due to increased lipophilicity and therefore di-TPP compounds **231** once again began to form. This can be minimised by

using a large excess of the dihalodecane but the overall concentration must be kept low as the desired mono-TPP product **230** is partially solubilised by the alkylating agent itself which leads to the bis-salt **231** being generated. Further work is required to optimise the synthesis of these longer-chain TPP-alkyl halides.

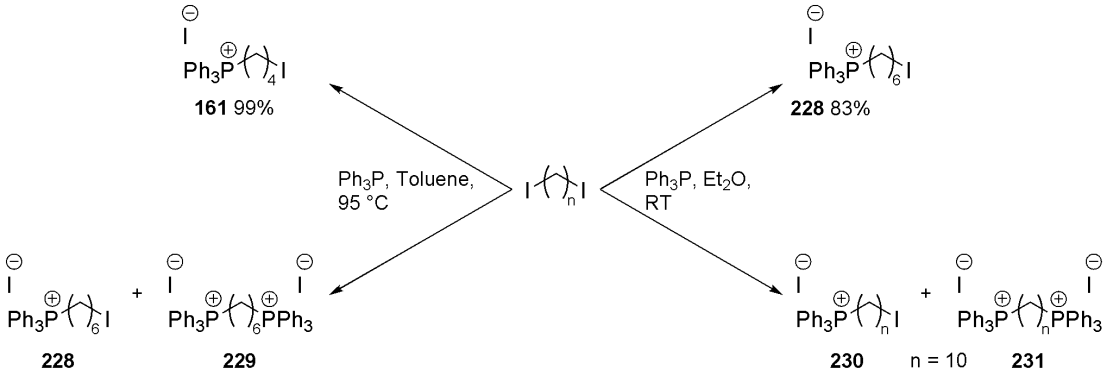

Scheme 67: Synthesis of TPP-alkyl halides

A range of other ready-to-attach linkers were also synthesised to enable the simple introduction of TPP groups. To improve the rates of subsequent alkylation reactions compared to the linear TPP-alkyl halides above, a TPP-benzylic bromide analogue **233** was prepared from α,α'-dibromoxylene **232** (Scheme 68). No reaction was observed when attempting to synthesise the direct nitrogen analogue **234** using triphenylamine, due to the differences in size of phosphorus and nitrogen atoms. The smaller nitrogen atom is more sterically hindered and the overlap of its lone pair with the aromatic rings is better than in the case of phosphorus, resulting in a significantly poorer nucleophile.

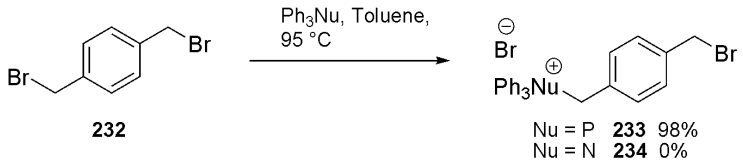

Scheme 68: Synthesis of TPP-benzylic bromide **233**

A carboxylic acid bearing variant **236** was synthesised to allow attachment *via* esters or amides (Scheme 69) either through the use of coupling agents or through the formation of an acid chloride intermediate. Through functional group interchange this compound could also potentially be used to access to the alcohol and aldehyde analogues and further derivatives thereof if necessary.

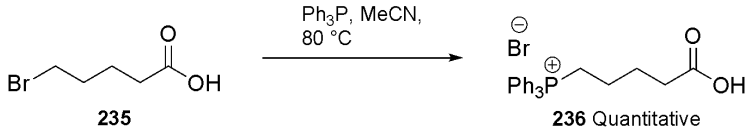

Scheme 69: Synthesis of TPP-carboxylic acid **236**

An attempt was also made to examine the possibility of introducing TPP groups through click chemistry (Scheme 70). Alkyl halides are readily converted into azides in near quantitative yields using sodium azide in refluxing aqueous alcohols. A subsequent trial click reaction to couple TPP-azide **238** with propargylic alcohol **239** was unsuccessful, although a thorough optimisation of conditions was not completed in this case. This approach has since been successfully used within the Hartley research group (albeit with reversal of azide/alkyne moieties in relation to the TPP group) using a CuI catalysed click reaction in DMF to introduce TPP moieties *via* a biologically stable triazole unit.

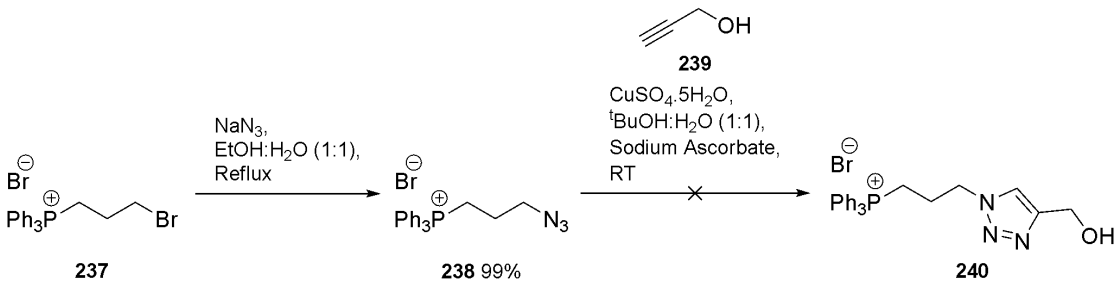

Scheme 70: Attempted TPP introduction using click-chemistry

7.5 Initial attempts towards MitoDNP-SUM and MitoFCCP-SUM

Initial synthetic approaches towards MitoSUMs focussed on modifying the boronate ester moiety of previously synthesised SUMs **210** and **211** to facilitate targeting group attachment (Scheme 71).[153]

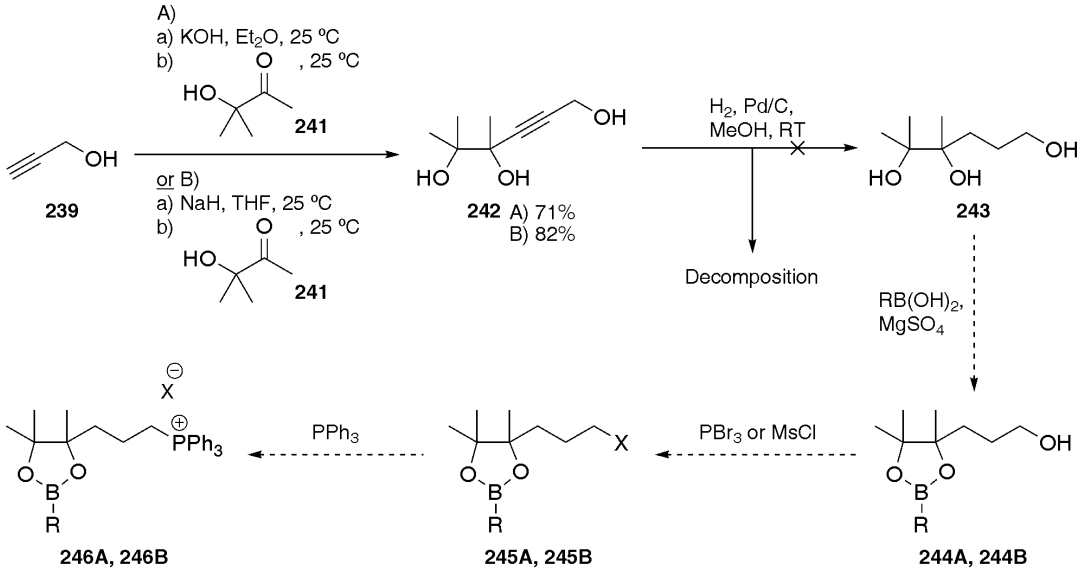

Scheme 71: Original proposed route to MitoSUMs

A: R = *p*-(C_6H_4)CH_2ODNB B: R = *p*-(C_6H_4)CH_2FCCP X = Br or OMs

Adapting the procedure of Li and Burgess[155] alkyne-triol **242** was synthesised, isolated and characterised for the first time. A literature reduction of crude alkyne-triol **242** used hydrogen over Raney nickel. Attempted reduction using hydrogen over Pd/C caused significant decomposition with multiple quartets observed in the ^{1}H NMR spectrum of the crude mixture. These could only arise after hydroxyl group loss and/or intramolecular methyl group migration. Although originally the aim was to use a saturated linker **243**, an alternative might be to use alkyne-triol **242** instead which would ensure the remoteness of the free hydroxyl to prevent potential mixtures of boronate esters forming (eg. 7- or 8-membered boronate ring formation).

Before either triol **242** or triol **243** could be coupled to form a boronate ester, conversion of DNP-SUM **210** or FCCP-SUM **211** to their corresponding boronic acids would be required. Boronate esters of 1,2-diols such as pinacol and boronic acids exist in equilibrium favouring the boronate ester due to the chelate effect. Sodium periodate was employed to convert free pinacol into acetone driving the equilibrium to the boronic acid side (Scheme 72). It was found that hydrolysis of DNP-SUM **210** or FCCP-SUM **211** to their boronic acid analogues was difficult to drive to completion above 80-85% conversion, despite repeated reaction attempts, with increased duration and sodium periodate excess.

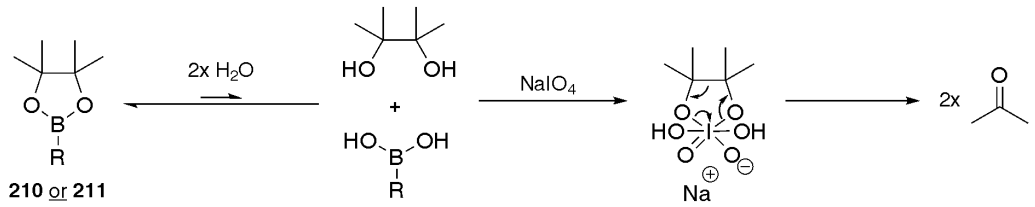

Scheme 72: $NaIO_4$ reaction with 1,2-diols

R = *p*-$(C_6H_4)CH_2$ODNB or *p*-$(C_6H_4)CH_2$FCCP

Alternative methods of boronate ester to boronic acid conversion not attempted employ transesterification using an excess of boron trichloride or a polymer-bound boronic acid as reported by Pennington *et al.*[156] Crude boronic acid **247** (~83:17 **247:210** by ^{1}H NMR) was coupled to alkyne-triol **242** with magnesium sulfate as a drying agent to drive the reaction to completion. ^{1}H NMR spectroscopy indicated clean coupling of the two partners to give boronate **248**, however upon attempted purification by column chromatography on silica the compound decomposed.

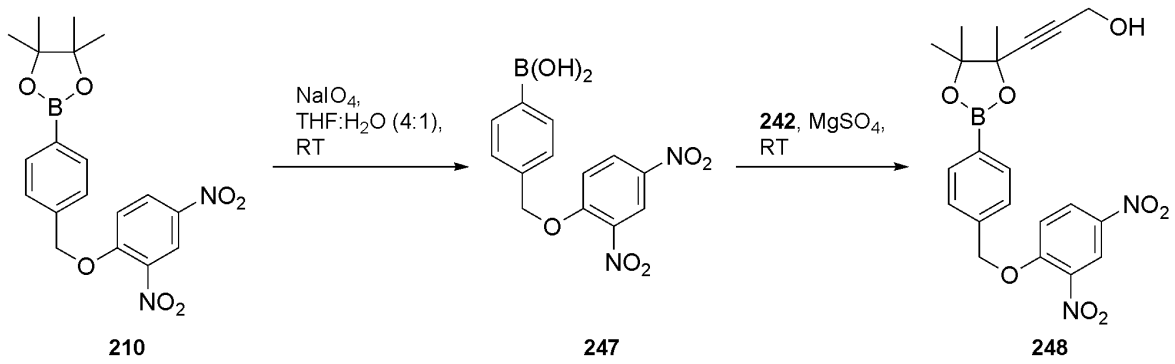

Scheme 73: Proposed boronate ester hydrolysis/formation

A test coupling reaction between alkyne-triol **242** and phenylboronic acid **249** appeared similarly successful by crude ^{1}H NMR spectroscopy but purification by column chromatography on silica again led to total decomposition of the alcohol **250** (Scheme 74).

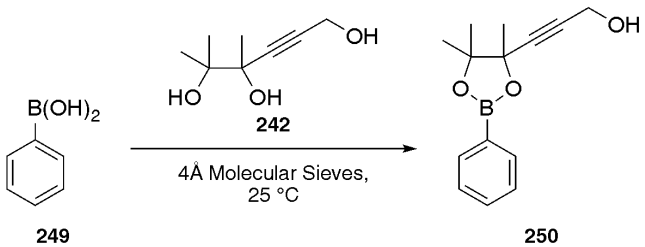

Scheme 74: Model boronic acid coupling to alkyne-triol **242**

Due to stability issues along with the potential loss of the targeting group *via* reversible hydrolysis of the boronate ester in aqueous environments, alternative structures for MitoSUMs were proposed.

7.6 Revised approach towards MitoDNP-SUM

The second synthetic MitoSUM target proposed would be directly analogous to DNP-SUM **210** but would include attachment of a TPP group through a stable ether linker attached directly to the aryl ring (Fig.46).

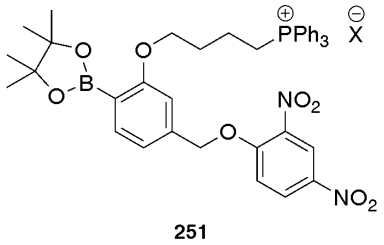

251

Fig.46: Revised structure for mitochondria-targeted DNP-SUM **251**

Phenol **252** was iodinated using the procedure of Whiting and Pilling[157] in moderate yield (Scheme 75). Esterification under acidic conditions and the following diisobutylaluminium hydride (DIBALH) reduction to benzylic alcohol **255** were both completed in near quantitative yield. On top of the two equivalences of DIBALH required to complete the reduction, a sacrificial equivalence is also required due to reagent co-ordination to the free phenol.

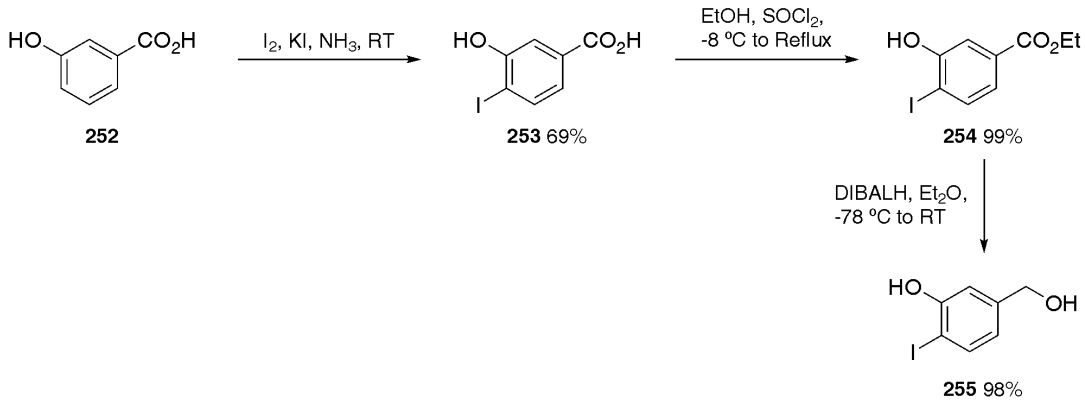

252 **253** 69% **254** 99% **255** 98%

Scheme 75: Synthesis of diol **255**

Originally $LiAlH_4$ was employed to reduce ethyl ester **254** but this led to a mixture of products including dehalogenated phenol **146** (Scheme 76). The significant halogen loss was probably a result of aluminium co-ordination by the phenoxyl moiety directing hydride transfer onto the carbon bearing the iodine atom. A similar mixture including iodide loss was observed upon the attempted reduction of carboxylic acid **253** with $THF.BH_3$ to give benzylic alcohol **255**.

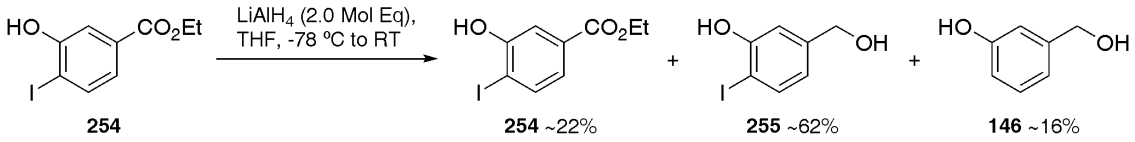

Scheme 76: Attempted reduction of ester **254** with $LiAlH_4$ (Crude yields from ^1H NMR)

Conversion of diol **255** into bis-acetal **257** was quantitative with no trace of phenol **256** present in the crude reaction mixture (^1H NMR). However, after purification by column chromatography on silica, partial loss of the phenolic acetal was observed indicating its higher lability under mildly acidic conditions compared to the benzylic acetal. No sign of any benzylic alcohol deprotection was detected. Isolated phenol **256** could be readily converted back into bis-acetal **257** through resubmission to protection conditions although this was never attempted as sufficient bis-acetal **257** had been obtained as a 1:1 mixture of diastereomers to continue the synthesis (Scheme 77).

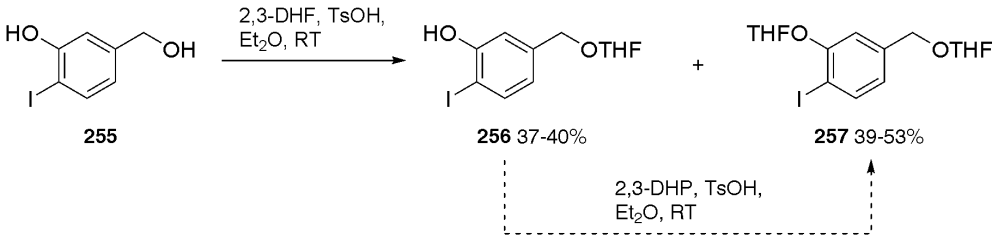

Scheme 77: Protection of diol **255**

Lithium-halogen exchange and borylation to give boronate ester **258** was less efficient than previously found for boronate esters **214** and **219** due to the increased steric bulk adjacent to the borylation site (Scheme 78). Bis-deprotection was readily achieved using aluminium trichloride although approximately 10% of material underwent proto-deborylation to give diol **146**. The crude mixture was taken forward to introduce the TPP group to the phenol moiety. Differentiation between hydroxyl groups could be achieved by differences in pKa values between the phenol (~10) and the benzylic alcohol (~15). However, upon phenoxide **262** formation by cesium carbonate, complete proto-

deborylation occurred as the directly conjugated oxyanion promotes protonation of the carbon attached to boron atom (Scheme 79). If the targeting group attachment had been successful, introduction of the uncoupling molecule would have completed the synthesis.

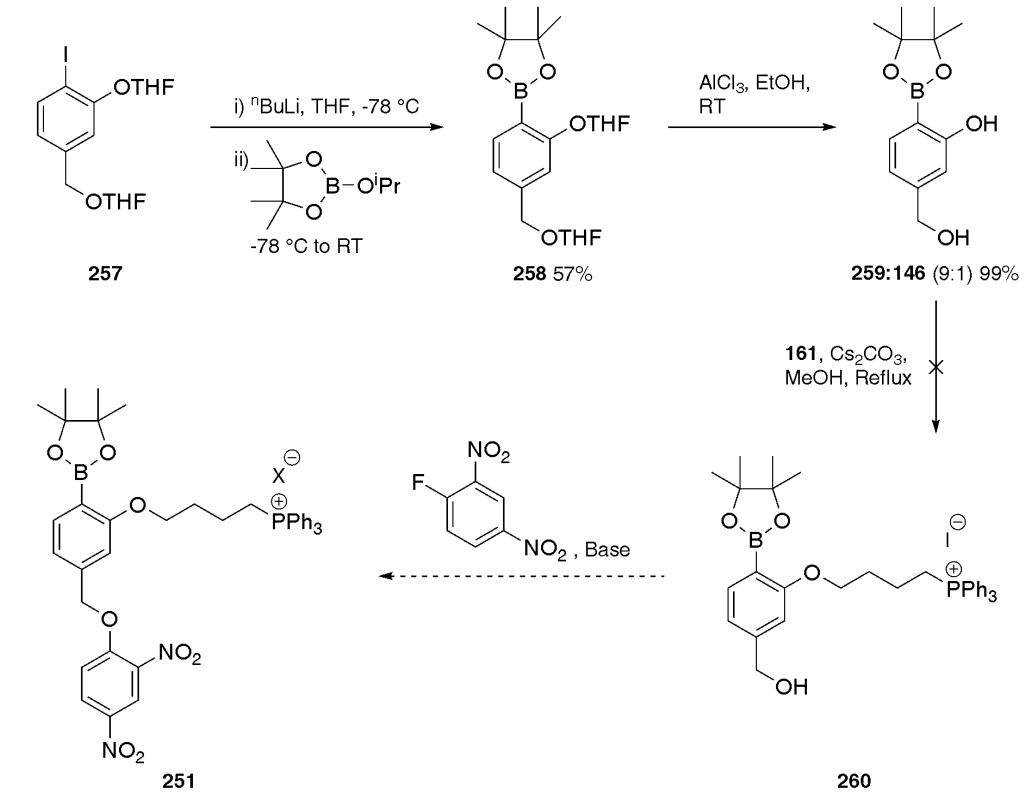

Scheme 78: Proposed route towards MitoSUM **251**

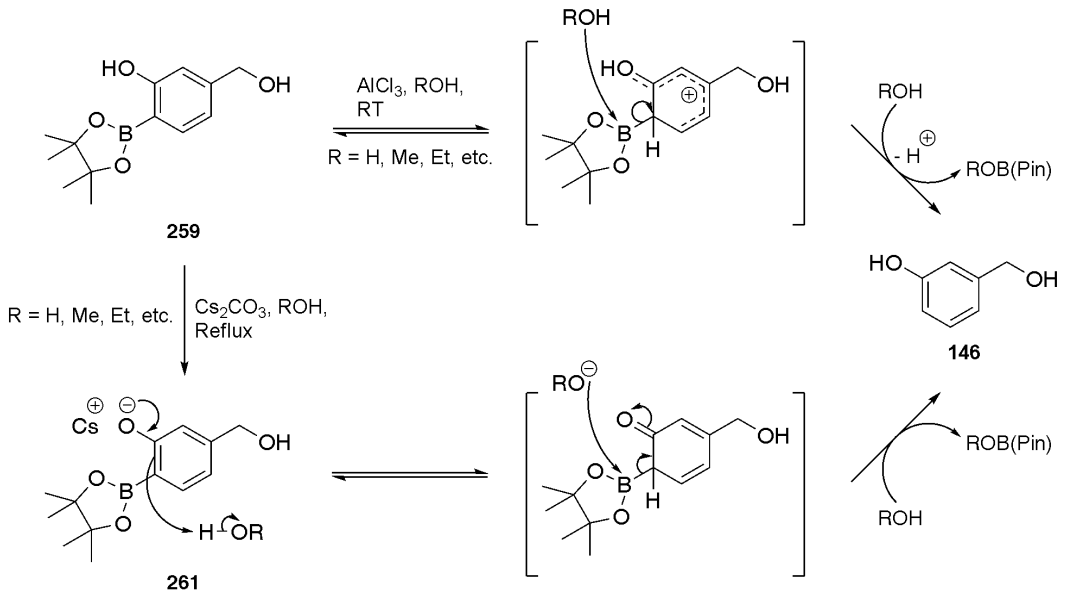

Scheme 79: Proto-deborylation occurs under acidic or basic conditions (The boronate cleavage step is likely to go *via* a step-wise mechanism)

In an attempt to prevent proto-deborylation by increasing the rate of the alkylation step an excess of α,α'-dibromoxylene **232** was used along with an anhydrous, aprotic solvent (Scheme 80). Significant loss of the boronate group was still observed indicating that this decomposition is significantly faster than the attempted alkylation reaction. Attempted targeting group introduction was unsuccessful.

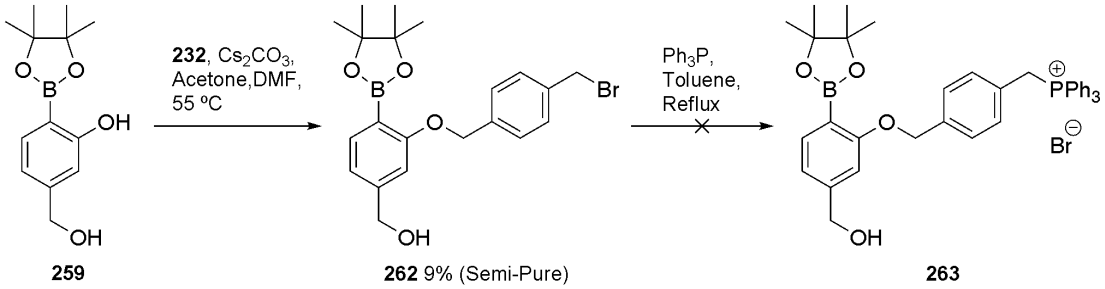

259 **262** 9% (Semi-Pure) **263**

Scheme 80: Alternative proposed route to MitoSUM intermediate

Synthetic steps were reversed to allow the introduction of the boronate trigger in the final step to prevent the problem of proto-deborylation (Schemes 81-83). MOM protection of previously synthesised ethyl ester **254** was achieved in high yield. As observed during the reduction of the unprotected ethyl ester **254**, reduction with lithium aluminium hydride gave a mixture of products including dehalogenated products **266** and **267** (Scheme 81). Therefore it appears that the methoxymethyl ether protecting group can sufficiently co-ordinate to aluminium to assist in directing hydride attack to the carbon atom attached to the iodine atom. The use of a bulky, non-co-ordinating phenol protecting group such as a *tert*-butyldimethylsilyl group could potentially prevent iodide loss by removing any directing effects and by sterically hindering hydride attack on the iodine-bearing carbon atom. However DIBALH was successfully employed due to its lower reactivity and greater steric bulk to reduce ethyl ester **264** to selectively give benzylic alcohol **265** in 63% yield.

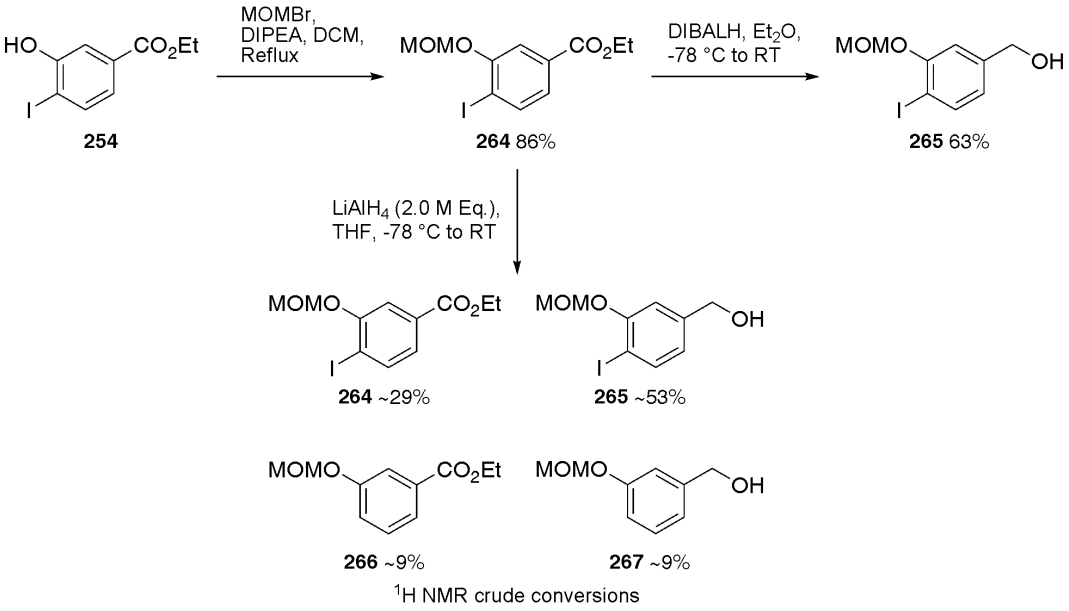

Scheme 81: Intermediate route towards MitoSUMs

The uncoupling molecule payload was incorporated using the standard S_NAr conditions (Scheme 82). Phenol deprotection was achieved in high yield under strongly acidic conditions after the same transformation had been attempted using the mild conditions of Breton.[158] $NaHSO_4$ supported on silica gave low but clean conversion to phenol **269** with addition of excess reagent unsuccessful at driving the reaction to completion. Phenol alkylation with TPP-benzylic bromide **233** was completed using mild alkylating conditions.

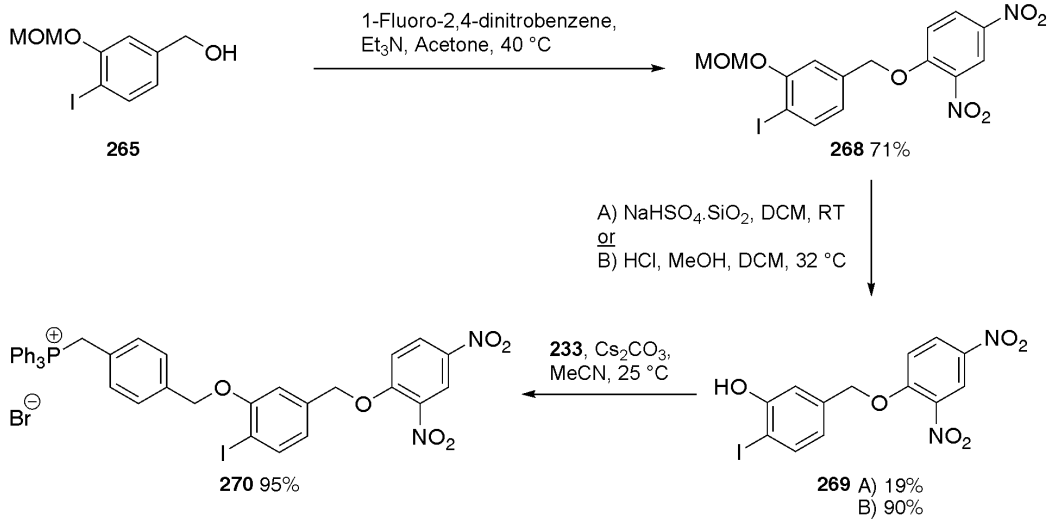

Scheme 82: Synthesis towards a DNP **201** bearing MitoSUM **292**

The final step introduction of the pinacol boronate ester group *via* a Miyaura borylation reaction was unsuccessful with no sign of borylation and significant compound degradation observed (Scheme 83). At this stage it was unclear if this degradation resulted from thermal decomposition and/or from the breakdown of the compound after palladium insertion.

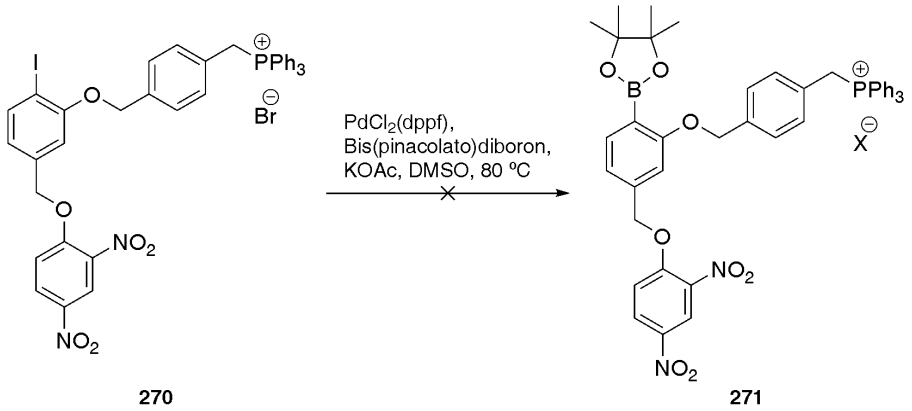

270 271

Scheme 83: Attempted Miyaura borylation

Other methods of introducing boronate esters are not compatable with the other functionality in aryl iodide **270**. A phosphorus ylide could form under basic conditions while the nitro groups of the DNP **201** moiety rule out lithiation procedures. Furthermore DNP **201** is a good leaving group precluding the use of many nucleophilic reagents or Grignard conditions. With this in mind and with only limited amounts of aryl iodide **270** in hand, further modifications to the structure of DNP-bearing MitoSUMs were made (Chapters 7.8-7.10).

7.7 Attempts towards MitoBHT-SUM

MitoBHT-SUM **278** was proposed and investigated in tandem with the DNP analogue **251** discussed previously. Initial esterification of carboxylic acid **252**, introduction of the methoxymethyl ether protecting group and ester reduction steps were all achieved in high yield on a multi-gram scale. Attempted functional group conversion of the benzylic alcohol **274** into the desired benzylic bromide **275** using the method previously used to generate benzylic bromide **220**, instead yielded deprotected benzylic bromide **145**. This is not unprecedented as acetal-type ethers have previously been reported by Kim *et al*[159] to be cleaved by soft nucleophiles such as bromide (eg. $MgBr_2$) or thiols in certain solvent systems. Benzylic bromide **145** had previously only been reported in the literature as an intermediate crude, unstable oil or as a purified brown solid with incomplete

characterisation.[130] The isolated crystals were indeed found to be unstable in light at RT. Whether one or both of these factors promote decomposition is unclear, although both are potentially a contributing factor. The solid itself appears to be stable for prolonged periods if stored in the dark at –18 °C. Upon decomposition the solid turns brown/black indicating bromide loss and becomes poorly soluble in organic solvents indicating polymerisation.

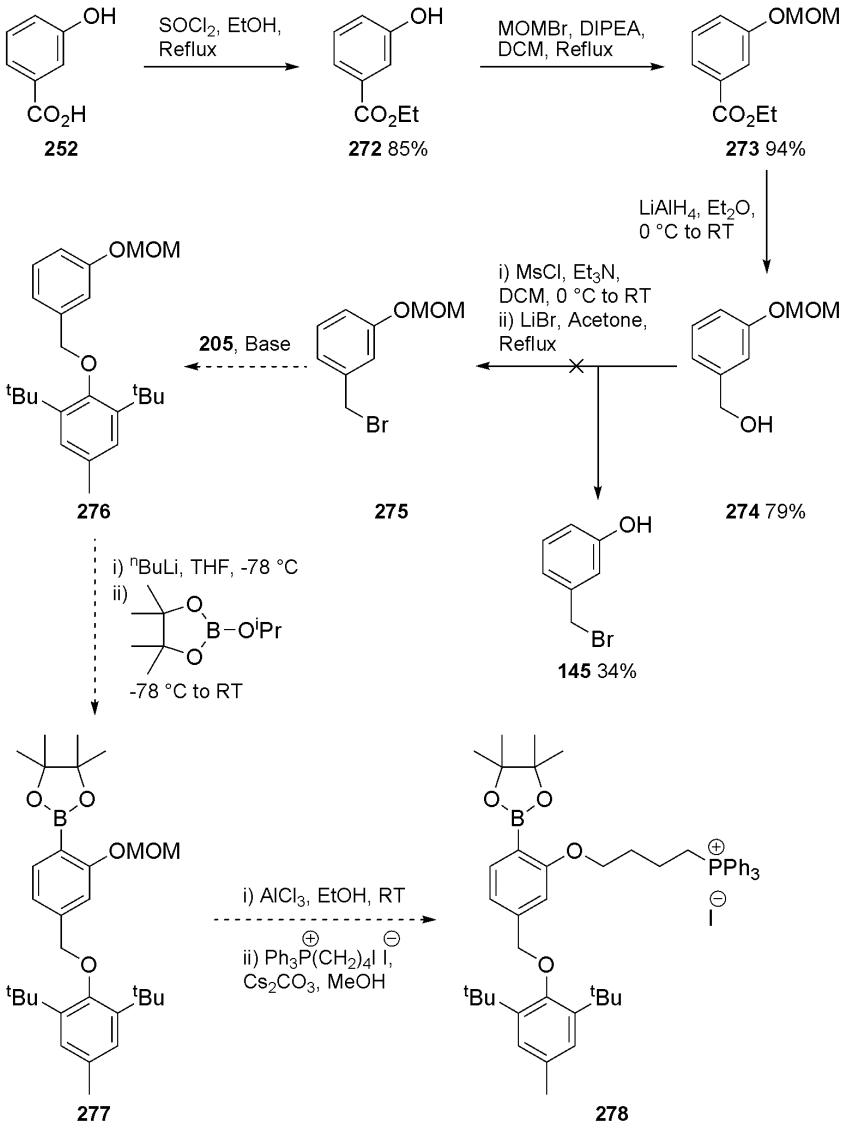

Scheme 84: Proposed synthesis of MitoBHT-SUM **278**

Conversion of benzylic alcohol **274** into benzylic bromide **275** could potentially be achieved using Appel reaction conditions or *via* mesylation followed by bromide displacement if an alternative protecting group was chosen. However, severe proto-deborylation issues observed during the parallel attempted synthesis of boronate **260** would be expected to occur similarly in MitoBHT-SUM **278** due to the closely related structures. Therefore no further efforts were made at completing this synthesis *via* this route.

7.8 Attempts towards AmidoMitoDNP-SUM and AmidoMitoFCCP-SUM

The new synthetic targets switched the targeting group attachment site away from the aryl ring bearing the boronate trigger to the same attachment site as the uncoupler molecule payload itself. Thus the newly proposed AmidoMitoDNP-SUM **279** and AmidoMitoFCCP-SUM **280** have the uncoupler attached to a secondary rather than a primary carbon atom (Fig.47). Although introducing an amide which is a potential site for metabolism by enzyme-catalysed hydrolysis that could result in targeting group loss, these structural modifications would remove the previous proto-deborylation issues and should have improved water solubility.

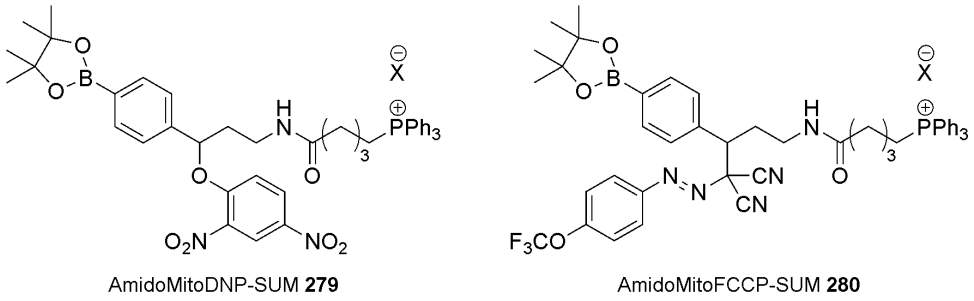

Fig.47: Proposed AmidoMito-SUMs

Phthalimido-aldehyde fragment **283** was readily synthesised from 3-aminopropan-1-ol **281** by phthalimide protection of the amino group under Dean-Stark conditions followed by Swern oxidation of alcohol **282** (Scheme 85).

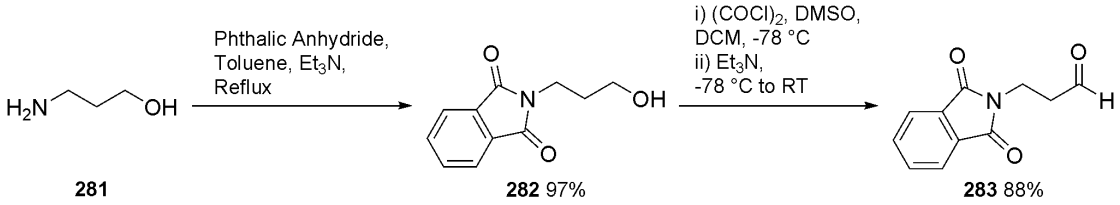

Scheme 85: Synthesis of phthalimido-aldehyde fragment **283**

Aryl iodide **155** was readily synthesised in excellent yield using the conditions of Knochel and co-workers (Scheme 86).[134,135]

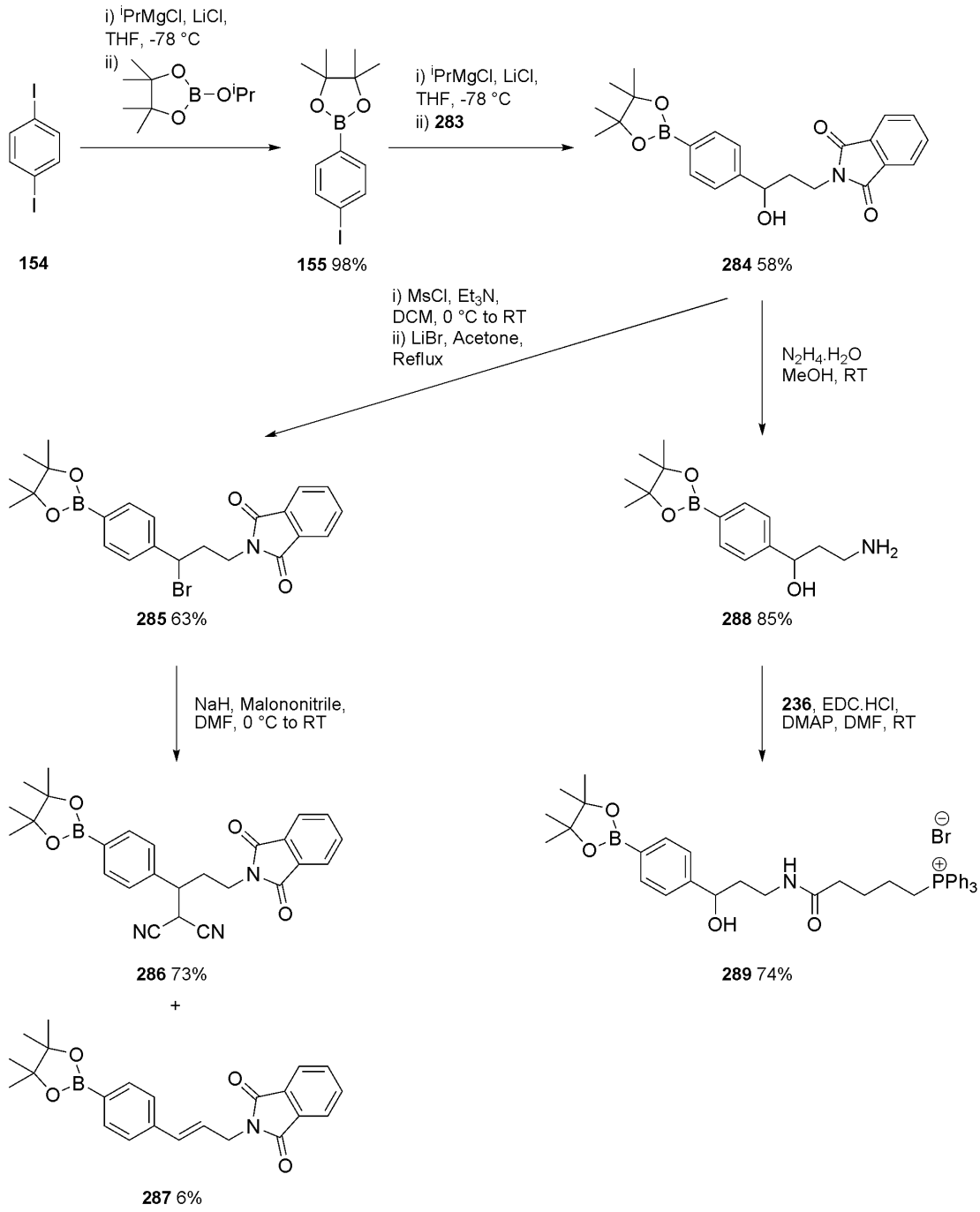

Scheme 86: Synthesis towards AmidoMito-SUMs **279** and **280**

The presence of LiCl breaks up the ^{i}PrMgCl dimer **290** or oligomer aggregates in solution to form an intermediate ^{i}PrMgCl.LiCl **291** complex that is more reactive than the parent Grignard dimer **290** and the resulting aryl Grignard LiCl complex **292** (Scheme 87).[135]

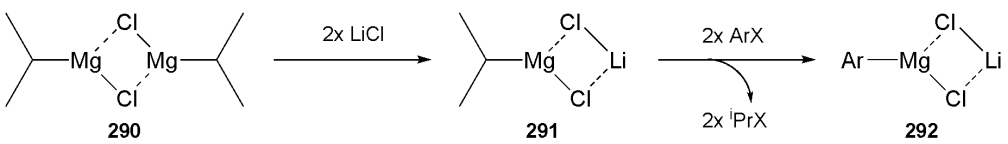

Scheme 87: Catalysis of Mg-halogen exchange reaction with LiCl

Employing identical Grignard conditions as for the previous step, but instead using aldehyde **283** as the electrophile gave key intermediate alcohol **284** in moderate yield (Scheme 86). Using LiCl in this second step prevents formation of the isopropylboronate resulting from Grignard attack at boron.[135] At this point the synthesis diverged towards the two synthetic targets and the subsequent two steps towards each AmidoMito-SUM were successful.

Mesylation and conversion to bromide **285** was followed by S_N2 displacement by malononitrile to take the synthesis towards AmidoMitoFCCP-SUM **280**. A small amount of elimination product **287** was observed in both steps and isolated after the latter.

Hydrazine deprotection of phthalimide **284** and amide formation using water-soluble coupling reagent *N*-(3-Dimethylaminopropyl)-*N′*-ethylcarbodiimide hydrochloride (EDC.HCl) and preformed TPP-carboxylic acid **236** gave alcohol **289** in yields of 85% and 74% respectively, one step from completion of AmidoMitoDNP-SUM **279**.

A number of attempts to complete the synthesis of AmidoMitoDNP-SUM **279** using the previously used S_NAr reaction conditions were unsuccessful (Scheme 88). The target compound was produced by the reaction but none of the conditions used gave complete conversion to product despite repeated attempts. Isolation attempts using column chromatography on silica and HPLC were unsuccessful at separating the different TPP salt components in the mixture.

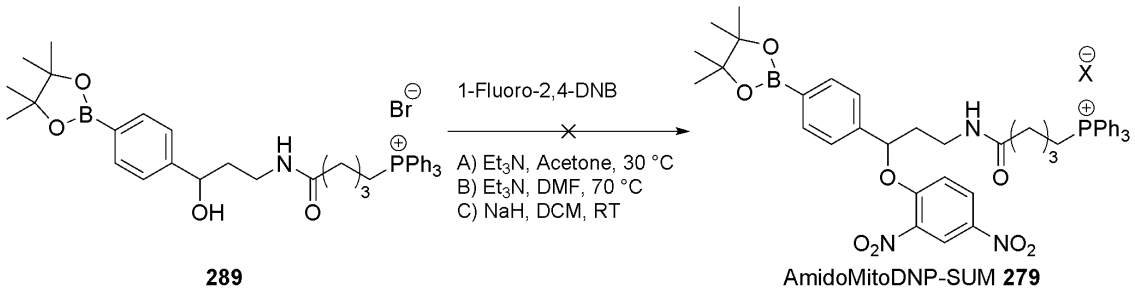

Scheme 88: Attempted synthesis of AmidoMitoDNP-SUM **279**

It is proposed that AmidoMitoFCCP-SUM **280** (Scheme 89) synthesis would be completed by reaction of phthalimide **286** with hydrazine followed by amide formation to introduce the TPP targeting group as before. FCCP **33** moiety formation *via* the diazonium salt of *p*-(trifluoromethoxy)aniline would complete the synthesis.

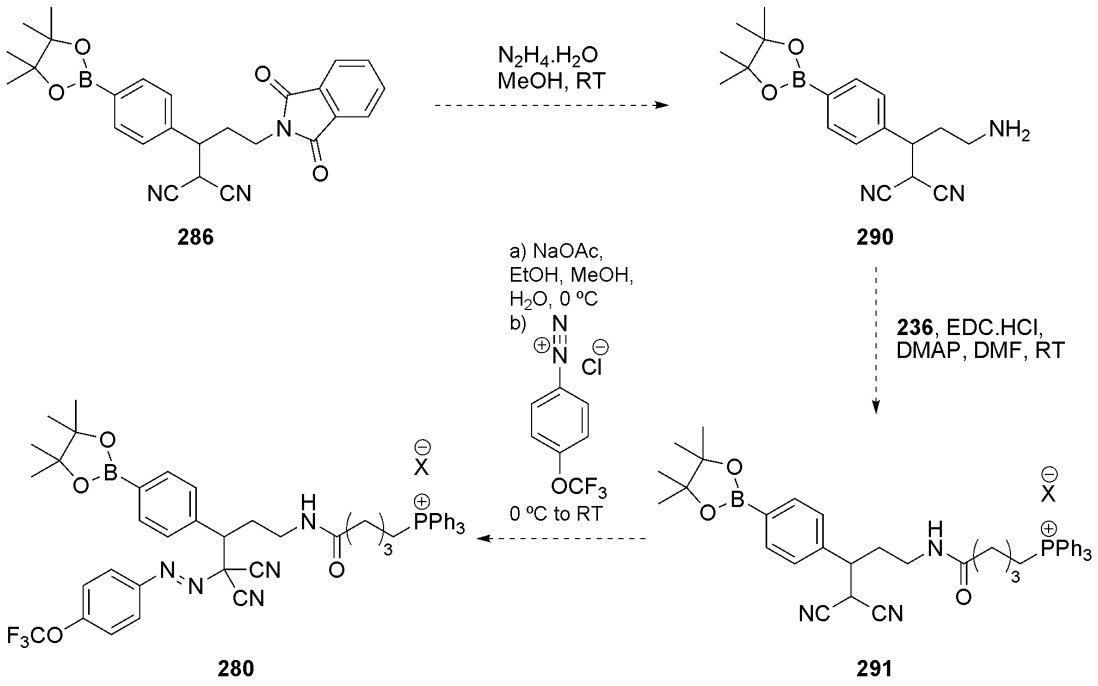

Scheme 89: Proposed end to AmidoMitoFCCP-SUM **280**

7.9 Synthesis of 1st generation MitoDNP-SUM

From the findings obtained during the previously unsuccessful MitoSUM attempts (Chapters 7.5-7.8) regarding synthetic approach, TPP attachment methods and position, a new structure for a DNP-bearing MitoSUM was proposed (Fig.48).

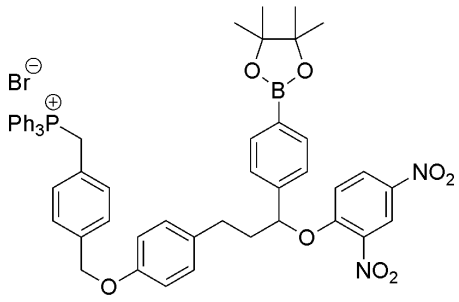

Fig.48: 1st Generation MitoDNP-SUM

Esterification of carboxylic acid **293** followed by methoxymethyl ether protection of the phenol moiety, reduction to a primary alcohol and Swern oxidation gave aldehyde **297** in excellent yields on multi-gram scales (Scheme 90).

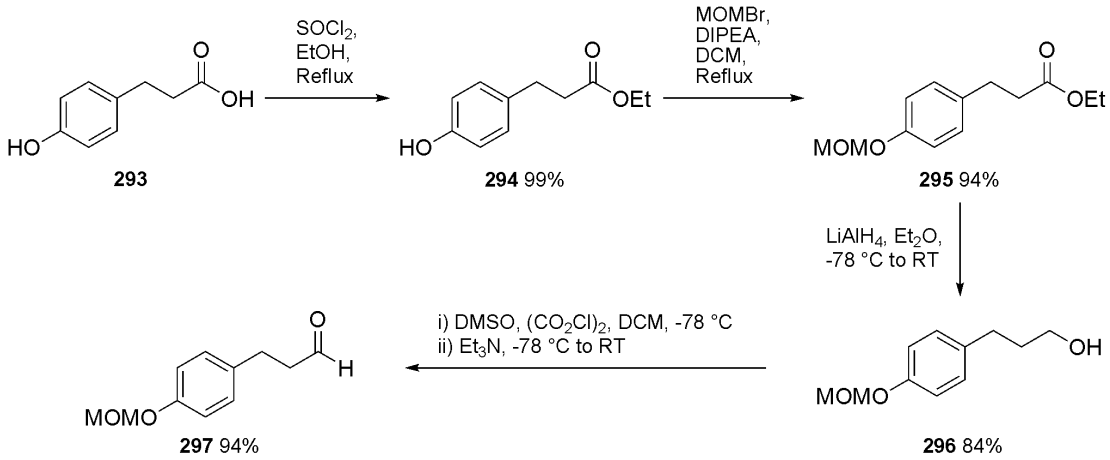

Scheme 90: Synthesis of aldehyde fragment **297**

Once again employing the Grignard conditions of Knochel[134,135] with aldehyde **297** as the electrophile (and as the limiting reagent) gave secondary alcohol **298** in excellent yield (Scheme 91). The propionaldehyde derivative **297** intermediate was chosen, as E2 elimination in alcohol **298** or ethers **292** or **299** would be less favourable as the aromatic rings would be sufficiently separated to prevent direct conjugation between the aryl units in the alkene product. Originally the S_NAr and MOM deprotection steps were conducted separately, however after incorporating the DNP **201** moiety, instability on silica and alumina led to reduced yields each time the purification was attempted. Furthermore the desired boronate ester form of phenol **299** was more readily separable from its boronic acid analogue than was the case for the intermediate boronate ester **300** and boronic acid **301** (Fig.49). Boronate ester **300** and boronic acid **301** were however identified in the crude ^1H NMR to monitor the reaction progress before the deprotection step is carried out. Thus combining these steps saved time and improved the overall yield.

Introduction of the TPP targeting group through mild alkylating conditions (cesium carbonate and benzylic bromide **233**) completed the synthesis of MitoDNP-SUM(1) **292**.

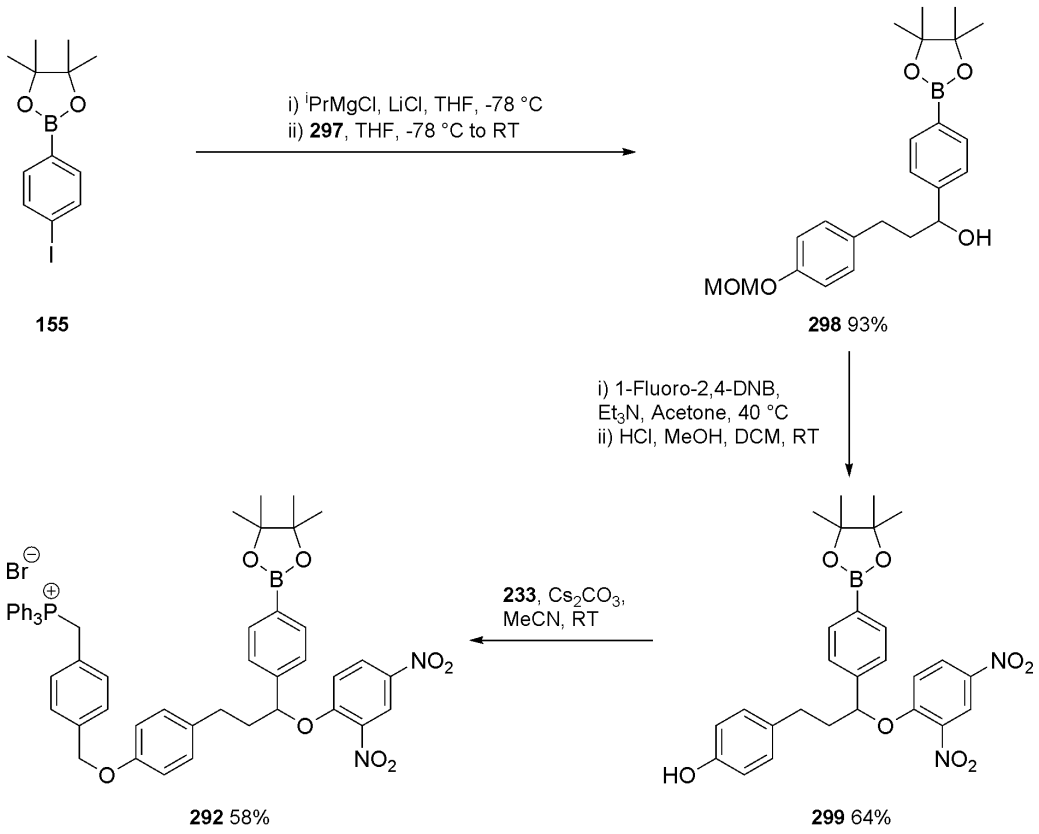

Scheme 91: Synthesis of MitoDNP-SUM(1) **292**

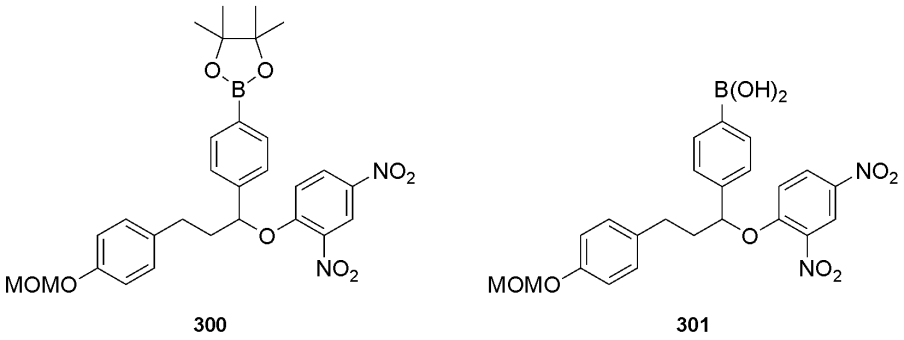

Fig.49: Intermediate mixture after S_NAr reaction with alcohol **298**

A small-scale assessment of the reversal of the final steps was made (Scheme 92). Phenol **298** deprotection yielded diol **302** in moderate yield followed by selective alkylation of the phenol over the secondary alcohol, again in moderate yield. An attempt to complete MitoDNP-SUM(1) **292** by an S_NAr reaction was unsuccessful although optimisation of this route could potentially allow it to be used to yield MitoSUMs in the future. At this point the target probe was completed *via* the original route (Scheme 91) and so no further experiments on this alternative route were conducted.

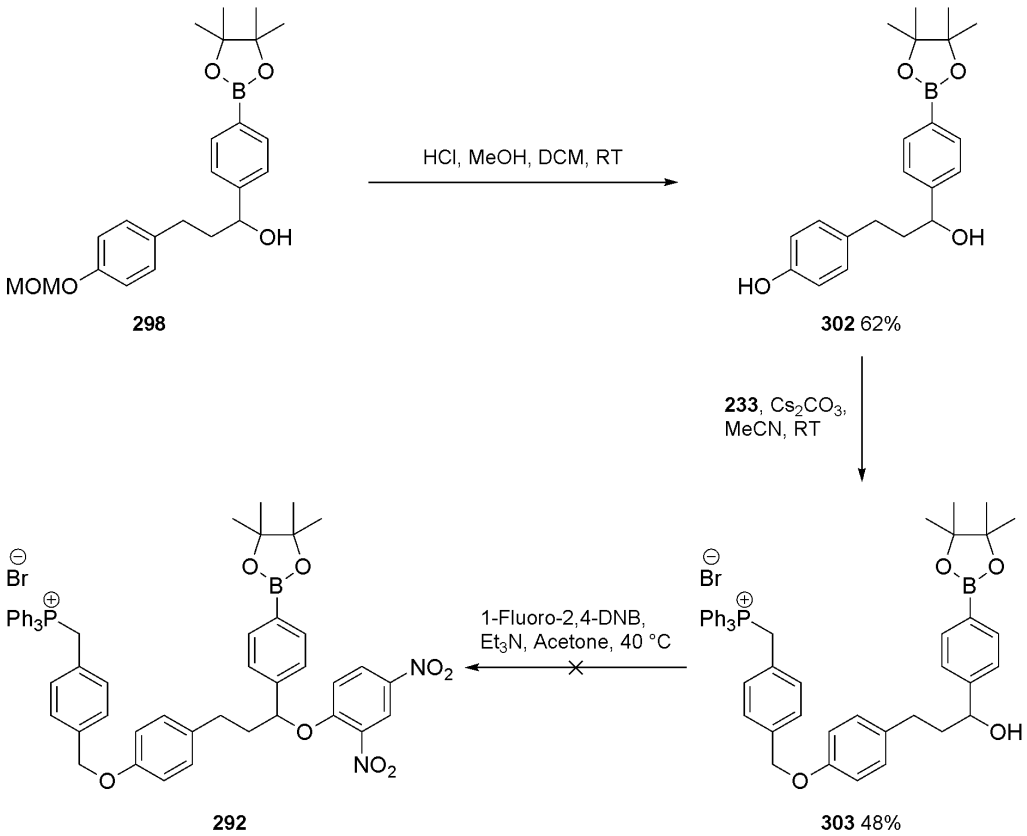

Scheme 92: Alternative proposed synthesis of MitoDNP-SUM(1) **292**

7.10 Synthesis of 2nd generation MitoDNP-SUM

A more compact, less lipophilic version of MitoDNP-SUM(1) **292** was designed to remove the apparently superfluous linkers between the caged uncoupling molecule and TPP group (Fig.50).

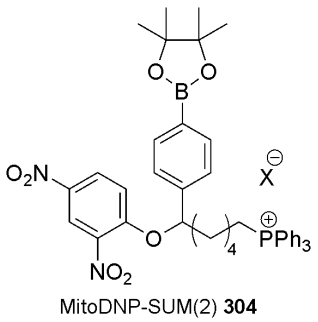

MitoDNP-SUM(2) **304**

Fig.50: 2nd Generation MitoDNP-SUM

Initial attempts looked at making an analogue with an aliphatic linker with one carbon shorter than MitoDNP-SUM(2) **304** (as carboxylic acid **235** was to hand) *via* an adaption of the method of Xu *et al.*[160] However using this aryl zincation method gave only dimerisation product **306** (Scheme 93). Introduction of a TPP moiety to alkyl bromide **305**

followed by ketone reduction with $NaBH_4$ and finally DNP **201** introduction by the standard S_NAr mechanism previously discussed would have completed the synthesis.

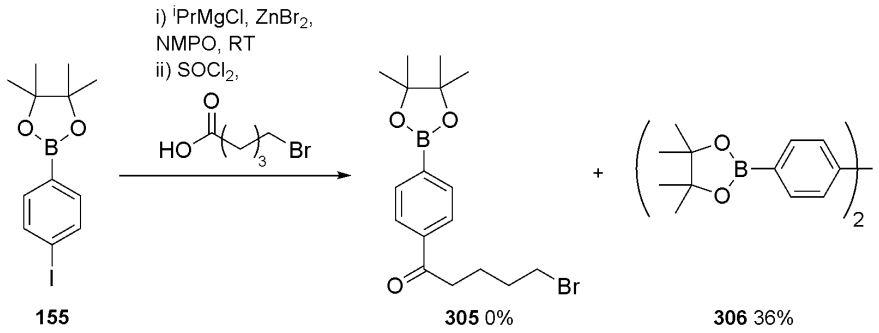

Scheme 93: Attempted synthesis of intermediate ketone **305** using aryl zincation

Synthesis of MitoDNP-SUM(2) **304** was completed *via* the direct modification of the MitoDNP-SUM(1) **292** route (Schemes 90 and 91) in which aldehyde **309** (Scheme 94) replaces aldehyde **297** as the electrophile in the second Grignard reaction (Schemes 91 and 95). Desymmetrisation of hexan-1,6-diol **307** by mono-acetal protection and subsequent Swern oxidation gave aldehyde **309** in excellent yield on a multi-gram scale.

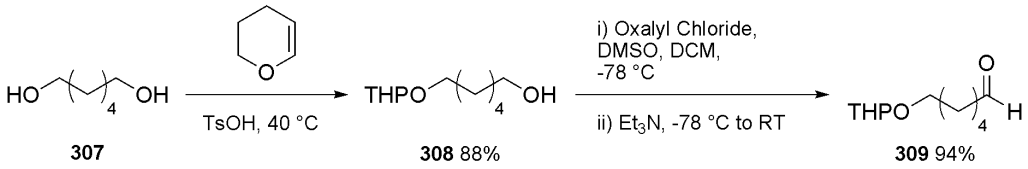

Scheme 94: Synthesis of aldehyde **309**

A subsequent Grignard reaction gave secondary alcohol **310** as a 1:1 mixture of diastereomers in high yield. DNP coupling and immediate deprotection under acidic conditions gave primary alcohol **311** in moderate yield, while diol **312** and secondary alcohol **313** were also isolated as minor by-products from this reaction (Scheme 95).

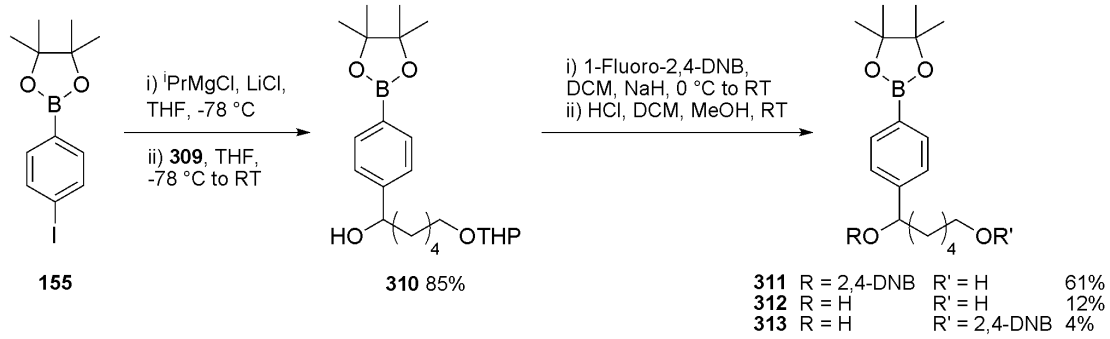

Scheme 95: Synthesis towards MitoDNP-SUM(2) **304**

The originally envisaged conversion of alcohol **311** directly into TPP salt **304** *via* an intermediate mesylate or triflate was unsuccessful. Appel reactions were employed to give alkyl halides **314** and **315** using CBr_4 and CI_4 respectively (Scheme 96).[161,162]

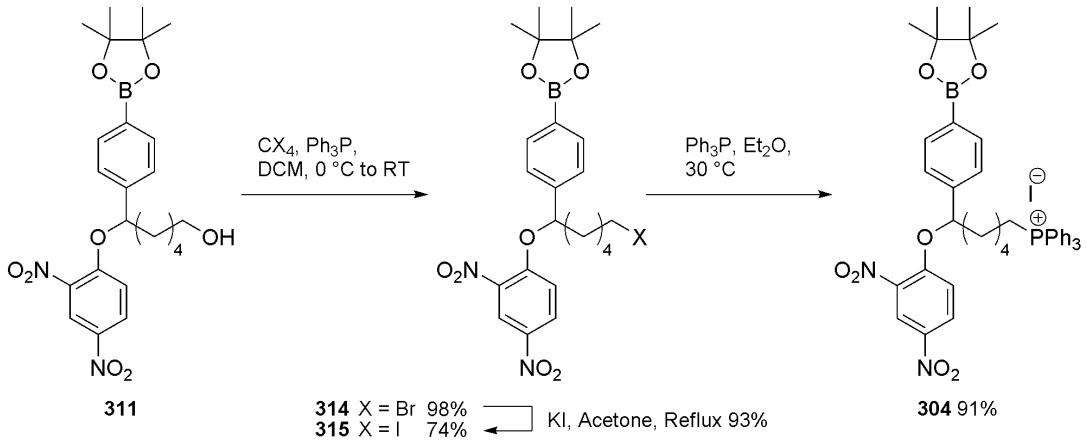

Scheme 96: Completion of MitoDNP-SUM(2) **304** synthesis

Direct TPP salt formation from bromide **314** failed under a number of conditions. Direct S_N2 displacement with triphenylphosphine heated under reflux in MeCN was sluggish and resulted in partial DNP **201** loss. Use of $AgNO_3$ as an additive to drive the reaction to completion through the precipitation of the silver bromide by-product led to no TPP formation and only gave a by-product, presumed to be the nitrate displacement product as identified by the shift in the adjacent CH_2 signal from ~3.4 ppm to ~4.4 ppm in ^{1}H NMR. The use of $AgClO_4$ gave more encouraging preliminary results with TPP formation occurring slowly but cleanly. However by this point synthesis was completed *via* iodide **315** by S_N2 displacement in diethyl ether. Although slow, the reaction can be accelerated by using a large excess of triphenylphosphine which is simply removed from the desired TPP salt product by precipitation of the salt product from stirring diethyl ether. Interconversion of bromide **314** into iodide **315** failed using the conditions of Firouzabadi *et al* ($ZrCl_4$ and NaI)[163] but was achieved in high yield using standard Finkelstein reaction conditions.

TPP salt formation was also observed in the reaction of bromide **314** with triphenylphosphine in MeCN under microwave conditions but the conversion was low and prolonged exposure to microwave energy led to many unidentified decomposition and/or side products. Therefore this approach was not explored any further.

7.11 Diastereotopicity in MitoDNP-SUMs

Once DNP **201** is attached, MitoDNP-SUM(1) **292**, MitoDNP-SUM(2) **304** and their caged-DNP containing precursors **299**, **311**, **314** and **315**, display diastereotopic pinacol methyl groups. In the precursor enantiomeric secondary alcohols **298** and **303** or diastereomeric alcohol **310**, no difference in chemical shift is observed. Once the large DNP **201** group is added the chiral centre is able to influence the chemical shifts of these distant groups.

As a result, geminal dimethyl groups become inequivalent and give rise to two 6H singlets in ^{1}H NMR spectra and two singlets in ^{13}C NMR. Distal methyl groups (ie. Me_A and Me_A' in Fig.**51**) remain equivalent due to free rotation about the boron-carbon bond while the proximal methyl groups (ie. Me_A and Me_B in Fig.**51**) which are equivalent in the precursors, become inequivalent due to the addition of this large group extending the influence of the chiral centre after the removal of the molecular mirror plane.

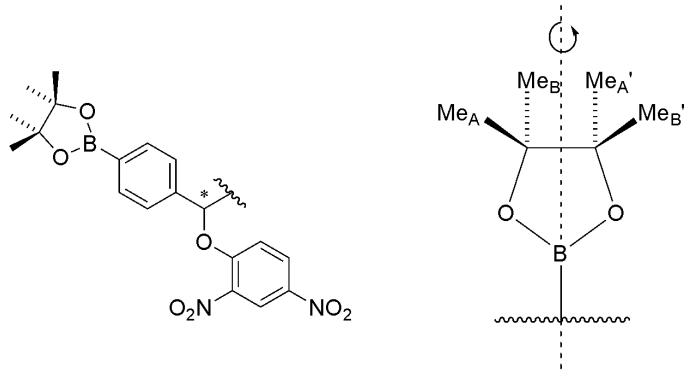

Fig.51: Diastereotopicity in MitoDNP-SUMs **292**/**304** and caged-DNP precursors

Surprisingly, chemical shift differences due to the presence of the chiral centre are also apparent in the remote methylene unit directly attached to phosphorus in MitoDNP-SUM(1) **292**. As this phenomenon is not observed in any of the other linking units, this must result from the manner in which the molecule folds in solution. An explanation for this is that the TPP group is held close enough to the chiral centre for the diastereotopicity to be observed, in a conformation perhaps resulting from a combination of the DNP unit π-stacking with the xylyl group and of dipole-dipole interactions between TPP and the oxygen atoms of the nitro groups of the DNP moiety. This may result in differential folding of the TPP unit towards either the front or rear faces of the DNP moiety which could potentially be influenced by π-stacking interactions between aryl units (Fig.52).

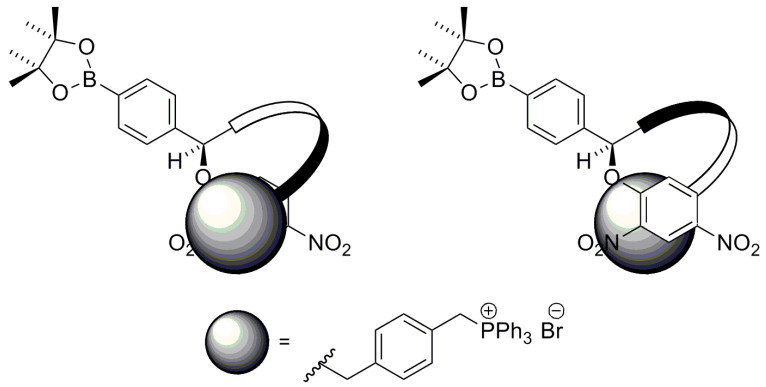

Fig.52: Possible folding in MitoDNP-SUM(1) **292**

7.12 SUM and MitoSUM stabilities and responsiveness to H_2O_2

The abilities of MitoDNP-SUMs **292** and **304** to release DNP **201** in response to H_2O_2 was assessed under *pseudo*-physiological conditions at both cytosolic pH (7.4) and mitochondrial matrix pH (8.0) at 37 ºC and were compared to the response of the untargeted DNP-SUM **210**. The stabilities of the three compounds under testing conditions were also assessed.

Initially the linearity of DNP **201** absorption (λ_{abs} = 410 nm) with increasing concentration was assessed in KHE buffer (Appendix 2):MeCN (3:1) at pHs 7.4 and 8.0 (Figs.53-55) and found to hold up to and including 60 μM DNP **201**. Towards 100 μM DNP **201**, absorption approaches 1 and linearity is lost. As a result, the maximum concentration of DNP **201** that could be released in the following experiments (assuming a 1:1 reaction stoichiometry and 100% conversion of H_2O_2) was kept below 60 μM. At both pHs the vast majority of DNP **201** is present in its anionic form and thus no significant difference in absorption is observed with a linear regression slope of 0.00946 ± 0.00008 for pH 7.4 and 0.00953 ± 0.00026 for pH 8.0 (Fig.55). Furthermore the presence of two equivalents of H_2O_2 had no impact on the absorption of DNP **201** (Orange and yellow graph lines, Figs.53 and 54). Absorption spectra graphs are truncated at 250 nm due to strong MeCN absorption below this wavelength.

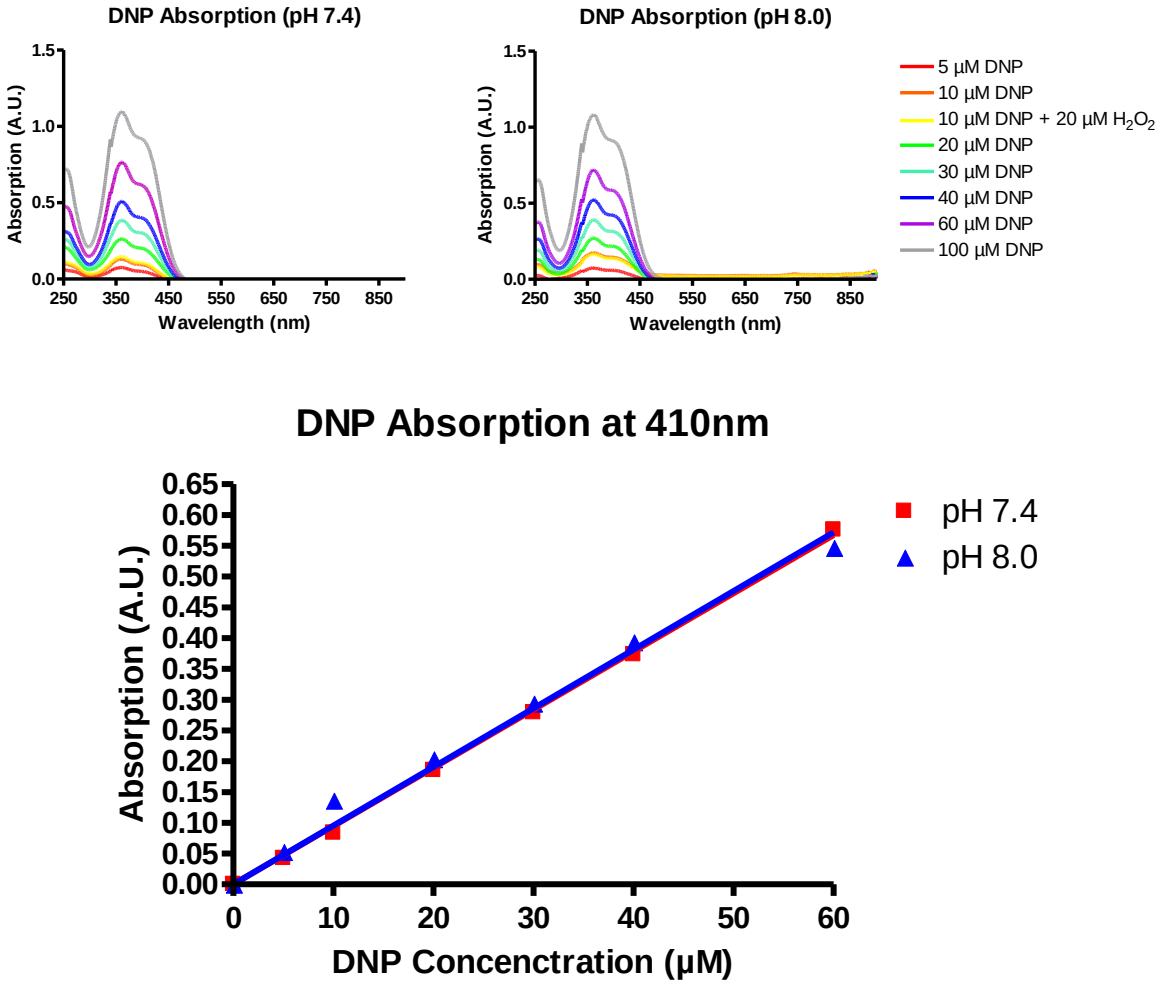

Figs.53-55: Linearity of DNP **201** absorption in KHE/MeCN buffer systems (n = 1)

In the following studies all time courses (TCs) were conducted over 2000 s with a full absorption spectrum scanned over 7 mins (100 nm min^{-1}, 900-200 nm) immediately afterwards. The following data presented are graphs of the spectral scans after each TC to monitor DNP **201** release. Corresponding TC graphs for MitoDNP-SUM(1) **292** and MitoDNP-SUM(2) **304** decomposition can be found in appendix 3 (Figs.83-86). Subsequent TCs began straight after completion of the preceding spectral scans. Probe concentrations of 200 µM were used to give *pseudo*-first order conditions. Additions of H_2O_2 noted in figure legends were added from freshly titrated stock solutions, followed by short inversion mixing prior to commencing TCs.

It was found that no decomposition of DNP-SUM **210** was observed at either pH 7.4 or 8.0, as spectra after TC1 and TC2 perfectly overlap (~1.4 h total incubation time, red and orange graph lines, Figs.56 and 57). Upon addition of H_2O_2, DNP **201** release was observed by monitoring the increased absorption at 410 nm while there was a decrease in

probe absorption maximum at 297 nm. The initial rapid jump in DNP **201** release slowed down over time as H_2O_2 was consumed.

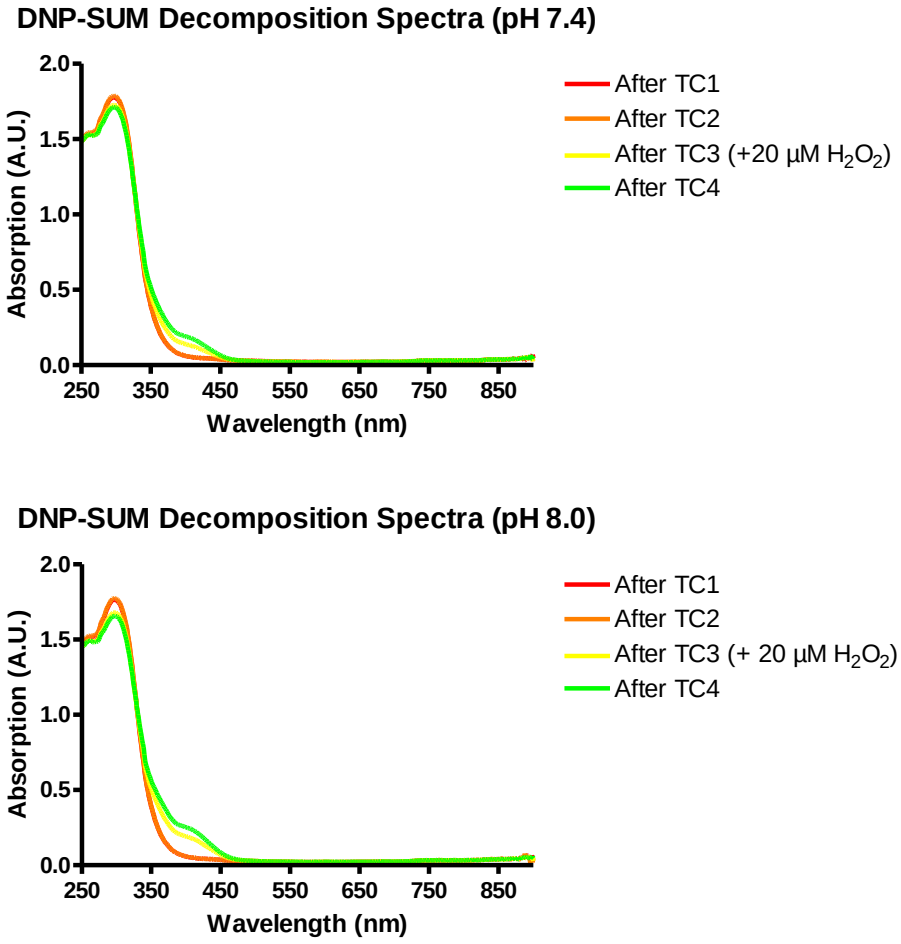

Figs.56 and 57: DNP-SUM **210** decomposition and reaction with H_2O_2

At pH 7.4, MitoDNP-SUM(1) **292** showed only very minor decomposition while MitoDNP-SUM(2) **304** gave a slow but steady, spontaneous release of DNP **201** (Figs.58 and 59, TCs 1-4). It is hypothesised that the greater instability of MitoDNP-SUM(2) **304** is due to the close proximity of the TPP moiety which can assist the leaving of the DNP anion **202** by stabilising the charge generated in the transition state. After more than 2.5 h incubation, both compounds still gave a rapid DNP **201** release upon addition of H_2O_2, the rate of which slowed as H_2O_2 was consumed (Fig.58, TCs 5 and 6) or gave an approximately linear step increase upon a subsequent H_2O_2 addition (Fig.59, TCs 5 and 6). Both probes display a λ_{abs} maximum at 300 nm which decreases as the reaction with H_2O_2 proceeds.

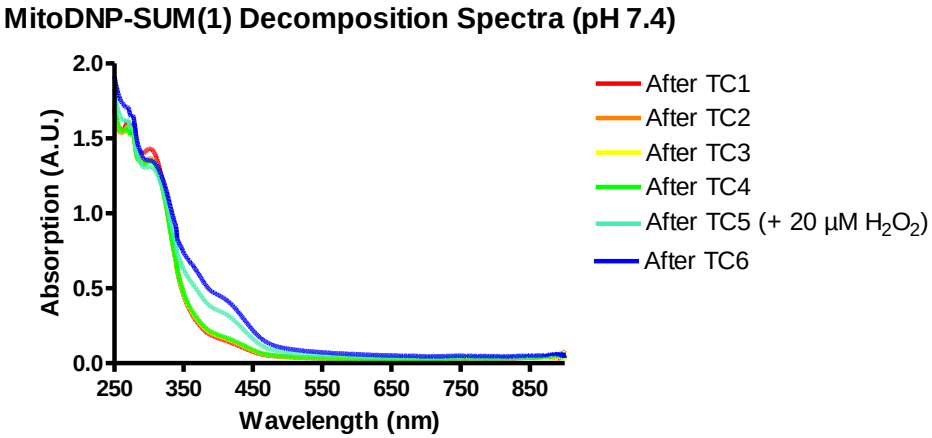

Fig.58: MitoDNP-SUM(1) **292** decomposition and reaction with H_2O_2

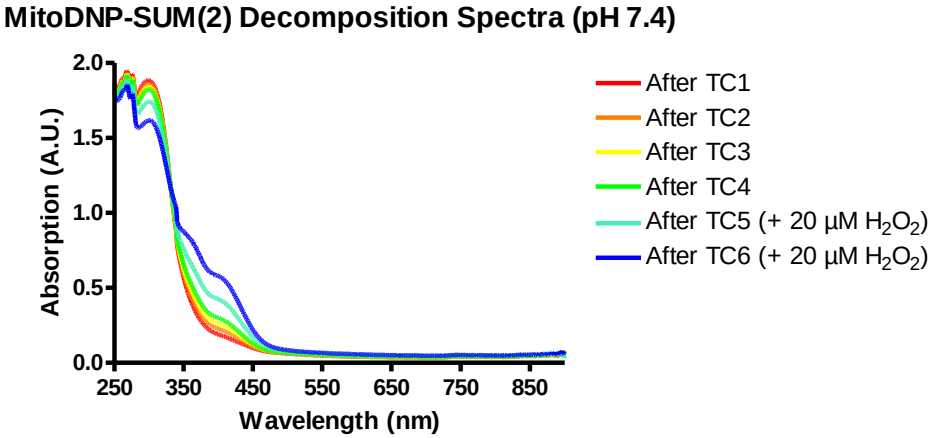

Fig.59: MitoDNP-SUM(2) **304** decomposition and reaction with H_2O_2

Significant decomposition of both MitoDNP-SUMs **292** and **304** occurred at pH 8.0 (Figs.60 and 61). Decomposition rates remained steady for the duration of the tests (over 2.5 h) and were faster than the corresponding rates measured at pH 7.4.

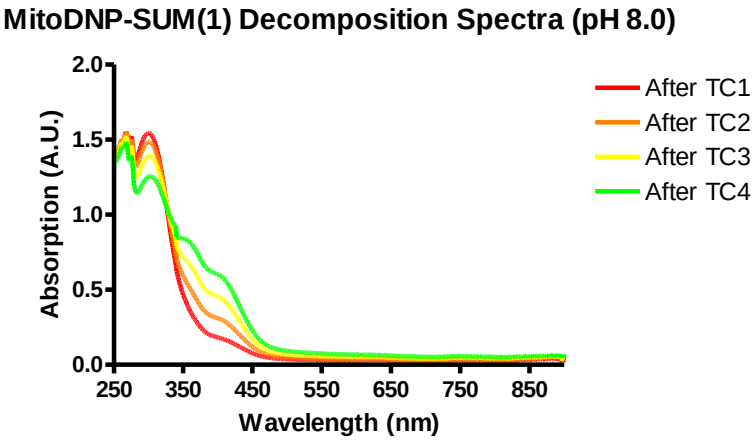

Fig.60: MitoDNP-SUM(1) **292** decomposition

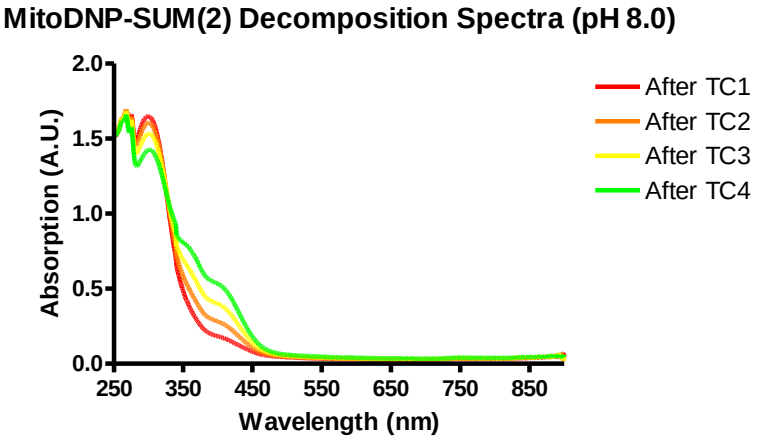

Fig.61: MitoDNP-SUM(2) **304** decomposition

From the apparent pH dependence of non-H_2O_2 initiated breakdown, it was therefore hypothesised that the spontaneous DNP **201** release is occurring due to the reversible attack at boron from hydroxide (Scheme 97), which is at a higher concentration at elevated pH. This would convert the electron-withdrawing boronate group into an electron-donating group with sufficient electron density to allow unimolecular fragmentation to occur, releasing DNP **201** in its anionic form **202**. The methylene group adjacent to the uncoupling molecule attachment site may stabilise the cationic character formed in the intermediate through hyperconjugation. This appears to be important for breakdown as no decomposition is observed in the case of the primary attachment site (DNP-SUM **210**, Fig.57). Therefore future MitoSUM target molecules would be envisaged to incorporate a primary attachment site for the leaving group with the targeting moiety attached *via* a short aliphatic chain linked to the aryl ring of the arylboronate unit.

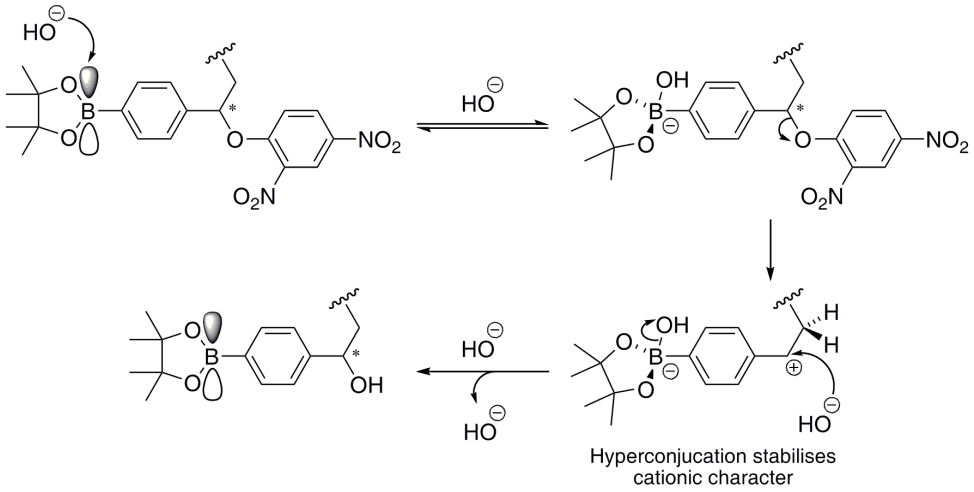

Scheme 97: pH dependent breakdown of MitoSUMs

MitoDNP-SUMs **292** and **304** were also assessed to determine as to whether or not they could react proportionally in response to varying levels of H_2O_2. Probes were exposed to specified concentrations of H_2O_2 and incubated for 2000 s after which a full spectral scan was taken. To account for spontaneous decomposition, MitoDNP-SUMs **292** or **304** were included in the reference cuvette throughout. Even with the elevated decomposition at pH 8.0, both probes responded to H_2O_2 addition and as predicted, with increasing H_2O_2 leading to an increased DNP **201** release (Fig.62 and 63).

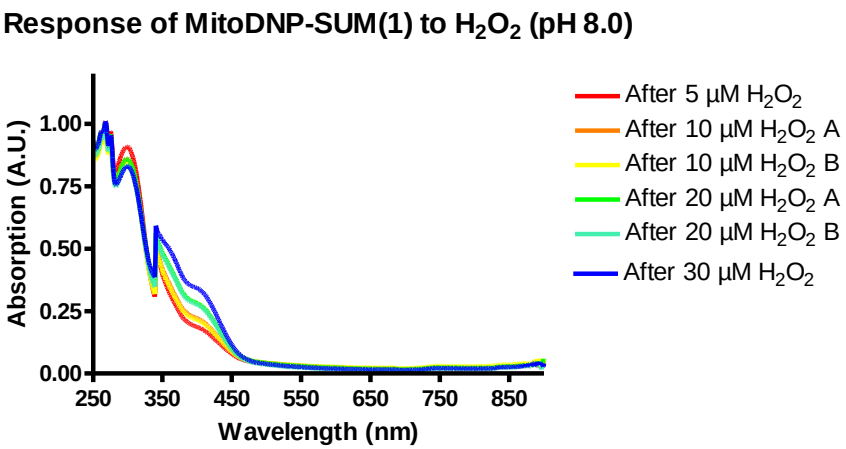

Fig.62: Responsiveness of MitoDNP-SUM(1) **292** to H_2O_2

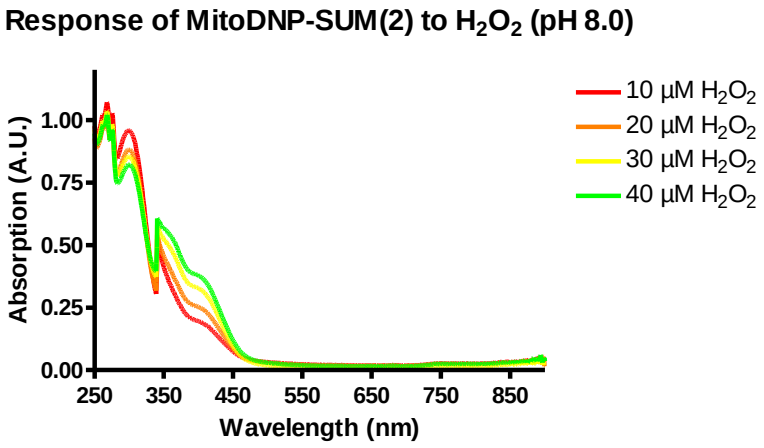

Fig.63: Responsiveness of MitoDNP-SUM(2) **304** to H_2O_2

Therefore MitoDNP-SUMs **292** and **304** have been shown to release DNP **201** upon reaction with H_2O_2 and are responsive to H_2O_2 concentrations under *pseudo*-physiological conditions. The above data are preliminary results with further replicates required for statistical analyses to be conducted.

It is proposed that mitochondria-targeted arylboronate esters containing a *para*-leaving group analogous to the MitoSUMs discussed above could potentially be used as a slow release mechanism for drugs designed to target mitochondria. The compounds would be more stable in the circulation and cytosol but slowly release their payload molecules in the mitochondrial matrix due to the elevated pH. For example, one such application may be the targeting of anti-cancer agents as cancer cells almost ubiquitously have elevated $\Delta\Psi_m$ and some also have elevated $\Delta\Psi_p$, which could be used to derive some degree of selectivity for delivery of chemotherapy agents to cancer cells over healthy cells.[164] It is also thought that perturbing this increased $\Delta\Psi_m$ may be a way to combat uncontrolled cell division, in part through the depletion of ATP **5**.

Chapter 8: MitoDNP-SUMs : Preliminary biological results

Biological studies were conducted at the Buck Institute for Research on Aging (Novato, CA, USA) in the laboratory of Professor Martin Brand with the assistance of Dr Casey Quinlan.

All of the biological tests herein were conducted on mitochondria isolated from rat skeletal muscle (Appendix 4). Muscle tissue is commonly chosen for studies on isolated mitochondria as it contains large numbers of mitochondria compared to many other tissue types, due to the need for sufficient local energy stores to allow the muscle to respond quickly to the need to perform work. Furthermore, alternatives such as liver mitochondria possess heightened levels of peroxidase enzymes which could result in the breaking down of H_2O_2 prior to its reaction with MitoDNP-SUMs **292** or **304** which could affect the results of these studies. All tests were conducted at physiological temperature (37 ºC) in either potassium (KHE) or sucrose based buffers (MAS1 or SHEP, Appendix 2).

Over the course of biological studies, the abilities of MitoDNP-SUMs **292** or **304** to behave as designed in a physiological environment were investigated. For example, could the probes:

i) Accumulate within the matrix of isolated mitochondria as a result of $\Delta\Psi_m$.
ii) React with endogenous H_2O_2 resulting in the release of the mitochondrial uncoupling molecule DNP **201**.
iii) Release sufficient DNP **201** to uncouple mitochondria.
iv) Reduce ROS production by reducing $\Delta\Psi_m$ as a result of mitochondrial uncoupling.
v) Self-limit DNP **201** release. Firstly as reducing ROS production would reduce H_2O_2 production which is required to trigger DNP **201** release and secondly by reducing $\Delta\Psi_m$, the compound could redistribute out of the mitochondrial matrix, reducing the rate of the trigger activation reaction.
vi) Control ROS production to reduce oxidative stress at a cellular level, slowing the onset of age-related diseases.

In initial biological testing, MitoDNP-SUM(2) **304** exhibited a poor stability profile in the biological systems, consistent with results previously discussed (Chapter 7.12, Figs.59 and 61). Therefore, the data presented hereafter relates solely to MitoDNP-SUM(1) **292** which was sufficiently stable for an evaluation of probe functions to be made.

A number of biologically active compounds are incorporated into the following biological experiments to modify the behaviour of the electron transport chain, including rotenone **316** (complex I inhibitor), antimycin A **317** (complex III inhibitor), oligomycin A **318** (ATPase inhibitor) and nigericin **319** (proton and potassium ion antiporter) (Fig.64). Rotenone **316** inhibits complex I by preventing electron transfer from the Rieske iron-sulphur centres to coenzyme Q **1** by reversibly binding to the ubiquinone binding site. Antimycin A **317** inhibits complex III by binding irreversibly to the Q_i site, preventing ubiquinone reduction. The inhibition of complex I or III impacts the ability to generate $\Delta\Psi_m$ as protons are no longer pumped into the IMS by the inhibited protein complex. Oligomycin A **318** inhibits ATPase by blocking the proton channel. Nigericin **319** addition results in the electroneutral exchange H^+ and K^+ ions across the MIM, resulting in the removal of the pH gradient component of the protomotive force.

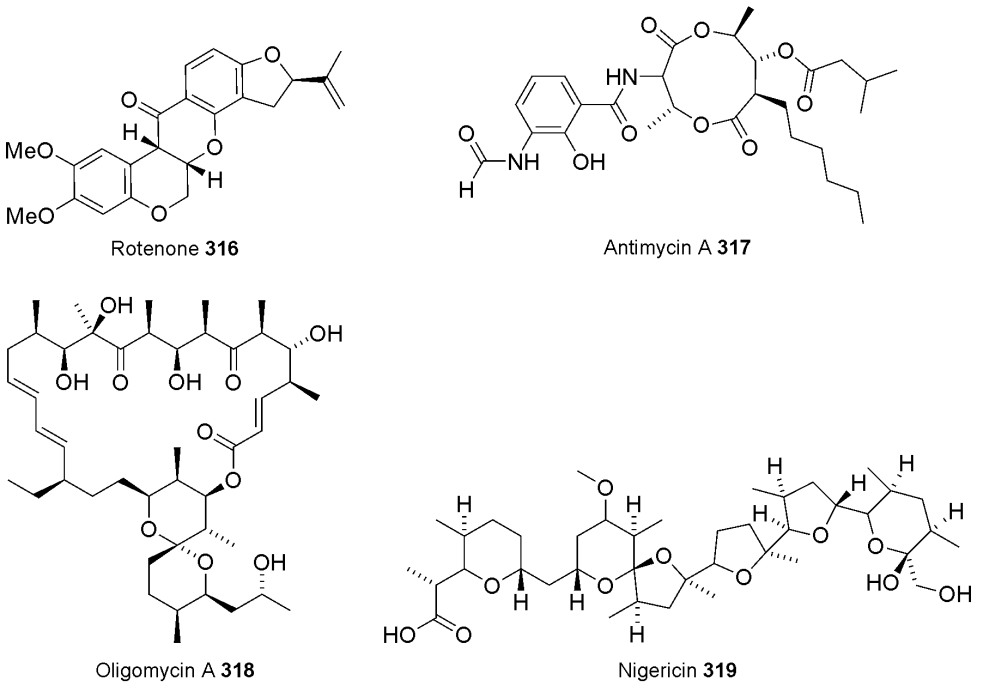

Fig.64: Structures of bioactive molecules incorporated into biological experiments

8.1 Mitochondrial uptake of MitoDNP-SUM(1)

An assessment of MitoDNP-SUM(1) **292** uptake into energised mitochondria was conducted using a MTPP (methyltriphenylphosphonium, aka TPMP) electrode which measures the voltage in the buffer across a semi-permeable membrane. The experimental set-up also allows for simultaneous measurements of oxygen concentration to be taken by a Clark electrode. Initial studies were conducted using potassium based buffer (KHE) but later repeated in a simplified sucrose based buffer (SHEP).

Analogous to the uptake experiment previously shown for MitoB **134** (Fig.31) or reference MTPP (Fig.65), MitoDNP-SUM(1) **292** would be added portionwise (five additions) to obtain a logarithmic calibration curve. This could be done with or without isolated mitochondria being present in the system from the start of the experimental calibration. In the latter case, the addition of mitochondria mid-experiment gives an indication of the level of non-specific lipophilic uptake (drop in voltage). In either case, the initiation of the electron transport chain *via* the addition of a substrate such as succinate or glycerol phosphate establishes a $\Delta\Psi_m$ and any lipophilic cations would accumulate in the mitochondrial matrix, resulting in a corresponding drop in voltage readings as the cations are removed from the bulk buffer. Using the calibration curve it is possible to determine the level of cation uptake into the mitochondrial matrix. Finally the addition of the strong mitochondrial uncoupling molecule FCCP **33** would dissipate the $\Delta\Psi_m$, releasing the cations back into the buffer solution. Experiments are generally run in a closed-system in which a finite amount of oxygen is present, allowing mitochondrial respiration rates to be monitored at different stages of the experiment. However in a closed system, mitochondria must be present throughout the entire experiment as late addition is not possible.

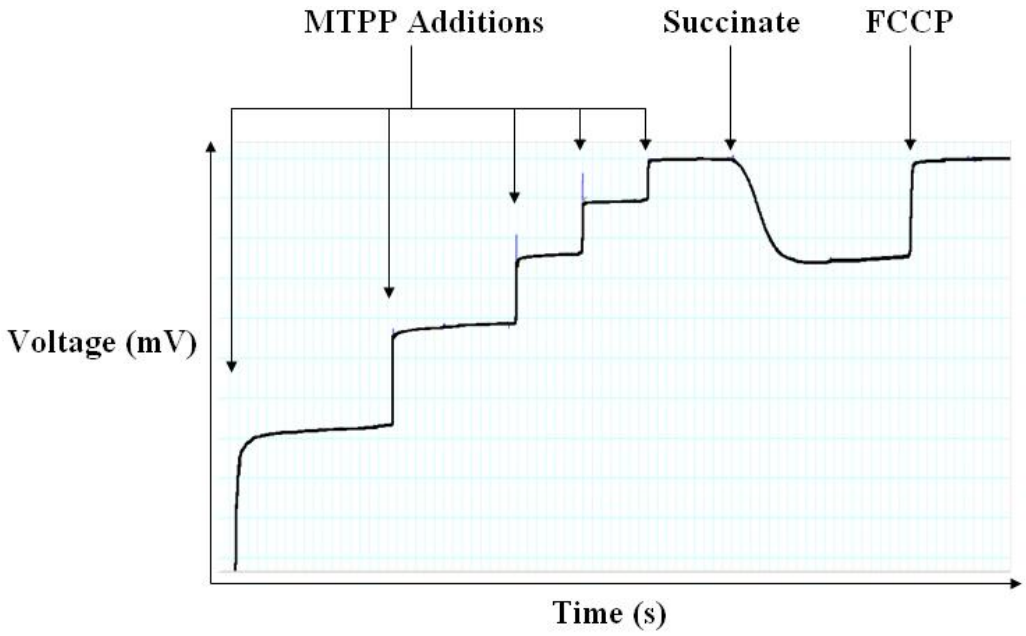

Fig.65: Representative of an optimal TPP salt uptake experiment graph (Closed system)

The MTPP electrode gave a very slow response to MitoDNP-SUM(1) **292** additions (particularly at higher doses) (Figs.66 and 67) compared to the reference MTPP (Fig.65) itself (min vs s). Lower additions (0.1-0.5 µM) gave significantly sharper responses, however the reduced magnitude of the voltage change resulted in increased signal noise. Addition of DNP **201** or FCCP **33** should release the probe by depleting the $\Delta\Psi_m$, however upon uncoupler addition the voltage readings gave an inconsistent response (falling/rising/ falling then rising/having no change). This phenomenon is likely related to the high lipophilicity of the probe and its binding to the electrode, experimental cell walls and/or the mitochondrial membranes, although the exact reasons were not confirmed. Similar issues have been observed by other research groups using this experimental set-up with lipophilic compounds, including Asin-Cayuela *et al* during the investigation of lipophilic analogues of MitoQ **29**.[60] Furthermore MTPP-electrode drift issues with these handmade electrodes are not uncommon and can change direction and magnitude between runs or even within a single run.

Once mitochondria are isolated from cells, their health deteriorates and can be used for 4-6 h after isolation if stored in highly concentrated stock solutions on ice. Once in dilute buffer solutions this degradation is accelerated which can affect test results. As the electrodes took a relatively long time to settle after MitoDNP-SUM(1) **292** additions, an experiment was run in an open system to allow mitochondria to be added during the experiment to prevent significant deterioration due to prolonged periods spent in the dilute buffer at 37 °C while the electrode stabilised. This allowed the observation of both initial

lipophilic uptake of MitoDNP-SUM(1) **292**, followed by active uptake after mitochondrial energisation by succinate (Fig.66). This showed that the probe was driven into the mitochondrial matrix by the $\Delta\Psi_m$ as designed but release upon de-energisation using mitochondrial uncoupler FCCP **33** was unsuccessful.

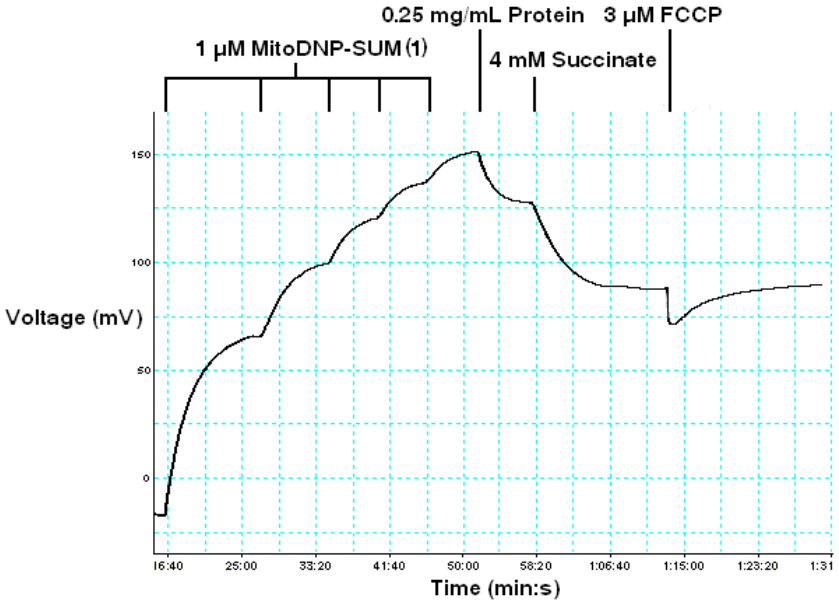

Fig.66: Open system: KHE buffer, 0.25 mg mL^{-1} protein, 1% BSA, pH 7.4, 5 µM rotenone **316**, 1 µg mL^{-1} oligomycin A **318**, 1 µM nigericin **319**.

Next, a closed system experiment was conducted in which mitochondria were present from the start (Fig.67). As a result of the slow electrode response to probe additions, only two calibration steps were made to prevent extensive mitochondrial deterioration. Upon energisation, $\Delta\Psi_m$ driven uptake was again observed. In this experiment the mitochondria present are allowed to consume all of the oxygen in the system. The resulting anaerobic conditions cause the mitochondria to become de-energised and this was observed to trigger probe release from the mitochondrial matrix.

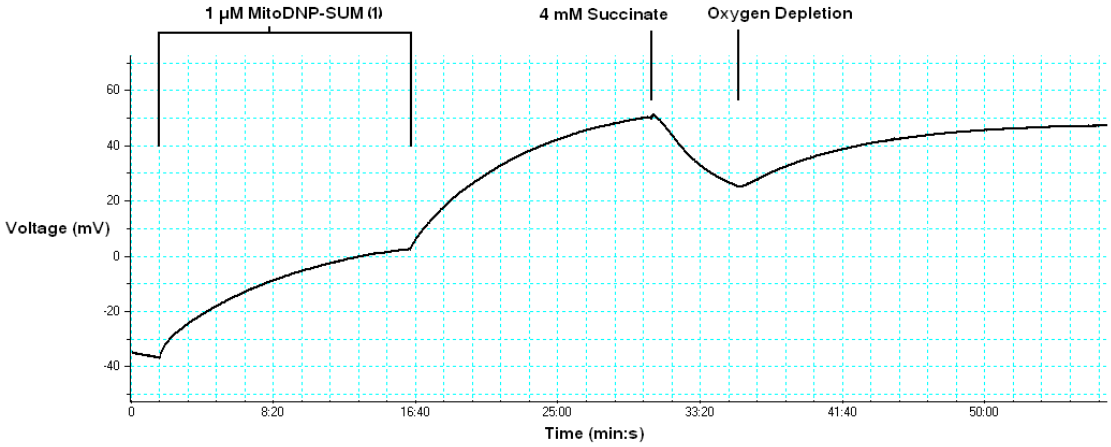

Fig.67: Closed system: KHE buffer, 0.25 mg mL^{-1} protein, 0.5% BSA, pH 7.4, 5 µM rotenone **316**, 1 µg mL^{-1} oligomycin A **318**, 110 nM nigericin **319**.

These uptake experiments have shown that MitoDNP-SUM(1) **292** is actively taken up into energised mitochondria due to the DLC targeting group and that depletion of the $\Delta\Psi_m$ caused by oxygen depletion releases the probe back into the buffer as designed.

8.2 The impact of MitoDNP-SUM(1) on mitochondrial ROS production rates

Experiments to determine the impact of MitoDNP-SUM(1) **292** on mitochondrial ROS production rates were conducted measuring changes in fluorescence using an Amplex UltraRed (Invitrogen, 50 µM, λ_{ex} = 563 nm, λ_{em} = 587 nm) and horseradish peroxidise (HRP, 5 U mL^{-1}) system.[165] Amplex UltraRed is a fluoregenic substrate for HRP, an enzyme which utilises H_2O_2 in a 1:1 stoichiometry to oxidise the substrate into Amplex UltroxRed, leading to a large increase in fluorescence at the λ_{em}. The exact structures of Amplex UltraRed and Amplex UltroxRed are unpublished but will likely be closely related to the structures of Amplex Red **320** (Invitrogen) and its oxidisation/deacetylation product resorufin **321** (Scheme 98). These fluorophores are particularly suited to biological systems as they emit red-fluorescence, resulting in little interference from blue or green autofluorescence occuring from natural biomolecules.

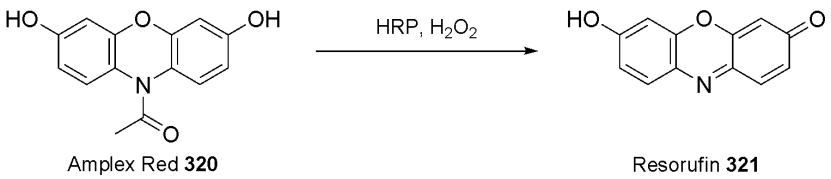

Amplex Red **320** Resorufin **321**

Scheme 98: Oxidation and fluorescence activation of Amplex Red **320** by HRP/H_2O_2

As the above system reports solely on H_2O_2 concentrations, excess superoxide dismutase (25 U mL^{-1}) was added to rapidly convert any $O_2^{\bullet-}$ generated by the system into H_2O_2 through a disproportionation reaction, to give a more accurate read on overall ROS production levels.

8.2.1 Membrane potential dependent ROS production

The following ROS experiments (Chapters 8.2.1 and 8.2.2) were conducted in SHEP buffer (pH 7.4), with 0.3 mg/mL protein (2 mL total cuvette volume) at 37 °C and used succinate (5 mM) as the mitochondrial substrate. Succinate addition after 1-2 min is readily observable by the immediate sharp increase in fluorescence (Figs.68-70 and 72) and MitoDNP-SUM(1) **292** or DNP **201** additions are subsequently made to the relevant runs between 4-5 min. After this any changes in the rate of fluorescence increase can be observed in the change in slope of the signal. All results in chapters 8.2.1 and 8.2.2 are preliminary and require further replication to obtain statistically analysed data sets.

Initially the ability of MitoDNP-SUM(1) **292** to reduce mitochondrial membrane dependent ROS production (combined $O_2^{\bullet-}$ and H_2O_2 production monitored as H_2O_2 using SOD/HRP/Amplex UltraRed system) as designed was assessed. In this experiment succinate would generate the $\Delta\Psi_m$ causing probe uptake into the mitochondrial matrix. Dissipation of the $\Delta\Psi_m$ through ATPase is prevented through inhibition by oligomycin A **318** (14.5 μg mL^{-1}). Therefore any significant lowering of $\Delta\Psi_m$ would result solely from DNP **201** released from MitoDNP-SUM(1) **292** uncoupling the mitochondria. Rotenone **316** inhibits electron transfer between Fe-S centres of complex I, resulting in a build up of electrons on $FMNH_2$ co-factors (the proportion of which is set by the $NADH/NAD^+$ ratio), and hence endogenously generated ROS is produced in the form of $O_2^{\bullet-}$.[166] H_2O_2 generated by SOD would react with the boronate moiety of the probe, triggering DNP **201** release which would then reduce $\Delta\Psi_m$ and therefore ROS production.

It was found that under these conditions MitoDNP-SUM(1) **292** reduced ROS production rates as seen by the reduced rates of fluorescence increase (Fig.68). Furthermore increasing the MitoDNP-SUM(1) **292** dose, increased the drop in ROS production rates consistent with increased mitochondrial uncoupling due to an increased DNP **201** concentration being released into the system.

Impact of MitoDNP-SUM(1) on $\Delta\Psi_m$ Dependent ROS

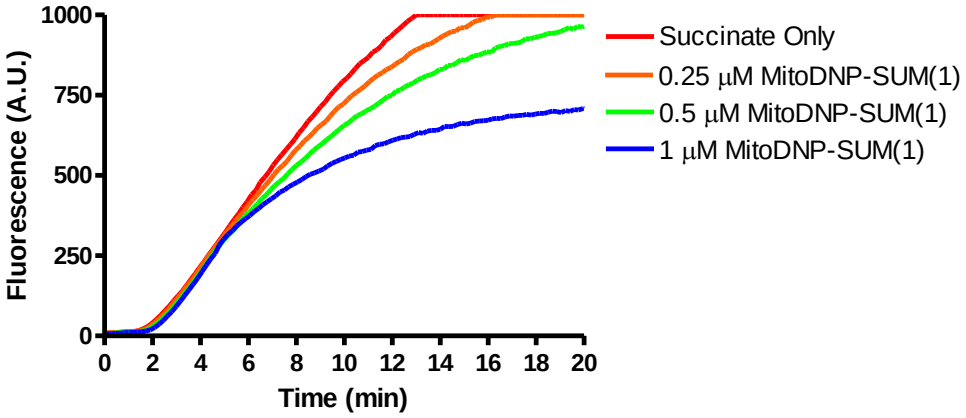

Figs.68: Impacts of MitoDNP-SUM(1) **292** on $\Delta\Psi_m$ dependent ROS

In comparison, the ability of free DNP **201** to moderate $\Delta\Psi_m$ was found to be significantly lower (Fig.69) than that of MitoDNP-SUM(1) **292** (Fig.68) under these conditions even at elevated concentrations. This is because the bulk of the DNP **201** will remain in the buffer as there is no force driving the uncoupler to the site of action while in the case of MitoDNP-SUM(1) **292**, DNP **201** is released directly into the mitochondrial matrix where it acts as an uncoupler.

Impact of DNP on $\Delta\Psi_m$ Dependent ROS

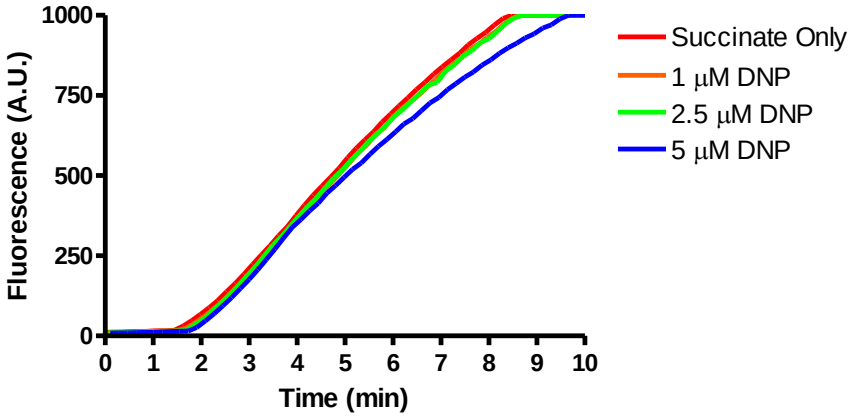

Figs. 69: Impacts of DNP **201** on $\Delta\Psi_m$ dependent ROS production rates

8.2.2 Membrane potential independent ROS production

To confirm that the reduction in ROS production rates previously observed through MitoDNP-SUM(1) **292** addition resulted solely from mitochondrial uncoupling and not from an unpredicted inhibition of mitochondrial machinery, two control experiments were conducted. Firstly an experiment was set up containing rotenone **316** (2 μM) and anitmycin A **317** (2 μM) to generate ROS, predominantly from complex III after succinate oxidation. As both complexes I and III are inhibited, no $\Delta\Psi_m$ can be established as protons cannot be pumped into the IMS. Therefore the ROS produced by this system is independent of $\Delta\Psi_m$. Addition of MitoDNP-SUM(1) **292** was found to have no impact on ROS production rates (Fig.70), even at concentrations higher than previously used.

Impact of MitoDNP-SUM(1) on $\Delta\Psi_m$ Independent ROS

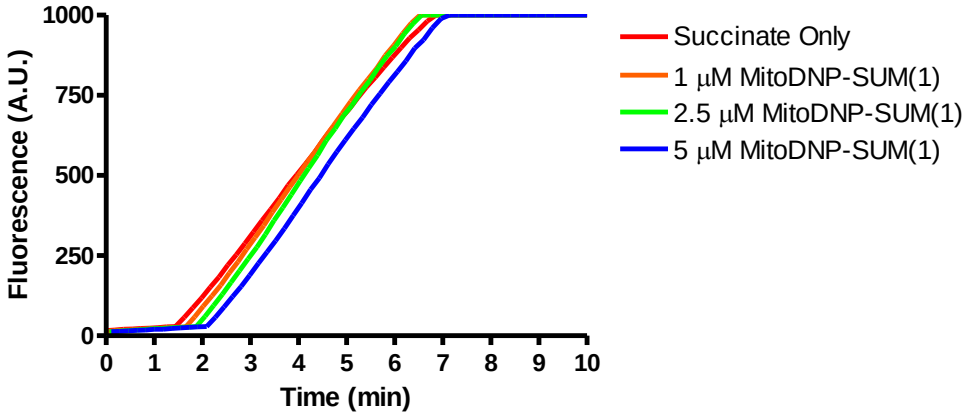

Fig.70: MitoDNP-SUM(1) **292** has no impact on $\Delta\Psi_m$ independent ROS

Secondly, to ensure that the lack of impact that MitoDNP-SUM(1) **292** had on the membrane potential independent ROS system above was not simply due to lack of compound uptake, $\Delta\Psi_m$ was generated *via* the reverse running of ATPase while using the same ROS producing conditions (Fig.71). This system converts excess ATP **5** into ADP **4** with the concomitant pumping of three protons from the mitochondrial matrix through ATPase into the IMS for each molecule of ATP **5** hydrolysed, establishing $\Delta\Psi_m$. To set up these conditions, excess ATP **5** (1 mM) is added while the additions of creatine kinase (20 U mL^{-1}) and an excess of phosphocreatine **322** (10 mM) regenerate ATP **5** from any ADP **4** produced (Scheme 99), which can then be rehydrolysed by ATPase to maintain $\Delta\Psi_m$.

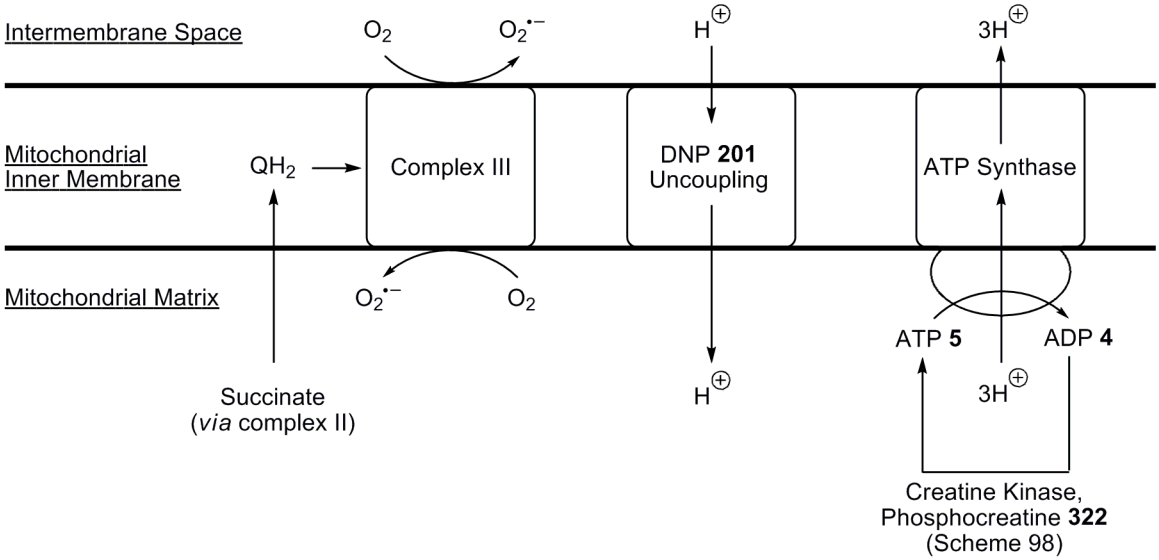

Fig.71: Reverse running of ATPase can be used to generate a $\Delta\Psi_m$

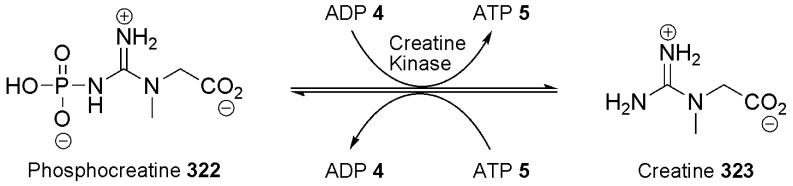

Scheme 99: Creatine Kinase and excess phosphocreatine **322** maintain high ATP **5** levels

As predicted under these conditions, MitoDNP-SUM(1) **292** was once again found to have no impact on $\Delta\Psi_m$ independent ROS production rates (Fig.72) despite probe uptake into the mitochondrial matrix.

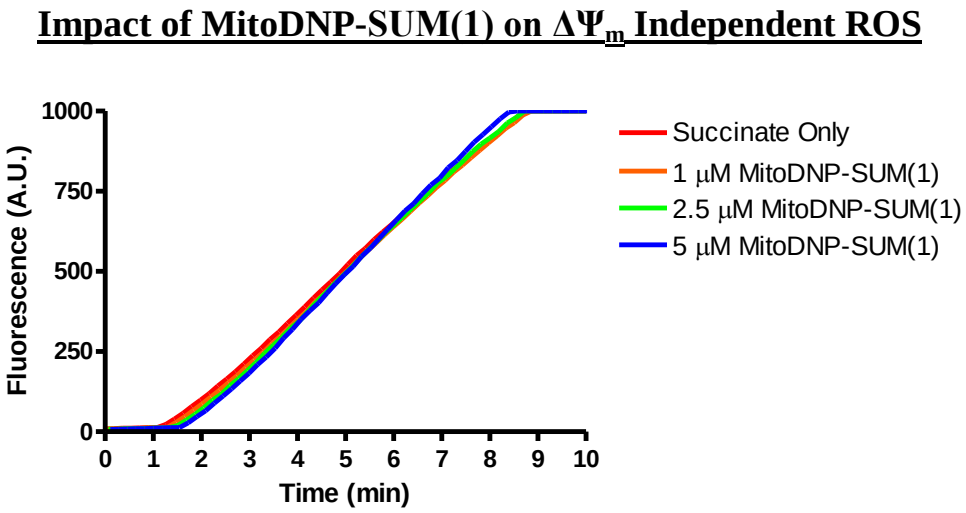

Fig.72: MitoDNP-SUM(1) **292** has no impact on $\Delta\Psi_m$ independent ROS

8.2.3 High versus low level ROS production

A key design of the MitoSUMs is that they should only modulate misbehaving mitochondria with high ROS production, but not uncouple healthy mitochondria. An investigation into the ability of MitoDNP-SUM(1) **292** to produce different levels of uncoupling depending on to varying levels of endogenous ROS was conducted by Dr Casey Quilan using a Seahorse XF24 analyzer. This microplate reader allows for the simultaneous monitoring of oxygen concentration and pH over the course of an experiment.

Parallel experiments with mitochondria possessing identical $\Delta\Psi_m$ (to ensure equal probe uptake) but varying in their ROS production rates were required to show any performance differences for the probe between high and low ROS conditions. To do this, the reverse ATPase system discussed previously (Chapter 8.2.2) was employed to maintain $\Delta\Psi_m$ while conditions with or without succinate yielded high (~1.4 nmol H_2O_2/min/mg protein) and low (~0.05 nmol H_2O_2/min/mg protein) ROS producing systems respectively.

During ATP **5** hydrolysis, protons are liberated resulting in a net acidification of the system. A greater degree of mitochondrial uncoupling results in increased ATP **5** hydrolysis and hence increased acidification of the system. Therefore the level of uncoupling resulting from any DNP **201** released from MitoDNP-SUM(1) **292** following reaction with H_2O_2 can be monitored as the rate of acidification of the buffer medium.

MitoDNP-SUM(1) **292** exhibited a dose dependent uncoupling response at both low and high ROS conditions (Fig.74). At low concentrations (10 μM) there was no difference between the differing ROS levels or from the DNP **201** control. This could potentially result from a number of factors such as free DNP **201** being present in the stock solution, or a high sensitivity to either low amounts ROS or to the mitochondrial matrix conditions (ie. pH, enzymes or biomolecules). However at higher concentrations (20 or 40 μM) MitoDNP-SUM(1) **292** exhibited a significant ROS-dependent uncoupling profile in line with DNP **201** controls, suggesting that high ROS conditions can lead to complete release of the uncoupler from the MitoSUM construct with only partial release in low ROS conditions. 40 μM DNP **201** was found to give the maximum uncoupling rates under these test conditions.

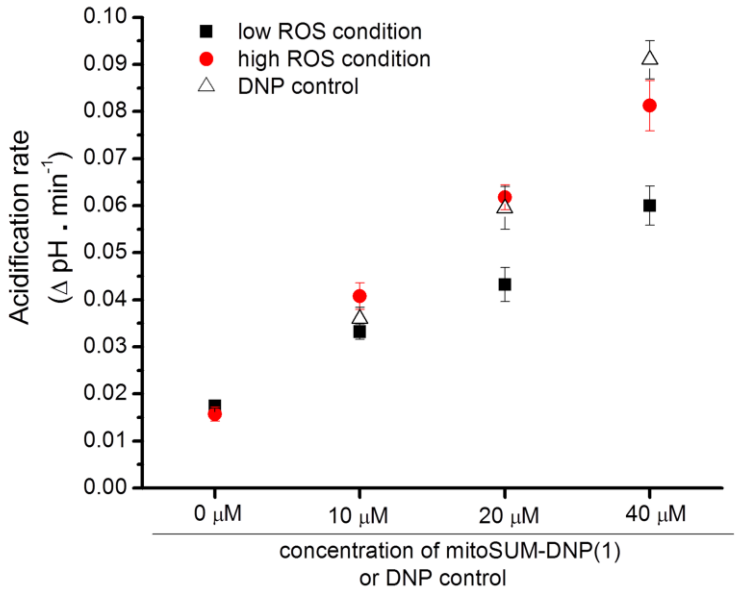

Fig.74: MitoDNP-SUM(1) **292** displays ROS dependent uncoupling

8.3 Conclusions

A number of the tenets proposed for the MitoSUMs project (Chapters 7-8) have been successfully proven. Firstly, it has been shown that MitoDNP-SUM(1) **292** will accumulate in the matrix of isolated energised mitochondria in response to $\Delta\Psi_m$ (as a result of the DLC targeting group) and that it will be subsequently be released upon de-energisation brought about by oxygen depletion (Chapter 8.1).

Secondly it has been demonstrated through spectrometric techniques that Mito-SUMs **292** and **304** react with exogenous H_2O_2 to release the uncoupling molecule DNP **201** in a dose dependent manner under *pseudo*-physiological conditions (Chapter 7.12). It was observed that the stability of both probes, particularly MitoDNP-SUM(2) **304**, deteriorates in increasingly basic environments but that this issue may be overcome by a structural modification to a primary benzylic attachment site for the uncoupling molecule (as in DNP-SUM **210**) instead of a secondary centre.

Furthermore, biological testing has confirmed that MitoDNP-SUM(1) **292** will release its uncoupling molecule cargo in response to endogenous ROS production, again in a dose dependent manner and that the level of DNP **201** released is sufficient to uncouple mitochondria as measured by acidification rates (Chapter 8.2.3).

Preliminary studies have indicated that the rates of mitochondrial ROS production can be attenuated by addition of MitoDNP-SUM(1) **292** (Chapters 8.2.1-8.2.2) and that this is more effective than free DNP **201** due to targeted delivery of the uncoupling molecule. An impact on ROS production rates was observed on $\Delta\Psi_m$ dependent ROS, consistent with this affect resulting from the modulation of $\Delta\Psi_m$ by the released uncoupling molecule. However, either a Clark electrode experiment measuring the rates of oxygen consumption during respiration or a fluorescence experiment that directly monitor $\Delta\Psi_m$ (ie. Safranin O **66**, Chapter 3.3) should be conducted to confirm this.

To date no evidence has been generated to indicate that the release of DNP **201** from the current MitoSUM constructs is self-limiting and no longer term studies into the affects that MitoSUMs might have on the onset of oxidative stress driven age-related diseases have been conducted. For the next round of MitoSUM compounds it is proposed that the uncoupling molecule attachment site is modified to a primary centre to improve alkaline stability and that a more potent uncoupler such as FCCP **33** be incorporated to reduce concentrations and therefore any potential undesired side-effect caused by high mitochondrial concentrations of DLCs or probe reaction by-products. Finally compound sensitivity towards H_2O_2 and lipophilicity may require optimisation.

Chapter 9: Mitochondria-targeted photo-activatable functional molecules

9.1 Project aims and photo-activation

Although the TPP delivery mechanism can robustly target materials to mitochondria, the challenge of delivering materials selectively to individual mitochondria within cells or tissues at any specific time persists. This is of particular interest as localised subpopulations of mitochondria within cells potentially play unique roles in various cellular mechanisms.[167] Furthermore temporal control of compound delivery to specific mitochondria is vital in developing a detailed understanding for a wide range of cellular pathways and interactions.

Compounds were designed that would accumulate in all mitochondria using the standard TPP delivery mechanism, but would only release their payload molecule after targeted stimulation. This would be achieved by laser induced photo-activation so that caged functional molecules in specific mitochondrial regions of interest could be activated while leaving others unaffected. A number of photo-cleavable protecting groups have been developed,[168] with the most successful based on *o*-nitrobenzyl-type (NB-type)[169,170,171] **324** and coumarin-type[172,173] **325** photo-activatable units.

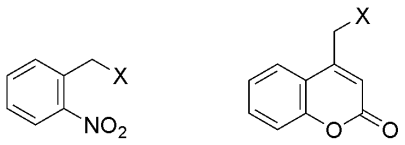

324 **325**

Fig.75: NB-type **324** and coumarin-type **325** photo-cleavable protecting groups (X = Leaving group)

Photo-activatable caged molecules can be irreversibly activated by light irradiation whereby the photo-labile group is permanently cleaved from a payload functional molecule of interest.[168,171] For use in biological systems the ideal caged precursors should be water soluble, stable to hydrolysis and both the probe itself and any photo-activation by-products should be non-toxic. Furthermore photo-activation should occur in high ϕ and at wavelengths >300 nm to minimise light-induced damage to cells.

NB-type **324** linkers are the most extensively employed photo-activatable caging groups and have been used for over three decades in both organic synthesis[174] and biochemistry applications.[175] The λ_{abs} for NB-type **324** units range between ~260-370 nm depending on

aryl substitution patterns with more electron-rich aryl units absorbing at the longer wavelengths albeit with reduced ϕ.[172,173] As normal laser excitation wavelengths range from approximately 330-385 nm, the maximum λ_{abs} for many NB-type **324** molecules (particularly those with electron poorer aromatics) are outside this range.

The exact nature of all photolysis intermediates have not been fully elucidated but it is known that upon irradiation, hydrogen atom abstraction from the benzylic position by the *ortho*-nitro group is followed by rapid tautomerisation (Scheme 100).[171] Subsequent loss of a leaving group is the rate determining step, resulting in the formation of a nitroso-carbonyl by-product **326**.

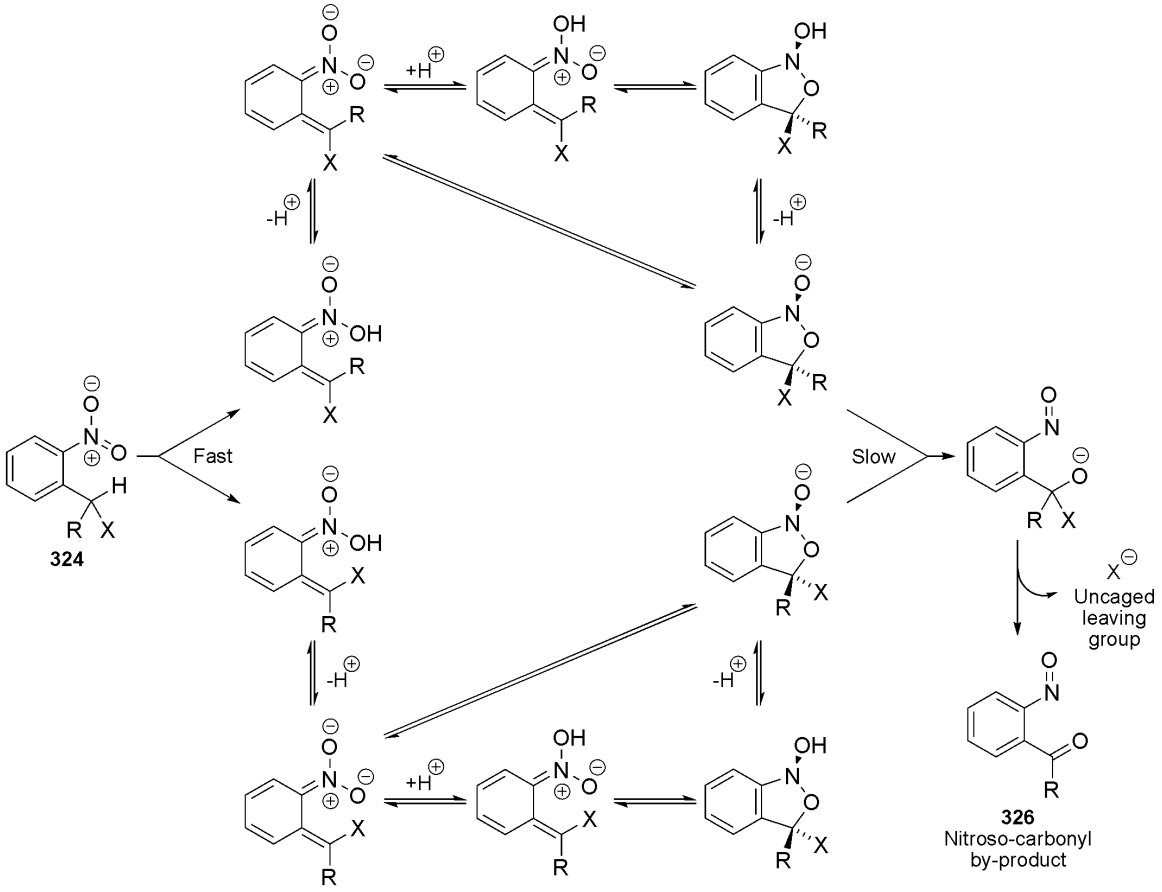

Scheme 100: Proposed NB-type **324** photo-cleavage mechanism

(R = H, alkyl X = Leaving group)

Commonly coumarin-type **325** photo-activatable units often suffer from a low ϕ but benefit from high absorption co-efficients, rapid photo-release and λ_{abs} ranges (~325-400 nm) that extend into the visible region of the electromagnetic spectrum.[171] As a result coumarin-type **325** linkers can be activated by one-photon photolysis using lower energy irradiation than required for NB-type **324** groups and are also potential candidates for

multiple-photon photolysis cleavage probes.[172,176] Activation by multiple photons in the IR region could be beneficial for a number of reasons. Firstly these low energy photons result in less damage to biological systems (in particular DNA) and have greater penetration due to their longer wavelength. In single-photon excitation, any absorbing molecule in the photons path will be excited regardless of depth until the light is completely absorbed and the probability of any scattered light resulting in a photo-activation event is high. In contrast, two-photon excitation will only occur at the focal point of both photon beams at which the combined energy is sufficient to activate the molecule (Fig.76, orange regions represent emission or uncaging events).[177]

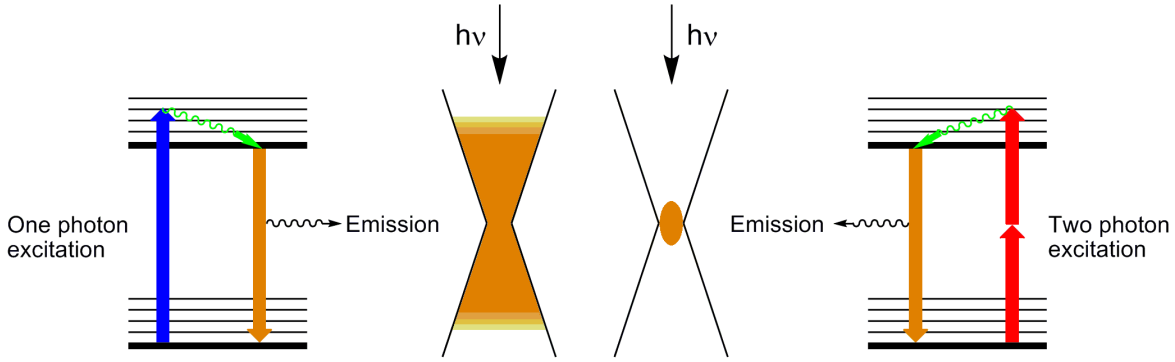

Fig.76: Two-photon excitation gives increased spatial precision for photo-activation

This could allow significant improvements in spatial selectivity in releasing bioactives as has been used for fluorescence based studies. The success of any such system will rely on the uncaging cross section of the molecule which is a product of the cross-section for two-photon absorption and the subsequent quantum yield of the uncaging process.[170] Unfortunately there currently are no reliable rules which dictate structural requirements for the two-photon excitation and uncaging processes.

However, MitoPhoto-DNP **328** was recently synthesised within the Hartley research group incorporating an NB-type **324** photo-linker and TPP targeting group (Scheme 101).[167] MitoPhoto-DNP **328** was shown to accumulate in the mitochondria of isolated smooth muscle cells and selective photo-activation (irradiated at 355 nm, probe maximum λ_{abs} = 306 nm in aqueous buffer with 0.1% DMSO) was found to successfully uncouple specific localised mitochondria after the probe released its uncoupling molecule payload (DNP **201**). The synthetic strategy employed allowed for the final step diversification of the probe by attaching a chosen payload molecule to benzylic alcohol **327** (Scheme 101). Therefore this general approach should allow a library of compounds containing alcohols

or phenols to be readily synthesised and subsequently delivered and released in mitochondria.

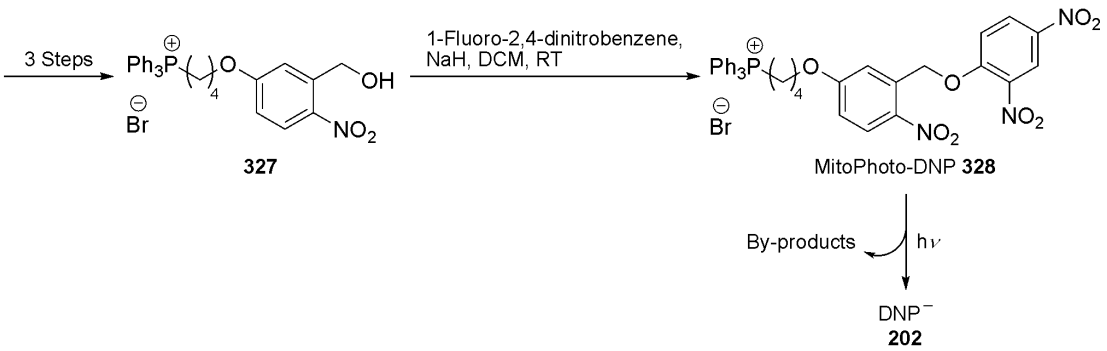

Scheme 101: Final step in the synthesis of MitoPhoto-DNP **328**

The long-term aims of this project were to:

i) Develop the scope of bioactive substrates that can be selectively delivered and released inside mitochondria using this targeted photo-release approach.

ii) Optimise the NB-type **324** photo-linker properties to so that the maximum λ_{abs} more closely matches the excitation wavelength used.

iii) Assess how various selectively released bioactives could impact mitochondria, as well as wider biological behaviour.

iv) Develop two-photon excitation analogues for increased spatial control of payload release.

The ether linker used in MitoPhoto-DNP **328** could easily be adapted into an ester to allow the attachment of molecules boasting carboxylic acid moieties, or into a carbamate to allow the attachment of any amine or amide containing compound. Two such examples would be for the selective delivery and release of reversible complex I inhibitor amobarbital[178] **329** or irreversible complex II inhibitor 3-nitropropionic acid (NPA)[179] **331** delivered as MitoPhoto-Amytal **331** and MitoPhoto-NPA **332** (Fig.77).

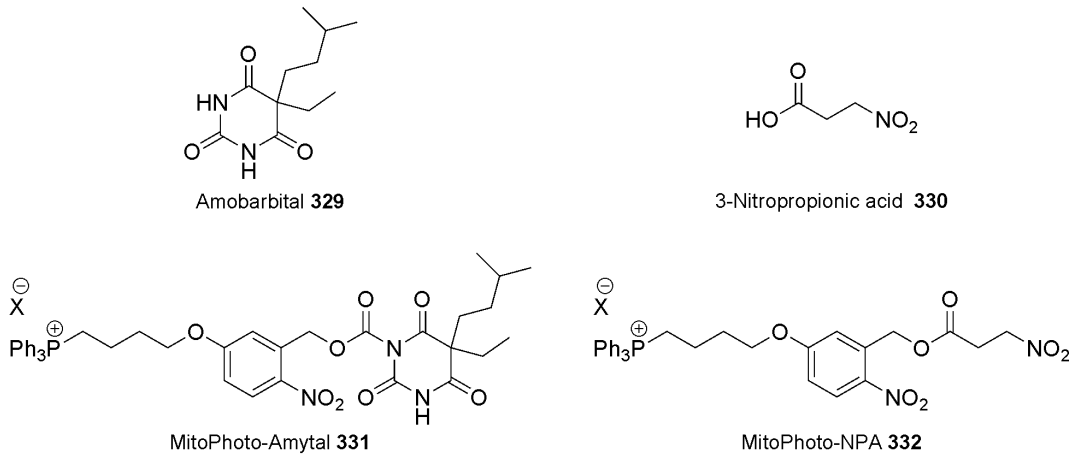

Fig.77: MitoPhoto probes to deliver carbamate or ester bound bioactives

It was proposed to further broaden the synthetic strategy to allow the selective delivery of bioactives through a photo-activatable acetal linker, analogous to the photo-labile protecting group for aldehydes and ketones developed by Hébert, Gravel and colleagues.[180,181] These would allow for the selective mitochondrial release of bioactive molecules containing aldehydes or ketones with general acetal structure **333** (Fig.78). A number of options are available for the spacer between the TPP and photo-activatable moieties as long as the chosen group does not quench the desired photo-cleavage mechanism. Initially, a butyl chain directly analogous to MitoPhoto-DNP **328** will be used as this has previously been successful.

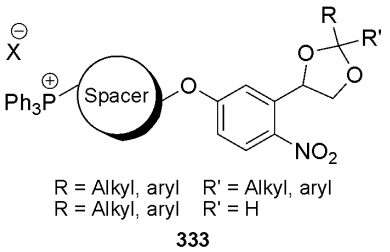

Fig.78: Proposed photo-activatable acetals to deliver aldehydes/ketones to mitochondria

9.2 Initial attempts towards mitochondria-targeted photo-labile acetals

The initial target for the acetal-project was to synthesise a mitochondria-targeted photo-activatable version of reversible isoflavonoid complex I inhibitor rotenone, as MitoPhoto-Rotenone **334** (Fig.79). The *R*-configuration assigned to the acetal centre stereochemistry is based on the curvature of the rotenone molecule which would likely block the formation of the alternative *S*-configuration.

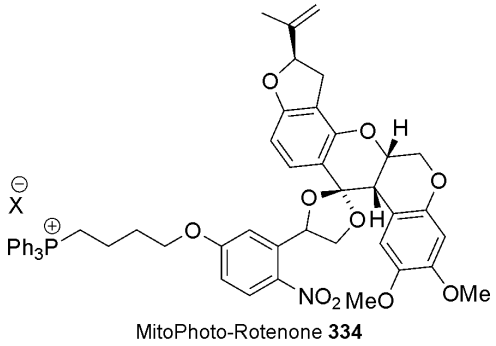

MitoPhoto-Rotenone **334**

Fig.79: Proposed mitochondria-targeted photo-activatable version of rotenone **316**

The synthesis would begin with the conversion of aldehyde **335** into triol **337** using methylenation and dihydroxylation conditions (Scheme 102). The subsequent order of targeting group and payload molecule attachment could be reversed (depending on the ease of synthesis) with a number of potential choices available for each. Ideally the bioactive molecule would be attached as the final step to access one common intermediate **338**, which would allow single-step diversification to a range of products. However the purification of desired TPP compounds from TPP containing starting materials (eg. **333** and **338**) or by-products with similar physical properties (dominated by the presence of the TPP group) can be problematic. It is however generally slightly easier to separate TPP compounds with significant differences in the sizes of attached organic substituents (eg. **161** and **333**) and it is simple to separate non-TPP compounds by precipitation (eg. **339**) from ethereal solvents.

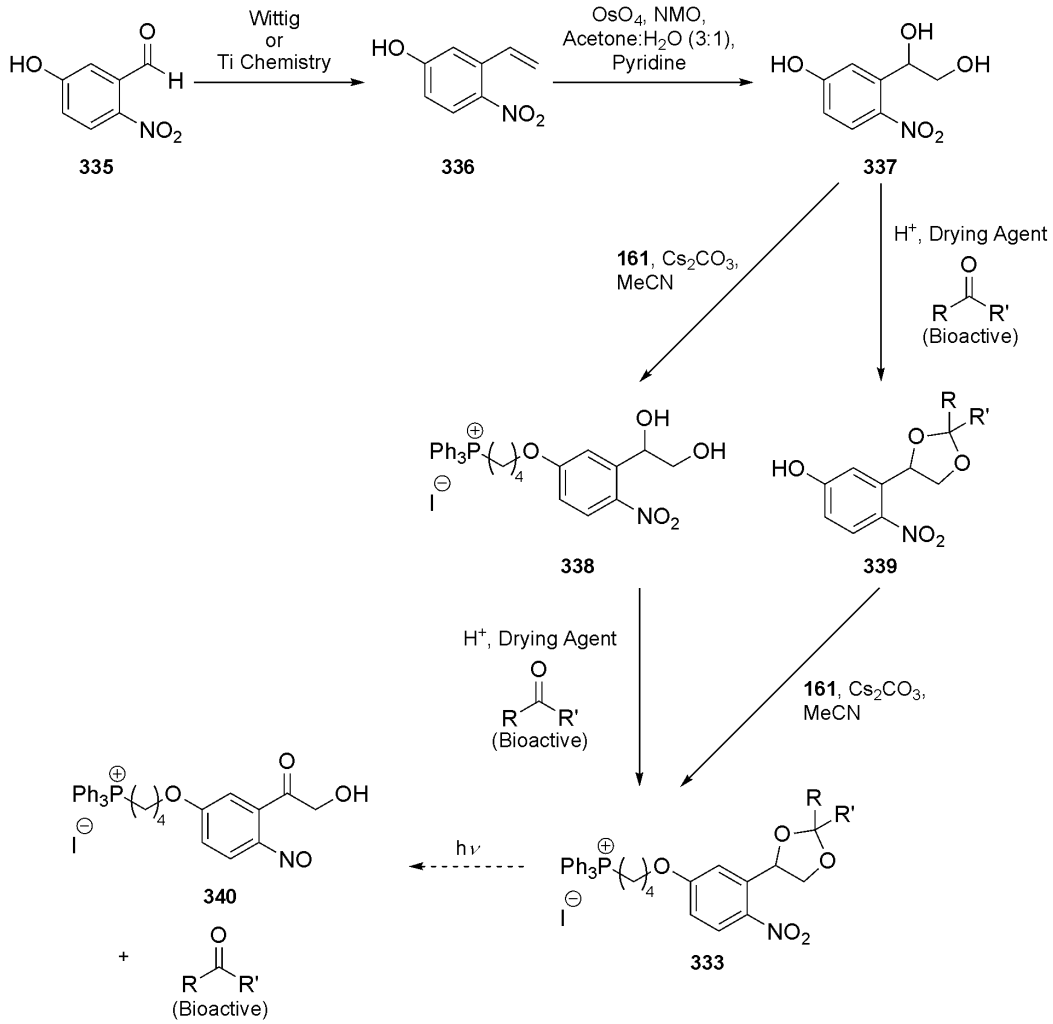

Scheme 102: Proposed general route to MitoPhoto-Acetals

Methylenation of aldehyde **335** (Scheme 103, Table 8) using standard Wittig conditions (Entry 1) or by titanium-based conditions developed in the Hartley research group for the methylenation of esters[182] (Entry 2) both gave complete conversion to alkene **336** as determined by ^{1}H NMR. However purification from the triphenylphosphine oxide by-product and excess MTPP bromide (Entry 1) or from titanium containing impurities (Entry 2) proved difficult and led to a substantial loss in yield in both cases.

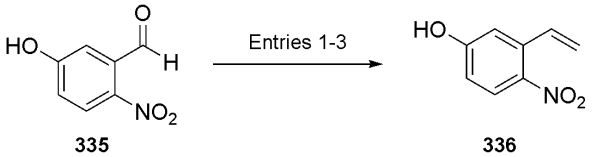

335 336

Scheme 103 and Table 8: Methylenation of 2-nitro-5-hydroxybenzaldehyde **335**

Entry	Conditions	Temperature	Isolated Yield (%)
1	i) ^{n}BuLi, $Ph_3PMe.Br$ (2 eq.), THF ii) Aldehyde **335**, THF	–78 °C to RT	43
2	i) Nysted Reagent **341** (1.5 eq.), Cp_2TiCl_2, (3 eq.), THF ii) Aldehyde **335**, THF	–78 °C to RT	39
3	Aldehyde **335**, Nysted Reagent **341** (1.5 eq.), $BF_3.OEt_2$ (1.2 eq.), THF	0 °C to RT	99

Ultimately using the geminal dizinc Nysted reagent **341** (Fig.80) under Lewis acid promoted conditions (Entry 3) again gave clean and complete conversion to the product with purification simplified (filtration through a short pad of Celite), giving the alkene **336** in a near quantitative yield. Furthermore this methylenation procedure is rapid and removes the need to cool to –78 °C or handle pyrophoric materials (^{n}BuLi). The Nysted reagent is often used to chemoselectively methylenate aldehydes and ketones in the presence of esters, to methylenate sterically hindered carbonyls or when basic Wittig reagents are incompatible with the molecule.[183]

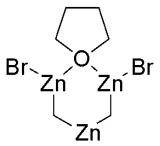

341

Fig.80: Nysted methylenation reagent

Preliminary attempts to isolate triol **337** after dihydroxylation of alkene **336** using catalytic osmium tetroxide with *N*-morpholine *N*-oxide (NMO) as the stoichiometric co-oxidant were unsuccessful, in part due to the partial water solubility of the product. Acetate **342** was synthesised in an attempt to make the dihydroxylation product simpler to isolate. Moreover it would help prevent the suspected polymerisation observed upon recrystallisation of alkene **336** during its initial synthesis, caused be phenol attack at the

terminal alkene (Scheme 104). However, subsequent attempts to isolate diol **343** were unsuccessful.

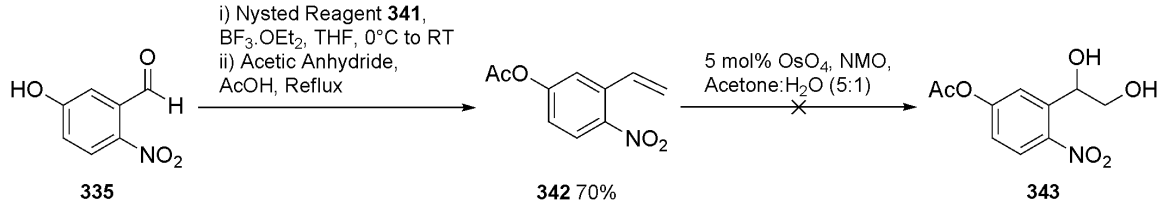

335 **342** 70% **343**

Scheme 104: Attempted dihydroxylation step towards MitoPhoto-Acetals

9.3 Revised synthetic targets

New synthetic targets were proposed in which the TPP component would be attached prior to setting up the bioactive attachment site to aid isolation. Simultaneously it was decided to optimise the absorption properties of the photo-activatable linker to more aptly match the intended excitation wavelength based on the laser that would be used for cell studies (355 nm). To red-shift the maximum λ_{abs} of the NB-type **324** photo-activatable probes, the target structures were modified to incorporate an additional electron-donating methoxy-group in the photo-excitable unit.[170,172] The greater absorption would go someway to compensate for the resultant drop in uncaging ϕ but photo-linker properties could be further optimised at a later date once a benchmark level of bioactive release had been achieved and their biological impacts assessed.

Revised targets included a direct analogue of MitoPhoto-DNP **328** (MethoxyMitoPhoto-DNP **344**) as well as MethoxyMitoPhoto-NPA **345** and MethoxyMitoPhoto-Rotenone conjugates **346**.

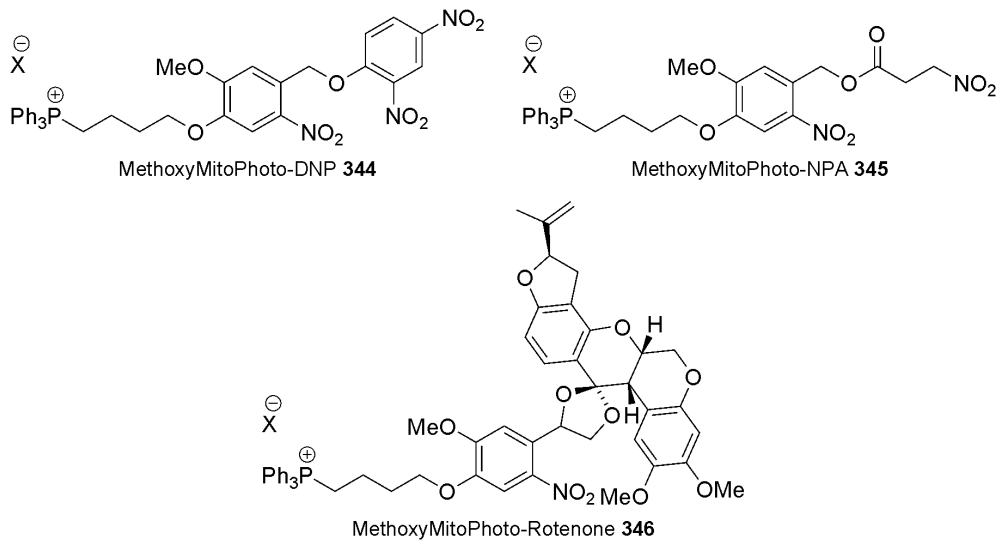

Fig.81: Revised mitochondria-targeted photo-activatable targets

9.3.1 Attempted synthesis of MethoxyMitoPhoto-DNP and MethoxyMitoPhoto-NPA

Firstly the chosen photo-activatable core had to be synthesised from vanillin **347** with the nitro group and bioactive leaving group attachment sites in an *ortho*-orientation. As expected, the direct nitration of vanillin **347** yielded solely the most electronically favoured product **348** in which the groups are in a *meta*-orientation (Scheme 105). Conversion was almost quantitative and was aldehyde **348** isolated in a moderate yield after recrystallisation. This reaction was attempted as all materials used were very cheap and readily scalable. Therefore, even if the desired aldehyde **350** could have generated and isolated as a minor reaction product, this would have reduced the number of synthetic steps by two.

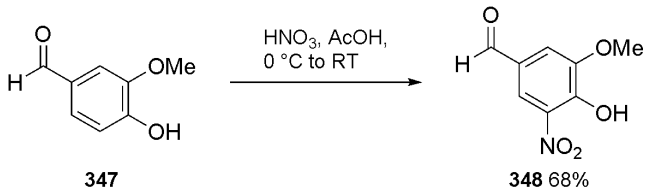

Scheme 105: Nitration of vanillin **347**

Modifying the procedure of Tsai and Klinman,[169] benzyl protection of vanillin **347** followed by nitration and subsequent deprotection gave aldehyde **350** with recrystallisations occurring between each step (Scheme 106). The change in nitration selectivity predominantly results from the change in ring electronics due to the reduced electron-donating ability of the phenol moiety, although increased steric interactions around the phenolic position are likely to also play a role in the observed selectivity.

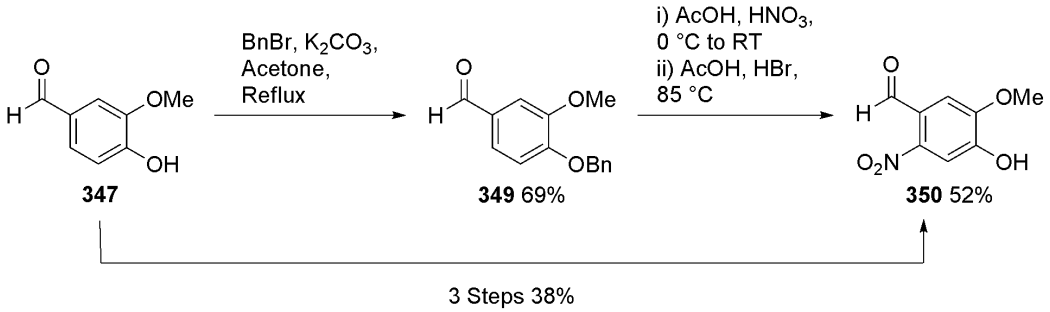

Scheme 106: Synthesis of photo-activatable probe core **350**

The recrystallisation of each step from hot EtOH as described by Tsai and Klinman[169] is not optimal as the crystallisation is hindered by the partial formation of the corresponding diethyl acetal and ethyl hemiacetal. It was found that recrystallisation from acetone is found to be more successful. Phenol protection, nitration and deprotection steps also were achieved in a slightly elevated overall yield with just a single recrystallisation after the third step which reduced the time taken to obtain aldehyde **350**. It is possible that this yield could be increased by further recrystallisations of the crude material, however due to time constraints, the initial ~10 g of the photo-activatable linker **350** obtained was sufficient to take the synthesis forward.

Direct alkylation of phenol **350** with alkyl iodide **161** proved unsuccessful (Scheme 107). This is most likely because of the poor nucleophilicity of the phenoxide due to the electron withdrawing effects of the nitro-group and the directly conjugated carbonyl. Therefore the step-wise synthesis of aldehyde **352** was accomplished by alkylation using an excess of 1,4-diiodobutane **160** at elevated temperatures followed by standard conversion to a TPP group. Yields for each step were reduced due to partial iodide elimination which gave the terminal alkene analogue of alkyl iodide **351**. This was particularly an issue in the alkylation step due to the presence of base which promoted this side-reaction.

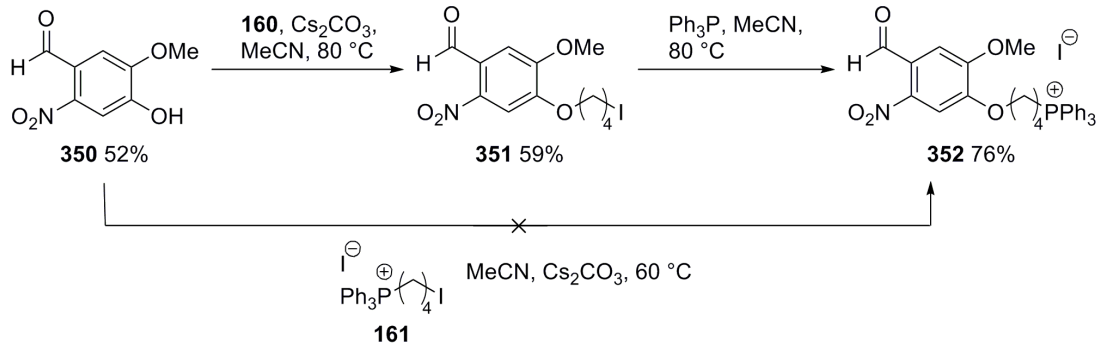

Scheme 107: Synthesis of a mitochondria-targeted photo-activatable core

The final steps towards MethoxyMitoPhoto-DNP **344** synthesis were attempted using identical procedures as had been used for the original MitoPhoto-DNP **328** synthesis (Scheme 108).[167] Reduction to benzylic alcohol **353** was readily achieved using sodium borohydride but instability similar to that noted during the original MitoPhoto-DNP **328** synthesis was observed. This instability could potentially occur through thermal and/or photo-activated decomposition to the related nitroso-aldehyde species, although the exact structures of breakdown products were not confirmed in this project.

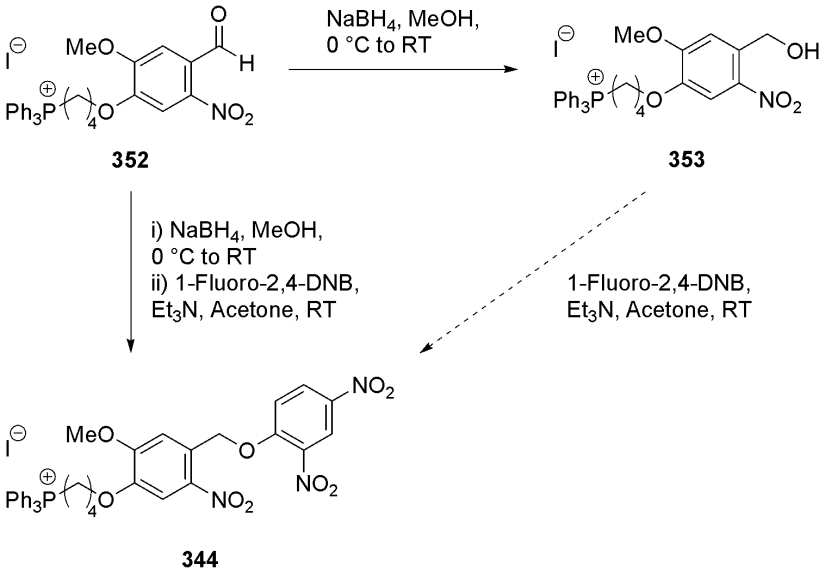

Scheme 108: Attempted completion of a MethoxyMitoPhoto-DNP **344**

Aldehyde reduction followed by immediate S_NAr coupling to 1-fluoro-2,4-dinitrobenzene gave significant and relatively clean conversion, with MethoxyMitoPhoto-DNP **344** as the major reaction product as determined by ^{1}H NMR. Partial purification was achieved by precipitation from diethyl ether to remove non-TPP salt impurities. Although significantly more stable than the precursor benzylic alcohol **353**, analogous to the findings from the synthesis of MitoPhoto-DNP **328**,[167] purification was not successful due to decomposition of the compound during column chromatography. It was noted that gradual but significant loss of DNP **201** occurred on both silica and alumina. It is likely that having the electron-donating ether moiety in direct conjugation, *para*- to the leaving group is sufficient to accelerate decomposition by stabilising the transition state. A small quantity of MethoxyMitoPhoto-DNP **344** was separated containing only a DNP **201** impurity. Attempts to wash this out with aqueous $NaHCO_3$ led to complete decomposition of remaining ether **344**. Due to issues isolating MethoxyMitoPhoto-DNP **344**, attention was turned to MethoxyMitoPhoto-NPA **345**. However attempts using the EDC.HCl coupling

agent and catalytic DMAP were unsuccessful and no coupling to NPA **330** was observed by ^{1}H NMR (Scheme 109).

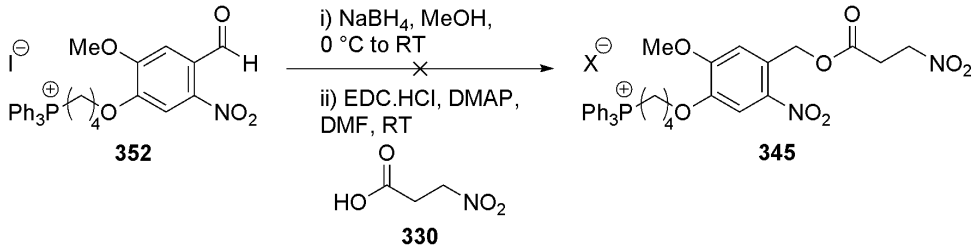

Scheme 109: Attempted synthesis of MethoxyMitoPhoto-NPA **345**

For each photo-activatable probe, a number of control molecules would be required for biological testing, to confirm that the specific roles that individual compound features play in uptake, photo-activation and release mechanisms are working as proposed **354-357** (Fig.82).[167] TPP **354** lacks the nitro group and therefore would assist in the identification of any non-photo-induced release of the bioactives due to interactions with, or general instability towards the biological environments under study. This control molecule would also be used to confirm that the uncaging mechanism requires the nitro group for activation. As the removal of the nitro group significantly changes the aromatic core electronics, this molecule would have to be assessed at the optimal λ_{abs} of both the MitoPhoto compound under study and of the control molecule itself. TPP compounds **355** and **356** have no cleavable unit or cleave a biologically innocuous molecule respectively and would be used to determine if any observed biological affects were being driven by photo-activation process or its by-products. Finally ether **357** would allow the confirmation as to whether or not the DLC driven mitochondria-targeting was playing a vital role in any observed effects.

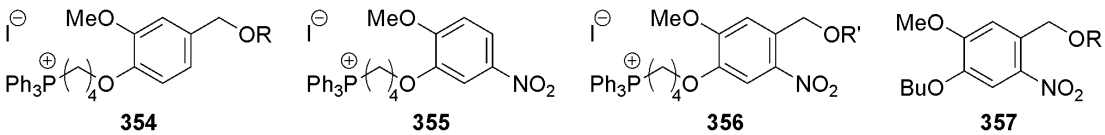

Fig.82: Proposed control molecules

R = caged bioactive, R' = biologically inactive molecule

Aldehyde **358** is a key intermediate towards the nitro group free control molecules for both the proposed photo-activatable ether and acetal compounds depending on the subsequent synthetic steps employed (Scheme 110). Vanillin **347** alkylation was achieved in moderate

yield using the conditions that had previously been unsuccessful for the more electron-deficient nitro analogue **352**.

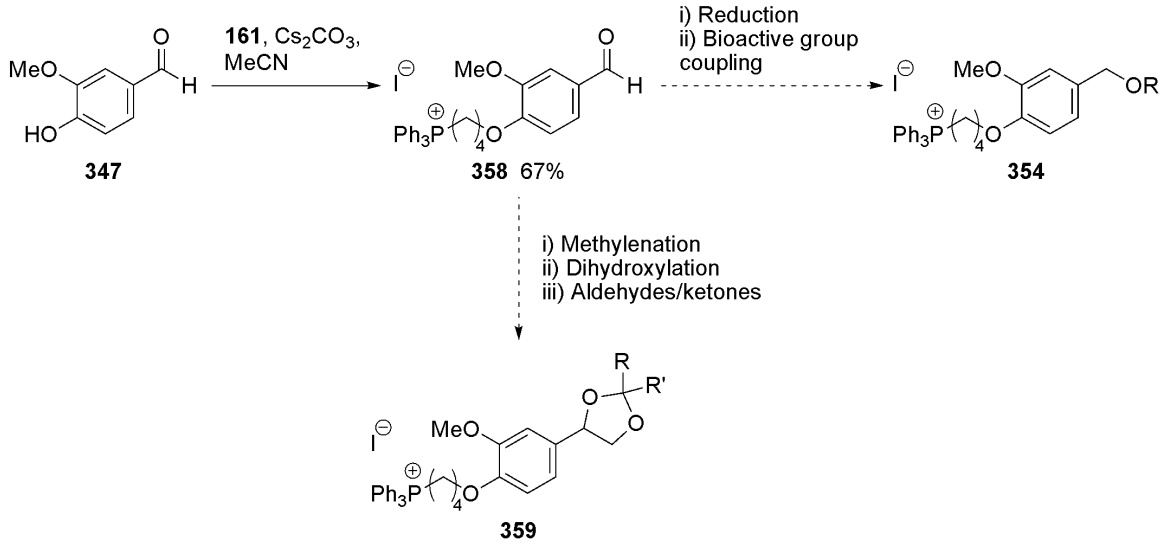

Scheme 110: Preliminary step towards control molecules **354** and **359**

9.3.2 Attempted synthesis of MethoxyMitoPhoto-Acetals

Previously synthesised aldehyde **352** was the key intermediate at which point synthesis would diverge to attach various payload molecules. Reduction to benzylic alcohol **353** could be followed by attachments *via* ether, ester, carbamate or carbonate linkers as described above while the targeted delivery of bioactive molecules containing aldehydes or ketones *via* acetals could be achieved after methylenation and subsequent dihydroxylation procedures.

Methylenation was attempted using the Nysted reagent **341** which gave slow and clean conversion of aldehyde **352** into styrene **360** as determined by ^{1}H NMR (Scheme 111), but complete conversion was never achieved. Resubmission of the reaction crude mixture to identical reaction conditions drove the reaction further towards completion (~50% in total) with aldehyde **352** and styrene **360** being the only products in the mixture. The failure to obtain complete conversion is possibly because TPP compounds are insoluble in THF (in which the Nysted suspension is purchased) and using DCM as a co-solvent led to a destabilisation of the Nysted reagent **341** which requires ethereal solvents for stabilisation. Nonetheless it is likely that using a larger excess of Nysted reagent **341** or the optimisation of the co-solvent system could be used to give complete methylenation in the presence of the TPP salt to yield styrene **360**.

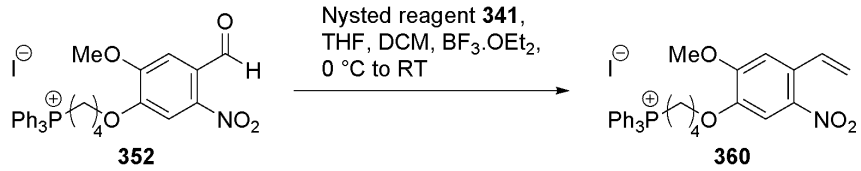

Scheme 111: Attempted methylenation of aldehyde **352**

Wittig methylenation conditions would be incompatible with aldehyde **352** as this could lead to the corresponding phosphonium ylide being generated, while Tebbe or Petasis conditions were not attempted. However an alternative approach in which aldehyde **352** is epoxidised by trimethylsulfoxonium iodide by a Corey-Chaykovsky reaction followed by epoxide opening and acetal formation was investigated (Schemes 112 and 113).

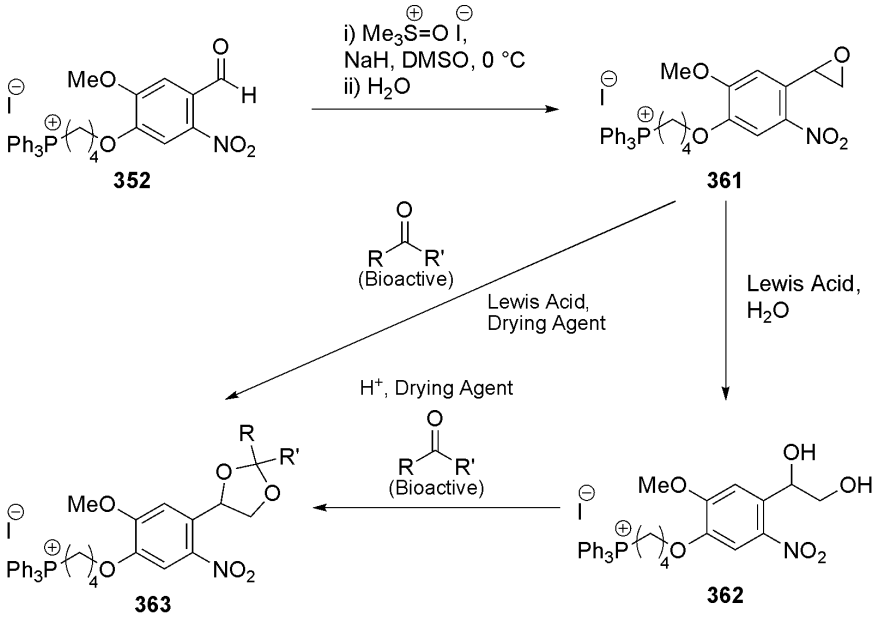

Scheme 112: Proposed final steps to MethoxyMitoPhoto-Acetals

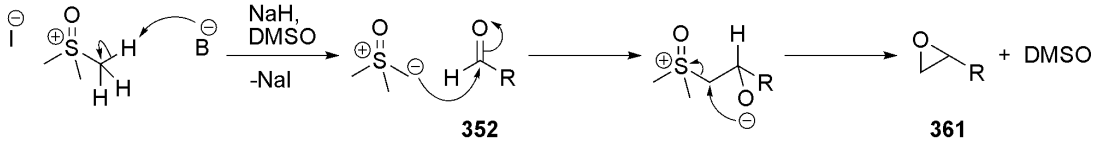

Scheme 113: Corey-Chaykovsky reaction mechanism

This epoxidation procedure rapidly generated the desired epoxide **361** but also oxidised the TPP moiety to a diphenylphosphine oxide when an excess of the sulfoxonium reagent was used. When stoichiometric reagent was used, a mixture of the epoxidation and phosphorus oxidation products were observed indicating comparable reaction rates.

Although anhydrous DMSO was used as a solvent, it is unclear as to whether or not phosphorus oxidation is occurring as a result of reaction with the oxygen from the trimethylsulfoxonium iodide reagent directly, or simply by hydroxide (Chapter 2.1, Scheme 17) generation from small amounts of residual moisture present in the small scale reactions. If hydroxide had been the cause it would be expected that some epoxide opening to diol **362** would have been observed, but this was not the case. Additionally, increasing the equivalences of the sulfoxonium reagent would not be expected to have any impact on the amount of phosphorus oxidation, unless this reagent was the source of moisture. If any of TPP **352** had been deprotonated by either residual base or the deprotonated sulphur reagent to form a phosphonium ylide, a much messier crude mixture would be expected after undergoing a Wittig reaction with a further molecule of aldehyde **352**. Oxidation caused by trimethylsulfoxonium iodide itself could be confirmed or ruled out by using an ^{18}O radiolabelled version of the reagent and assessing if any of the labelled oxygen becomes incorporated in the phosphorus oxidation products.

An alternative route reversing the methylenation and targeting group attachment steps was started (Scheme **114**). Alkene **362** was readily isolated in good yield using an excess of Nysted reagent to account for any lost through co-ordination of the zinc reagent to the free phenol. Alkene **362** could then be used to complete the synthesis of MitoPhoto-Acetals *via* the original proposed route, directly analogous to non-methoxy analogue **336** (Scheme **102**).

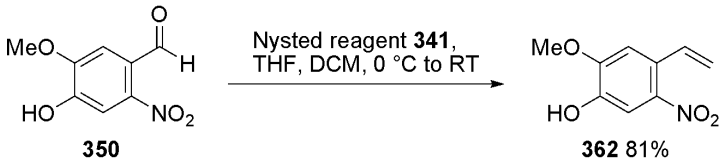

350 **362** 81%

Scheme 114: Alternative intermediate for MitoPhoto-Acetals

9.4 Conclusions

A number of steps towards new generations of mitochondria-targeted photo-activatable probes have been made. Most significantly, the synthesis of a mitochondria-targeted core **352** that could potentially be used as a common precursor for the delivery of a plethora of bioactive molecules linked through ethers, esters, carbamates and acetals was achieved. It is possible that with further optimisation of the final reaction steps and with increased experience handling light unstable materials, that new probes to investigate mitochondria could be developed based on this synthetic route.

Chapter 10: Research conclusions and future work

Over the course of the above projects (Chapters 6-9), a number of novel functional molecules have been produced that assist in advancing the understanding of mitochondrial behaviour and the free radical theory of ageing.

10.1 Ratiometric mass spectrometry probes for ROS/RNS quantification

The first ratiometric mass spectrometry (MS) probe (MitoB **134**) has been produced and allows the levels of H_2O_2 to be accurately measured *in vivo* (also applicable *in vitro*) for the first time, *via* the conversion of a boronic acid to a phenol moiety.[127,129] To date studies require a tissue sample to be taken, but preliminary studies suggest that further optimisation of this technique will allow for the first completely non-invasive measurements in larger organisms through urine sampling.

For the first time, a plethora of biological interventions and environmental conditions can be assessed directly for their impacts on H_2O_2 concentrations in whole organisms. This begins to allow studies to look at separating a whole host of ROS production, detoxification and repair pathways from each other.

For example, the widely held theory that dietary restriction extended lifespan as a result of reducing ROS levels has been now been shown to be incorrect. Conformation of the increasing H_2O_2 level in an organism as it ages has been found to be independent of lifespan, suggesting that the concentration may be a result of ageing rather than causative. The influence of many other chemical or environmental factors such as oxygen concentration, paraquat addition, differing levels of physical activity, etc. can now also be probed. This approach will ultimately allow for the development of a ranking table in which the various factors that modify H_2O_2 concentration can be ranked and assessed against each other and against different organism/cell types. In particular, optimising the procedures may allow for many behavioural and dietary variables such as smoking or alcohol consumption (which are known to lead to accelerated ageing and disease) to be studied for their impacts on ROS production in whole organisms, such as humans.

This approach is also applicable to *in vitro* studies complementing existing fluorescent techniques, or replacing them where necessary. This method has a broad scope as it could

be used in the detection and quantification of many biologically relevant species as long as the reaction between the probe and the species in question can be sufficiently selective and yield a stable, MS identifiable product. For example, the assessment of the analogous nitric oxide MS probe (MitoDA **156**, Chapter 6.3) in biological systems is underway and the development of further ROS/RNS MS probes is ongoing within the Hartley research group. Once biologically suitable, selective probe transformations have been established for each ROS/RNS of interest, alterations of the targeting group will allow this ratiometric MS approach to give quantification of these species in cellular compartments other than the mitochondria (eg. as discussed in ExoCellB **147**, Chapter 6.2).

10.2 Prodrugs activated in response to endogenous ROS

A novel class of compounds, mitochondria-targeted selective uncoupling molecules (MitoSUMs) have been developed and their impact on isolated mitochondria assessed. In line with the project aims, MitoSUMs were shown to accumulate in the matrix of isolated energised mitochondria in response to $\Delta\Psi_m$ and release uncoupling molecules in a dose dependent manner in response to elevated mitochondrial ROS production, leading to a reduction in ROS production rates. Additionally these constructs were shown to be significantly more potent than untargeted uncoupler, which would reduce any unwanted side-effects of DNP **201** interaction with biological systems outside of the mitochondria.

These molecules are a new class of prodrug that with further payload molecule variation, could be used to selectively release a wide range of biologically active compounds inside mitochondria in response to elevated H_2O_2 production. This could allow the biological effects of many compounds to be studied *in vitro* in relation to ROS production rates, detoxification or repair mechanisms.

Further studies are required to assess whether or not prolonged exposure to MitoSUMs in whole organisms can lead to a reduction in the onset of age-related disease resulting from oxidative stress, as proposed in the free radical theory of ageing. For the next round of MitoSUM compounds it is proposed that modifications of the payload molecule, uncoupling molecule attachment site and trigger electronics/sterics could be made to optimise compound stability, reactivity and potency. Theoretically the trigger mechanism could be altered so as to give selective payload molecule release in response to some other biologically produced species of interest. Similarly, the targeting group could be modified to target different cellular compartments.

10.3 Photo-activatable constructs for highly controlled bioactive release

A future goal of this research is to produce mitochondria-targeted compounds that will allow temporal and spatial selectivity with regards to bioactive release following targeted photo-activation. This would allow theories related to localised mitochondria subpopulations to be investigated and a greater understanding of the roles individual mitochondria play to be developed. The scope of this research following on from the first such probe developed within the Hartley research group, MitoPhoto-DNP **328**,[167] is vast. Of particular interest is the possibility of selectively releasing respiratory chain inhibitors so as to monitor the effects of altering biological pathways of specific mitochondria and assessing how this impacts the cell and organism as a whole.

A number of steps towards novel mitochondria-targeted photo-activatable probes have been made. These include the synthesis of a mitochondria-targeted core **352** precursor that could allow for the delivery of bioactive molecules linked through ethers, esters, carbamates and acetals. Completion of this synthetic route (Schemes 106 and 107) will lead to a library of targeted bioactives that may be selectively released inside mitochondria of interest that may be used in a wide range of potential studies. Three key areas of optimisation for these molecules exist. Firstly, optimisation of the photo-activatable core may be required to allow these functional molecules to more aptly match the preferred wavelengths of lasers used by different research groups and improve stability in the visible light region if required. Secondly, changing of the targeting group will allow studies to examine bioactive molecule interactions with areas of an organism other than mitochondria. Finally developing a range of new photo-activatable cores which are suitable for two-photon excitation will allow improved spatial resolution, which will be hugely beneficially for *in vivo* studies. This is particularly useful as the lower energy, longer wavelength photons required can penetrate tissues more readily and cause less damage to cells. One such application may be to selective release apoptosis inducing agents from inactive caged precursors, selectively in tumour tissues.

Chapter 11: Experimental

11.1 General experimental

All reactions under an inert atmosphere were carried out using oven-dried or flame-dried glassware. Solutions were added *via* syringe or canula. Acetonitrile, diethyl ether, tetrahydrofuran, dichloromethane, and toluene were dried where necessary using a solvent drying system, Puresolv^{TM}, in which solvent is pushed from its storage container under low nitrogen pressure through two stainless steel columns containing activated alumina and copper. Acetone was dried by distillation from calcium sulphate and dimethylformamide was dried by distillation from calcium hydride or purchased anhydrous from commercial suppliers. Reagents were obtained from commercial suppliers and used without further purification unless otherwise stated. ^{1}H, ^{13}C, ^{11}B, ^{19}F and ^{31}P NMR spectra were obtained on a Bruker DPX/400 spectrometer operating at 400, 100, 128, 376 and 162 MHz respectively or on a Bruker AVIII spectrometer operating at 500, 126, 160, 470 and 202 MHz respectively. All coupling constants are measured in Hz. DEPT was used to assign the signals in the ^{13}C NMR spectra as C, CH, CH_2 or CH_3. COSY, NOESY, HMBC and HSQC NMR were used to confirm assignments where required. Aromatic carbons directly attached to boron are not observed in ^{13}C NMR spectra due to extensive splitting by ^{10}B and ^{11}B. Standard abbreviations for signal multiplicities are used (eg. s, d, t, q, dd, dt, m, etc.). ^{1}H NMR data for partially deuterated aromatic rings $P(C_6D_4H)$ are reported and integrated relative to other ^{1}H NMR signals unless the signals are otherwise obscured by other aromatic region signals. Proton assignments in THP ethers are as described by Abraham *et al*, with protons assigned to the major ring conformer in which the 2-oxo substituent is axial due to the anomeric effect.[184] Mass spectra (MS) were recorded on a Jeol JMS700 (MStation) spectrometer except ESI^+, ESI^- and certain CI^+ analyses, which were recorded on a Thermofisher LTQ Orbitrap XL. Infra-red (IR) spectra were obtained on a Shimadzu FTIR-8400S spectrometer using attenuated total reflectance (ATR) so that the IR spectrum of the compound (solid or liquid) could be directly detected (thin layer) without any sample preparation. R_f values for phosphonium salts and carboxylic acids are concentration dependant and are reported as the maximum observed R_f. Microanalyses were obtained on an Exeter Analytical CE440. This instrument cannot distinguish between hydrogen and deuterium and the percentage H and D found in deuterated compounds are calculated from raw data with any deviation from theoretical appearing in the percentage D.

11.2 Synthesis

(3-Dihydroxyboronylbenzyl)triphenylphosphonium bromide (MitoB) 134[127]

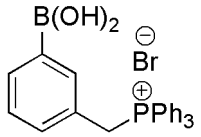

3-(Bromomethyl)phenylboronic acid **143** (400 mg, 95%, 1.77 mmol) and triphenylphosphine (513 mg, 1.96 mmol) were heated at reflux in toluene (10 mL) for 6 h during which a white precipitate formed. The mixture was concentrated under reduced pressure and the residue was recrystallised from minimal DMSO-toluene. The solid was dissolved in hot H_2O (400 mL) and H_2O was removed under reduced pressure until precipitation began, upon which the mixture was allowed to cool to RT and crystallise slowly. The mixture was centrifuged, and solvent pipetted off. Crystals were washed with a little ice-cold H_2O (5 mL) and dried under reduced pressure to yield phosphonium bromide **134** as needles. Further phosphonium bromide **134** was obtained by multiple repetitions of the recrystallisation and centrifugation processes with material obtained by concentration of the combined aqueous liqueur (Combined yield 732 mg, 87%). Mp: 304-305 °C (H_2O). ν_{max} (ATR): 3322 (OH), 2928 (CH), 2882 (CH), 2789 (CH), 1549 (Ar), 1485 (Ar), 1435 (Ar) cm^{-1}. δ_H (400 MHz, d_6–DMSO): 7.94 [2H, s, $B(OH)_2$], 7.92-7.86 (3H, m, 3 × *p*-H PPh_3), 7.77-7.69 (7H, m, 6 × *o*-H PPh_3 and H-4), 7.68-7.60 (6H, m, 6 × *m*-H PPh_3), 7.46 (1H, broad s, H-2), 7.17 (1H, t, J = 7.5 Hz, H-5), 6.96 (1H, broad d, J = 7.4 Hz, H-6), 5.14 (2H, d, J = 15.6 Hz, CH_2). δ_C (100 MHz, d_6–DMSO): 136.88 (d, J = 5.6 Hz, CH), 134.94 (d, J = 2.4 Hz, CH), 133.93 (d, J = 9.8 Hz, CH), 133.78 (d, J = 3.6 Hz, CH), 132.25 (d, J = 5.2 Hz, CH), 129.95 (d, J = 12.5 Hz, CH), 127.60 (d, J = 2.8 Hz, CH), 126.67 (d, J = 8.5 Hz, C), 117.75 (d, J = 85.5 Hz, C), 28.15 (d, J = 46.5 Hz, CH_2). δ_P (162 MHz, d_6–DMSO): 23.52-22.76 (broad s). δ_P {^{1}H} (162 MHz, d_6–DMSO): 23.15 (s). LRMS (ESI^+): 397 (cation, 100%). HRMS: 397.1518 and 396.1557. $C_{25}H_{23}{}^{11}BO_2P$ requires cation, 397.1524 and $C_{25}H_{23}{}^{10}BO_2P$ requires cation, 396.1560. Microanalysis: $C_{25}H_{23}BBrO_2P$ requires C: 62.93% H: 4.86%, found C: 62.90% H: 4.80%. Structure confirmed by x-ray crystallography: Cambridge Crystalographic Data Centre deposition number CCDC 900923.

(3-Dihydroxyboronylbenzyl)tri(pentadeuterophenyl)phosphonium bromide (MitoB-d_{15}) 135[127]

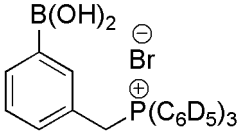

A stirring solution of 3-(bromomethyl)phenylboronic acid **143** (155 mg, 95%, 0.69 mmol) and tri(pentadeuterophenyl)phosphine (200 mg, 0.72 mmol) was heated at reflux in toluene (4 mL) for 6 h during which a white precipitate formed. The mixture was concentrated under reduced pressure and the residue was recrystallised from DMSO-toluene, followed by recrystallisation from hot H_2O. The mixture was centrifuged, and solvent pipetted off. Crystals were washed with a little ice-cold H_2O and dried under reduced pressure to yield phosphonium bromide **135** as needles. The solvent pipetted off after centrifugation and the aqueous washings were concentrated under reduced pressure until further crystallisation was observed to begin and the crystallisation and centrifugation processes repeated to yield further phosphonium bromide **135** (Combined yield 179 mg, 50%). The compound was isolated as a 92:8 mixture of H_8D_{15}:H_9D_{14}. Mp: 303-304 °C (H_2O). ν_{max} (ATR): 3236 (OH), 2928 (CH), 2882 (CH), 1543 (Ar), 1485 (Ar), 1424 (Ar,) cm^{-1}. δ_H (400 MHz, d_6–DMSO): 7.96 [2H, s, $B(OH)_2$], 7.72 (1H, broad d, *J* = 7.4 Hz, H-4), 7.46 (1H, broad s, H-2), 7.17 (1H, t, *J* = 7.6 Hz, H-5), 6.94 (1H, broad d, *J* = 7.6 Hz, H-6), 5.12 (2H, d, *J* = 15.6 Hz, CH_2). δ_C (100 MHz, d_6–DMSO): 137.02 (d, *J* = 5.6 Hz, CH), 135.08-134.22 (m, CD), 133.92 (d, *J* = 2.7 Hz, CH), 134.22-133.12 (m, CD), 132.43 (d, *J* = 5.5 Hz, CH), 130.05-129.15 (m, CD), 127.75 (d, *J* = 2.6 Hz, CH), 126.84 (d, *J* = 8.6 Hz, C), 117.67 (d, *J* = 85.4 Hz, C), 28.27 (d, *J* = 46.5 Hz, CH_2). δ_P (162 MHz, d_6–DMSO): 23.01 (broad t, *J* = 15.5 Hz). δ_P {^{1}H} (162 MHz, d_6–DMSO): 23.12-22.94 (broad s). LRMS (ESI^+): 412 (cation, 100%). HRMS: 412.2460 and 411.2479. $C_{25}H_8D_{15}{}^{11}BO_2P$ requires cation, 412.2465 and $C_{25}H_8D_{15}{}^{10}BO_2P$ requires cation, 411.2501. Microanalysis: $C_{25}H_8D_{15}BBrO_2P$ requires C: 61.00% H: 1.64% D: 6.14%, found C: 60.90% H: 1.64% D: 6.17%.

(3-Hydroxybenzyl)triphenylphosphonium bromide (MitoP) 136[127]

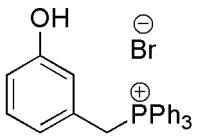

Method A:

A stirring solution of benzylic bromide **145** (134 mg, 0.72 mmol) and triphenylphosphine (200 mg, 0.76 mmol) was heated at reflux in toluene (4 mL) for 24 h during which a white precipitate formed. The reaction mixture was concentrated under reduced pressure and the

resultant solid recrystallised from EtOH-hexane. The solid was washed with a little ice-cold H_2O and dried under reduced pressure to yield phosphonium bromide **136** as an amorphous solid (190 mg, 59%). Mp: >290 °C (Decomp.) [Lit.[128] 290.5-291.5 °C (EtOH)]. ν_{max} (ATR): 3079 (OH), 2889 (CH), 2858 (CH), 2787 (CH), 1611 (Ar), 1568 (Ar) cm^{-1}. δ_H (400 MHz, d_6–DMSO): 9.54 (1H, s, OH), 7.94-7.86 (3H, m, 3 × *p*-H PPh_3), 7.78-7.70 (6H, m, 6 × *o*-H PPh_3), 7.70-7.60 (6H, m, 6 × *m*-H PPh_3), 7.00 (1H, t, *J* = 7.8 Hz, H-5), 6.68 (1H, broad d, *J* = 8.0 Hz, H-4), 6.41 (1H, broad s, H-2), 6.36 (1H, broad d, *J* = 7.1 Hz, H-6), 5.06 (2H, d, *J* = 15.6 Hz, CH_2). δ_C (100 MHz, d_6–DMSO): 157.54 (d, *J* = 3.2 Hz, C), 135.10 (d, *J* = 1.9 Hz, CH), 134.03 (d, *J* = 9.8 Hz, CH), 130.11 (d, *J* = 12.5 Hz, CH), 129.75 (d, *J* = 2.2 Hz, CH), 129.05 (d, *J* = 8.3 Hz, C), 121.39 (d, *J* = 5.5 Hz, CH), 117.98 (d, *J* = 85.6 Hz, C), 117.83 (d, *J* = 5.6 Hz, CH), 115.33 (d, *J* = 3.1 Hz, CH), 28.13 (d, *J* = 46.6 Hz, CH_2). δ_P (162 MHz, d_6–DMSO): 23.38-22.70 (broad s). δ_P {^{1}H} (162 MHz, d_6–DMSO): 23.03 (s). LRMS (ESI^+): 369 (cation, 100%). HRMS: 369.1399. $C_{25}H_{22}OP$ requires cation, 369.1403. Microanalysis: $C_{25}H_{22}BrOP$ requires C: 66.83% H: 4.94%, found C: 66.89% H: 4.98%. ^{1}H NMR data agree with literature.[128]

Method B:

Adapting the procedure of Dawson *et al.*[128] PBr_3 (0.95 mL, 1.0 M in DCM, 3.50 mmol) and anhydrous pyridine (150 µL, 1.85 mmol) were added to anhydrous MeCN (1 mL) at –8 °C under argon and stirred for 5 min. A solution of 3-hydroxybenzyl alcohol 146 (1.00 g, 8.06 mmol) and anhydrous pyridine (50 µl, 0.62 mmol) in anhydrous MeCN (2.5 mL) was added slowly and the resulting solution stirred for 10 min at –8 °C under argon. The solution was allowed to warm to RT and stirred at 20 °C for 15 h before being concentrated under reduced pressure. H_2O (10 mL) was added and extracted with DCM (2 × 10 mL). The extracts were eluted through a short silica column with EtOAc-DCM (1:19 then 1:9). Toluene (8 mL) was added to the crude yellow, unstable oil (1.13 g) followed by triphenylphosphine (3.58 g, 13.6 mmol) and stirred at reflux for 16 h. After cooling to RT the precipitate was collected by filtration, washed with hot toluene, then Et_2O and dried under reduced pressure. Slow recrystallisation from EtOH yielded phosphonium bromide **136** as prisms (2.31 g, 64%). *Characterisation as previous.*

(3-Hydroxybenzyl)tri(pentadeuterophenyl)phosphonium bromide (MitoP-d_{15}) 137[127]

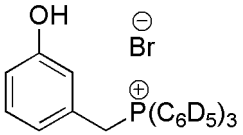

A stirring solution of benzylic bromide **145** (128 mg, 0.68 mmol) and tri(pentadeuterophenyl)phosphine (200 mg, 0.72 mmol) was heated at reflux in toluene (4 mL) for 24 h during which a white precipitate formed. The reaction mixture was concentrated under reduced pressure and the resultant solid recrystallised from EtOH-hexane. The solid was washed with a little ice-cold H_2O and dried under reduced pressure to yield phosphonium bromide **137** as an amorphous solid (153 mg, 48%). The compound was isolated as a 92:8 mixture of H_7D_{15}:H_8D_{14}. Mp: >290 °C (Decomp.). ν_{max} (ATR): 3080 (OH), 2889 (CH), 2858 (CH), 2787 (CH), 1617 (Ar), 1609 (Ar), 1587 (Ar) cm^{-1}. δ_H (400 MHz, d_6–DMSO): 9.55 (1H, s, OH), 7.00 (1H, t, *J* = 7.8 Hz, H-5), 6.69 (1H, broad d, *J* = 8.0 Hz, H-4), 6.42 (1H, broad s, H-2), 6.36 (1H, broad d, *J* = 7.2 Hz, H-6), 5.08 (2H, d, *J* = 15.7 Hz, CH_2). δ_C (100 MHz, d_6–DMSO): 157.54 (d, *J* = 3.1 Hz, C), 134.90-134.23 (m, CD), 134.08-133.12 (m, CD), 130.08-129.20 (m, CD), 129.73 (d, *J* = 3.4 Hz, CH), 128.57 (d, *J* = 8.6 Hz, C), 121.39 (d, *J* = 5.6 Hz, CH), 117.85 (d, *J* = 5.5 Hz, CH), 117.76 (d, *J* = 85.4 Hz, C), 115.32 (d, *J* = 3.4 Hz, CH), 28.16 (d, *J* = 46.6 Hz, CH_2). δ_P (162 MHz, d_6–DMSO): 22.92 (broad t, *J* = 15.4 Hz). δ_P {^{1}H} (162 MHz, d_6–DMSO): 23.08-22.74 (broad s). LRMS (ESI^+): 384 (cation, 100%). HRMS: 384.2336. $C_{25}H_7D_{15}OP$ requires cation, 384.2344. Microanalysis: $C_{25}H_7D_{15}BrOP$ requires C: 64.66% H: 1.52% D: 6.51%, found C: 64.69% H: 1.52% D: 6.69%. ^{1}H NMR data for partially deuterated aromatic ring $P(C_6D_4H)$ integrated relative to other signals in ^{1}H NMR: 7.90 (0.018H, d, *J* = 0.9 Hz, *p*-H PPh_3), 7.74 (0.030H, d, *J* = 3.0 Hz, *m*-H PPh_3), 7.65 (0.032H, d, *J* = 12.5 Hz, *o*-H PPh_3).

3-Hydroxybenzyl bromide 145

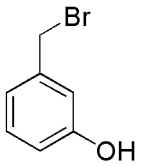

A stirring solution of benzylic alcohol **274** (3.00 g, 17.8 mmol) and anhydrous triethylamine (3.7 mL, 27 mmol) in anhydrous DCM (90 mL) were degassed with argon for 10 min. The solution was cooled to 0 °C and methanesulfonyl chloride (1.8 mL, 23.2 mmol) was added dropwise. The solution was stirred at 0 °C for 1 h and then allowed to warm to RT over 1 h. The solution was washed with H_2O (2 × 20 mL), dried over $MgSO_4$ and concentrated under reduced pressure. Anhydrous acetone (90 mL) and anhydrous

LiBr (15.85 g, 178 mmol) were added to the residual oil and the resulting mixture stirred for 22 h at reflux under argon. The mixture was concentrated under reduced pressure and the residue redissolved in DCM (80 mL). Organics were washed with H_2O (2 × 30 mL), dried over $MgSO_4$ and concentrated under reduced pressure to give a brown gum. Column chromatography [SiO_2, petroleum ether-EtOAc (3:2)] yielded benzylic bromide **145** as needles (1.14 g, 34%). R_f [SiO_2, petroleum ether-EtOAc (3:2)]: 0.71. Mp: 61-62 °C. ν_{max} (ATR): 3248 (OH), 2955 (CH), 2851 (CH), 1586 (Ar) cm^{-1}. δ_H (400 MHz, $CDCl_3$): 7.21 (1H, t, *J* = 7.9 Hz, H-5), 6.96 (1H, d, *J* = 7.9 Hz, H-6), 6.89-6.86 (1H, m, H-2), 6.77 (1H, ddd, *J* = 8.1, 2.5 and 0.8 Hz, H-4), 5.04 (1H, broad s, OH), 4.34 (2H, s, CH_2). δ_C (100 MHz, $CDCl_3$): 155.62 (C), 139.42 (C) 130.07 (CH), 121.47 (CH), 115.90 (CH), 115.53 (CH), 33.14 (CH_2). LRMS (EI^+): 188 [$M^{+\bullet}$ (^{81}Br), 20%], 186 [$M^{+\bullet}$ (^{79}Br), 19], 107 ($M^{+\bullet}$ – $Br^{\bullet}$, 100), 86 (100), 84 (100), 49 (100). HRMS: 187.9650 and 185.9689. $C_7H_7{}^{81}BrO$ requires $M^{+\bullet}$, 187.9660 and $C_7H_7{}^{79}BrO$ requires $M^{+\bullet}$, 185.9680.

<u>2-(3'-Iodophenyl)-4,4,5,5-tetramethyl-1,3,2-dioxaborolane</u> 152[134]

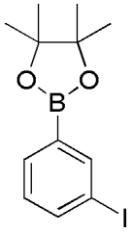

Anhydrous THF (25 mL) was added under argon to 1,3-diiodobenzene **151** (1.50 g, 4.55 mmol) and anhydrous LiCl (212 mg, 5.00 mmol). The stirring mixture was cooled to –78 °C and ^{i}PrMgCl (2.0 M in THF, 2.5 mL, 5.00 mmol) was added dropwise and stirred for 3 h. 2-Isopropoxy-4,4,5,5-tetramethyl-1,3,2-dioxaborolane (930 μL, 4.6 mmol) was added dropwise and the solution allowed to warm slowly to RT overnight. Saturated aqueous NH_4Cl (2 mL) was added to quench. The resulting mixture was stirred until the precipitate settled before being filtered through a pad of Celite and washed through with Et_2O. Organics were dried over $MgSO_4$ and concentrated under reduced pressure. Column chromatography [SiO_2, petroleum ether-EtOAc (9:1)] yielded dioxaborolane **152** as an amorphous solid (545 mg, 36%). R_f [SiO_2, petroleum ether-EtOAc (9:1)]: 0.54. Mp: 70-71 °C [Lit.[134] 71.1-71.9 °C (Et_2O)]. δ_H (500 MHz, $CDCl_3$): 8.14 (1H, broad t, *J* = 1.2 Hz, H-2'), 7.78 (1H, ddd, *J* = 7.9, 1.9 and 1.2 Hz, H-4' or H-6'), 7.75 (1H, td, *J* = 7.4 and 1.1 Hz, H-4' or H-6'), 7.10 (1H, td, *J* = 7.6 and 0.3 Hz, H-5'), 1.33 (12H, s, 4 × Me). δ_C (126 MHz, $CDCl_3$): 143.39 (CH), 140.06 (CH), 133.62 (CH), 129.62 (CH), 94.50 (C), 84.10 (C), 24.84 (CH_3). ^{11}B (160 MHz, $CDCl_3$): 30.30 (s). ^{11}B {^{1}H} (160 MHz, $CDCl_3$): 30.27

(s). LRMS (EI^+): 330 ($M^{+\bullet}$, 90%), 315 (57), 244 (100), 231 (70), 104 (60), 84 (51), 49 (53). ^1H and ^{13}C NMR data agree with literature.[134]

2-(4'-Iodophenyl)-4,4,5,5-tetramethyl-1,3,2-dioxaborolane 155[134]

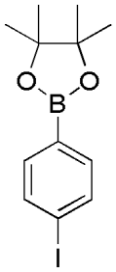

Anhydrous THF (500 mL) was added to 1,4-diiodobenzene **154** (25.00 g, 75.8 mmol) and anhydrous LiCl (3.48 g, 82.1 mmol) under argon. The stirring mixture was cooled to –78 °C and ^{i}PrMgCl (2.0 M in THF, 41 mL, 82 mmol) was added dropwise over 50 min. After stirring for 3 h at –78 °C, 2-isopropoxy-4,4,5,5-tetramethyl-1,3,2-dioxaborolane (15.5 ml, 75.8 mmol) was added dropwise and the mixture allowed to warm slowly to RT overnight. Saturated aqueous NH_4Cl (50 mL) was added to quench. The resulting mixture was stirred until the precipitate settled before being filtered through a pad of Celite and washed through with Et_2O. Organics were dried over $MgSO_4$ and concentrated under reduced pressure. Column chromatography [SiO_2, petroleum ether-EtOAc (9:1)] yielded dioxaborolane **155** as a solid (24.58 g, 98%). R_f [SiO_2, petroleum ether-EtOAc (9:1)]: 0.45. Mp: 95-96 °C [Lit.[134] 93.9-98.4 °C (Et_2O)]. δ_H (400 MHz, $CDCl_3$): 7.72 (2H, d, J = 8.2 Hz, H-2' and H-6'), 7.51 (2H, d, J = 8.1 Hz, H-3' and H-5'), 1.33 (12H, s, 4 × Me). δ_C (100 MHz, $CDCl_3$): 136.90 (CH), 136.26 (CH), 98.83 (C), 84.01 (C), 24.84 (CH_3). ^1H and ^{13}C NMR data agree with literature.[134]

{4-[(2'-Aminophenyl)amino]but-1-yl}triphenylphosphonium methanesulfonate (MitoDA) 156

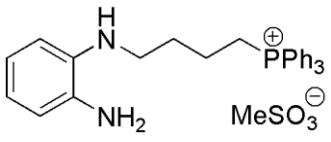

Method A:

Pd/C (281 mg, 10% Pd on C, 0.26 mmol) was added to a solution of azide **163** (950 mg, 1.9 mmol) in MeOH (12 mL) and H_2 (g) was bubbled through for 24 h. The mixture was filtered and concentrated until reduced pressure. The crude oil was dissolved in anhydrous MeCN (15 mL) under argon. 1-Fluoro-2,4-dinitrobenzene (0.6 mL, 5.9 mmol) and anhydrous triethylamine (0.9 mL, 6.3 mmol) were added and the solution stirred at 40 °C

for 18 h before concentrating under reduced pressure. The residue was dissolved in $CHCl_3$ (8 mL) and the salt was precipitated by adding the solution dropwise to vigourously stirring Et_2O (300 mL). The precipitate was collected by filtration, washed with Et_2O and dried under reduced pressure. The crude orange glass was dissolved in EtOH:H_2O (35 mL:25 mL). $NaHCO_3$ (727 mg, 8.7 mmol) and $Na_2S_2O_4$ (1.84 g, 82%, 8.7 mmol) were added and the solution stirred at 30 °C for 1 h. A further $Na_2S_2O_4$ (1.84 g, 82%, 8.7 mmol) was added and the mixture stirred at 30 °C for a further 1 h. The mixture was filtered and the precipitate washed with $CHCl_3$. The filtrate was concentrated under reduced pressure and column chromatography [SiO_2, DCM-EtOH (1:0) to (4:1)] gave the target phophonium salt with a mixture of anions. The mixed salt was washed through an ion-exchange resin (7 g) loaded with methanesulfonate anions (Appendix 1) in a MeOH-H_2O (1:1) solution. Concentration of the eluent under reduced pressure yielded phosphonium methanesulfonate **156** as a sticky light brown glass (189 g, 23%). The compound was stored under argon. R_f [SiO_2, DCM-EtOH (9:1)]: 0.17. ν_{max} (ATR): 3358 (NH_2), 3059 (CH), 2932 (CH), 2870 (CH), 1651 (Ar), 1591 (Ar), 1520 (Ar), 1180 (S=O) cm^{-1}. δ_H (400 MHz, $CDCl_3$): 7.79-7.71 (9H, m, 6 × *o*-H PPh_3 and 3 × *p*-H PPh_3), 7.69-7.62 (6H, m, 6 × *m*-H PPh_3), 6.63 (1H, td, J = 7.5 and 1.5 Hz, H-5'), 6.58 (1H, dd, J = 7.6 and 1.6 Hz, H-3'), 6.53 (1H, td, J = 7.4 and 1.1 Hz, H-4'), 6.48 (1H, dd, J = 7.8 and 1.0 Hz, H-6'), 3.68 (3H, broad s, NH and NH_2), 3.67-3.59 (2H, m, 2 × H-1), 3.44 (2H, broad t, J = 5.9 Hz, 2 × H-4), 2.06-1.98 (2H, m, 2 × H-3), 1.85-1.75 (2H, m, 2 × H-2). δ_C (100 MHz, $CDCl_3$): 136.57 (C), 134.91 (d, J = 3.0 Hz, CH), 134.86 (C), 133.60 (d, J = 9.8 Hz, CH), 130.44 (d, J = 12.7 Hz, CH), 118.94 (CH), 118.48 (d, J = 85.7 Hz, C), 117.68 (CH), 115.28 (CH), 110.75 (CH), 42.97 (CH_2), 39.55 (CH_3), 28.70 (d, J = 6.4 Hz, CH_2), 21.84 (d, J = 50.2 Hz, CH_2), 20.61 (d, J = 4.2 Hz, CH_2). δ_P {^{1}H} (162 MHz, $CDCl_3$): 24.14 (s). LRMS (ESI^+): 425 (cation, 100%). HRMS: 425.2130. $C_{28}H_{30}N_2P$ requires cation, 425.2141. LRMS (ESI^-): 95 (MsO^-, 100%).

Method B:

EtOH (0.9 mL) and H_2O (0.9 mL) were added to a stirring mixture of phosphonium bromide **173** (40 mg, 75 μmol), $NaHCO_3$ (44 mg, 524 μmol) and $Na_2S_2O_4$ (112 mg, 82%, 527 μmol) under argon. The resulting mixture was stirred at RT for 45 min before concentrating under reduced pressure. Extracts from the solid residue were made with $CHCl_3$ (2 × 5 mL). Combined organic extracts were dried over Na_2SO_4 and concentrated under reduced pressure. Flash column chromatography [SiO_2, DCM-EtOH (1:0) to (4:1)] yielded the target phophonium salt with a mixture of anions. The mixed salt was washed

through an ion-exchange resin (7 g) loaded with methanesulfonate anions (Appendix 1) in a MeOH-H_2O (1:1) solution. Concentration of the eluent under reduced pressure yielded phosphonium methanesulfonate **156** as a sticky light brown glass (16.1 mg, 41%). *Characterisation as previous.*

{4-[(2'-Aminophenyl)amino]but-1'-yl}tri(pentadeuterophenyl)phosphonium methanesulfonate (MitoDA-d_{15}) 157

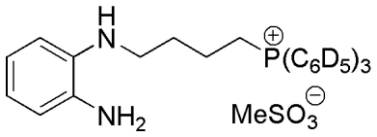

EtOH (0.9 mL) and H_2O (0.9 mL) were added to a stirring mixture of phosphonium bromide **174** (40 mg, 73 μmol), $NaHCO_3$ (37 mg, 440 μmol) and $Na_2S_2O_4$ (55 mg, 82%, 438 μmol) under argon. The resulting mixture was stirred at RT for 45 min before concentrating under reduced pressure. Extracts from the solid residue were made with $CHCl_3$ (2 × 5 mL). Combined organic extracts were dried over Na_2SO_4 and concentrated under reduced pressure. Flash column chromatography [SiO_2, DCM-EtOH (1:0) to (4:1)] yielded phophonium salt with a mixture of anions. The mixed salt was washed through an ion-exchange resin (7 g) loaded with methanesulfonate anions (Appendix 1) in a MeOH-H_2O (1:1) solution. Concentration of the eluent under reduced pressure yielded phosphonium methanesulfonate **157** as a sticky light brown glass (22.0 mg, 57%). The compound was stored under argon. R_f [SiO_2, DCM-EtOH (9:1)]: 0.17. ν_{max} (ATR): 3362 (NH), 2992 (CH), 2932 (CH), 2866 (CH), 2274 (CD), 2234 (CD), 1649 (Ar), 1597 (Ar), 1519 (Ar), 1182 (S=O) cm^{-1}. δ_H (500 MHz, $CDCl_3$): 6.63 (1H, td, *J* = 7.4 and 1.7 Hz, H-5'), 6.58 (1H, dd, *J* = 7.6 and 1.7 Hz, H-3'), 6.53 (1H, td, *J* = 7.4 and 1.3 Hz, H-4'), 6.47 (1H, dd, *J* = 7.8 and 1.2 Hz, H-6'), 3.97 (3H, broad s, NH and NH_2), 3.81-3.65 (2H, m, 2 × H-1), 3.24 (2H, broad t, *J* = 5.6 Hz, 2 × H-4), 2.72 (3H, s, Me), 2.10-1.98 (2H, m, 2 × H-3), 1.88-1.74 (2H, m, 2 × H-2). δ_C (126 MHz, $CDCl_3$): 136.35 (C), 135.12 (C), 134.64-134.11 (m, CD), 133.53-132.94 (m, CD), 130.25-129.60 (m, CD), 118.61 (CH), 118.35 (d, *J* = 85.3 Hz, C), 117.45 (CH), 114.93 (CH), 110.38 (CH), 42.91 (CH_2), 39.60 (CH_3), 28.53 (d, *J* = 16.4 Hz, CH_2), 21.87 (d, *J* = 49.9 Hz, CH_2), 20.70 (d, *J* = 4.0 Hz, CH_2). δ_P {^{1}H} (162 MHz, $CDCl_3$): 24.46-24.02 (m). LRMS (ESI^+): 440 (cation, 100%). HRMS: 440.3082. $C_{28}H_{15}D_{15}N_2P$ requires cation, 440.3083. LRMS (ESI^-): 95 (MsO^-, 100%). ^{1}H NMR data for partially deuterated aromatic ring P(C_6D_4H) integrated relative to other signals in ^{1}H NMR: 7.78 (0.031H, d, *J* = 12.7 Hz, *o*-H PPh_3), 7.75 (0.018H, d, *J* = 1.8 Hz, *p*-H PPh_3), 7.65 (0.028H, d, *J* = 3.4 Hz, *m*-H PPh_3).

[4-(1'*H*-1',2',3'-benzotriazol-1'-yl)but-1-yl]triphenylphosphonium iodide (MitoBT) 158

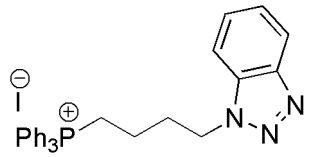

A solution of alkyl iodide **180** (135 mg, 0.45 mmol) and triphenylphosphine (1.18 g, 4.5 mmol) in DCM (1.2 mL) was stirred at 30 °C for 48 h. $CHCl_3$ (2.5 mL) was added and the salt precipitated by adding the solution dropwise to vigouously stirring Et_2O (80 mL). After filtering, the residue was loaded onto a pad of silica in $CHCl_3$, washed with EtOAc before $CHCl_3$-EtOH (9:1) was used to elute the product. Drying under reduced pressure yielded phophonium iodide **158** as a sticky glass (240 mg, 95%). ν_{max} (ATR): 3053 (CH), 3009 (CH), 2990 (CH), 2920 (CH), 2895 (CH), 1613 (Ar), 1587 (Ar) cm^{-1}. δ_H (500 MHz, $CDCl_3$): 7.96 (1H, broad d, *J* = 8.4 Hz, H-4'), 7.81 (1H, broad d, *J* = 8.4 Hz, H-7'), 7.79-7.72 (9H, m, 6 × *o*-H PPh_3 and 3 × *p*-H PPh_3), 7.68-7.62 (m, 6 × *m*-H PPh_3), 7.46 (ddd, *J* = 8.4, 7.0 and 0.9 Hz, H-6'), 7.34 (ddd, *J* = 8.4, 6.9 and 0.9 Hz, H-5'), 4.87 (2H, t, *J* = 6.5 Hz, 2 × H-4), 3.89-3.77 (2H, m, 2 × H-1), 2.55-2.45 (2H, m, 2 × H-3), 1.86-1.72 (2H, m, 2 × H-2). δ_C (126 MHz, $CDCl_3$): 145.78 (C), 135.16 (d, *J* = 3.0 Hz, CH), 133.65 (d, *J* = 10.1 Hz, CH), 132.97 (C), 130.54 (d, *J* = 12.3 Hz, CH), 127.55 (CH), 124.01 (CH), 119.52 (CH), 117.72 (d, *J* = 86.2 Hz, C), 110.39 (CH), 46.98 (CH_2), 29.32 (d, *J* = 17.1 Hz, CH_2), 22.28 (d, *J* = 51.2 Hz, CH_2), 19.49 (d, *J* = 3.6 Hz, CH_2). δ_P {^{1}H} (202 MHz, $CDCl_3$): 24.30 (s). LRMS (ESI^+): 451 (cation, 100%). HRMS: 436.1927. $C_{28}H_{27}N_3P$ requires cation, 436.1937. LRMS (ESI^-): 127 (I^-, 100%).

[4-(1'*H*-1',2',3'-benzotriazol-1'-yl)butyl]tri(pentadeuterophenyl)phosphonium iodide (MitoBT-d_{15}) 159

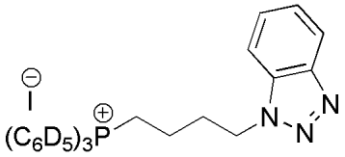

A solution of alkyl iodide **180** (181 mg, 0.60 mmol) and tri(pentadeuterophenyl)phosphine (200 mg, 0.72 mmol) in DCM (0.5 mL) was stirred at 30 °C for 72 h. $CHCl_3$ (1.5 mL) was added and the salt precipitated by adding the solution dropwise to vigouously stirring Et_2O (60 mL). After filtering, the residue was loaded onto a pad of silica in $CHCl_3$, washed with EtOAc before $CHCl_3$-EtOH (9:1) was used to elute the product. Drying under reduced pressure yielded phophonium iodide **159** as a sticky glass (302 mg, 87%). ν_{max} (ATR): 2918 (CH), 2868 (CH), 2793 (CH), 2255 (CD), 2191 (CD), 1613 (Ar), 1549 (Ar) cm^{-1}. δ_H

(500 MHz, $CDCl_3$): 7.99 (1H, broad d, *J* = 8.4 Hz, H-4'), 7.80 (1H, broad d, *J* = 8.4 Hz, H-7'), 7.48 (1H, ddd, *J* = 8.4, 7.0 and 0.8 Hz, H-6'), 7.35 (1H, ddd, *J* = 8.4, 6.9 and 0.8 Hz, H-5'), 4.89 (2H, t, *J* = 6.4 Hz, 2 × H-4), 3.94-3.84 (2H, m, 2 × H-1), 2.58-2.48 (2H, m, 2 × H-3), 1.69-1.59 (2H, m, 2 × H-2). δ_C (126 MHz, $CDCl_3$): 145.86 (C), 134.88-134.14 (m, CD), 133.59-132.94 (m, CD), 132.99 (C), 130.35-129.69 (m, CD), 127.58 (CH), 124.01 (CH), 119.58 (CH), 117.62 (d, *J* = 86.1 Hz, C), 110.35 (CH), 46.88 (CH_2), 29.14 (d, *J* = 17.3 Hz, CH_2), 22.40 (d, *J* = 51.1 Hz, CH_2), 19.42 (d, *J* = 3.6 Hz, CH_2). δ_P {^{1}H} (202 MHz, $CDCl_3$): 24.53-24.20 (m). LRMS (ESI^+): 451 (cation, 100%). HRMS: 451.2867. $C_{28}H_{12}D_{15}N_3P$ requires cation, 451.2879. LRMS (ESI^-): 127 (I^-, 100%). ^{1}H NMR data for partially deuterated aromatic ring P(C_6D_4H) integrated relative to other signals in ^{1}H NMR: 7.76 (d, *J* = 12.9 Hz, *o*-H PPh_3), 7.65 (0.031H, d, *J* = 3.4 Hz, *m*-H PPh_3). The *p*-H PPh_3 signal and the integration for the *o*-H PPh_3 obscured due to other aromatic signals.

(4-Iodobutyl)triphenylphosphonium iodide 161

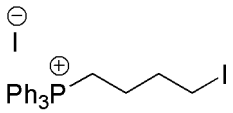

1,4-Diiodobutane **160** (3.0 mL, 22.7 mmol) was added to a solution of triphenylphosphine (3.00 g, 11.4 mmol) in toluene (30 mL) and the resulting solution stirred at 95 °C for 48 h. After cooling to RT the precipitate was collected by filtration, washed with Et_2O (30 mL) and residual solvent removed under reduced pressure to yield phosphonium iodide **161** as an amorphous solid (6.46 g, 99%). A portion of the solid was dissolved in minimal $CHCl_3$ and allowed to re-crystallise slowly through evaporation to give phosphonium iodide **161** as needles. Mp: 168-169 °C (Needles). ν_{max} (ATR): 3074 (CH), 3052 (CH), 3007 (CH), 2952 (CH), 2889 (CH), 2858 (CH), 2785 (CH), 1587 (Ar), 1484 (Ar) cm^{-1}. δ_H (400 MHz, $CDCl_3$): 7.90-7.79 (9H, m, 6 × *o*-H PPh_3 and 3 × *p*-H PPh_3), 7375-7.69 (6H, m, 6 × *m*-H PPh_3), 3.88-3.78 (2H, m, 2 × H-1), 3.35 (2H, t, *J* = 6.2 Hz, 2 × H-4), 2.28-2.19 (2H, m, 2 × H-2), 1.88-1.76 (2H, m, 2 × H-3). δ_C (100 MHz, $CDCl_3$): 135.24 (d, *J* = 3.0 Hz, CH), 133.76 (d, *J* = 10.1 Hz, CH), 130.63 (d, *J* = 12.5 Hz, CH), 117.90 (d, *J* = 86.1 Hz, C), 32.52 (d, *J* = 17.0 Hz, CH_2), 23.23 (d, *J* = 3.6 Hz, CH_2), 21.98 (d, *J* = 51.2 Hz, CH_2), 7.41 (CH_2). δ_P {^{1}H} (162 MHz, $CDCl_3$): 24.34 (s). LRMS (ESI^+): 445 (cation, 100%), 289 (18). HRMS: 445.0564. $C_{22}H_{23}IP$ requires cation, 445.0577. LRMS (ESI^-): 127 (I^-, 100%).

(4-Iodobut-1-yl)tri(pentadeuterophenyl)phosphonium iodide 162

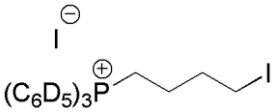

1,4-Diiodobutane **160** (0.57 mL, 4.3 mmol) was added to a solution of tri(pentadeuterophenyl)phosphine (300 mg, 1.1 mmol) in toluene (5 mL). The resulting solution was stirred at 80 °C for 24 h under argon. After cooling to RT the precipitate was collected by filtration, washed with Et_2O and residual solvent removed under reduced pressure to yield phosphonium iodide **162** as an amorphous solid (574 mg, 88%). Mp: 169-170 °C. ν_{max} (ATR): 2929 (CH), 2889 (CH), 2857 (CH), 2784 (CH), 1547 (Ar) cm^{-1}. δ_H (400 MHz, $CDCl_3$): 3.78-3.66 (2H, m, 2 × H-1), 3.31 (2H, t, J = 6.5 Hz, 2 × H-4), 2.30-2.18 (2H, m, 2 × H-3), 1.90-1.77 (2H, m, 2 × H-2). δ_C (100 MHz, $CDCl_3$): 135.06-134.27 (m, CD), 133.55-132.61 (m, CD), 130.54-129.52 (m, CD), 117.31 (d, J = 86.0 Hz, C), 32.60 (d, J = 16.9 Hz, CH_2), 23.09 (d, J = 3.5 Hz, CH_2), 21.75 (d, J = 51.4 Hz, CH_2), 7.18 (CH_2). δ_P (162 MHz, $CDCl_3$): 23.90-23.49 (m). LRMS (ESI^+): 460 (cation, 100%). HRMS (ESI^+): 460.1507. $C_{22}H_8D_{15}IP$ requires cation, 460.1518. LRMS (ESI^-): 127 (I^-, 100%). ^1H NMR data for partially deuterated aromatic ring $P(C_6D_4H)$ integrated relative to other signals in ^1H NMR: 7.88 (0.031H, d, J = 12.6 Hz, *o*-H PPh_3), 7.87 (0.019H, d, J = 2.5 Hz, *p*-H PPh_3), 7.77 (0.030H, d, J = 3.5 Hz, *m*-H PPh_3).

(4-Azidobut-1-yl)triphenylphosphonium iodide 163

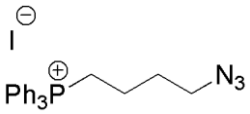

A solution of alkyl iodide **161** (3.25 g, 5.7 mmol) and NaN_3 (741 mg, 11.4 mmol) in EtOH (20 mL) and H_2O (20 mL) was stirred at 70 °C for 18 h. After cooling to RT, extracts were made with $CHCl_3$ (2 × 50 mL). Combined organics were dried over Na_2SO_4 and concentrated under reduced pressure to yield phophonium iodide **161** as an amorphous solid (2.74 g, 99%). Mp: 145-146 °C. ν_{max} (ATR): 3053 (CH), 3007 (CH), 2945 (CH), 2893 (CH), 2868 (CH), 2789 (CH), 2097 (N_3), 1993 (N_3), 1587 (Ar), 1574 (Ar) cm^{-1}. δ_H (400 MHz, $CDCl_3$): 7.88-7.79 (9H, m, 6 × *o*-H PPh_3 and 3 × *p*-H PPh_3), 7.78-7.70 (6H, m, 6 × *m*-H PPh_3), 3.79-3.66 (2H, m, 2 × H-1), 3.45 (2H, t, J = 6.3 Hz, 2 × H-4), 2.06-1.96 (2H, m, 2 × H-3), 1.83-1.70 (2H, m, 2 × H-2). δ_C (100 MHz, $CDCl_3$): 135.04 (d, J = 2.9 Hz, CH), 133.43 (d, J = 10.1 Hz, CH), 130.43 (d, J = 12.5 Hz, CH), 117.60 (d, J = 86.2 Hz, C), 50.35 (CH_2), 29.06 (d, J = 16.6 Hz, CH_2), 22.30 (d, J = 51.1 Hz, CH_2), 19.61 (d, J = 3.9 Hz, CH_2). δ_P (162 MHz, $CDCl_3$): 24.02 (broad s). LRMS (ESI^+): 847 [(2 × cation) + I^-,

6%], 360 (cation, 100), 332 (28), 289 (65). HRMS (ESI^+): 360.1622. $C_{22}H_{23}N_3P$ requires cation, 360.1624. LRMS (ESI^-): 127 (I^-, 100%).

(4-Azidobut-1-yl)tri(pentadeuterophenyl)phosphonium iodide 164

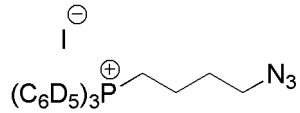

A solution of alkyl iodide **162** (250 mg, 0.43 mmol) and NaN_3 (55 mg, 0.85 mmol) in EtOH (1.5 mL) and H_2O (1.5 mL) was stirred at 70 °C for 18 h. H_2O (2 mL) was added and extracts made with $CHCl_3$ (2 × 5 mL). Combined organics were dried over Na_2SO_4 and concentrated under reduced pressure to yield phophonium iodide **164** as an amorphous solid (210 mg, 98%). Mp: 153-154 °C. ν_{max} (ATR): 2940 (CH), 2893 (CH), 2868 (CH), 2797 (CH), 2247 (CD), 2153 (CD), 2095 (N_3), 1547 (Ar) cm^{-1}. δ_H (400 MHz, $CDCl_3$): 3.79-3.65 (2H, m, 2 × H-1), 3.44 (2H, t, J = 6.4 Hz, 2 × H-4), 2.10-1.96 (2H, m, 2 × H-3), 1.86-1.72 (2H, m, 2 × H-2). δ_C (100 MHz, $CDCl_3$): 134.31-133.54 (m, CD), 132.78-131.94 (m, CD), 129.72-128.87 (m, CD), 116.64 (d, J = 86.0 Hz, C), 49.70 (CH_2), 28.44 (d, J = 16.6 Hz, CH_2), 21.68 (d, J = 51.2 Hz, CH_2), 18.93 (d, J = 3.7 Hz, CH_2). δ_P {^{1}H} (162 MHz, $CDCl_3$): 23.82-22.90 (m). LRMS (ESI^+): 375 (cation, 100%). HRMS: 375.2561. $C_{22}H_8D_{15}N_3P$ requires cation, 375.2566. LRMS (ESI^-): 127 (I^-, 100%). ^{1}H NMR data for partially deuterated aromatic ring $P(C_6D_4H)$ integrated relative to other signals in ^{1}H NMR: 7.86 (0.031H, d, J = 12.7 Hz, *o*-H PPh_3), 7.86 (0.018H, d, J = 1.5 Hz, *p*-H PPh_3), 7.76 (0.031H, d, J = 3.4 Hz, *m*-H PPh_3).

[4-(*N*-Phthalimido)but-1-yl]triphenylphosphonium bromide 169

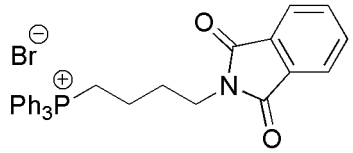

N-(4-Bromobut-1-yl)phthalimide **168** (600 mg, 2.1 mmol) and triphenylphosphine (7.4 g, 28 mmol) in toluene (50 mL) were stirred at 95 °C for 24 h during which a white precipitate formed. After cooling to RT, toluene was decanted off. The residue was dissolved in (5 mL) $CHCl_3$ and the salt precipitated by adding the solution dropwise to vigouously stirring Et_2O (80 mL). The precipitate was collected by filtration, washed with Et_2O and dried under reduced pressure to yield phophonium bromide **169** as an oil (521 mg, 45%). ν_{max} (ATR): 3048 (CH), 2953 (CH), 2872 (CH), 2799 (CH), 1705 (C=O), 1624 (Ar), 1610 (Ar), 1586 (Ar) cm^{-1}. δ_H (500 MHz, $CDCl_3$): 7.88-7.81 (6H, m, 6 × *o*-H PPh_3), 7.79-7.71 (7H, m, 3 × *p*-H PPh_3 and 4 × H Phthal), 7.70-7.64 (6H, m, 6 × *m*-H PPh_3),

4.03-3.92 (2H, m, 2 × H-1), 3.76 (2H, t, J = 6.3 Hz, 2 × H-4), 2.20-2.10 (2H, m, 2 × H-3), 1.67-1.53 (2H, m, 2 × H-2). δ_C (126 MHz, $CDCl_3$): 167.73 (C), 134.52 (d, J = 2.5 Hz, CH), 133.77 (CH), 133.08 (d, J = 10.0 Hz, CH), 130.99 (C), 129.09 (d, J = 12.5 Hz, CH), 122.56 (CH), 117.34 (d, J = 86.0 Hz, C), 35.64 (CH_2), 27.92 (d, J = 16.8 Hz, CH_2), 21.05 (d, J = 50.9 Hz, CH_2), 18.81 (d, J = 2.9 Hz, CH_2). δ_P {^{1}H} (162 MHz, $CDCl_3$): 24.36 (s). LRMS (ESI^+): 464 (cation, 100%). HRMS: 464.1768. $C_{28}H_{27}NO_2P$ requires cation, 464.1774. LRMS (ESI^-): 81 ($^{81}Br^-$, 98%) and 79 ($^{79}Br^-$, 100).

[4-(*N*-Phthalimido)but-1-yl]tri(pentadeuterophenyl)phosphonium bromide 170

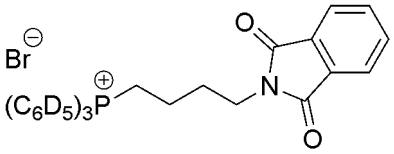

N-(4-Bromobutyl)phthalimide **169** (183 mg, 0.65 mmol) and tri(pentadeuterophenyl)phosphine (150 mg, 0.54 mmol) in toluene (6 mL) were stirred at 95 °C for 24 h during which a white precipitate formed. After cooling to RT, toluene was decanted off. The residue was dissolved in $CHCl_3$ and the salt precipitated by adding the solution dropwise to vigouously stirring Et_2O (80 mL). The precipitate was collected by filtration, washed with Et_2O and dried under reduced pressure to yield phophonium bromide **170** as an oil (169 mg, 56%). ν_{max} (ATR): 2915 (CH), 2251 (CD), 1703 (C=O), 1613 (Ar), 1549 (Ar) cm^{-1}. δ_H (500 MHz, $CDCl_3$): 7.77-7.70 (4H, m, 4 × Phthalimide), 4.07-3.98 (2H, m, 2 × H-1), 3.77 (2H, t, J = 6.3 Hz, 2 × H-4), 2.20-2.12 (2H, m, 2 × H-3), 1.66-1.57 (2H, m, 2 × H-2). δ_C (126 MHz, $CDCl_3$): 168.33 (C), 134.72-134.28 (m, CD), 134.06 (CH), 133.75-133.08 (m, CD), 131.82 (C), 130.28-129.60 (m, CD), 123.15 (CH), 117.34 (d, J = 86.0 Hz, C), 36.40 (CH_2), 28.50 (d, J = 16.8 Hz, CH_2), 21.69 (d, J = 50.8 Hz, CH_2), 19.47 (d, J = 3.8 Hz, CH_2). δ_P {^{1}H} (162 MHz, $CDCl_3$): 24.93-24.53 (m). LRMS (ESI^+): 479 (cation, 100%). (ESI^-): 81 ($^{81}Br^-$, 98%) and 79 ($^{79}Br^-$, 100). HRMS: 479.2707. $C_{30}H_{12}D_{15}NO_2P$ requires cation, 479.2715.

(4-Aminobut-1-yl)triphenylphosphonium bromide 171

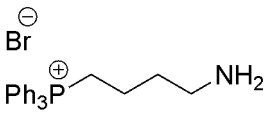

$N_2H_4.H_2O$ (31 µL, 64%, 0.41 mmol) was added to a stirring solution of phthalimide **169** (150 mg, 0.33 mmol) in MeOH (0.2 mL) and the resultant solution was stirred overnight at RT. After concentrating under reduced pressure, $CHCl_3$ (5 mL) was added followed by Na_2SO_4. The suspension was filtered and the filtrate concentrated under reduced pressure

to yield amine **171** as a pale yellow oil (165 mg, 89%). ν_{max} (ATR): 3368 (NH_2), 2985 (CH), 2924 (CH), 2864 (CH), 1614 (Ar), 1589 (Ar) cm^{-1}. δ_H (500 MHz, $CDCl_3$): 7.88-7.77 (9H, m, 6 × *o*-H PPh_3 and 3 × *p*-H PPh_3), 7.77-7.68 (6H, m, 6 × *m*-H PPh_3), 3.76-3.61 (2H, m, 2 × H-1), 2.78 (2H, t, J = 6.7 Hz, 2 × H-4), 2.34 (2H, broad s, NH_2), 1.94-1.83 (2H, m, 2 × H-3), 1.81-1.78 (2H, m, 2 × H-2). δ_C (126 MHz, $CDCl_3$): 135.02 (d, J = 3.0 Hz, CH), 133.45 (d, J = 10.0 Hz, CH), 130.41 (d, J = 12.6 Hz, CH), 117.91 (d, J = 86.0 Hz, C), 40.79 (CH_2), 32.85 (d, J = 7.6 Hz, CH_2), 22.62 (d, J = 50.1 Hz, CH_2), 19.97 (d, J = 3.9 Hz, CH_2). δ_P (162 MHz, $CDCl_3$): 24.06 (s). LRMS (ESI^+): 334 (cation, 100%). HRMS (ESI^+): 334.1725. $C_{22}H_{25}NP$ requires cation, 334.1719. LRMS (ESI^-): 81 ($^{81}Br^-$, 98%) and 79 ($^{79}Br^-$, 100).

(4-Aminobut-1-yl)tri(pentadeuterophenyl)phosphonium iodide 172

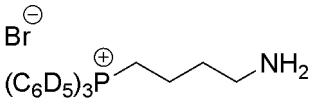

$N_2H_4.H_2O$ (35 µL, 64%, 0.46 mmol) was added to a stirring solution of phthalimide **170** (160 mg, 0.29 mmol) in MeOH (0.3 mL) and the resultant solution was stirred overnight at RT. After concentrating under reduced pressure, $CHCl_3$ (5 mL) was added followed by Na_2SO_4. The suspension was filtered and the filtrate concentrated under reduced pressure to yield amine **172** a pale yellow oil (116 mg, 94%). ν_{max} (ATR): 3358 (NH_2), 2916 (CH), 2870 (CH), 1589 (Ar) cm^{-1}. δ_H (500 MHz, $CDCl_3$): 3.84-3.73 (2H, m, 2 × H-1), 2.79 (4H, broad s, 2 × H-4 and NH_2), 1.96-1.83 (2H, m, 2 × H-3), 1.81-1.67 (2H, m, 2 × H-2). δ_C (126 MHz, $CDCl_3$): 134.96-134.20 (m, CD), 133.66-132.94 (m, CD), 130.44-129.68 (m, CD), 118.06 (d, J = 85.8 Hz, C), 40.74 (CH_2), 32.88 (d, J = 7.6 Hz, CH_2), 22.58 (d, J = 50.0 Hz, CH_2), 20.05 (d, J = 4.1 Hz, CH_2). δ_P (162 MHz, $CDCl_3$): 24.29-23.82 (m). LRMS (ESI^+): 349 (cation, 100%). HRMS (ESI^+): 349.2663. $C_{21}H_{10}D_{15}NP$ requires cation, 349.2661. LRMS (ESI^-): 81 ($^{81}Br^-$, 98%) and 79 ($^{79}Br^-$, 100). ^1H NMR data for partially deuterated aromatic ring $P(C_6D_4H)$ integrated relative to other signals in ^1H NMR: 7.83 (0.032H, d, J = 12.7 Hz, *o*-H PPh_3), 7.80 (0.018H, d, J = 1.8 Hz, *p*-H PPh_3), 7.71 (0.030H, d, J = 3.4 Hz, *m*-H PPh_3).

{4-[(2'-Nitrophenyl)amino]but-1-yl}triphenylphosphonium bromide 173

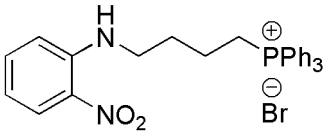

1-Fluoro-2-nitrobenzene (85 μL, 0.81 mmol) was added to a stirring solution of amine **171** (110 mg, 0.3 mmol) in anhydrous MeCN (0.5 mL) under argon. Anhydrous triethylamine (120 μL, 0.86 mmol) was added dropwise and the resulting solution stirred at 40 °C overnight. After cooling to RT the solution was concentrated under reduced pressure then re-dissolved in $CHCl_3$ (3 mL). The solution was added dropwise to vigourously stirring Et_2O (90 mL) and the precipitate collected by filtration. The solid was dissolved in $CHCl_3$ (8 mL) and washed with H_2O (5 mL). Organics were dried over Na_2SO_4 and concentrated under reduced pressure to yield phosphonium bromide **173** as an orange glass (135 mg, 95%). R_f [SiO_2, DCM-EtOH (9:1)]: 0.48. ν_{max} (ATR): 3377 (NH), 3053 (CH), 3007 (CH), 2866 (CH), 2793 (CH), 1614 (Ar), 1570 (Ar), 1352 (NO_2) cm^{-1}. δ_H (500 MHz, $CDCl_3$): 8.07 (1H, dd, J = 8.6 and 1.5 Hz, H-3'), 7.92 (1H, broad t, J = 5.1 Hz, NH), 7.89-7.81 (6H, m, 6 × *o*-H PPh_3), 7.81-7.74 (3H, m, 3 × *p*-H PPh_3), 7.72-7.64 (6H, m, 6 × *m*-H PPh_3), 7.43 (1H, ddd, J = 8.5, 7.0 and 1.3 Hz, H-5'), 6.99 (1H, dd, J = 8.6 and 0.6 Hz, H-6'), 6.60 (1H, ddd, J = 8.6, 6.9 and 1.1 Hz, H-4'), 4.03-3.87 (2H, m, 2 × H-1), 3.51 (2H, td, J = 6.4 and 5.6 Hz, 2 × H-4), 2.21-2.08 (2H, m, 2 × H-3), 1.89-1.73 (2H, m, 2 × H-2). δ_C (126 MHz, $CDCl_3$): 145.47 (C), 136.61 (CH), 135.08 (d, J = 2.8 Hz, CH), 133.68 (d, J = 10.0 Hz, CH), 131.66 (C), 130.52 (d, J = 12.7 Hz, CH), 126.56 (CH), 118.11 (d, J = 85.8 Hz, C), 115.41 (CH), 114.56 (CH), 41.84 (CH_2), 29.07 (d, J = 16.4 Hz, CH_2), 22.34 (d, J = 50.6 Hz, CH_2), 19.92 (d, J = 3.8 Hz, CH_2). δ_P {^{1}H} (162 MHz, $CDCl_3$): 24.40 (s). LRMS (ESI^+): 455 (cation, 100%). HRMS: 455.1873. $C_{28}H_{28}N_2O_2P$ requires cation, 455.1883. LRMS (ESI^-): 81 (Br^-, 100) and 79 (Br^-, 94%).

{4-[(2'-Nitrophenyl)amino]but-1-yl}tri(pentadeuterophenyl)phosphonium bromide 174

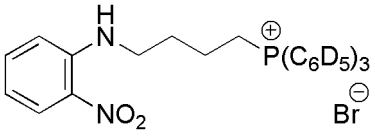

1-Fluoro-2-nitrobenzene (0.2 mL, 1.9 mmol) was added to a stirring solution of amine **172** (102 mg, 0.24 mmol) in anhydrous MeCN (0.5 mL) under argon. Anhydrous triethylamine (150 μL, 1.1 mmol) was added dropwise and the resulting solution stirred at 40 °C overnight. After cooling to RT the solution was concentrated under reduced pressure then re-dissolved in $CHCl_3$ (3 mL). The solution was added dropwise to vigourously stirring

Et_2O (80 mL) and the precipitate collected by filtration. The solid was dissolved in $CHCl_3$ (8 mL) and washed with H_2O (5 mL). Organics were dried over Na_2SO_4 and concentrated under reduced pressure to yield phosphonium bromide **174** as an orange glass (118 mg, 83%). ν_{max} (ATR): 3377 (NH), 2866 (CH), 2793 (CH), 2251 (CD), 1616 (Ar), 1570 (Ar), 1352 (NO_2) cm^{-1}. δ_H (500 MHz, $CDCl_3$): 8.06 (1H, dd, *J* = 8.7 and 1.6 Hz, H-3'), 7.91 (1H, broad t, *J* = 5.1 Hz, NH), 7.42 (1H, ddd, *J* = 8.6, 7.1 and 1.4 Hz, H-5'), 6.98 (1H, broad d, *J* = 8.7 Hz, H-6'), 6.60 (1H, ddd, *J* = 8.6, 7.0 and 1.1 Hz, H-4'), 3.98-3.89 (2H, m, 2 × H-1), 3.51 (2H, broad td, *J* = 6.5 and 5.7 Hz, 2 × H-4), 2.18-2.10 (2H, m, 2 × H-3), 1.86-1.76 (2H, m, 2 × H-2). δ_C (126 MHz, $CDCl_3$): 145.46 (C), 136.60 (CH), 134.97-134.25 (m, CD), 133.63-132.94 (CD), 131.65 (C), 130.46-129.66 (m, CD), 126.55 (CH), 117.87 (d, *J* = 85.8 Hz, C), 115.40 (CH), 114.56 (CH), 41.85 (CH_2), 29.08 (d, *J* = 16.5 Hz, CH_2), 22.36 (d, *J* = 50.6 Hz, CH_2), 19.90 (d, *J* = 3.8 Hz, CH_2). δ_P {^{1}H} (162 MHz, $CDCl_3$): 24.46-24.02 (m). LRMS (ESI^+): 470 (cation, 100%). HRMS: 470.2819. $C_{28}H_{13}D_{15}N_2O_2P$ requires cation, 470.2824. LRMS (ESI^-): 81 ($^{81}Br^-$, 98%) and 79 ($^{79}Br^-$, 100). ^{1}H NMR data for partially deuterated aromatic ring P(C_6D_4H) integrated relative to other signals in ^{1}H NMR: 7.85 (d, *J* = 12.7 Hz, *o*-H PPh_3), 7.65 (0.021H, d, *J* = 1.8 Hz, *p*-H PPh_3). The *m*-H PPh_3 signal and the integration for the *o*-H PPh_3 are obscured due to other aromatic signals.

4-[(2'-Nitrophenyl)amino]butan-1-ol 176

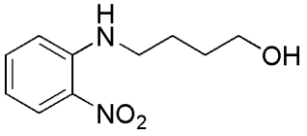

4-Aminobutan-1-ol **175** (340 μL, 3.3 mmol) was added to a stirring solution of 1-fluoro-2-nitrobenzene (300 μL, 3.3 mmol) in MeCN (1.5 mL) followed by the dropwise addition of triethylamine (680 μL, 4.9 mmol). The resulting solution was stirred at 50 °C overnight. After cooling to RT the solution was concentrated under reduced pressure. The residue was dissolved in DCM and flushed through a short pad of silica with DCM followed by DCM-EtOH (19:1) to elute the product. Concentration under reduced pressure yielded alcohol **176** as orange needles (572 mg, 84%). R_f (SiO_2, DCM): 0.10. Mp: 42-43 °C (Lit.[185] 40-41 °C). ν_{max} (ATR): 3378 (NH and OH), 2936 (CH), 2863 (CH), 1616 (Ar), 1571 (Ar), 1507 (NO_2), 1351 (NO_2) cm^{-1}. δ_H (400 MHz, $CDCl_3$): 8.14 (1H, ddd, *J* = 8.6, 1.6 and 0.3 Hz, H-3'), 8.08 (1H, broad t, *J* = 4.0 Hz, NH), 7.42 (1H, dddd, *J* = 8.6, 7.0, 1.6 and 0.6 Hz, H-5'), 6.85 (1H, dd, *J* = 8.7 and 1.2 Hz, H-6'), 6.62 (1H, ddd, *J* = 8.6, 6.9 and 1.2 Hz, H-4'), 3.72 (2H, t, *J* = 6.2 Hz, 2 × H-1), 3.34 (2H, td, *J* = 6.9 and 5.4 Hz, 2 × H-

4), 2.21 (1H, broad s, OH), 1.87-1.78 (2H, m, 2 × H-3), 1.76-1.67 (2H, m, 2 × H-2). δ_C (100 MHz, $CDCl_3$): 145.56 (C), 136.31 (CH), 131.62 (C), 126.83 (CH), 115.17 (CH), 113.81 (CH), 62.18 (CH_2), 42.80 (CH_2), 29.98 (CH_2), 25.41 (CH_2). LRMS (CI^+): 211 [$(M + H)^+$, 100%]. HRMS: 211.1082. $C_{10}H_{15}N_3O_3$ requires $(M + H)^+$, 211.1083.

1-(4'-Iodobut-1-yl)-1*H*-1,2,3-benzotriazole 180

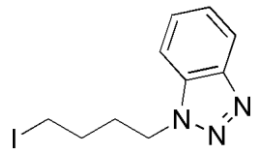

Anhydrous MeCN (40 mL) was added to a stirring mixture of 1*H*-1,2,3-benzotriazole **179** (1.00 g, 8.4 mmol) and K_2CO_3 (1.07 g, 10.1 mmol) followed by 1,4-diiodobutane **160** (4.4 mL, 33.6 mmol) under argon. The resultant mixture stirred at 50 °C for 48 h. After cooling to RT the mixture was concentrated under reduced pressure. $CHCl_3$ (60 mL) was added and the mixture washed with H_2O (2 × 30 mL). Organics were dried over Na_2SO_4 and concentrated under reduced pressure. Column chromatography [SiO_2, petroleum ether-EtOAc (1:0) to (1:1)] yielded alkyl iodide **180** as a pale yellow oil (1.56 g, 46%). R_f [SiO_2, petroleum ether-EtOAc (1:1)]: 0.53. ν_{max} (ATR): 3062 (CH), 2941 (CH), 2852 (CH), 1614 (Ar), 1589 (Ar) cm^{-1}. δ_H (400 MHz, $CDCl_3$): 8.06 (1H, broad dt, *J* = 8.4 and 0.8 Hz, H-4), 7.55 (1H, broad dt, *J* = 8.3 and 1.0 Hz, H-7), 7.50 (1H, ddd, *J* = 8.3, 6.7 and 0.9 Hz, H-6), 7.38 (1H, ddd, *J* = 8.1, 6.7 and 1.2 Hz, H-5), 4.67 (2H, t, *J* = 6.9 Hz, 2 × H-1'), 3.20 (2H, t, *J* = 6.7 Hz, 2 × H-4'), 2.20-2.11 (2H, m, 2 × H-2'), 1.90-1.81 (2H, m, 2 × H-3'). δ_C (100 MHz, $CDCl_3$): 145.97 (C), 132.78 (C), 127.36 (CH), 123.92 (CH), 120.05 (CH), 109.18 (CH), 46.89 (CH_2), 30.27 (CH_2), 30.02 (CH_2), 5.37 (CH_2). LRMS (CI^+): 302 [$(M + H)^+$, 100%]. HRMS: 302.0157. $C_{10}H_{13}N_3I$ requires $(M + H)^+$, 302.0154.

2-(4'-Iodobut-1-yl)-2*H*-1,2,3-benzotriazole 181

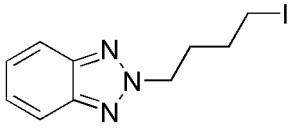

Column chromatography of the mixture that produced alkyl iodide **180** above also gave alkyl iodide **181** (814 mg, 32%) as an oil that solidified on standing. R_f [SiO_2, petroleum ether-EtOAc (1:1)]: 0.67. Mp: 45-46 °C. ν_{max} (ATR): 2955 (CH), 2930 (CH), 2862 (CH), 1568 (Ar) cm^{-1}. δ_H (400 MHz, $CDCl_3$): 7.86 (2H, dd, *J* = 6.5 and 3.1 Hz, H-4 and H-7), 7.37 (2H, dd, *J* = 6.5 and 3.1 Hz, H-5 and H-6), 4.75 (2H, t, *J* = 6.8 Hz, 2 × H-1'), 3.19 (2H, t, *J* = 6.8 Hz, 2 × H-4'), 2.28-2.19 (2H, m, 2 × H-2'), 1.89-1.80 (2H, m, 2 × H-3').

δ_C (100 MHz, $CDCl_3$): 144.28 (C), 126.26 (CH), 117.93 (CH), 55.18 (CH_2), 30.66 (CH_2), 30.06 (CH_2), 5.14 (CH_2). LRMS (CI^+): 302 [$(M + H)^+$, 100%], 189 (72), 133 (42). HRMS: 302.0150. $C_{10}H_{13}IN_3$ requires $(M + H)^+$, 302.0149.

1-[4'-(1''*H*-1'',2'',3''-benzotriazol-1''-yl)but-1'-yl]-1*H*-1,2,3-benzotriazole 182

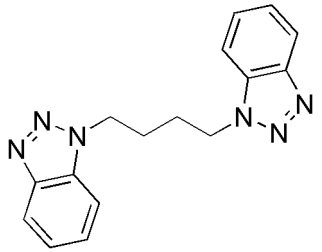

By-product isolated during the attempted synthesis of alkyl iodide **180**. NaH (88 mg, 60% in mineral oil, 2.2 mmol) was added to a stirring solution of 1*H*-1,2,3-benzotriazole (250 mg, 2.1 mmol) and 1,4-diiodobutane (1.1 mL, 8.4 mmol) in anhydrous DMF (4 mL) at 0 °C. The resultant solution was stirred at RT for 2 h. H_2O (8 mL) was added and extracted with $CHCl_3$ (3 × 8 mL). Combined organics were dried over Na_2SO_4 and concentrated under reduced pressure. Column chromatography [SiO_2, petroleum ether-EtOAc (1:0) to (1:1)] yielded benzotriazole **182** as an amorphous off-white solid (3 mg, <1%). R_f [SiO_2, petroleum ether-EtOAc (1:1)]: 0.15. δ_H (500 MHz, $CDCl_3$): 8.06 (2H, broad dt, *J* = 8.4 and 0.7 Hz, H-4 and H-4''), 7.50-7.47 (4H, m, H-6, H-7, H-6'' and H-7''), 7.37 (2H, ddd, *J* = 8.2, 5.6 and 1.4 Hz, H-5 and H-5''), 4.72-4.66 (4H, m, 2 × H-1' and 2 × H-4'), 2.09-2.04 (4H, m, 2 × H-2' and 2 × H-3'). LRMS (CI^+): 293 [$(M + H)^+$, 100%]. HRMS: 293.1510. $C_{16}H_{17}N_6$ requires $(M + H)^+$, 293.1509.

1-[4'-(2''*H*-1'',2'',3''-benzotriazol-2''-yl)but-1'-yl]-1*H*-1,2,3-benzotriazole 183

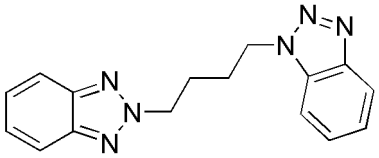

Column chromatography of the experiment that yielded bis(benzotriazole) **182** above also gave bis(benzotriazole) **183** as an amorphous solid (14 mg, 2%). R_f [SiO_2, petroleum ether-EtOAc (1:1)]: 0.33. Mp: 77-78 °C. ν_{max} (ATR): 3055 (CH), 2947 (CH), 2878 (CH), 1614 (Ar), 1589 (Ar), 1568 (Ar) cm^{-1}. δ_H (500 MHz, $CDCl_3$): 8.06 (1H, d, *J* = 8.4 Hz, H-4), 7.85 (2H, dd, *J* = 6.5 and 3.1 Hz, H-4'' and H-7''), 7.51-7.43 (2H, m, H-6 and H-7), 7.39 (2H, dd, *J* = 6.5 and 3.1 Hz, H-5'' and H-6''), 7.36 (1H, ddd, *J* = 8.0, 6.6 and 1.4 Hz, H-5), 4.79 (2H, t, *J* = 6.6 Hz, 2 × H-4'), 4.68 (2H, t, *J* = 6.9 Hz, 2 × H-1'), 2.22-2.14 (2H, m, 2 × H-3'), 2.09-2.02 (2H, m, 2 × H-2'). δ_C (126 MHz, $CDCl_3$): 146.13 (C), 144.40 (C), 132.91

(C), 127.34 (CH), 126.42 (CH), 123.90 (CH), 120.16 (CH), 117.98 (CH), 109.13 (CH), 55.46 (CH_2), 47.20 (CH_2), 26.96 (CH_2), 26.50 (CH_2). LRMS (CI^+): 293 [$(M + H)^+$, 100%]. HRMS: 293.1510. $C_{16}H_{17}N_6$ requires $(M + H)^+$, 293.1509.

1,3-Bis(4'-iodobut-1-yl)-1*H*-1,2,3-benzotriazol-3-ium iodide 185

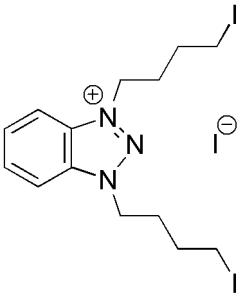

Column chromatography of the mixture that produced alkyl iodide **180** above also gave alkyl iodide **185** as an amorphous yellow solid (617 mg, 12%). R_f [SiO_2, DCM-EtOH (9:1)]: 0.04. Mp: 114-115 °C. ν_{max} (ATR): 3032 (CH), 2999 (CH), 2934 (CH), 2891 (CH), 2862 (CH), 1603 (Ar) cm^{-1}. δ_H (400 MHz, $CDCl_3$): 8.55 (2H, dd, *J* = 6.6 and 3.0 Hz, H-4 and H-7), 7.96 (2H, dd, *J* = 6.6 and 3.0 Hz, H-5 and H-6), 5.28 (4H, t, *J* = 7.2 Hz, 4 × H-1'), 3.28 (4H, t, *J* = 6.6 Hz, 4 × H-4'), 2.39-2.30 (4H, m, 4 × H-2'), 2.10-2.01 (4H, m, 4 × H-3'). δ_C (100 MHz, $CDCl_3$): 144.28 (C), 126.26 (CH), 117.93 (CH), 55.18 (CH_2), 30.66 (CH_2), 30.06 (CH_2), 5.14 (CH_2). LRMS (ESI^+): 484 (cation, 100%). HRMS: 483.9729. $C_{28}H_{12}D_{15}N_2P$ requires cation, 483.9741. LRMS (ESI^-): 127 (I^-, 100%).

***tert*-Butyl *N*-(8-{[(*tert*-butoxy)carbonyl]amino}-6-phenylphenanthridin-3-yl) carbamate 199**[142]

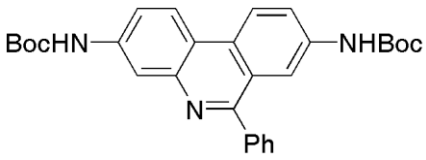

Method A:

THF (10 mL) was added to 3,8-diamino-6-phenylphenanthridine **198** (500 mg, 1.8 mmol) and potassium carbonate (969 mg, 7.0 mmol) followed by H_2O (1 mL). Di-*tert*-butyl dicarbonate (1.53 g, 7.0 mmol) was added drop-wise to the vigourously stirring biphasic solution. After stirring for 96 h at RT, the precipitate was collected by filtration, washed with THF (3 mL) and H_2O (3 mL) and dried under reduced pressure to yield dicarbamate **199** as an amorphous yellow solid (724 mg, 85%). Mp: 209-210 °C. ν_{max} (ATR): 3323 (NH), 3009 (CH), 2981 (CH), 2833 (CH), 1695 (C=O), 1622 (Ar), 1583 (Ar), 1573 (Ar), 1549 (Ar) cm^{-1}. δ_H (400 MHz, d_6-DMSO): 9.75 (1H, s, NH), 9.71 (1H, s, NH), 8.71 (1H,

d, *J* = 9.1 Hz, H-10), 8.60 (1H, d, *J* = 9.0 Hz, H-1), 8.21 (1H, d, *J* = 1.5 Hz, H-7), 8.19 (1H, d, *J* = 2.0 Hz, H-4), 8.01 (1H, broad d, *J* = 8.4 Hz, H-9), 7.81 (1H, d, *J* = 9.0 and 2.2 Hz, H-2), 7.72-7.67 (2H, m, 2 × *m*-H Ph), 7.62-7.54 (3H, m, 2 × *o*-H Ph and *p*-H Ph), 1.53 (9H, s, Boc), 1.45 (9H, s, Boc). δ_C (100 MHz, d_6-DMSO): 160.27 (C), 152.81 (C), 152.76 (C), 143.25 (C), 139.58 (C), 139.55 (C), 138.17 (C), 129.59 (CH), 128.61 (CH), 128.22 (CH), 128.08 (C), 124.33 (C), 123.02 (CH), 122.82 (CH), 122.58 (CH), 118.94 (CH), 118.29 (C), 116.35 (CH), 115.00 (CH), 79.41 (C), 79.18 (C), 28.15 (CH_3), 28.07 (CH_3). LRMS (CI^+): 1457 {[(3 × M) + H]$^+$, 1%}, 971 {[(2 × M) + H]$^+$, 32], 486 [(M + H)$^+$, 100]. HRMS: 1456.6966, 971.4698 and 486.2380. $C_{87}H_{94}N_9O_{12}$ requires [(3 × M) + H]$^+$, 1456.7016, $C_{58}H_{63}N_6O_8$ requires [(2 × M) + H]$^+$, 971.4702 and $C_{29}H_{32}N_3O_4$ requires (M + H)$^+$, 486.2387. ^{1}H NMR data broadly agree with literature.[142]

Method B:

3,8-Diamino-6-phenylphenanthridine **198** (700 mg, 2.45 mmol) in $CHCl_3$ (16 mL) was added slowly to stirring di-*tert*-butyl dicarbonate (1.07 g, 4.91 mmol) in $CHCl_3$ (6 mL) under argon. The resulting orange solution was stirred at RT for 66 h before concentrating under reduced pressure. Column chromatography [SiO_2, petroleum ether-EtOAc (1:1)] yielded dicarbamate **199** as an amorphous yellow solid (226 mg, 20%). R_f [SiO_2, petroleum ether-EtOAc (9:1)]: 0.51. *Characterisation as previous.*

2-[4'-(2'',4''-Dinitrophenoxymethyl)phenyl]-4,4,5,5-tetramethyl-1,3,2-dioxaborolane (DNP-SUM) 210[153]

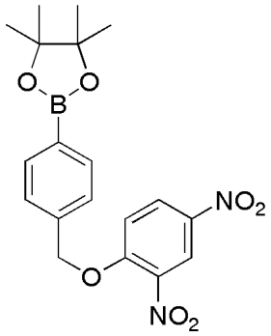

Method A:

Benzylic alcohol **215** (200 mg, 0.85 mmol) was mixed with 1-fluoro-2,4-dinitrobenzene (0.5 mL, 4.1 mmol) and 3 drops of anhydrous triethylamine added. The reaction mixture was stirred overnight at RT and then concentrated under reduced pressure. The mixture was dissolved in DCM (15 mL) and washed with $NaHCO_3$ (2 × 20 mL), H_2O (2 × 10 mL) and brine (10 mL). Organics were dried over $MgSO_4$ and concentrated under reduced pressure to give a yellow oil. Column chromatography [SiO_2, petroleum ether-EtOAc

(4:1)] gave an oil, which was triturated with hexane. The mixture was heated until the solid whitened, then the hexane was removed by pipette. The hexane washings were then concentrated under reduced pressure and the resulting oil treated in the same way. The process was repeated until no further solid was collected. The solid residues were combined to yield DNP-SUM **210** as an amorphous solid (54 mg, 16%). R_f [SiO_2, petroleum ether-EtOAc (4:1)]: 0.23. Mp: 143-145 °C. ν_{max} (ATR): 2981 (CH), 2931 (CH), 2894 (CH), 1604 (Ar), 1521 (NO_2), 1342 (NO_2) cm^{-1}. δ_H ($CDCl_3$, 400 MHz): 8.74 (1H, d, *J* = 2.8 Hz, H-3''), 8.34 (1H, dd, *J* = 9.3 and 2.8 Hz, H-5''), 7.85 (2H, d, *J* = 8.1 Hz, H-2' and H-6'), 7.44 (2H, d, *J* = 8.1 Hz, H-3' and H-6'), 7.21 (1H, d, *J* = 9.3 Hz, H-6''), 5.39 (2H, s, $ArCH_2$), 1.35 (12H, s, 4 × Me). δ_C ($CDCl_3$, 100 MHz): 156.21 (C), 140.23 (C), 139.24 (C), 136.90 (C), 135.39 (CH), 128.95 (CH), 126.15 (CH), 121.96 (CH), 114.98 (CH), 84.01 (C), 71.98 (CH_2), 24.86 (CH_3). LRMS (CI^+): 401 [$(M + H)^+$, 50%], 234 [$(M + H)^+ - C_6H_3(NO_2)^+$ 95], 219 (100), 145 (43). HRMS: 401.1521 and 400.1564. $C_{13}H_{22}{}^{11}BN_2O_7$ requires $(M + H)^+$, 401.1520 and $C_{13}H_{22}{}^{10}BN_2O_7$ requires $(M + H)^+$, 400.1556.

Method B:

NaH (28 mg, 60% in mineral oil, 0.69 mmol) was added to stirring benzylic alcohol **215** (125 mg, 0.53 mmol) and 1-fluoro-2,4-dinitrobenzene (135 µL, 1.1 mmol) in anhydrous DCM (1.5 mL) under argon. The resulting mixture was stirred at RT for 16 h. H_2O (8 mL) was added to quench and extracts made with DCM (2 × 5 mL). Organics were dried over Na_2SO_4 and concentrated under reduced pressure. Column chromatography [SiO_2, petroleum ether-EtOAc (1:0) to (1:1)] yielded DNP-SUM **210** as an amorphous solid (134 mg, 63%). *Characterisation as previous.*

2-Cyano-3-[4'-(4",4",5",5"-Tetramethyl-1",3",2"-dioxaborolan-2"-yl)phenyl]-2-(4"'-trifluoromethoxyphenyldiazo)propionitrile (FCCP-SUM) 211[153]

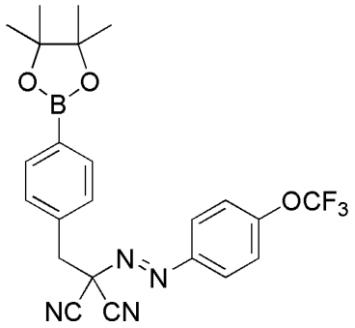

A solution of $NaNO_2$ (25 mg, 0.36 mmol) in H_2O (0.3 mL) was cooled to 0 °C and added dropwise to a stirring solution of 4-trifluoromethoxyaniline (62.8 mg, 0.36 mmol) and HCl

(1.5 M, 1.7 mL) at 0 °C. The resulting solution was stirred for 5 min and then added dropwise to a stirring solution of boronate ester **227** (100 mg, 354 μmol) and NaOAc (116 mg, 1.42 mmol) in a mixture of H_2O (1.3 mL), MeOH (1.5 mL) and EtOH (1.5 mL) at 0 °C. The resultant solution was stirred at 0 °C for 1 h and then overnight at RT. The precipitate was filtered, washed with ice-cold H_2O (4 mL) and dried under reduced pressure to yield FCCP-SUM **211** as an amorphous yellow solid. Further material was obtained by concentration of the filtrate under reduced pressure and extraction with DCM. Concentration under reduced pressure followed by column chromatography [SiO_2, petroleum ether-EtOAc (9:1)] yielded further FCCP-SUM **211** (Combined yield 77 mg, 46%). R_f [SiO_2, petroleum ether-EtOAc (9:1)]: 0.34. Mp: 120-122 °C. ν_{max} (ATR): 2937 (CH), 2162 (CN), 1614 (Ar) cm^{-1}. δ_H ($CDCl_3$, 400 MHz): 7.90 (2H, d, J = 9.0 Hz, H-2''' and H-6'''), 7.82 (2H, d, J = 8.0 Hz, H-3' and H-5'), 7.39-7.36 (4H, m, H-2', H-6', H-3''' and H-5'''), 3.69 (2H, s, 2 × H-3), 1.34 (12H, s, 4 × Me). δ_F ($CDCl_3$, 376 MHz): –57.58 (s). δ_C ($CDCl_3$, 100 MHz): 153.08 (C), 147.71 (C), 135.51 (CH), 132.86 (C), 130.15 (CH), 125.81 (CH), 121.48 (CH), 120.38 (q, J = 259.2 Hz, CF_3), 111.85 (C), 84.17 (C), 69.35 (C), 36.62 (CH_2), 24.99 (CH_3). LRMS (CI^+): 471 [$(M + H)^+$ (^{11}B), 11%], 446 (39), 337 (40), 283 (95), 219 (91), 189 ($F_3COArN_2^+$, 100). HRMS: 471.1821. $C_{23}H_{23}{}^{11}BF_3N_4O_3$ requires $(M + H)^+$, 471.1820.

2-(4'-Bromobenzyloxy)tetrahydrofuran 213[153]

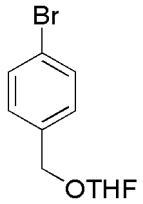

A solution of 4-bromobenzyl alcohol **212** (13.00 g, 69.5 mmol), 2,3-dihydrofuran (6.3 mL, 83.5 mmol) and *para*-toluene sulfonic acid monohydrate (20 mg, 0.1 mmol) in DCM (50 mL) was stirred at RT for 1.5 h. The reaction mixture was then washed with H_2O (2 × 100 mL) and saturated aqueous $NaHCO_3$ (100 mL). Organics were dried over $MgSO_4$ and concentrated under reduced pressure to yield acetal **213** as a yellow oil (17.17 g, 96%). ν_{max} (ATR): 2982 (CH), 2951 (CH), 2882 (CH), 1487 (Ar) cm^{-1}. δ_H ($CDCl_3$, 400 MHz): 7.45 (2H, d, J = 8.3 Hz, H-3' and H-5'), 7.20 (2H, d, J = 8.3 Hz, H-2' and H-6'), 5.19 (1H, dd, J = 3.7 and 2.6 Hz, H-2), 4.65 (1H, d, J = 12.4 Hz, ArCH^AH^B), 4.42 (1H, d, J = 12.4 Hz, ArCH^AH^B), 3.95-3.84 (2H, m, 2 × H-5), 2.07-1.80 (4H, m, 2 × H-3 and 2 × H-4). δ_C ($CDCl_3$, 100 MHz): 137.44 (C), 131.41 (CH), 129.43 (CH), 121.29 (C), 103.17 (CH), 67.97 (CH_2), 67.08 (CH_2), 32.34 (CH_2), 23.44 (CH_2). LRMS (EI^+): 258 [$M^{+\bullet}$ (^{81}Br), 13%],

256 [$M^{+\bullet}$ (^{79}Br), 13], 171 ($^{81}BrC_6H_4CH_2^+$, 100), 169 ($^{79}BrC_6H_4CH_2^+$, 100), 71 ($C_4H_7O^+$, 100). HRMS: 258.0079 and 256.0099. $C_{11}H_{13}{}^{81}BrO_2$ requires $M^{+\bullet}$, 258.0085 and $C_{11}H_{13}{}^{79}BrO_2$ requires $M^{+\bullet}$, 256.0097.

2-[4'-(4'',4'',5'',5''-Tetramethyl-1'',3'',2''-dioxaborolan-2''-yl)benzyloxy] tetrahydrofuran 214[153]

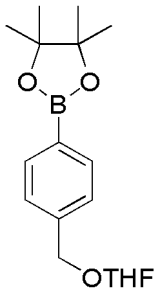

A stirring solution of aryl bromide **213** (12.00 g, 46.7 mmol) in anhydrous THF (130 mL) was cooled to –78 °C and degassed with argon for 15 min. Under argon, ^{n}BuLi (1.68 M in hexanes, 31.7 mL, 56.0 mmol) was added dropwise over 3 h and the mixture allowed to stir for 15 min. 2-Isopropoxy-4,4,5,5-tetramethyl-1,3,2-dioxaborolane (11.4 mL, 56.0 mmol) was added dropwise and the resulting solution allowed to stir for 2 h –78 °C before warming to RT. The reaction was quenched with H_2O (100 mL) and the product extracted with DCM (3 × 100 mL). Combined organics were washed with brine (100 mL), dried over $MgSO_4$ and concentrated under reduced pressure to give a yellow oil. Impurities were removed by Kugelrohr distillation to yield acetal **214** as a yellow oil, which solidified on standing (11.87 g, 84%). Mp: 41-44 °C. ν_{max} (ATR): 2978 (CH), 2932 (CH), 2882 (CH), 1614 (Ar) cm^{-1}. δ_H ($CDCl_3$, 400 MHz): 7.78 (2H, d, *J* = 7.7 Hz, H-2' and H-5'), 7.34 (2H, d, *J* = 7.7 Hz, H-4' and H-6'), 5.20 (1H, dd, *J* = 4.2 and 1.2 Hz, H-2), 4.72 (1H, d, *J* = 12.4 Hz, ArC*H*^{A}H^B), 4.50 (1H, d, *J* = 12.4 Hz, ArCH^A*H*^{B}), 3.97-3.86 (2H, m, 2 × H-5), 2.09-1.83 (4H, m, 2 × H-3 and 2 × H-4), 1.34 (12H, s, 4 × Me). δ_C ($CDCl_3$, 100 MHz): 141.60 (C), 134.86 (CH), 126.99 (CH), 103.09 (CH), 83.73 (C), 68.60 (CH_2), 67.02 (CH_2), 32.33 (CH_2), 24.84 (CH_3), 23.44 (CH_2). LRMS (EI^+): 304 ($M^{+\bullet}$, 4%), 217 (75), 83 (100). HRMS: 304.1842. $C_{17}H_{25}{}^{11}BO_4$ requires $M^{+\bullet}$, 304.1846.

[4-(4',4',5',5'-Tetramethyl-1',3',2'-dioxaborolan-2'-yl)phenyl]methanol 215[153, 154]

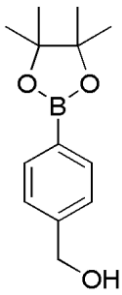

Adapting the procedure of De Filippis *et al*,[154] aluminium trichloride (40 mg, 0.30 mmol) was added to a stirring solution of acetal **214** (1.00 g, 3.29 mmol) in anhydrous EtOH (10 mL) under argon. The mixture was stirred overnight at RT and then concentrated under reduced pressure. The residue was dissolved in Et_2O and filtered. The filtrate was concentrated under reduced pressure and redissolved in anhydrous EtOH (10 mL) under argon. Aluminium chloride (30 mg, 0.22 mmol) was added and the solution was stirred overnight at RT. The residue was concentrated under reduced pressure, dissolved in Et_2O and filtered. The filtrate was concentrated under reduced pressure to yield the benzylic alcohol **215** as an oil (517 mg, 67%). ν_{max} (ATR): 3312 (OH), 2978 (CH), 2930 (CH), 2880 (CH), 1614 (Ar) cm^{-1}. δ_H ($CDCl_3$, 400 MHz): 7.78 (2H, d, J = 7.6 Hz, H-3 and H-5), 7.33 (2H, d, J = 7.7 Hz, H-2 and H-6), 4.66 (2H, s, $ArCH_2$), 2.34 (1H, broad s, OH), 1.33 (12H, s, 4 × Me). δ_C ($CDCl_3$, 100 MHz): 144.07 (C), 134.99 (CH), 126.06 (CH), 83.82 (C), 65.05 (CH_2), 24.83 (CH_3). LRMS (EI^+): 234 [$M^{+\bullet}$, 50%], 135 [$HOCH_2C_6H_4{}^{11}BOH^{+\bullet}$, 100]. HRMS: 234.1426. $C_{13}H_{19}{}^{11}BO_3$, requires $M^{+\bullet}$, 234.1427. ^1H and ^{13}C NMR data agree with literature.[154]

4,4,5,5-Tetramethyl-2-(*para*-tolyl)-1,3,2-dioxaborolane 219[153,186]

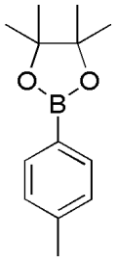

^{n}BuLi (2.5 M in hexanes, 33.7 mL, 84.2 mmol) was added dropwise to a stirred solution of 4-bromotoluene **218** (12.00 g, 70.2 mmol) in anhydrous THF (200 mL) under argon at –78 °C over 3 h and the reaction was stirred for a further 15 min. 2-Isopropoxy-4,4,5,5-tetramethyl-1,3,2-dioxaborolane (17.2 mL, 84.2 mmol) was added dropwise and the reaction stirred for a further 1.5 h at –78 ºC, before being allowed to warm to RT overnight. The reaction mixture was quenched with H_2O (100 mL) and extracted with EtOAc (2 × 100 mL). Combined organics were washed with brine (100 mL), dried over

$MgSO_4$ and concentrated under reduced pressure. Impurities were removed by Kugelrohr distillation to yield boronate ester **219** as an oil, which solidified on standing (14.89 g, 97%). Mp: 38-40 °C. ν_{max} (ATR): 2978 (CH), 2924 (CH), 2864 (CH), 1611 (Ar) cm^{-1}. δ_H (400 MHz, $CDCl_3$): 7.71 (2H, d, *J* = 7.7 Hz, H-2' and H-6'), 7.17 (2H, d, *J* = 7.6 Hz, H-3' and H-5'), 2.35 (3H, s, Me), 1.33 (12H, s, 4 × Me). δ_C (100 MHz, $CDCl_3$): 141.42 (C), 134.89 (CH), 128.58 (CH), 83.65 (C), 24.91 (CH_3), 21.78 (CH_3). LRMS (EI^+): 218 ($M^{+\bullet}$, 28%), 83 (100). HRMS: 218.1474. $C_{13}H_{19}{}^{11}BO_2$ requires $M^{+\bullet}$, 218.1478. ^1H and ^{13}C NMR data agree with literature.[186]

2-(4'-Bromomethylphenyl)-4,4,5,5-tetramethyl-1,3,2-dioxaborolane 220[153,154]

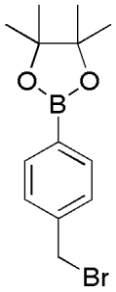

Following the procedure of De Filippis *et al*,[154] stirring benzylic alcohol **215** (500 mg, 2.14 mmol) in anhydrous DCM (15 mL) was degassed with argon for 15 min. The solution was cooled to 0 °C and anhydrous triethylamine (324 mg, 3.20 mmol) was added. Methanesulfonyl chloride (0.2 mL, 2.56 mmol) was added and the solution was allowed to stir for 1 h. Organics were washed with H_2O (3 × 4 mL), dried over $MgSO_4$ and concentrated under reduced pressure. The resultant solid was dissolved in anhydrous acetone (15 mL) and degassed with argon for 15 min. Anhydrous LiBr (1.90 g, 21.4 mmol) was added and the resultant solution was heated at reflux overnight. The solution was concentrated under reduced pressure and the residue dissolved in DCM (15 mL) and washed with H_2O (8 mL). Organics were dried over $MgSO_4$ and concentrated under reduced pressure. Column chromatography [SiO_2, hexane-EtOAc (3:1)] yielded benzylic bromide **220** as an amorphous solid (413 mg, 63%). R_f [SiO_2, hexane-EtOAc (3:1)]: 0.64. Mp: 76-78 °C (Lit.[154] 76-78 °C). ν_{max} (ATR): 2976 (CH), 2930 (CH), 2872 (CH), 1613 (Ar) cm^{-1}. δ_H (400 MHz, $CDCl_3$): 7.79 (2H, d, *J* = 7.7 Hz, H-2' and H-6'), 7.39 (2H, d, *J* = 7.7 Hz, H-3' and H-5'), 4.49 (2H, s, CH_2), 1.34 (12H, s, 4 × Me). δ_C (100 MHz, $CDCl_3$): 140.65 (C), 135.21 (CH), 128.30 (CH), 83.90 (C), 33.33 (CH_2), 24.84 (CH_3). LRMS (EI^+): 298 [$M^{+\bullet}$, (^{11}B and ^{81}Br), 4%], 296 [$M^{+\bullet}$, (^{11}B and ^{79}Br), 4], 217 [$M^{+\bullet}$ (^{11}B) – $Br^{\bullet}$, 100], 216 [$M^{+\bullet}$ (^{10}B) – $Br^{\bullet}$, 24]. HRMS: 298.0549 and 296.0567. $C_{13}H_{18}{}^{11}B^{81}BrO_2$ requires $M^{+\bullet}$, 298.0563 and $C_{13}H_{18}{}^{11}B^{79}BrO_2$ requires $M^{+\bullet}$, 296.0583. ^{13}C NMR data agree with literature.[154]

2-Cyano-3-[4'-(4",4",5",5"-tetramethyl-1",3",2"-dioxaborolan-2"-yl)phenyl]propionitrile 227[153]

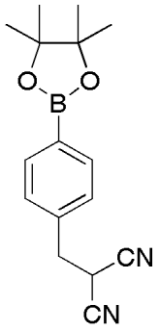

Malononitrile (0.12 mL, 2.3 mmol) in anhydrous THF (2 mL) and anhydrous DMF (1.6 mL) was added dropwise to a stirring suspension of NaH (70 mg, 80% in mineral oil, 2.3 mmol) in anhydrous THF (16 mL) at RT under argon. The reaction was stirred at RT for 30 min then cooled to 0 °C. A solution of benzylic bromide **220** (329 mg, 1.1 mmol) in anhydrous THF (4 mL) was added dropwise and stirred overnight allowing to warm to RT. Saturated aqueous NH_4Cl (40 mL) was added to quench the reaction and the mixture extracted with EtOAc (3 × 20 mL). Combined organics were washed with H_2O (3 × 20 mL), dried over $MgSO_4$ and concentrated under reduced pressure. Column chromatography [SiO_2, hexane-EtOAc (4:1)] yielded boronate ester **227** as an amorphous solid. (281 mg, 90%). R_f [SiO_2, hexane-EtOAc (4:1)]: 0.13. Mp: 135-137 °C. ν_{max} (ATR): 2982 (CH), 2361 (CN), 1614 (Ar) cm^{-1}. δ_H (400 MHz, $CDCl_3$): 7.84 (2H, d, J = 7.1 Hz, H-3' and H-5'), 7.32 (2H, d, J = 7.2 Hz, H-2' and H-6'), 3.94 (1H, t, J = 6.8 Hz, H-2), 3.26 (2H, d, J = 6.8 Hz, 2 × H-3), 1.34 (12H, s, 4 × Me). δ_C (100 MHz, $CDCl_3$): 135.86 (C), 135.61 (CH), 128.46 (CH), 112.19 (C), 84.00 (C), 77.30 (CH), 36.66 (CH_2), 24.85 (CH_3). LRMS (CI^+): 283 [$(M + H)^+$ (^{11}B), 100%]. HRMS: 283.1613. $C_{16}H_{20}{}^{11}BN_2O_2$ requires $(M + H)^+$, 283.1621.

(6-Iodohexyl)triphenylphosphonium iodide 228

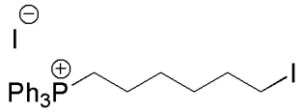

1,6-Diiodohexane (3 mL, 18.19 mmol) was added to a solution of triphenylphosphine (1.19 g, 4.55 mmol) in Et_2O (10 mL) and the resulting solution allowed to stand at RT for 6 d. Crystals were collected by filtration, washed with Et_2O and dried under reduced pressure. The filtrate was allowed to evaporate to ~5 mL and further crystals were collected as above after 5 d standing at RT. This process was repeated one more time to yield **228** as needles (Combined yield 2.24 g, 83%). Mp: 128-129 °C. ν_{max} (ATR): 3040 (CH), 3006 (CH), 2929 (CH), 2858 (CH), 2794 (CH), 1587 (Ar), 1483 (Ar) cm^{-1}. δ_H (400 MHz, $CDCl_3$): 7.89-7.78

(9H, m, 6 × *o*-H PPh_3 and 3 × *p*-H PPh_3), 7.74-768 (6H, m, 6 × *m*-H PPh_3), 3.85-3.76 (2H, m, 2 × H-1), 3.17 (2H, t, *J* = 6.8 Hz, 2 × H-6), 1.82-1.61 (6H, m, 2 × H-2, 2 × H-3 and 2 × H-5), 1.47-1.37 (2H, m, 2 × H-4). δ_C (100 MHz, $CDCl_3$): 135.14 (d, *J* = 3.0 Hz, CH), 133.74 (d, *J* = 10.1 Hz, CH), 130.58 (d, *J* = 12.5 Hz, CH), 118.18 (d, *J* = 85.9 Hz, C), 32.86 (CH_2), 29.96 (CH_2), 29.24 (d, *J* = 16.0 Hz, CH_2), 23.12 (d, *J* = 50.1 Hz, CH_2), 22.51 (d, *J* = 4.4 Hz, CH_2), 7.52 (CH_2). δ_P {^{1}H} (162 MHz, $CDCl_3$): 24.34 (s). LRMS (ESI^+): 473 (cation, 100%). HRMS: 473.0876. $C_{24}H_{27}IP$ requires cation, 473.0890. LRMS (ESI^-): 127 (I^-, 100%).

[4-(Bromomethyl)benzyl]triphenylphosphonium bromide 233

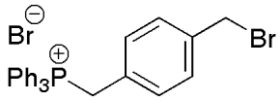

A solution of triphenylphosphine (100 mg, 0.38 mmol) in anhydrous toluene (1.25 mL) was added dropwise to a stirring solution of α, α'-*para*-dibromoxylene **232** (604 mg, 2.3 mmol) in anhydrous toluene (2.5 mL) at 95 °C under argon and stirred for 1 h. A further solution of triphenylphosphine (100 mg, 0.38 mmol) in anhydrous toluene (2.5 mL) was added dropwise and the resulting mixture was stirred for 5 h at 95 °C under argon. The hot mixture was filtered and the precipitate washed with hot toluene and then Et_2O. The solid was dried under reduced pressure to yield phosphonium bromide **233** as an amorphous solid (391 mg, 98%). Mp: >220 °C (Decomp.). ν_{max} (ATR): 3054 (CH), 3010 (CH), 2990 (CH), 2965 (CH), 2887 (CH), 2850 (CH), 2779 (CH), 1604 (Ar), 1588 (Ar), 1572 (Ar). δ_H (400 MHz, CD_3CN): 7.91-7.84 (3H, m, 3 × *p*-H PPh_3), 7.72-7.64 (6H, m, 6 × *o*-H PPh_3), 7.61-7.51 (6H, m, 6 × *m*-H PPh_3), 7.27 (2H, d, *J* = 7.7 Hz, H-3 and H-5), 6.94 (2H, dd, *J* = 7.9 and 1.8 Hz, H-2 and H-6), 4.68 (2H, d, *J* = 14.3 Hz, CH_2P), 4.52 (2H, s, CH_2Br). δ_C (100 MHz, CD_3CN): 138.89 (d, *J* = 4.6 Hz, C), 134.95 (d, *J* = 2.9 Hz, CH), 133.89 (d, *J* = 9.8 Hz, CH), 131.01 (d, *J* = 5.4 Hz, CH), 129.77 (d, *J* = 12.6 Hz, CH), 129.29 (d, *J* = 3.0 Hz, CH), 127.21 (d, *J* = 7.8 Hz, C), 117.06 (d, *J* = 86.0 Hz, C), 32.36 (s, CH_2), 29.16 (d, *J* = 48.3 Hz, CH_2). δ_P {^{1}H} (162 MHz, CD_3CN): 22.71 (s). LRMS (ESI^+): 447 [cation (^{81}Br), 100%], 445 [cation (^{79}Br), 93]. HRMS: 447.0683 and 445.0707. $C_{26}H_{26}{}^{81}BrP$ requires cation, 447.0695 and $C_{26}H_{26}{}^{79}BrP$ requires cation, 445.0715. LRMS (ESI^-): 81 ($^{81}Br^-$, 99%) and 79 ($^{79}Br^-$, 100).

(4-Carboxybutyl)triphenylphosphonium bromide 236[187]

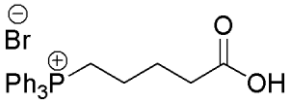

5-Bromovaleric acid **235** (6.00 g, 33.1 mmol) and triphenylphosphine (9.56 g, 36.5 mmol) were dissolved in anhydrous MeCN (15 mL) and stirred at 80 °C under argon for 70 h. After cooling to RT, the mixture was concentrated under reduced pressure. The resulting solid was triturated with Et_2O, liquid removed *via* pipette and the solid dried under reduced pressure to yield phosphonium bromide **236** as an amorphous solid (14.69 g, 100%). Mp: 199-200 °C. δ_H (400 MHz, $CDCl_3$): 10.44 (1H, broad s, CO_2H), 7.84-7.75 (9H, m, 6 × *o*-H PPh_3 and 3 × *p*-H PPh_3), 7.74-7.67 (6H, m, 6 × *m*-H PPh_3), 3.70-3.59 (2H, m, 2 × H-1), 2.64 (2H, t, J = 7.0 Hz, 2 × H-4), 1.94 (2H, quintet, J = 6.9 Hz, 2 × H-3), 1.78-1.67 (2H, m, 2 × H-2). δ_C (100 MHz, $CDCl_3$): 175.06 (C), 135.20 (d, J = 2.9 Hz, CH), 133.63 (d, J = 9.9 Hz, CH), 130.61 (d, J = 12.5 Hz, CH), 118.00 (d, J = 86.1 Hz, C), 33.76 (CH_2), 25.54 (d, J = 17.1 Hz, CH_2), 22.31 (d, J = 51.3 Hz, CH_2), 21.54 (d, J = 4.2 Hz, CH_2). δ_P {^{1}H} (162 MHz, $CDCl_3$): 23.67 (s). LRMS (ESI^+): 363 (cation, 100%). HRMS (ESI^+): 363.1499. $C_{23}H_{24}O_2P$ requires cation, 363.1508. LRMS (ESI^-): 81 ($^{81}Br^-$, 98%) and 79 ($^{79}Br^-$, 100). ^{1}H NMR data agree with literature.[187]

(3-Azidopropyl)triphenylphosphonium bromide 238[189]

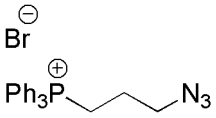

A solution of (3-bromopropyl)triphenylphosphonium bromide **237** (500 mg, 1.08 mmol) and NaN_3 (105 mg, 1.62 mmol) in EtOH (3 mL) and H_2O (3 mL) was stirred at 72 °C for 18 h. Extracts were made with DCM (3 × 4 mL). Combined organics were dried over $MgSO_4$ and concentrated under reduced pressure to yield phosphonium bromide **238** as an amorphous solid (441 mg, 99%). Mp: 161-162 °C (Lit.[188] 181-182 °C). ν_{max} (ATR): 3079 (CH), 3004 (CH), 2991 (CH), 2890 (CH), 2869 (CH), 2801 (CH), 2286 (N_3), 2112 (N_3), 1587 (Ar) cm^{-1}. δ_H (500 MHz, $CDCl_3$): 7.88-7.79 (9H, m, 6 × *o*-H PPh_3 and 3 × *p*-H PPh_3), 7.75-7.69 (6H, m, 6 × *m*-H PPh_3), 4.04-3.96 (2H, m, 2 × H-1), 3.84 (2H, dt, J = 6.3 and 0.9 Hz, 2 × H-3), 1.95-1.86 (2H, m, 2 × H-2). δ_C (126 MHz, $CDCl_3$): 135.18 (d, J = 3.0 Hz, CH), 133.67 (d, J = 10.1 Hz, CH), 130.59 (d, J = 12.6 Hz, CH), 118.00 (d, J = 86.3 Hz, C), 50.74 (d, J = 18.3 Hz, CH_2), 22.71 (d, J = 3.2 Hz, CH_2), 20.07 (d, J = 52.7 Hz, CH_2). δ_P {^{1}H} (202 MHz, $CDCl_3$): 24.52 (s). LRMS (ESI^+): 346 (cation, 100%). HRMS

(ESI$^+$): 346.1468. $C_{21}H_{21}N_3P$ requires cation, 346.1468. LRMS (ESI$^-$): 81 ($^{81}Br^-$, 98%) and 79 ($^{79}Br^-$, 100). ^1H and ^{13}C NMR data agree with literature.[189]

4,5-Dimethylhex-2-yne-1,4,5-triol 242[155]

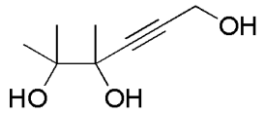

Method A:

Adapting the procedure of Li and Burgess,[155] KOH (7.71 g, 137.4 mmol) and H_2O (5 ml) were added to propargyl alcohol **239** (4.0 mL, 68.7 mmol) in Et_2O (200 mL). The resultant mixture stirred for 1 h at 25 °C. 3-Hydroxy-3-methyl-2-butanone **241** (3.35 mL, 32.7 mmol) was added and the reaction stirred overnight at 25 °C. The solution was concentrated under reduced pressure, acidified with H_2SO_4 (1 M, 68.7 mL) and concentrated under reduced pressure. Eextracts were made with EtOAc, filtered and concentrated under reduced pressure to yield triol **242** as an oil (3.559 g, 71%). ν_{max} (ATR): 3351 (OH) cm^{-1}. δ_H (400 MHz, $CDCl_3$): 4.29 (2H, s, 2 × H-1), 4.11 (3H, broad s, 3 × OH) 1.43 (3H, s, Me), 1.37 (3H, s, Me), 1.27 (3H, s, Me). δ_C (100 MHz, $CDCl_3$): 88.04 (C), 82.78 (C), 75.67 (C), 73.93 (C), 50.44 (CH_2), 25.57 (CH_3), 24.40 (CH_3), 22.79 (CH_3). LRMS (CI$^+$): 141 [(M + H)$^+$ – H_2O, 100%], 123 [(M + H)$^+$ – (2 × H_2O), 47]. HRMS: 141.0914. $C_8H_{13}O_2$ requires [(M + H)$^+$ – H_2O], 141.0916. Compound reported in literature without characterisation data.[155]

Method B:

Propargyl alcohol **239** (0.32 mL, 6.62 mmol) in anhydrous THF (10 mL) was degassed with argon for 15 min. NaH (370 mg, 80% in mineral oil, 12.3 mmol) was added and the mixture stirred for 1 h under argon at 25 °C. 3-Hydroxy-3-methyl-2-butanone **241** (0.32 mL, 2.9 mmol) in anhydrous THF (10 mL) was added and the reaction stirred overnight at 25 °C under argon. Saturated aqueous NH_4Cl (15 mL) was added to quench and the resultant mixture concentrated under reduced pressure. The solid residue was washed with EtOAc, filtered and concentrated under reduced pressure to yield triol **242** as an oil (368 mg, 82%). *Characterisation as previous.*

3-(4',5',5'-Trimethyl-2'-phenyl-1',3',2'-dioxaborolan-4'-yl)prop-2-yn-1-ol 250

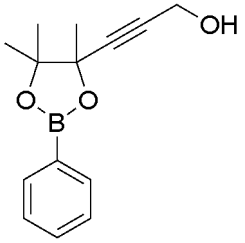

Phenylboronic acid **249** (200 mg, 1.63 mmol) and molecular sieves (4Å, 815 mg) were added to triol **242** (259 mg, 1.63 mmol) in anhydrous THF (10 mL). The resultant mixture was stirred for 72 h at 25 °C. The mixture was filtered and concentrated under reduced pressure to yield the crude boronate ester **250** as an oil. Attempted purification by column chromatography (SiO_2) resulted in decomposition. Selected data from crude: δ_H (400 MHz, $CDCl_3$): 7.82 (2H, d, *J* = 6.8 Hz, H-2'' and H-6''), 7.47 (1H, t, *J* = 7.4 Hz, H-4''), 7.37 (2H, t, *J* = 7.3 Hz, H-3'' and H-5''), 4.32 (2H, d, *J* = 5.9 Hz, 2 × H-1), 2.06 (1H, broad s, OH) 1.60 (3H, s, Me), 1.55 (3H, s, Me), 1.39 (3H, s, Me). δ_C (100 MHz, $CDCl_3$): 134.90 (CH), 131.64 (CH), 127.77 (CH), 85.00 (C), 85.42 (C), 84.25 (C), 81.00 (C), 51.07 (CH_2), 27.27 (CH_3), 25.43 (CH_3), 24.02 (CH_3).

3-Hydroxy-4-iodobenzoic acid 253[157,190]

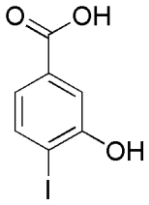

Following the procedure of Whiting and Pilling,[157] a solution of I_2 (23.40 g, 92 mmol) and KI (18.26 g, 110 mmol) in H_2O (100 mL) was added dropwise to a stirring solution of 3-hydroxybenzoic acid **252** (13.95 g, 100 mmol) in concentrated aqueous NH_3 (200 mL) over 1.5 h at RT. The resultant green solution was stirred for 30 min before cooling to 0 °C. Concentrated HCl (180 mL) was added slowly during which a precipitate formed. After cooling to RT, the precipitate was filtered off and washed with ice-cold H_2O (40 mL). The precipitate was recrystallised from H_2O-EtOH (5:1) and washed with ice-cold H_2O (40 mL) before drying under reduced pressure to yield carboxylic acid **253** as an amorphous solid (18.82 g, 69%). Mp: 222-224 °C [H_2O-EtOH (5:1)] [Lit.[157] 224-225 °C H_2O-EtOH (5:1)]. ν_{max} (ATR): 3547 (OH), 3302 (very broad, CO_2H) 1680 (C=O) cm^{-1}. δ_H (400 MHz, $CDCl_3$): 13.00 (1H, s, CO_2H), 10.68 (1H, s, OH), 7.80 (1H, d, *J* = 8.1 Hz, H-5), 7.42 (1H, d, *J* = 1.9 Hz, H-2), 7.14 (1H, dd, *J* = 8.1 and 1.9 Hz, H-6). δ_C (100 MHz, $CDCl_3$): 166.80 (C), 156.70 (C), 138.98 (CH), 131.99 (C), 121.39 (CH), 114.90 (CH),

90.84 (C). LRMS (CI^+): 265 [$(M + H)^+$, 79%], 264 (46), 157 (59), 139 (65), 79 (100). HRMS: 264.9366. $C_7H_6IO_2$ requires $(M + H)^+$, 264.9362. ^1H NMR data agree with literature.[190]

Ethyl 3-hydroxy-4-iodobenzoate 254[191]

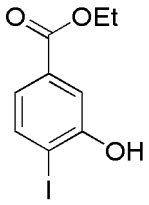

Carboxylic acid **253** (10.91 g, 41.3 mmol) in EtOH (40 mL) was cooled to –8 °C and thionyl chloride (9.3 mL, 0.13 mol) was added dropwise. The solution was then stirred at reflux for 3 h before cooling to RT. The solution was concentrated under reduced pressure. The resultant solid was dissolved in DCM (100 mL), washed with saturated aqueous $NaHCO_3$ (2 × 50 mL) and H_2O (50 mL). Organics were dried over $MgSO_4$ and concentrated under reduced pressure. Recrystallisation from EtOAc-hexane yielded ethyl ester **254** as plates (11.90 g, 99%). Mp: 118-119 °C (EtOAc-hexane) [Lit.[191] 119-120 °C (toluene)]. ν_{max} (ATR): 3374 (broad OH), 1694 (C=O) cm^{-1}. δ_H (400 MHz, $CDCl_3$): 7.75 (1H, d, J = 8.2 Hz, H-5), 7.65 (1H, d, J = 1.7 Hz, H-2), 7.33 (1H, dd, J = 8.2 and 1.7 Hz, H-6), 5.81 (1H, s, OH), 4.37 (2H, q, J = 7.1 Hz, CH_2), 1.39 (3H, t, J = 7.1 Hz, CH_3). δ_C (100 MHz, $CDCl_3$): 166.00 (C), 155.09 (C), 138.53 (CH), 132.55 (C), 122.99 (CH), 115.77 (CH), 91.51 (C), 61.44 (CH_2), 14.24 (CH_3). LRMS (EI^+): 292 [$M^{+\bullet}$, 79%], 247 [$M^{+\bullet} – EtO^\bullet$, 100], 83 (71). HRMS: 291.9594. $C_9H_9IO_3$ requires $M^{+\bullet}$, 291.9596. ^1H NMR data agree with literature.[191]

3-Hydroxy-4-iodobenzyl alcohol 255

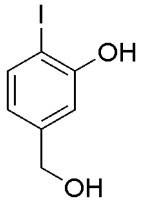

Ethyl ester **254** (2.20 g, 7.53 mmol) in anhydrous Et_2O (40 mL) was degassed with argon for 15 min. The stirring solution was cooled to –78 °C and diisobutylaluminium hydride (22.6 mL, 1.0 M in hexanes, 22.6 mmol) was added dropwise. The resultant solution stirred at –78 °C for 1 h and then stirred overnight, allowing to warm to RT. Saturated aqueous NH_4Cl (15 mL) and Et_2O (60 mL) were added and the resulting solution stirred for 1.5 h until the precipitate settled. The Et_2O layer was filtered through a Celite pad and

washed through with Et_2O. Organics were dried over $MgSO_4$, and concentrated under reduced pressure to yield diol **255** as an amorphous solid (1.84 g, 98%). Mp: 107-109 °C. ν_{max} (ATR): 3406 (OH), 3134 (CH), 3086 (CH), 1589 (Ar) cm^{-1}. δ_H (400 MHz, MeOD): 7.60 (1H, d, *J* = 7.8 Hz, H-5), 6.86 (1H, s, H-2), 6.58 (1H, d, *J* = 7.8 Hz, H-6), 4.49 (2H, s, CH_2). δ_C (100 MHz, MeOD): 158.07 (C), 144.91 (C), 140.19 (CH), 120.75 (CH), 114.25 (CH), 82.74 (C), 64.53 (CH_2). LRMS (EI^+): 250 ($M^{+\bullet}$, 100%), 123 ($M^{+\bullet} - I^{\bullet}$, 27), 95 (91). HRMS: 249.9493. $C_7H_7IO_2$ requires $M^{+\bullet}$, 249.9491.

2-Iodo-5-(tetrahydrofuran-2'-yloxymethyl)phenol 256

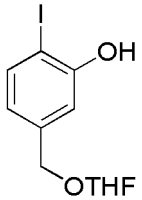

By-product isolated during the synthesis of diacetal **257.** Diol **255** (2.61 g, 10.4 mmol) in anhydrous Et_2O (50 mL) was degassed with argon for 15 min. The solution was cooled to 0 °C and 2,3-dihydrofuran (0.96 mL, 12.5 mmol) and *para*-toluene sulfonic acid monohydrate (19 mg, 0.1 mmol) were added. The solution was stirred at 0 ºC for 1 h before 2,3-dihydrofuran (0.96 mL, 12.5 mmol) was added followed by stirring at 0 ºC for 1 h then at RT for a further 1 h. The solution was concentrated under reduced pressure and the resultant yellow oil taken up in DCM (40 mL). Organics were washed with saturated aqueous $NaHCO_3$ (25 mL) and H_2O (2 × 20 mL), dried over $MgSO_4$ and concentrated under reduced pressure. Column chromatography [SiO_2, petroleum ether-EtOAc (4:1)] yielded phenol **256** as an amorphous solid (1.32 g, 40%). This reaction also yielded diacetal **257** as an oil (1.60 g, 39%). Mp: 60-61 °C. R_f [SiO_2, petroleum ether-EtOAc (4:1)]: 0.23. ν_{max} (ATR): 3201 (OH), 2980 (CH), 2945 (CH), 2907 (CH), 1589 (Ar) cm^{-1}. δ_H (400 MHz, $CDCl_3$): 7.60 (1H, d, *J* = 8.1 Hz, H-3), 6.96 (1H, s, H-6), 6.65 (1H, d, *J* = 8.0 Hz, H-4), 5.60 (1H, broad s, OH), 5.27-5.14 (1H, m, H-2'), 4.63 (1H, d, *J* = 12.3 Hz, $ArCH^AH^B$), 4.41 (1H, d, *J* = 12.3 Hz, $ArCH^AH^B$), 4.01-3.83 (2H, m, 2 × H-5'), 2.10-1.79 (4H, m, 2 × H-3' and 2 × H-4'). δ_C (100 MHz, $CDCl_3$): 154.07 (C), 141.22 (C), 138.16 (CH), 121.65 (CH), 114.25 (CH), 103.20 (CH), 84.00 (C), 67.82 (CH_2), 67.15 (CH_2), 32.34 (CH_2), 23.41 (CH_2). LRMS (CI^+): 321 [$(M + H)^+$, 62%], 71 ($C_4H_7O^+$, 100). HRMS: 320.9988. $C_{11}H_{14}IO_3$ requires $(M + H)^+$, 320.9988.

2-(Tetrahydrofuran-2'-yloxy)-4-(tetrahydrofuran-2''-yloxymethyl)iodobenzene 257

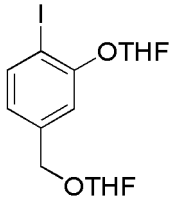

Diol **255** (1.97 g, 7.87 mmol) and 2,3-dihydrofuran (1.8 mL, 32.6 mmol) in anhydrous Et_2O (30 mL) were degassed with argon for 10 min. *para*-Toluene sulfonic acid monohydrate (20 mg, 0.11 mmol) was added and the resulting solution degassed with argon for a further 10 min before stirring at RT for 24 h. The solution was washed with saturated aqueous $NaHCO_3$ (10 mL) and H_2O (2 × 10 mL). Organics were dried over $MgSO_4$ and concentrated under reduced pressure. Column chromatography [SiO_2, petroleum ether-EtOAc (4:1)] yielded diacetal **257** as an oil in a 1:1 mixture of diastereomers (X and Y) (1.63 g, 53%). R_f [SiO_2, petroleum ether-EtOAc (4:1)]: 0.44 and 0.50. ν_{max} (ATR): 2978 (CH), 2947 (CH), 2886 (CH), 1574 (Ar) cm^{-1}. δ_H (400 MHz, $CDCl_3$): 7.69 (1H, d, J = 8.0 Hz, H-6), 7.11 (1H, s, H-3), 6.73 (1H, d, J = 8.0 Hz, H-5), 5.82 (1H, t, J = 3.9 Hz, H-2'), 5.19 (1H, dd, J = 3.9 and 2.0 Hz, H-2''), 4.64 (1H, d, J = 12.2 Hz, ArCH^AH^B), 4.42 (1H, d, J = 12.2 Hz, ArCH$^A H^B$), 4.09 (1H, dt, J = 8.0, 5.6 Hz, H^A-5'), 4.00-3.83 (3H, m, H^B-5' and 2 × H-5''), 2.37-2.18 (2H, m, 2 × H-3'), 2.17-1.78 (6H, m, 2 × H-4', 2 × H-3'' and 2 × H-4''). δ_C (100 MHz, $CDCl_3$): 155.97 (C), 140.31 (C), 140.25 (C), 138.89 (CH), 122.69 (CH), 115.05 (CH), 103.17 (CH), 103.12 (CH), 86.65 (C), 86.61 (C), 68.29 (CH_2), 68.09 (CH_2), 66.99 (CH_2), 32.76 (CH_2), 32.29 (CH_2), 23.38 (CH_2), 23.26 (CH_2). LRMS (EI^+): 390 ($M^{+\bullet}$, 100%), 320 ($M^{+\bullet}$ – C_4H_6O, 51), 234 ($M^{+\bullet}$ – C_4H_6O and – $C_4H_6O_2$, 100), 71 ($C_4H_7O^+$, 100). HRMS: 390.0331. $C_{15}H_{19}IO_4$ requires $M^{+\bullet}$, 390.0328.

2-[2'-(Tetrahydrofuran-2''-yloxy)-4'-(tetrahydrofuran-2'''-yloxymethyl)phenol-4,4,5,5-tetramethyl-1,3,2-dioxaborolane 258

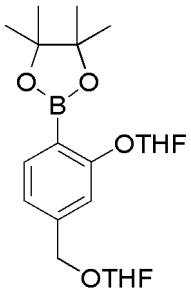

Aryl iodide **257** (1.63 g, 4.18 mmol) was dried by azeotrope with toluene (×3) and dried under reduced pressure. Anhydrous THF (20 mL) was added and the resulting stirring solution degassed with argon for 20 min. The solution was cooled to –78 °C and ^{n}BuLi

(1.6 M in hexanes, 3.14 mL, 5.02 mmol) was added dropwise over 2 min. The resulting solution was stirred for a further 10 min before 2-isopropoxy-4,4,5,5-tetramethyl-1,3,2-dioxaborolane (1.02 mL, 5.02 mmol) was added dropwise. This solution was stirred at –78 °C for 1.5 h and then was allowed to warm to RT overnight. The reaction was quenched with H_2O (10 mL) and extracted with EtOAc (4 × 25 mL). Column chromatography [SiO_2, petroleum ether-EtOAc (4:1)] yielded diacetal **258** as an oil as a 1:1 mixture of diastereomers (924 mg, 57%). R_f [SiO_2, petroleum ether-EtOAc (4:1)]: 0.28. ν_{max} (ATR): 2976 (CH), 2955 (CH), 2886 (CH), 1611 (Ar). δ_H (400 MHz, $CDCl_3$): 7.61 (1H, d, *J* = 7.5 Hz, H-6'), 7.08 (1H, s, H-3'), 6.97 (1H, d, *J* = 7.5 Hz, H-5'), 5.80 (1H, t, *J* = 4.3 Hz, H-2''), 5.19 (1H, dd, *J* = 4.5 and 1.4 Hz, H-2'''), 4.68 (1H, d, *J* = 12.5 Hz, ArC*H*^{A}H^B), 4.47 (1H, d, *J* = 12.5 Hz, ArCH^A*H*^{B}), 4.14-4.06 (1H, m, H^A-5''), 3.98-3.84 (3H, m, H^B-5'' and 2 × H-5'''), 2.31-2.14 (2H, m, 2 × H-3''), 2.11-1.77 (6H, m, 2 × H-4'', 2 × H-3''' and 2 × H-4'''), 1.33 (12H, s, 4 × Me). δ_C (100 MHz, $CDCl_3$): 161.91 (C), 143.08 (C), 143.05 (C), 136.34 (CH), 120.86 (CH), 120.83 (CH), 115.69 (CH), 115.64 (CH), 103.40 (CH), 103.34 (CH), 103.09 (CH), 83.23 (C), 68.52 (CH_2), 67.96 (CH_2), 67.00 (CH_2), 32.68 (CH_2), 32.33 (CH_2), 24.86 (CH_3), 23.43 (CH_2), 23.21 (CH_2). LRMS (CI^+): 391 [$(M + H)^+$, 19%], 321 [$(M + H)^+ – C_4H_6O$, 100), 303 [$(M + H)^+ – C_4H_6O$ and $– H_2O$, 83], 233 [$(M + H)^+ – (2 × C_4H_6O)$ and $– H_2O$, 56], 177 (68), 71 ($C_4H_7O^+$, 57). HRMS: 391.2285. $C_{21}H_{32}{}^{11}BO_6$ requires $(M + H)^+$, 391.2292.

<u>5-Hydroxymethyl-2-(4',4',5',5'-tetramethyl-1',3',2'-dioxaborolan-2'-yl)phenol</u> 259

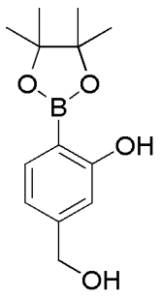

Aluminium trichloride (32 mg, 0.24 mmol) was added to a stirring solution of diacetal **258** (461 mg, 1.2 mmol) in EtOH (9.5 mL). The reaction mixture was stirred under argon at RT for 45 min. The solution was concentrated under reduced pressure and the resulting grey oil dissolved in Et_2O (40 mL) and filtered. Concentrating under reduced pressure yielded diol **259** as a 10:1 mixture with 3-hydroxybenzyl alcohol **146** by-product as the minor component (296 mg, 99%). ν_{max} (ATR): 3436 (OH), 2979 (CH), 2934 (CH), 2869 (CH), 1629 (Ar). δ_H (400 MHz, $CDCl_3$): 7.85 (1H, broad s, OH), 7.58 (1H, d, *J* = 7.8 Hz, H-3), 6.91-6.70 (2H, m, H-4 and H-6), 4.65 (2H, s, CH_2), 2.05 (1H, broad s, OH), 1.36 (12H, s, 4 × Me). δ_C (100 MHz, $CDCl_3$): 163.87 (C), 147.23 (C), 136.01 (CH), 117.79

(CH), 113.40 (CH), 84.50 (C), 65.00 (CH_2), 24.81 (CH_3). LRMS (CI^+): 251 [$(M + H)^+$, 100%], 233 [$(M + H)^+ - H_2O$, 44]. HRMS: 251.1459 and 250.1425. $C_{13}H_{20}{}^{11}BO_4$ requires $(M + H)^+$, 251.1455 and $C_{13}H_{20}{}^{10}BO_4$ requires $(M + H)^+$, 250.1491.

3-[4'-(Bromomethyl)benzyloxy]-4-(4'',4'',5'',5''-tetramethyl-1'',3'',2''-dioxaborolan-2''-yl)benzyl alcohol 262

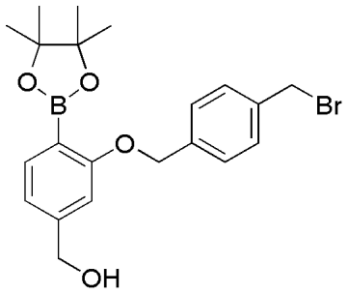

Cs_2CO_3 (74 mg, 0.23 mmol) was added to stirring α, α'-*para*-dibromoxylene **232** (218 mg, 0.83 mmol) in anhydrous acteone (2 mL) and the mixture degassed with argon for 30 min. The mixture was heated to reflux and a degassed solution of phenol **259** (26 mg, 0.11 mmol) in anhydrous acetone (0.2 mL) and anhydrous THF (0.5 mL) was added dropwise. After 45 min anhydrous DMF (0.1 mL) was added to aid solubility. After a further 1.75 h, a further degassed solution of phenol **259** (26 mg, 0.11 mmol) in anhydrous acetone (0.2 mL) and anhydrous THF (0.3 mL) was added dropwise. After a further 2.5 h, the reaction mixture was cooled to RT. H_2O (15 mL) was added and extracted with Et_2O (4 × 15 mL). Combined organics were dried over $MgSO_4$ and concentrated under reduced pressure. Column chromatography [SiO_2, petroleum ether-EtOAc (4:1)] yielded benzylic bromide **262** as a semi-pure oil (18 mg, 9%). Selected data from crude: δ_H (400 MHz, $CDCl_3$): 7.69 (1H, broad d, *J* = 7.4 Hz, H-5), 7.61 (2H, d, *J* = 8.2 Hz, H-2' and H-6'), 7.40 (2H, *J* = 8.2 Hz, H-3' and H-5'), 6.96 (1H, broad s, H-2), 6.94 (1H, broad d, *J* = 7.5 Hz, H-6), 5.11 (2H, s, $ArCH_2O$), 4.70 (2H, s, C*H*$_2$OH), 4.52 (2H, s, CH_2Br), 1.37 (12H, s, 4 × Me). δ_C (100 MHz, $CDCl_3$): 163.52 (C), 145.88 (C), 137.99 (C), 137.08 (CH), 136.79 (C), 128.90 (CH), 127.05 (CH), 118.78 (CH), 109.95 (CH), 83.50 (C), 69.38 (CH_2), 65.17 (CH_2), 33.51 (CH_2), 24.96 (CH_3).

Ethyl 3-(methoxymethoxy)-4-iodobenzoate 264

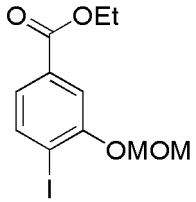

Phenol **254** (1.00 g, 3.4 mmol) and diisopropylethylamine (1.2 mL, 6.9 mmol) in anhydrous DCM (25 mL) were degassed with argon for 10 min. Bromomethyl methyl ether (0.62 mL, 6.9 mmol) was added and the solution stirred at reflux for 24 h. After cooling to RT, the mixture was washed with aqueous HCl (1 M, 25 mL) and H_2O (50 mL). Organics were dried over $MgSO_4$ and concentrated under reduced pressure to give a yellow oil. Column chromatography [SiO_2, petroleum ether-EtOAc (9:1)] yielded ethyl ester **264** as an oil (984 mg, 86%). R_f [SiO_2, petroleum ether-EtOAc (9:1)]: 0.41. ν_{max} (ATR): 2970 (CH), 2919 (CH), 2830 (CH), 1717 (C=O), 1586 (Ar), 1570 (Ar) cm^{-1}. δ_H (400 MHz, $CDCl_3$): 7.85 (1H, d, *J* = 8.1 Hz, H-5), 7.66 (1H, d, *J* = 1.8 Hz, H-2), 7.41 (1H, dd, *J* = 8.1 and 1.8 Hz, H-6), 5.30 (2H, s, OCH_2O), 4.37 (2H, q, *J* = 7.1 Hz, CH_2CH_3), 3.52 (3H, s, OMe), 1.39 (3H, t, *J* = 7.1 Hz, CH_2CH_3). δ_C (100 MHz, $CDCl_3$): 165.89 (C), 155.97 (C), 139.48 (CH), 132.01 (C), 124.32 (CH), 114.96 (CH), 94.90 (CH_2), 93.61 (C), 61.31 (CH_2), 55.80 (CH_3), 14.30 (CH_3). LRMS (FAB^+): 337 [$(M + H)^+$, 100%], 336 (96), 291 [$(M + H)^+ – CH_3OCH_2$, 60]. HRMS: 336.9938. $C_{11}H_{14}IO_4$ requires $(M + H)^+$, 336.9937.

4-Iodo-3-(methoxymethoxy)benzyl alcohol 265[192]

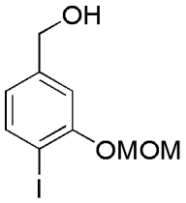

A stirring solution of ethyl ester **264** (8.00 g, 23.8 mmol) in anhydrous Et_2O (120 mL) was degassed with argon for 15 min. The solution was cooled to –78 °C and diisobutylaluminium hydride (1.0 M in THF, 52.4 mL, 52.4 mmol) was added over 20 min and the resulting mixture stirred for 2.5 h before warming to RT, followed by 40 min further stirring. Saturated aqueous NH_4Cl (80 mL) and Et_2O (50 mL) were added and the mixture stirred until the precipitate settled. The organic layer was filtered through a pad of Celite and washed through with Et_2O (350 mL). Organics were dried over $MgSO_4$ and concentrated under reduced pressure. Column chromatography [SiO_2, petroleum ether-EtOAc (4:1)] gave alcohol **265** as an oil (4.40 g, 63%). R_f [SiO_2, petroleum ether-EtOAc (4:1)]: 0.13. ν_{max} (ATR): 3373 (Broad, OH), 2957 (CH), 2905 (CH), 2827 (CH), 1588 (Ar),

1575 (Ar). δ_H [400 MHz, $(CD_3)_2CO$]: 7.73 (1H, d, *J* = 8.0 Hz, H-5), 7.16 (1H, d, *J* = 1.5 Hz, H-2), 6.81 (1H, broad dd, *J* = 8.0 and 1.7 Hz, H-6), 5.27 (2H, s, OCH_2O), 4.60 (2H, s, CH_2OH), 4.33 (1H, broad s, OH), 3.47 (3H, s, OMe). δ_C (100 MHz, $CDCl_3$): 155.78 (C), 142.89 (C), 139.23 (CH), 121.93 (CH), 113.05 (CH), 94.64 (CH_2), 85.54 (C), 64.07 (CH_2), 56.41 (CH_3). LRMS (EI^+): 294 ($M^{+\bullet}$, 95%), 45 ($CH_3OCH_2^+$, 100). HRMS: 293.9749. $C_9H_{11}IO_3$ requires $M^{+\bullet}$, 293.9753. Compound is reported in the literature although analysed in an alternative NMR solvent (CCl_4).[192]

4-(2',4'-Dinitrophenoxymethyl)-1-iodo-2-(methoxymethoxy)benzene 268

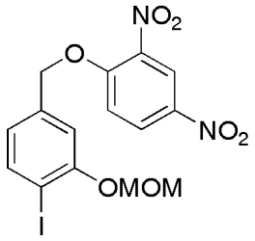

Benzylic alcohol **265** (700 mg, 2.38 mmol), 1-fluoro-2,4-dinitrobenzene (0.3 mL, 2.38 mmol) and anhydrous triethylamine (3.3 mL, 2.38 mmol) were stirred in anhydrous acetone (3.5 mL) at 40 °C under argon for 72 h. EtOAc (20 mL) was added and the mixture washed with saturated aqueous $NaHCO_3$ (15 mL) and H_2O (15 mL). Organics were dried over $MgSO_4$ and concentrated under reduced pressure. Column chromatography [SiO_2, petroleum ether-EtOAc (4:1) to (1:1)] yielded aryl iodide **268** as an oil (774 mg, 71%). R_f [SiO_2, petroleum ether-EtOAc (1:1)]: 0.57. Mp: 137-138 °C. ν_{max} (ATR): 3114 (CH), 3083 (CH), 2964 (CH), 2939 (CH), 2915 (CH), 2868 (CH), 2830 (CH), 1605 (Ar), 1573 (Ar). δ_H [400 MHz, $(CD_3)_2CO$]: 8.77 (1H, d, *J* = 2.6 Hz, H-3'), 8.53 (1H, dd, *J* = 9.3 and 2.6 Hz, H-5'), 7.86 (1H, d, *J* = 8.0 Hz, H-6), 7.70 (1H, d, *J* = 9.3 Hz, H-6'), 7.33 (1H, s, H-3), 6.99 (1H, d, *J* = 8.0 Hz, H-5), 5.53 (2H, s, $ArCH_2$), 5.31 (2H, s, OCH_2O), 3.48 (3H, s, OMe). δ_C [100 MHz, $(CD_3)_2CO$]: 157.26 (C), 156.78 (C), 141.29 (C), 140.53 (CH), 140.18 (C), 138.18 (C), 129.92 (CH), 123.38 (CH), 122.13 (CH), 116.73 (CH), 114.83 (CH), 95.69 (CH_2), 87.31 (C), 72.06 (CH_2), 56.60 (CH_3). LRMS (EI^+): 460 ($M^{+\bullet}$, 26%), 277 ($M^{+\bullet}$ – $(O_2N)_2C_6H_3O^\bullet$, 65), 184 ($DNP^{+\bullet}$, 18), 45 ($CH_3OCH_2^+$, 100). HRMS: 459.9771. $C_{15}H_{15}IN_2O_7$ requires $M^{+\bullet}$, 459.9768.

5-(2',4'-Dinitrophenoxymethyl)-2-iodophenol 269

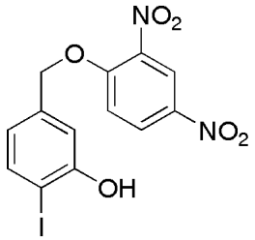

Method A:

$NaHSO_4.SiO_2$ was synthesised following the procedure of Breton.[158] $NaHSO_4.SiO_2$ (47 mg) was added to a stirring solution of acetal **268** (80 mg, 0.17 mmol) in DCM (2 mL) at RT. The reaction was monitored *via* TLC every 30 min. After 2 h the reaction had ceased and was incomplete. A further 70 mg of $NaHSO_4.SiO_2$ was added and stirring continued for a further 2.25 h. With no further change observed by TLC, the mixture was filtered and concentrated under reduced pressure. Column chromatography [SiO_2, petroleum ether-EtOAc (9:1) to (1:1)] yielded phenol **269** as an oil (17.3 mg, 19%). R_f [SiO_2, petroleum ether-EtOAc (1:1)]: 0.47. Mp: >200 °C (Decomp.). ν_{max} (ATR): 3439 (OH), 3120 (CH), 3111 (CH), 3089 (CH), 3074 (CH), 2923 (CH), 2861 (CH), 1607 (Ar), 1571 (Ar). δ_H [400 MHz, $(CD_3)_2CO$]: 8.76 (1H, d, *J* = 2.8 Hz, H-3'), 8.52 (1H, dd, *J* = 9.3 and 2.8 Hz, H-5'), 7.77 (1H, d, *J* = 8.0 Hz, H-3), 7.67 (1H, d, *J* = 9.3 Hz, H-6'), 7.12 (1H, d, *J* = 1.9 Hz, H-6), 6.82 (1H, dd, *J* = 8.0 and 1.9 Hz, H-4), 5.47 (2H, s, CH_2). δ_C [100 MHz, $(CD_3)_2CO$]: 157.80 (C), 156.78 (C), 141.31 (C), 140.43 (CH), 140.22 (C), 138.19 (C), 129.89 (CH), 122.07 (CH), 121.17 (CH), 116.72 (CH), 114.53 (CH), 84.24 (C), 71.96 (CH_2). LRMS (EI^+): 416 ($M^{+\bullet}$, 10%), 233 [$(HO)IC_6H_3CH_2^+$, 100]. HRMS: 415.9504. $C_{13}H_9IN_2O_6$ requires $M^{+\bullet}$, 415.9505.

Method B:

Concentrated HCl (4 mL) in MeOH (16 mL) was added to a stirring solution of acetal **268** (506 mg, 1.1 mmol) in DCM (10 mL). A further DCM (8 mL) was added to dissolve a resulting precipitate. After stirring for 4 h at 32 °C, the solution was poured into aqueous HCl (1 M, 15 mL) and extracted with DCM (3 × 20 mL). Combined organics were dried over $MgSO_4$ and concentrated under reduced pressure. Column chromatography [SiO_2, petroleum ether-EtOAc (9:1) to (7:3)] yielded phenol **269** as an oil (413 mg, 90%). *Characterisation as previous.*

{4-[5'-(2'',4''-Dinitrophenoxymethyl)-2'-iodophenoxymethyl]benzyl} triphenylphosphonium bromide 270

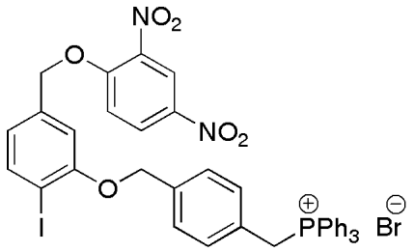

Anhydrous MeCN (3 mL) was added to a mixture of phenol **269** (40 mg, 9.6×10^{-5} mol), phosphonium bromide **233** (50.6 mg, 9.6×10^{-5} mol) and Cs_2CO_3 (31.3 mg, 0.12 mmol). The resulting mixture was stirred at 25 °C for 4.5 h under argon, resulting in a yellow liquid over a white precipitate. Liquid was pipetted off and filtered. Residual solid was washed multiple times with anhydrous MeCN and pipetted off and filtered each time until only a small residue remained. Combined MeCN washings were concentrated under reduced pressure, redissolved in DCM (3 mL) and washed with H_2O (3 mL). Organics were dried over $MgSO_4$ and concentrated under reduced pressure to yield phosphonium bromide **270** as a pale yellow solid (79 mg, 95%). Mp: >140 °C (Decomp.). ν_{max} (ATR): 3053 (CH), 3110 (CH), 3089 (CH), 2960 (CH), 2892 (CH), 2852 (CH), 2779 (CH), 1607 (Ar). δ_H (400 MHz, CD_3CN): 8.68 (1H, d, *J* = 2.8 Hz, H-3''), 8.43 (1H, dd, *J* = 9.3 and 2.8 Hz, H-5''), 7.89-7.82 (4H, m, 3 × *p*-H PPh_3 and H-3'), 7.69-7.62 (6H, m, 6 × *o*-H PPh_3), 7.60-7.51 (6H, m, 6 × *m*-H PPh_3), 7.43 (1H, d, *J* = 9.3 Hz, H-6''), 7.34 (2H, broad d, *J* = 7.9 Hz, H-3 and H-5), 7.12 (1H, d, *J* = 1.6 Hz, H-6'), 6.97 (2H, dd, *J* = 8.2 and 2.4 Hz, H-2 and H-6), 6.88 (1H, dd, *J* = 8.0 and 1.6 Hz, H-4'), 5.33 (2H, s, CH_2ODNB), 5.16 (2H, d, *J* = 1.7 Hz, C*H*$_2$ArCH$_2$P), 4.69 (2H, d, *J* = 14.7 Hz, CH_2P). δ_C (100 MHz, CD_3CN): 157.10 (C), 156.07 (C), 140.24 (C), 139.64 (CH), 138.85 (C), 136.78 (d, *J* = 3.3 Hz, C), 136.43 (C), 135.08 (d, *J* = 2.3 Hz, CH), 134.31 (d, *J* = 9.8 Hz, CH), 131.57 (d, *J* = 5.4 Hz, CH), 130.20 (d, *J* = 12.6 Hz, CH), 129.50 (CH), 127.40 (d, *J* = 2.8 Hz, CH), 126.43 (d, *J* = 9.3 Hz, C), 121.84 (CH), 121.13 (CH), 117.62 (d, *J* = 85.8 Hz, C), 115.85 (CH), 111.56 (CH), 86.43 (C), 71.28 (CH_2), 70.17 (CH_2), 30.55 (d, *J* = 46.8 Hz, CH_2). δ_P {^{1}H} (162 MHz, CD_3CN): 23.04 (s). LRMS (ESI^+): 781 (cation, 100%). HRMS: 781.0940. $C_{39}H_{31}IN_2O_6P$ requires, 781.0959.

Ethyl 3-hydroxybenzoate 272[193]

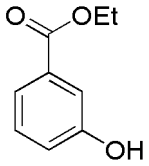

3-Hydroxybenzoic acid **252** (10.10 g, 72.4 mmol) in EtOH (70 mL) was cooled to –8 ºC and thionyl chloride (16.3 mL, 217 mmol) was added dropwise to the stirring solution. After stirring at reflux for 3 h the solution was allowed to cool to RT and then concentrated under reduced pressure. The residue was dissolved in DCM (70 mL) and washed with saturated aqueous $NaHCO_3$ (25 mL) and H_2O (2 × 50 mL). Organics were dried over $MgSO_4$ and concentrated under reduced pressure. Recrystallisation from EtOAc-hexane yielded ethyl ester **272** as an amorphous solid (10.25 g, 85%). Mp: 71-72 °C (EtOAc-hexane) [Lit.[193] 72-73 °C (EtOH)]. ν_{max} (ATR): 3318 (OH), 2986 (CH), 1674 (C=O), 1589 (Ar) cm^{-1}. δ_H (400 MHz, $CDCl_3$): 7.64-7.58 (2H, m, H-2 and H-6), 7.31 (1H, t, J = 8.1 Hz, H-5), 7.07 (1H, ddd, J = 8.1, 2.5 and 1.2 Hz, H-4), 5.97 (1H, broad s, OH), 4.38 (2H, q, J = 7.1 Hz, CH_2), 1.39 (3H, t, J = 7.1 Hz, CH_3). δ_C (100 MHz, $CDCl_3$): 167.05 (C), 155.98 (C), 131.56 (C), 129.71 (CH), 121.77 (CH), 120.32 (CH), 116.37 (CH), 61.41 (CH_2), 14.24 (CH_3). ^1H and ^{13}C NMR data broadly agree with literature.[193]

Ethyl 3-(methoxymethoxy)benzoate 273

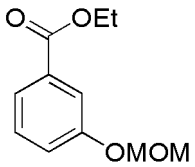

A stirring solution of phenol **272** (6.00 g, 36.1 mmol) in anhydrous DCM (200 mL) was degassed with argon for 20 min. Bromomethyl methyl ether (0.62 mL, 6.9 mmol) was added and the solution stirred at reflux for 24 h under argon. After cooling to RT, the mixture was washed with aqueous HCl (1 M, 75 mL) and H_2O (2 × 150 mL). Organics were dried over $MgSO_4$ and concentrated under reduced pressure to give a yellow oil. Column chromatography [SiO_2, petroleum ether-EtOAc (4:1)] yielded ethyl ester **273** as an oil (7.59 g, 94%). R_f [SiO_2, petroleum ether-EtOAc (4:1)]: 0.70. ν_{max} (ATR): 2982 (CH), 2959 (CH), 2938 (CH), 2905 (CH), 1717 (C=O), 1586 (Ar) cm^{-1}. δ_H (400 MHz, $CDCl_3$): 7.72-7.66 (2H, m, H-2 and H-6), 7.37-7.32 (1H, m, H-5), 7.25-7.19 (1H, m, H-4), 5.21 (2H, s, OCH_2O), 4.37 (2H, q, J = 7.1 Hz, CH_2CH_3), 3.48 (3H, s, OMe), 1.39 (3H, t, J = 7.1 Hz, CH_2CH_3). δ_C (100 MHz, $CDCl_3$): 166.31 (C), 157.13 (C) 131.90 (C), 129.69 (CH), 123.06 (CH), 120.89 (CH), 117.04 (CH), 94.38 (CH_2), 61.07 (CH_2), 56.09 (CH_3), 14.33

(CH_3). LRMS (EI^+): 210 ($M^{+\bullet}$, 100%), 165 ($M^{+\bullet}$ – $EtO^\bullet$ or – $CH_3OCH_2^\bullet$, 48), 45 ($CH_3OCH_2^{+\bullet}$, 50). HRMS: 210.0888. $C_{11}H_{14}O_4$ requires $M^{+\bullet}$, 210.0892.

3-(Methoxymethoxy)benzyl alcohol 274[194]

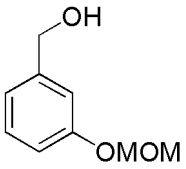

A stirring solution of ethyl ester **273** (500 mg, 2.38 mmol) in anhydrous Et_2O (20 mL) was degassed with argon for 10 min. The solution was cooled to 0 °C and lithium aluminium hydride (332 mg, 8.32 mmol) was added slowly. The mixture was stirred at 0 °C for 1.5 h and then at RT for 4 h. H_2O (1.5 mL) was added dropwise to quench the reaction followed by 3 drops aqueous HCl (1 M). The solution was diluted with H_2O (20 mL) and extracted with Et_2O (3 × 20 mL). Combined organics were dried over $MgSO_4$ and concentrated under reduced pressure. Column chromatography [SiO_2, petroleum ether-EtOAc (4:1)] yielded benzylic alcohol **274** as an oil (393 mg, 79%). R_f [SiO_2, petroleum ether-EtOAc (4:1)]: 0.13. ν_{max} (ATR): 3393 (OH), 2934 (CH), 2903 (CH), 2828 (CH), 1587 (Ar) cm^{-1}. δ_H (400 MHz, $CDCl_3$): 7.25 (1H, t, J = 7.9 Hz, H-5), 7.04-7.00 (1H, m, H-2), 6.96 (1H, d, J = 7.6 Hz, H-4 or H-6), 6.93 (1H, dd, J = 8.2 and 2.4 Hz, H-4 or H-6), 5.12 (2H, s, CH_2OH), 4.60 (2H, s, OCH_2O), 3.45 (3H, s, OMe), 2.55 (1H, broad s, OH). δ_C (100 MHz, $CDCl_3$): 157.27 (C), 142.74 (C) 129.55 (CH), 120.34 (CH), 115.31 (CH), 114.55 (CH), 94.23 (CH_2), 64.74 (CH_2), 55.93 (CH_3). LRMS (EI^+): 168 ($M^{+\bullet}$, 77%), 107 ($M^{+\bullet}$ – $CH_3OCH_2O^\bullet$, 15), 45 ($CH_3OCH_2^{+\bullet}$, 100). HRMS: 168.0788. $C_9H_{12}O_3$ requires $M^{+\bullet}$, 168.0786. ^1H and ^{13}C NMR data agree with literature.[194]

3-(1',3'-Dioxo-2',3'-dihydro-1*H*-isoindol-2'-yl)propan-1-ol 282[195]

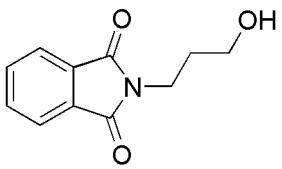

3-Aminopropan-1-ol **281** (8.0 mL, 105 mmol), phthalic anhydride (15.49 g, 105 mmol) and triethylamine (14.6 mL, 105 mmol) were dissolved in anhydrous toluene (150 mL) and stirred at reflux using a Dean-Stark apparatus for 5 h. After cooling to RT organics were washed with H_2O (80 mL) and dried over Na_2SO_4. Concentration under reduced pressure yielded alcohol **282** as an amorphous solid (20.80 g, 97%). Mp: 70-71 °C (Lit.[195] 73-75 °C). ν_{max} (ATR): 3329 (OH), 2949 (CH), 2941 (CH), 2929 (CH), 2874 (CH), 1699 (C=O), 1692 (C=O), 1604 (Ar), 1556 (Ar) cm^{-1}. δ_H (400 MHz, $CDCl_3$): 7.86 (2H, dd, J = 5.4 and

3.1 Hz, H-4' and H-7'), 7.73 (2H, dd, J = 5.4 and 3.1 Hz, H-5' and H-6'), 3.86 (2H, t, J = 6.3 Hz, 2 × H-1), 3.62 (2H, t, J = 5.8 Hz, 2 × H-3), 2.50 (1H, broad s, OH), 1.89 (2H, tt, J = 6.3 and 5.9 Hz, 2 × H-2). δ_C (100 MHz, $CDCl_3$): 168.91 (C), 134.11 (CH), 132.00 (C), 123.37 (CH), 59.06 (CH_2), 34.27 (CH_2), 31.34 (CH_2). LRMS (CI^+): 206 [$(M + H)^+$, 100%], 188 [$(M + H)^+ – H_2O$, 28]. HRMS: 206.0820. $C_{11}H_{12}NO_3$ requires $(M + H)^+$, 206.0817. ^1H and ^{13}C NMR data agree with literature.[195]

3-(1',3'-Dioxo-2',3'-dihydro-1*H*-isoindol-2'-yl)propanal 283[195]

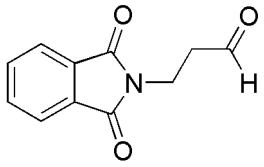

Oxalyl chloride (10.3 mL, 122 mmol) was added slowly to anhydrous DCM (350 mL) at –78 °C under argon and stirred for 5 min. Anhydrous DMSO (20.2 mL, 285 mmol) was added slowly and the resulting solution stirred for 30 min. A solution of alcohol **282** (16.71 g, 81.4 mmol) in anhydrous DCM (120 mL) was added slowly and the resulting solution stirred for 30 min. Triethylamine (40.9 mL, 293 mmol) was added and after stirring for 30 min at –78 °C, the solution was warmed to RT and stirred for a further 1.75 h. The reaction mixture was poured into H_2O (200 mL) and organics separated. Organics were washed with H_2O (2 × 150 mL), dried over Na_2SO_4 and concentrated under reduced pressure. Column chromatography [SiO_2, petroleum ether-EtOAc (4:1) to (1:1)] yielded aldehyde **283** as a viscous oil that solidified on standing (16.54 g, 88%). R_f [SiO_2, petroleum ether-EtOAc (1:1)]: 0.45. Mp: 119-120 °C (Lit.[195] 119-121 °C). ν_{max} (ATR): 2949 (CH), 2926 (CH), 2845 (CH), 2743 (CH), 1702 (C=O), 1677 (C=O), 1613 (Ar) cm^{-1}. δ_H (400 MHz, $CDCl_3$): 9.83 (1H, t, J = 1.3 Hz, H-1), 7.85 (2H, dd, J = 5.4 and 3.1 Hz, H-4' and H-7'), 7.73 (2H, dd, J = 5.4 and 3.1 Hz, H-5' and H-6'), 4.04 (2H, t, J = 7.0, 2 × H-3), 2.88 (2H, dt, J = 1.3 and 7.0 Hz, 2 × H-2). δ_C (100 MHz, $CDCl_3$): 199.51 (CH), 168.05 (C), 134.29 (CH), 131.92 (C), 123.40 (CH), 42.36 (CH_2), 31.66 (CH_2). LRMS (EI^+): 203 ($M^{+\bullet}$, 16%), 175 [($M^{+\bullet}$ – CO), 53], 160 ($PhthNCH_2^+$, 87), 85 (93), 83 (100), 76 (41), 47 (27). HRMS: 203.0579. $C_{11}H_9NO_3$ requires $M^{+\bullet}$, 203.0582. ^1H and ^{13}C NMR data agree with literature.[195]

3-(1',3'-Dioxo-2',3'-dihydro-1*H*-isoindol-2'-yl)-1-[4''-(4''',4''',5''',5'''-tetramethyl-1''',3''',2'''-dioxaborolan-2'''-yl)phenyl]propan-1-ol 284

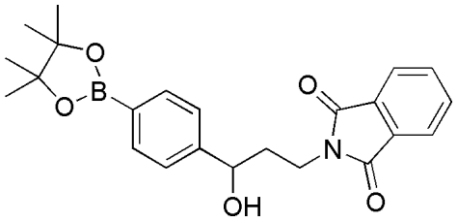

Anhydrous THF (35 mL) was added to aryl iodide **155** (2.50 g, 7.6 mmol) and anhydrous LiCl (385 mg, 9.1 mmol) under argon. The stirring mixture was cooled to –78 °C and ^{i}PrMgCl (2.0 M in THF, 4.6 mL, 9.1 mmol) was added dropwise. After stirring for 4.5 h, a solution of aldehyde **283** (1.54 g, 7.6 mmol) in anhydrous THF (15 mL) and anhydrous DCM (8 mL) was added dropwise and the mixture allowed to warm to RT overnight. Saturated aqueous NH_4Cl (15 mL) was added to quench and the mixture stirred until the precipitate settled. The mixture was filtered through a pad of Celite and washed through with Et_2O. Organics were dried over Na_2SO_4 and concentrated under reduced pressure. Column chromatography [SiO_2, petroleum ether-EtOAc (9:1) to (1:1)] yielded alcohol **284** as an oil (1.79 g, 58%). R_f [SiO_2, petroleum ether-EtOAc (1:1)]: 0.50. Mp: 126-127 °C. ν_{max} (ATR): 3502 (OH), 3042 (CH), 2994 (CH), 2942 (CH), 2871 (CH), 1699 (C=O), 1610 (Ar) cm^{-1}. δ_H (400 MHz, $CDCl_3$): 7.84 (2H, dd, *J* = 5.4 and 3.1 Hz, H-4' and H-7'), 7.74 (2H, d, *J* = 8.1 Hz, H-3'' and H-5''), 7.71 (2H, dd, *J* = 5.4 and 3.1 Hz, H-5' and H-6'), 7.34 (2H, d, *J* = 8.0 Hz, H-2'' and H-6''), 4.70 (1H, dt, *J* = 8.5 and 4.4 Hz, H-1), 3.91 (2H, dt, *J* = 6.5 and 1.2 Hz, 2 × H-3), 2.91 (1H, broad d, *J* = 4.2 Hz, OH), 2.15-2.00 (2H, m, 2 × H-2), 1.33 (12H, s, 4 × Me). δ_C (100 MHz, $CDCl_3$): 168.77 (C), 146.72 (C), 134.97 (CH), 134.02 (CH), 132.04 (C), 124.92 (CH), 123.33 (CH), 83.74 (C), 71.18 (CH), 37.61 (CH_2), 34.83 (CH_2), 24.86 (CH_3). LRMS (EI^+): 407 ($M^{+\bullet}$, 72%), 233 {[(Pinacol)B(C_6H_4)CHOH]$^+$, 66}, 175 [(PhthNEt)$^{+\bullet}$, 65], 160 (PhthNCH_2^+, 100), 105 ($PhCO^+$, 58), 83 ($C_6H_{11}^+$, 50) , 77 (Ph^+, 28). HRMS: 407.1905 and 406.1939. $C_{23}H_{26}{}^{11}BNO_5$ requires $M^{+\bullet}$, 407.1904 and $C_{23}H_{26}{}^{10}BNO_5$ requires $M^{+\bullet}$, 406.1940.

2-{3'-Bromo-3'-[4''-(4''',4''',5''',5'''-tetramethyl-1''',3''',2'''-dioxaborolan-2'''-yl)phenyl]propyl}-2,3-dihydro-1*H*-isoindole-1,3-dione 285

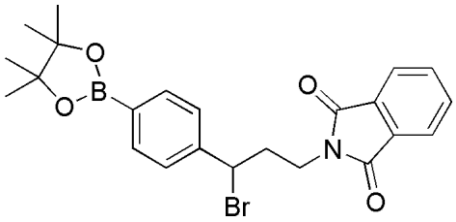

Methanesulfonyl chloride (15 µL, 0.20 mmol) was added to stirring alcohol **284** (67 mg, 0.17 mmol) in anhydrous DCM (1.1 mL) under argon at 0 °C followed by anhydrous triethylamine (34 µL, 0.25 mmol). After stirring for 1.5 h at RT, DCM (1.6 mL) was added and organics washed with H_2O (2 × 1.6 mL). Organics were dried over Na_2SO_4 and concentrated under reduced pressure. The residue was dissolved in anhydrous acetone (2 mL) under argon and anhydrous LiBr (143 mg, 1.65 mmol) added. The resultant mixture was stirred at reflux for 14 h. After cooling to RT, the mixture was concentrated under reduced pressure. DCM (4 mL) was added and washed with H_2O (2 × 3 mL). Organics were dried over Na_2SO_4 and concentrated under reduced pressure. Column chromatography [SiO_2, petroleum ether-EtOAc (4:1) to (1:1)] yielded semi-pure bromide **285** as amorphous solid (49 mg, 63%) (~85:15 bromide **285**:alkene **287**). R_f [SiO_2, petroleum ether-EtOAc (1:1)]: 0.58 (bromide **285** and alkene **287**). Selected data for bromide **285** from mixture: δ_H (500 MHz, $CDCl_3$): 7.79 (2H, dd, *J* = 5.4 and 3.1 Hz, H-4 and H-7), 7.72 (2H, d, *J* = 8.0 Hz, H-3'' and H-5''), 7.68 (2H, dd, *J* = 5.5 and 3.0 Hz, H-5 and H-6), 7.39 (2H, d, *J* = 8.1 Hz, H-2'' and H-6''), 5.00 (1H, t, *J* = 7.5 Hz, H-3'), 3.87-3.74 (2H, m, 2 × H-1'), 2.69-2.60 (2H, m, 2 × H-2'), 1.34 (12H, s, 4 × Me). δ_C (126 MHz, $CDCl_3$): 168.08 (C), 143.96 (C), 135.21 (CH), 133.94 (CH), 131.94 (C), 126.51 (CH), 123.23 (CH), 83.84 (C), 51.28 (CH), 37.80 (CH_2), 36.70 (CH_2), 24.84 (CH_3).

2-Cyano-5-(1',3'-dioxo-2',3'-dihydro-1*H*-isoindol-2'-yl)-3-[4''-(4''',4''',5''',5'''-tetramethyl-1''',3''',2'''-dioxaborolan-2'''-yl)phenyl]pentanenitrile 286

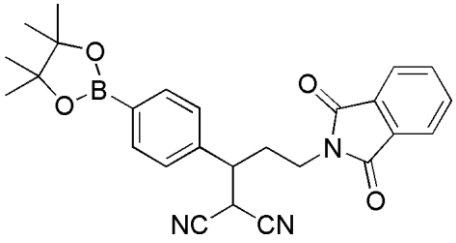

Anhydrous DMF (0.2 mL) was added to NaH (8.3 mg, 60% in mineral oil, 0.21 mmol) under argon at 0 °C. Malononitrile (4 drops) was added and and the solution stirred for 30 min. A solution of alkyl bromide (40 mg, 85 µmol) **285** in anhydrous DMF (0.4 mL) was

added dropwise and washed in with further anhydrous DMF (0.3 mL). The resultant solution was stirred overnight allowing to warm to RT. After 14.5 h, saturated NH_4Cl (2 mL) was added and extracts made with DCM (3 × 2 mL). Combined organics were dried over Na_2SO_4 and concentrated under reduced pressure. Column chromatography [SiO_2, petroleum ether-EtOAc (1:0) to (1:1)] yielded dinitrile **286** as amorphous solid (28 mg, 73%). R_f [SiO_2, petroleum ether-EtOAc (1:1)]: 0.60. δ_H (500 MHz, $CDCl_3$): 7.76 (2H, dd, *J* = 5.5 and 3.0 Hz, H-5' and H-6'), 7.75 (2H, d, *J* = 8.2 Hz, H-3'' and H-5''), 7.68 (2H, dd, *J* = 5.5 and 3.0 Hz, H-4' and H-7'), 7.34 (2H, d, *J* = 8.1 Hz, H-3'' and H-5''), 4.07 (1H, d, *J* = 6.2 Hz, H-2), 3.70 (2H, t, *J* = 6.7 Hz, H-5), 3.32 (1H, dt, *J* = 10.7 and 6.4 Hz, H-3), 2.60-2.50 (1H, m, H^A-4'), 2.37-2.29 (1H, m, H^B-4'), 1.33 (12H, s, 4 × Me). δ_C (126 MHz, $CDCl_3$): 168.08 (C), 138.27 (C), 135.69 (CH), 134.05 (CH), 131.70 (C), 127.14 (CH), 123.31 (CH), 111.42 (C), 111.39 (C), 83.94 (C), 44.51 (CH), 35.42 (CH_2), 30.43 (CH_2), 30.05 (CH), 24.85 (CH_3). LRMS (EI^+): 455 ($M^{+\bullet}$, 35%), 160 (100), 84 (94). HRMS: 455.2018 and 454.2052. $C_{26}H_{26}{}^{11}BN_3O_4$ requires $M^{+\bullet}$, 455.2016 and $C_{26}H_{26}{}^{10}BN_3O_4$ requires $M^{+\bullet}$, 454.2053.

2-{(2E)-3-[4'-(4'',4'',5'',5''-Tetramethyl-1'',3'',2''-dioxaborolan-2''-yl)phenyl]prop-2-en-1-yl}-2,3-dihydro-1*H*-isoindole-1,3-dione 287

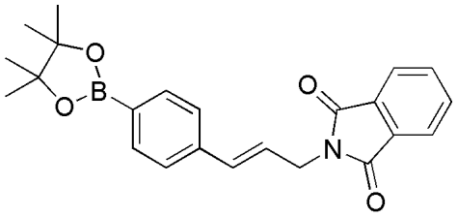

By-product isolated during the synthesis of dinitrile **286** as a glass (3 mg, 8%). R_f [SiO_2, petroleum ether-EtOAc (1:1)]: 0.58. δ_H (500 MHz, $CDCl_3$): 7.87 (2H, dd, *J* = 5.5 and 3.0 Hz, H-5 and H-6), 7.74-7.71 (4H, m, H-3, H-5, H-4'' and H-7''), 7.35 (2H, d, *J* = 8.1 Hz, H-2 and H-6), 6.65 (1H, d, *J* = 15.9 Hz, C*H*CHCH$_2$N), 6.32 (1H, dt, *J* = 15.9 and 6.4 Hz, C*H*CH$_2$N), 4.45 (2H, dd, *J* = 6.4 and 1.3 Hz, CH$_2$N), 1.33 (12H, s, 4 × Me). δ_C (126 MHz, $CDCl_3$): 167.97 (C), 138.90 (C), 135.00 (CH), 134.01 (CH), 133.64 (CH), 132.18 (C), 125.83 (CH), 123.79 (CH), 123.36 (CH), 83.78 (C), 39.65 (CH_2), 24.87 (CH_3). LRMS (EI^+): 389 ($M^{+\bullet}$, 95%), 242 (100), 160 (PhthNCH$_2^+$, 90), 142 (85), 83 ($C_6H_{11}^+$, 80). HRMS: 389.1800 and 388.1853. $C_{23}H_{24}{}^{11}BNO_4$ requires $M^{+\bullet}$, 389.1798 and $C_{23}H_{24}{}^{10}BNO_4$ requires $M^{+\bullet}$, 388.1835.

3-Amino-1-[4'-(4'',4'',5'',5''-tetramethyl-1'',3'',2''-dioxaborolan-2''-yl)phenyl]propan-1-ol 288

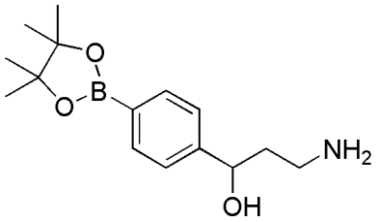

$N_2H_4.H_2O$ (50 µL, 64%, 0.66 mmol) was added to phthalimide **284** (200 mg, 0.49 mmol) in MeOH (1.5 mL) at 25 °C and stirred for 1.25 h before concentrating under reduced pressure. $CHCl_3$ (3 mL) was added and the residual solid removed by filtration. Organics were dried over Na_2SO_4 and concentrated under reduced pressure to yield amine **288** as an oil (115 mg, 85%). ν_{max} (ATR): 3365 (NH_2 and OH), 2976 (CH), 2927 (CH), 2868 (CH), 1611 (Ar), 1516 (Ar) cm^{-1}. δ_H (400 MHz, $CDCl_3$): 7.79 (2H, d, J = 7.6 Hz, H-3'' and H-5''), 7.39 (2H, d, J = 7.8 Hz, H-2'' and H-6''), 4.99 (1H, dd, J = 8.1 and 1.9 Hz, H-1), 3.13-3.03 (1H, m, H^A-3), 3.01-2.90 (1H, m, H^B-3), 1.95 (3H, broad s, NH_2 and OH), 1.92-1.83 (1H, m, H^A-2), 1.79-1.67 (1H, m, H^B-2), 1.34 (12H, s, 4 × Me). δ_C (100 MHz, $CDCl_3$): 148.42 (C), 134.78 (CH), 124.98 (CH), 83.68 (C), 74.63 (CH), 40.67 (CH_2), 39.99 (CH_2), 24.86 (CH_3). δ_B (128 MHz, $CDCl_3$): 30.96 (s). LRMS (EI^+): 277 ($M^{+\bullet}$, 24%), 260 [($M^{+\bullet}$ – NH_3), 39], 231 (30), 177 [$(OB(C_6H_4)CHOHCH_2CH_2NH_2)^{+\bullet}$, 25], 160 (40), 133 (47), 116 (42), 84 (100). HRMS: 277.1851 and 276.1892. $C_{15}H_{24}{}^{11}BNO_3$ requires $M^{+\bullet}$, 277.1852 and $C_{15}H_{24}{}^{10}BNO_3$ requires $M^{+\bullet}$, 276.1886.

[4-({3'-Hydroxy-3'-[4''-(tetramethyl-1''',3''',2'''-dioxaborolan-2'''-yl)phenyl]propyl}carbamoyl)butyl]triphenylphosphonium bromide 289

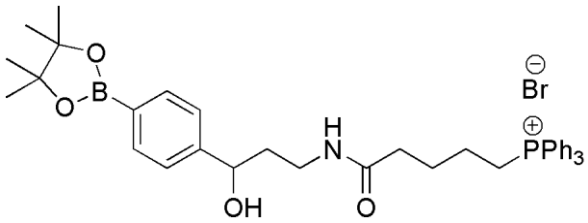

Anhydrous DMF (6 mL) was added to a stirring mixture of amine **288** (388 mg, 1.4 mmol), carboxylic acid **236** (604 mg, 1.4 mmol), 1-ethyl-3-(3-dimethylaminopropyl) carbodiimide (314 mg, 1.6 mmol) and 4-dimethylaminopyridine (17 mg, 0.14 mmol) at 25 °C under argon. The resulting solution was stirred for 24 h. DCM (15 mL) was added and organics washed with H_2O (18 mL), saturated aqueous LiBr (16 mL), dried over Na_2SO_4 and concentrated under reduced pressure. Column chromatography [SiO_2, DCM-MeOH (1:0) to (9:1)] yielded phosphonium bromide **289** as a glass (713 mg, 74%). R_f [SiO_2, DCM-MeOH (9:1)]: 0.30. ν_{max} (ATR): 3329 (OH and NH), 3055 (CH), 2976 (CH), 2932

(CH), 2870 (CH), 1643 (C=O), 1613 (Ar), 1543 (Ar) cm^{-1}. δ_H (400 MHz, $CDCl_3$): 8.72 (1H, t, *J* = 6.2 Hz, NH), 7.84-7.71 (11H, m, 6 × *o*-H PPh_3, 3 × *p*-H PPh_3, H-3'' and H-5''), 7.70-7.63 (6H, m, 6 × *m*-H PPh_3), 7.33 (2H, d, *J* = 8.0 Hz, H-2'' and H-6''), 4.82 (1H, broad s, OH), 4.70 (1H, broad d, *J* = 9.7 Hz, H-3'), 3.82-3.50 (3H, m, 2 × H-1 and H^A-1'), 3.36-3.25 (1H, m, H^B-1'), 2.77-2.61 (2H, m, 2 × H-4), 2.06-1.89 (3H, m, 2 × H-3 and H^A-2'), 1.81-1.62 (3H, m, 2 × H-2 and H^B-2'), 1.34 (12H, s, 2 × Me). δ_C (100 MHz, $CDCl_3$): 173.90 (C), 148.28 (C), 135.13 (d, *J* = 2.9 Hz, CH), 134.63 (CH), 133.60 (d, *J* = 10.1 Hz, CH), 130.52 (d, *J* = 12.6 Hz, CH), 125.05 (CH), 118.04 (d, *J* = 86.0 Hz, C), 83.61 (C), 69.88 (CH), 39.41 (CH_2), 35.87 (CH_2), 34.09 (CH_2), 26.04 (d, *J* = 17.0 Hz, CH_2), 24.88 (CH_3), 22.41 (d, *J* = 51.1 Hz, CH_2), 21.07 (d, *J* = 4.1 Hz, CH_2). LRMS (ESI^+): 622 (cation, 100%). HRMS (ESI^+): 622.3236 and 621.3277. $C_{38}H_{46}{}^{11}BNO_4P$ requires cation, 622.3259 and $C_{38}H_{46}{}^{10}BNO_4P$ requires cation, 621.3288. LRMS (ESI^-): 81 ($^{81}Br^-$, 98%) and 79 ($^{79}Br^-$, 100).

[(4-{4'-[3''-(2''',4'''-Dinitrophenoxy)-3''-[4''''-(4''''',4''''',5''''',5''''''-tetramethyl-1''''',3''''',2''''''-dioxaborolan-2''''''-yl)phenyl]prop-1''-yl]phenoxymethyl}phenyl)methyl]triphenylphosphonium bromide [MitoDNP-SUM(1)] 292

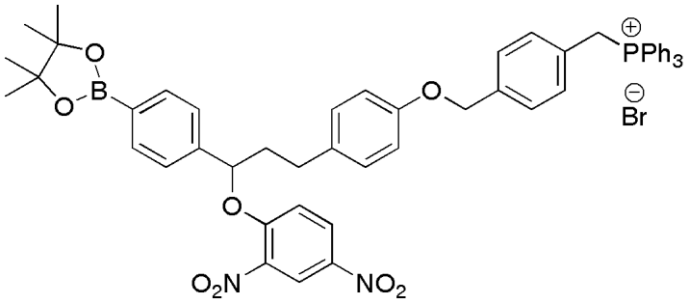

Cs_2CO_3 (178 mg, 0.55 mmol) was added to phenol **299** (178 mg, 0.34 mmol) in anhydrous MeCN (1.2 mL) and stirred under argon for 5 min. Benzylic bromide **233** (180 mg, 0.34 mmol) in anhydrous DCM (0.4 mL) was added. The resulting solution was stirred at RT for 10.5 h under argon before being concentrated under reduced pressure. H_2O (5 mL) was added and the product extracted with $CHCl_3$ (3 × 5 mL). Combined organics were dried over $MgSO_4$ and concentrated under reduced pressure. The solid was dissolved in DCM and precipitated by adding dropwise to stirring Et_2O. The liquor was pipetted off and the solid washed with Et_2O. Column chromatography of the residual solid [SiO_2, DCM-EtOH (9:1)] yielded phosphonium bromide **292** as an yellow glass (192 mg, 58%). R_f [SiO_2, DCM-EtOH (9:1)]: 0.20. ν_{max} (ATR): 3059 (CH), 3051 (CH), 2978 (CH), 2918 (CH), 2868 (CH), 2853 (CH), 1605 (Ar), 1524 (Ar), 1510 (NO_2), 1343 (NO_2). δ_H (500 MHz, $CDCl_3$):

8.69 (1H, d, *J* = 2.8 Hz, H-3’’’), 8.14 (1H, dd, *J* = 9.3 and 2.8 Hz, H-5’’’), 7.82-7.72 (11H, m, 6 × *o*-H PPh_3, 3 × *p*-H PPh_3, H-3 and H-5), 7.66-7.59 (6H, m, 6 × *m*-H PPh_3), 7.31 (2H, d, *J* = 8.1 Hz, H-3’’’’ and H-5’’’’), 7.19 (2H, d, *J* = 8.0 Hz, H-2’’’’ and H-6’’’’), 7.13 (2H, dd, *J* = 8.3 and 2.8 Hz, H-2 and H-6), 7.05 (2H, d, *J* = 8.7 Hz, H-3’ and H-5’), 6.86 (1H, d, *J* = 9.4 Hz, H-6’’’), 6.81 (2H, d, *J* = 8.7 Hz, H-2’ and H-6’), 5.50-5.42 (2H, m, CH_2P), 5.26 (1H, dd, *J* = 8.4 and 4.5 Hz, H-3’’), 4.96 (2H, d, *J* = 2.0 Hz, CH_2O), 2.77 (2H, t, *J* = 7.5 Hz, H-1’’), 2.45-2.36 (1H, m, H^A-2’’), 2.21-2.12 (1H, m, H^B-2’’), 1.324 (6H, s, 2 × Me), 1.319 (6H, s, 2 × Me). δ_C (126 MHz, $CDCl_3$): 156.86 (C), 155.73 (C), 141.79 (C), 139.77 (C), 139.22 (C), 137.53 (d, *J* = 4.2 Hz, C), 135.54 (CH), 135.07 (d, *J* = 2.4 Hz, CH), 134.32 (d, *J* = 9.8 Hz, CH), 133.05 (C), 131.63 (d, *J* = 5.6 Hz, CH), 130.18 (d, *J* = 12.7 Hz, CH), 129.41 (CH), 128.72 (CH), 127.66 (d, *J* = 3.0 Hz, CH), 126.62 (d, *J* = 8.6 Hz, C), 125.14 (CH), 121.59 (CH), 117.61 (d, *J* = 85.6 Hz, C), 116.32 (CH), 114.95 (CH), 83.99 (C), 82.10 (CH), 69.29 (CH_2), 39.89 (CH_2), 30.49 (d, *J* = 47.3 Hz, CH_2), 30.46 (CH_2), 24.86 (CH_3), 24.81 (CH_3). δ_P {^{1}H} (162 MHz, $CDCl_3$): 23.00 (s). LRMS (ESI^+): 885 (cation, 100%). HRMS (ESI^+): 885.3478 and 884.3517. $C_{53}H_{51}{}^{11}BN_2O_8P$ requires cation, 885.3479 and $C_{53}H_{51}{}^{10}BN_2O_8P$ requires cation, 884.3507. LRMS (ESI^-): 81 ($^{81}Br^-$, 98%) and 79 ($^{79}Br^-$, 100).

<u>Ethyl 3-(4’-hydroxyphenyl)propionate</u> 294[196]

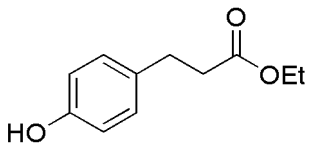

Thionyl chloride (10.54 mL, 144.4 mmol) was added dropwise to a stirring solution of 3-(4’-hydroxyphenyl)propionic acid **293** (8.00 g, 48.1 mmol) in EtOH (150 mL). The solution was stirred at reflux for 4.5 h. After cooling to RT, the solution was concentrated under reduced pressure to give a crude orange oil. Column chromatography [SiO_2, petroleum ether-EtOAc (9:1) to (3:2)] yielded ethyl ester **294** as an oil that solidified on standing (9.30 g, 99%). R_f [SiO_2, petroleum ether-EtOAc (7:3)]: 0.47. Mp: 42-43 °C. ν_{max} (ATR): 3364 (OH), 2998 (CH), 2981 (CH), 2962 (CH), 2942 (CH), 2904 (CH), 2870 (CH), 1701 (C=O), 1611 (Ar), 1596 (Ar) cm^{-1}. δ_H (400 MHz, $CDCl_3$): 7.04 (2H, d, *J* = 8.6 Hz, H-2’ and H-6’), 6.74 (2H, d, *J* = 8.6 Hz, H-3’ and H-5’), 6.02 (1H, broad s, OH), 4.13 (2H, q, *J* = 7.1 Hz, C*H*$_2$CH$_3$), 2.87 (2H, t, *J* = 7.9 Hz, 2 × H-3), 2.59 (2H, t, *J* = 7.8 Hz, 2 × H-2), 1.23 (3H, t, *J* = 7.2 Hz, CH_3). δ_C (100 MHz, $CDCl_3$): 173.75 (C), 154.24 (C), 132.23 (C), 129.38 (CH), 115.33 (CH), 60.72 (CH_2), 36.32 (CH_2), 30.10 (CH_2), 14.15 (CH_3). LRMS (EI^+): 194 ($M^{+\bullet}$, 33%), 149 ($M^{+\bullet}$ – $EtO^\bullet$, 9), 120 ($M^{+\bullet}$ – EtOH and – CO_2,

78), 107 ($HOC_6H_4CH_2^+$, 100), 83 (68). HRMS: 194.0945. $C_{11}H_{14}O_3$ requires $M^{+\bullet}$, 194.0943. ^{1}H NMR data agree with literature.[196]

Ethyl 3-(4'-methoxymethoxyphenyl)propionate 295[197]

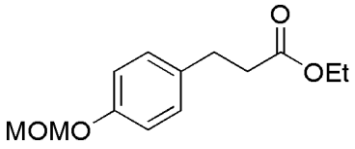

A stirring solution of ethyl ester **294** (27.00 g, 139 mmol) and DIPEA (31.5 mL, 181 mmol) in anhydrous DCM (400 mL) was degassed with argon for 30 min. Bromomethyl methyl ether (16.5 mL, 90%, 181 mmol) was added dropwise and the resulting solution stirred at reflux overnight under argon. After cooling to RT, the mixture was washed with aqueous HCl (1 M, 150 mL), H_2O (2 × 150 mL), dried over $MgSO_4$ and concentrated under reduced pressure. Column chromatography [SiO_2, petroleum ether-EtOAc (19:1) to (65:35)] yielded ethyl ester **295** as an oil (31.12 g, 94%). R_f [SiO_2, petroleum ether-EtOAc (4:1)]: 0.49. ν_{max} (ATR): 2982 (CH), 2955 (CH), 2936 (CH), 2826 (CH), 1732 (C=O), 1613 (Ar), 1586 (Ar) cm^{-1}. δ_H (400 MHz, $CDCl_3$): 7.11 (2H, d, *J* = 8.7 Hz, H-2' and H-6'), 6.94 (2H, d, *J* = 8.7 Hz, H-3' and H-5'), 5.13 (2H, s, OCH_2O), 4.11 (2H, q, *J* = 7.1 Hz, CH_2CH_3), 3.45 (3H, s, OMe), 2.88 (2H, t, *J* = 7.8 Hz, 2 × H-3), 2.57 (2H, t, *J* = 7.9 Hz, 2 × H-2), 1.22 (3H, t, *J* = 7.2 Hz, CH_2CH_3). δ_C (100 MHz, $CDCl_3$): 172.87 (C), 155.72 (C), 133.98 (C), 129.29 (CH), 116.30 (CH), 94.49 (CH_2), 60.33 (CH_2), 55.85 (CH_3), 36.15 (CH_2), 30.17 (CH_2), 14.21 (CH_3). LRMS (EI^+): 238 ($M^{+\bullet}$, 51%), 45 ($CH_3OCH_2^+$, 100). HRMS: 238.1209. $C_{13}H_{18}O_4$ requires $M^{+\bullet}$, 238.1205. Compound reported in literature without characterisation data.[197]

3-(4'-Methoxymethoxyphenyl)propan-1-ol 296[198]

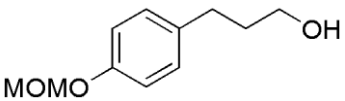

A stirring solution of ethyl ester **295** (8.73 g, 36.6 mmol) in anhydrous Et_2O (140 mL) was cooled to 0 °C under argon and $LiAlH_4$ (4.17 g, 109.8 mmol) was added portionwise. The solution was stirred at 0 °C under argon for 45 min before being allowed to warm to RT overnight. H_2O (25 mL) was added dropwise to quench. H_2O (20 mL) and Et_2O (100 mL) were added to dilute and the mixture stirred until the precipitate settled. The organic layer was filtered through a pad of Celite and washed through with Et_2O. Organics were dried over $MgSO_4$ and concentrated under reduced pressure to yield alcohol **296** as an oil (6.05 g, 84%). ν_{max} (ATR): 3347 (OH), 2994 (CH), 2937 (CH), 2902 (CH), 2861 (CH), 2827

(CH), 2785 (CH), 1612 (Ar), 1585 (Ar) cm^{-1}. δ_H (400 MHz, $CDCl_3$): 7.08 (2H, d, J = 8.7 Hz, H-2' and H-6'), 6.94 (2H, d, J = 8.7 Hz, H-3' and H-5'), 5.11 (2H, s, OCH_2O), 3.59 (2H, broad t, J = 5.9 Hz, 2 × H-1), 3.44 (3H, s, OMe), 3.00 (1H, broad s, OH), 2.61 (2H, t, J = 7.7 Hz, 2 × H-3), 1.86-1.77 (2H, m, 2 × H-2). δ_C (100 MHz, $CDCl_3$): 155.31 (C), 135.36 (C), 129.33 (CH), 116.23 (CH), 94.50 (CH_2), 61.81 (CH_2), 55.84 (CH_3), 34.34 (CH_2), 31.17 (CH_2). LRMS (CI^+): 197 [$(M + H)^+$, 46%], 165 [$(M + H)^+$ – MeOH, 100]. HRMS: 197.1179. $C_{11}H_{17}O_3$ requires $(M + H)^+$, 197.1178. ^1H and ^{13}C NMR are in agreement with literature, excluding the misreported ^{13}C NMR peak at 192.25 ppm (corresponds to peak the CH at 129.33 ppm above).[198]

3-(4'-Methoxymethoxyphenyl)propionaldehyde 297[198]

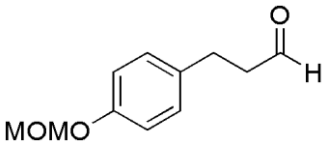

Oxalyl chloride (1.9 mL, 21.6 mmol) was added to anhydrous DCM (70 mL) at –78 °C under argon and stirred for 5 min. Anhydrous DMSO (2.7 mL, 38.0 mmol) was added and the resulting solution stirred at –78 °C for 30 min. A solution of alcohol **296** (3.00 g, 15.3 mmol) in anhydrous DCM (20 mL) was added slowly. After stirring for 30 min, anhydrous triethylamine (10.65 mL, 76.4 mmol) was added. After stirring for a further 30 min at –78 °C, the solution was allowed to warm to RT and stir for a further 2.5 h. The reaction was concentrated under reduced pressure. H_2O (50 mL) was added and extractions were made with DCM (3 × 30 mL). Combined organics were dried over $MgSO_4$ and concentrated under reduced pressure. Column chromatography [SiO_2, petroleum ether-EtOAc (9:1) to (7:3)] yielded aldehyde **297** as an oil (2.97 g, 94%). R_f [SiO_2, petroleum ether-EtOAc (4:1)]: 0.44. ν_{max} (ATR): 2996 (CH), 2957 (CH), 2933 (CH), 2898 (CH), 2848 (CH), 2826 (CH), 2792 (CH), 1722 (C=O), 1611 (Ar), 1585 (Ar) cm^{-1}. δ_H (400 MHz, $CDCl_3$): 9.78 (1H, t, J = 1.4 Hz, H-1), 7.10 (2H, d, J = 8.7 Hz, H-2' and H-6'), 6.96 (2H, d, J = 8.6 Hz, H-3' and H-5'), 5.13 (2H, s, OCH_2O), 3.45 (3H, s, OMe), 2.89 (2H, t, 2 × H-3, J = 7.5 Hz), 2.73 (2H, broad t, 2 × H-2, J = 7.5 Hz). δ_C (100 MHz, $CDCl_3$): 201.60 (CH), 155.73 (C), 133.72 (C), 129.26 (CH), 116.42 (CH), 94.48 (CH_2), 55.84 (CH_3), 45.39 (CH_2), 27.27 (CH_2). ^1H and ^{13}C NMR data agree with literature.[198]

3-(4'-Methoxymethoxyphenyl)-1-[4''-(4''',4''',5''',5'''-tetramethyl-1''',3''',2'''-dioxaborolan-2'''-yl)phenyl]propan-1-ol 298

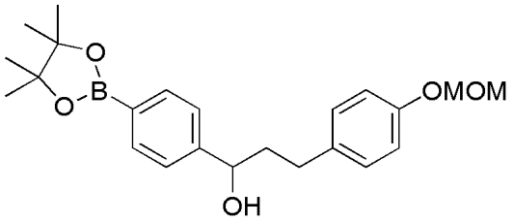

Anhydrous THF (60 mL) was added to aryl iodide **155** (3.91 g, 11.8 mmol) and anhydrous LiCl (552 mg, 13.0 mmol) under argon. The stirring mixture was cooled to –78 °C and ^{i}PrMgCl (2.0 M in THF, 6.5 mL, 13.0 mmol) was added dropwise over 20 min. After stirring for 3.5 h at –78 °C, aldehyde **297** (1.64 g, 8.4 mmol) in anhydrous THF (10 mL) was added dropwise and the solution allowed to warm to RT overnight. Saturated aqueous NH_4Cl (7 mL) was added to quench. H_2O (40 mL) was added and extractions made with Et_2O (3 × 40 mL). Combined organics were filtered through a pad of Celite and washed through with Et_2O. Organics were dried over $MgSO_4$ and concentrated under reduced pressure. Column chromatography [SiO_2, petroleum ether-EtOAc (19:1) to (55:45)] yielded alcohol **298** as an oil (3.36 g, 93%). R_f [SiO_2, petroleum ether-EtOAc (4:1)]: 0.22. ν_{max} (ATR): 3458 (OH), 2979 (CH), 2932 (CH), 2865 (CH), 2826 (CH), 1611 (Ar), 1586 (Ar) cm^{-1}. δ_H (400 MHz, $CDCl_3$): 7.78 (2H, d, J = 8.1 Hz, H-3'' and H-5''), 7.32 (2H, d, J = 8.0 Hz, H-2'' and H-6''), 7.07 (2H, d, J = 8.6 Hz, H-2' and H-6'), 6.93 (2H, d, J = 8.6 Hz, H-3' and H-5'), 5.11 (2H, s, OCH_2O), 4.68-4.60 (1H, m, H-1), 3.44 (3H, s, OMe), 2.70-2.52 (2H, m, 2 × H-3), 2.33 (1H, broad s, OH), 2.12-1.87 (2H, m, 2 × H-2), 1.33 (12H, s, 4 × Me). δ_C (100 MHz, $CDCl_3$): 155.36 (C), 147.84 (C), 135.15 (C), 134.97 (CH), 129.34 (CH), 125.24 (CH), 116.25 (CH), 94.53 (CH_2), 83.76 (C), 73.60 (CH), 55.85 (CH_3), 40.57 (CH_2), 31.06 (CH_2), 24.83 (CH_3). δ_B (128 MHz, $CDCl_3$): 30.54 (s). LRMS (EI^+): 398 ($M^{+\bullet}$, 53%), 380 ($M^{+\bullet}$ – H_2O, 43), 233 [$(C_6H_{12}O_2)B(C_6H_4)CHOH^+$, 33], 230 (60), 165 [$MOMO(C_6H_4)CH_2CH_2^+$, 10], 107 ($HOC_6H_4CH_2^+$, 45), 45 ($CH_3OCH_2^+$, 100). HRMS: 398.2260. $C_{23}H_{31}{}^{11}BO_5$ requires $M^{+\bullet}$, 398.2265.

4-{3'-(2'',4''-Dinitrophenoxy)-3'-[4'''-(4'''',4'''',5'''',5''''-tetramethyl-1'''',3'''',2''''-dioxaborolan-2''''-yl)phenyl]propyl}phenol 299

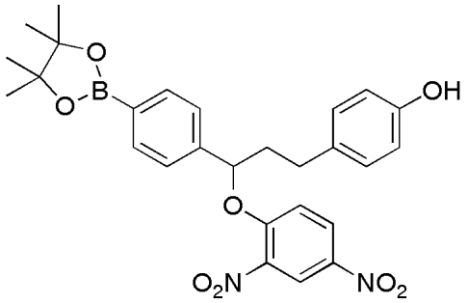

Anhydrous triethylamine (525 μL, 3.77 mmol) was added to a stirring solution of alcohol **298** (500 mg, 1.26 mmol) and 1-fluoro-2,4-dinitrobenzene (470 μL, 3.77 mmol) in anhydrous acetone (0.2 mL) and under argon. The resulting solution was stirred at 40 °C for 72 h, then concentrated under reduced pressure. EtOAc (12 mL) was added and washed with saturated aqueous $NaHCO_3$ (6 mL) and H_2O (2 × 6 mL). Organics were dried over $MgSO_4$ and concentrated under reduced pressure. DCM (16 mL) and MeOH (16 mL) were added followed by concentrated HCl (4 mL) dropwise. The resulting solution was stirred vigourously at 32 °C for 3.5 h. Pinacol (35 mg, 296 μmol) was added and stirred at RT for 1 h. The reaction mixture was poured into aqueous HCl (1 M, 12 mL) and organics separated before extracts were made with DCM (3 × 10 mL). Combined organics were dried over $MgSO_4$ and concentrated under reduced pressure. Column chromatography [SiO_2, petroleum ether-EtOAc (9:1) to (2:1)] yielded phenol **299** as an oil (417 mg, 64%). R_f [SiO_2, petroleum ether-EtOAc (7:3)]: 0.33. ν_{max} (ATR): 3399 (OH), 3114 (CH), 3094 (CH), 2980 (CH), 2932 (CH), 2863 (CH), 1606 (Ar), 1528 (NO_2), 1514 (NO_2), 1359 (NO_2), 1342 (NO_2) cm^{-1}. δ_H (500 MHz, $CDCl_3$): 8.70 (1H, d, J = 2.8 Hz, H-3''), 8.14 (1H, dd, J = 9.3 and 2.8 Hz, H-5''), 7.80 (2H, d, J = 7.9 Hz, H-3''' and H-5'''), 7.31 (2H, d, J = 8.0 Hz, H-2''' and H-6'''), 7.02 (2H, d, J = 8.4 Hz, H-3 and H-5), 6.85 (1H, d, J = 9.4 Hz, H-6''), 6.74 (2H, d, J = 8.4 Hz, H-2 and H-6), 5.25 (1H, dd, J = 8.4 and 4.5 Hz, H-3'), 4.81 (1H, broad s, OH), 2.77 (2H, t, J = 7.5 Hz, 2 × H-1'), 2.46-2.36 (1H, m, H^A-2'), 2.21-2.11 (1H, m, H^B-2'), 1.33 (6H, s, 2 × Me), 1.32 (6H, s, 2 × Me). δ_C (126 MHz, $CDCl_3$): 155.71 (C), 153.96 (C), 141.82 (C), 139.92 (C), 139.40 (C), 135.61 (CH), 132.59 (C), 129.60 (CH), 128.56 (CH), 125.10 (CH), 121.69 (CH), 116.00 (CH), 115.46 (CH), 84.06 (C), 82.12 (CH), 32.92 (CH_2), 30.48 (CH_2), 24.87 (CH_3), 24.82 (CH_3). LRMS (EI^+): 520 ($M^{+\bullet}$, 7%), 336 ($M^{+\bullet}$ – DNP, 7), 184 ($DNP^{+\bullet}$, 10), 107 ($HOArCH_2^+$, 100), 91 (16). HRMS: 520.2018 and 519.2049. $C_{27}H_{29}{}^{11}BN_2O_8$ requires $M^{+\bullet}$, 520.2017 and $C_{27}H_{29}{}^{10}BN_2O_8$ requires $M^{+\bullet}$, 519.2053.

2-{4'-[1''-(2''',4'''-Dinitrophenoxy)-3''-[4''''-(methoxymethoxy)phenyl]prop-1''-yl] phenyl}-4,4,5,5-tetramethyl-1,3,2-dioxaborolane 300

and

{4-[1'-(2'',4''-Dinitrophenoxy)-3'-[4'''-(methoxymethoxy)phenyl]prop-1''-yl]phenyl}boranediol 301

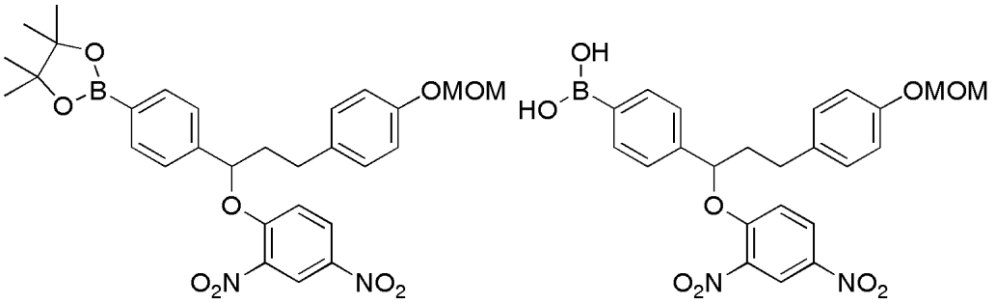

Anhydrous triethylamine (210 μL, 1.5 mmol) was added to stirring alcohol **298** (200 mg, 0.5 mmol), 1-fluoro-2,4-dinitrobenzene (189 μL, 1.5 mmol) and anhydrous acetone (0.1 mL) at RT under argon. The resulting solution was stirred at 40 °C for 72 h before being concentrated under reduced pressure. The residue was dissolved in DCM (6 mL) and washed with saturated aqueous $NaHCO_3$ (4 mL) and H_2O (2 × 4 mL). Organics were dried over $MgSO_4$ and concentrated under reduced pressure. Column chromatography [SiO_2, petroleum ether-EtOAc (95:5) to (5:95)] yielded an approximate 2:1 mixture of boronate ester **300** and boronic acid **301**. Selected data for boronate ester **300** from mixture: δ_H (400 MHz, $CDCl_3$): 8.69 (1H, d, *J* = 2.8 Hz, H-3'''), 8.15 (1H, dd, *J* = 9.3 and 2.8 Hz, H-5'''), 7.81 (2H, d, *J* = 8.1 Hz, H-2' and H-6'), 7.07 (2H, d, *J* = 8.6 Hz), 5.30 (1H, dd, *J* = 8.3 and 4.6 Hz, H-1''), 5.14 (2H, s, OCH_2O), 3.47 (3H, s, OMe), 2.78 (2H, t, *J* = 7.4 Hz, 2 × H-3''), 2.47-2.33 (1H, m, H^A-2''), 2.23-2.12 (1H, m, H^B-2''), 1.332 (6H, s, 2 × Me), 1.327 (6H, s, 2 × Me).

Selected data for boronic acid **301** from mixture: δ_H (400 MHz, $CDCl_3$): 8.65 (1H, d, *J* = 2.8 Hz, H-3''), 8.10 (1H, dd, *J* = 9.3 and 2.8 Hz, H-5''), 7.51 (2H, d, *J* = 7.9 Hz), 7.06 (2H, d, *J* = 8.6 Hz), 5.26 (1H, dd, *J* = 8.1 and 4.9 Hz, H-1'), 5.14 (2H, s, OCH_2O), 3.47 (3H, s, OMe), 2.75 (2H, t, *J* = 7.1 Hz, 2 × H-3'), 2.47-2.33 (1H, m, H^A-2'), 2.23-2.12 (1H, m, H^B-2').

4-{3'-Hydroxy-3'-[4''-(4''',4''',5''',5'''-tetramethyl-1''',3''',2'''-dioxaborolan-2'''-yl)phenyl]prop-1'-yl}phenol 302

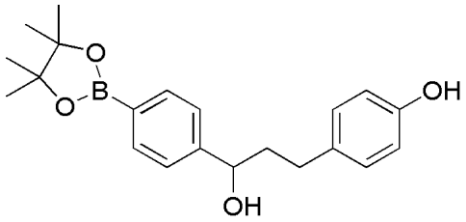

Concentrated HCl (2 mL) was added dropwise to stirring acetal **298** (250 mg, 0.63 mmol) in DCM (8 mL) and MeOH (8 mL). The resulting solution was stirred at 32 °C for 3.5 h. The solution was poured into aqueous HCl (1 M, 5 mL) and extracted with DCM (3 × 5 mL). Combined organics were dried over $MgSO_4$ and concentrated under reduced pressure. Column chromatography [SiO_2, petroleum ether-EtOAc (7:3)] gave diol **302** as an oil that solidified on standing (137 mg, 62%). R_f [SiO_2, petroleum ether-EtOAc (7:3)]: 0.19. Mp: 120-121 °C. ν_{max} (ATR): 3352 (OH), 3128 (CH), 3030 (CH), 3018 (CH), 2985 (CH), 2937 (CH), 2918 (CH), 2855 (CH), 1614 (Ar), 1600 (Ar) cm^{-1}. δ_H (400 MHz, $CDCl_3$): 7.80 (2H, d, *J* = 8.0 Hz, H-3'' and H-5''), 7.35 (2H, d, *J* = 8.0 Hz, H-2'' and H-6''), 7.04 (2H, d, *J* = 8.5 Hz, H-3 and H-5), 6.74 (2H, d, *J* = 8.5 Hz, H-2 and H-6), 4.84 (1H, broad s, OH), 4.72-4.65 (1H, m, H-3'), 2.70-2.54 (2H, m, 2 × H-1'), 2.14-1.92 (2H, m, 2 × H-2'), 1.90 (1H, broad s, OH), 1.35 (12H, s, 4 × Me). δ_C (100 MHz, $CDCl_3$): 153.68 (C), 147.67 (C), 135.03 (CH), 133.78 (C), 129.51 (CH), 125.24 (CH), 115.22 (CH), 83.84 (C), 73.80 (CH), 40.60 (CH_2), 31.01 (CH_2), 24.85 (CH_3). LRMS (EI^+): 354 ($M^{+\bullet}$, 33%), 336 ($M^{+\bullet} - H_2O$, 22), 233 [$(C_6H_{12}O_2)B(C_6H_4)CHOH^+$, 80], 208 (40), 121 (40), 107 [$HO(C_6H_4)CH_2^+$, 100], 83 (38). HRMS: 353.2016 and 354.2009. $C_{21}H_{27}{}^{10}BO_4$ requires $M^{+\bullet}$, 353.2039 and $C_{21}H_{27}{}^{11}BO_4$ requires $M^{+\bullet}$, 354.2002.

4-(4'-{3''-Hydroxy-3''-[4'''-(4'''',4'''',5'''',5''''-tetramethyl-1'''',3'''',2''''-dioxaborolan-2''''-yl)phenyl]prop-1''-yl}phenoxymethyl)benzyltriphenylphosphonium bromide 303

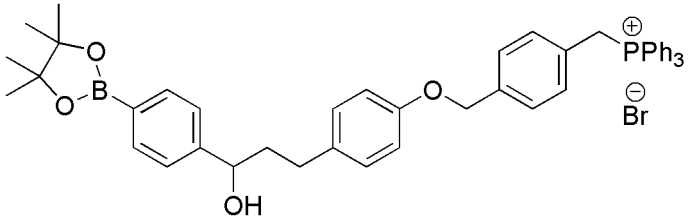

Cs_2CO_3 (44 mg, 0.14 mmol) was added to phenol **302** (40 mg, 0.11 mmol) in anhydrous MeCN (2 mL). After stirring under argon for 5 min, benzylic bromide **233** (59.4 mg, 1.1 mmol) in anhydrous DCM (0.5 mL) was added. The resulting solution was stirred at RT for 4 h under argon before being concentrated under reduced pressure. H_2O (3 mL) was

added and extracted with $CHCl_3$ (3 × 3 mL). Combined organics were dried over $MgSO_4$ and concentrated under reduced pressure. The solid was dissolved in DCM and precipitated by adding dropwise to stirring Et_2O. Liquid was pipetted off and the solid rinsed with Et_2O. Column chromatography [SiO_2, DCM-EtOH (9:1)] yielded phosphonium bromide **303** as an amorphous solid (43 mg, 48%). R_f [SiO_2, DCM-EtOH (9:1)]: 0.20. Mp: >190 °C (Decomp.). ν_{max} (ATR): 3323 (OH), 3055 (CH), 2976 (CH), 2926 (CH), 2862 (CH), 2785 (CH), 1611 (Ar), 1587 (Ar). δ_H (400 MHz, $CDCl_3$): 7.80-7.68 (11H, m, 6 × *o*-H PPh_3, 3 × *p*-H PPh_3, H-3''' and H-5'''), 7.60 (6H, m, 6 × *m*-H PPh_3), 7.34 (2H, d, *J* = 8.0 Hz, H-2''' and H-6'''), 7.16 (2H, d, *J* = 8.0 Hz, H-2 and H-6), 7.13-7.04 (4H, m, H-3, H-5, H-3' and H-5'), 6.80 (2H, d, *J* = 8.6 Hz, H-2' and H-6'), 5.74 (2H, d, *J* = 14.4 Hz, CH_2P), 4.93 (2H, d, *J* = 1.7 Hz, CH_2O), 4.69 (1H, dd, *J* = 7.6 and 5.4 Hz, H-3''), 2.71-2.54 (2H, m, 2 × H-1''), 2.20 (1H, broad s, OH), 2.13-1.91 (2H, m 2 × H-2''), 1.34 (12H, s, 4 × Me). δ_C (100 MHz, $CDCl_3$): 156.66 (C), 147.99 (C), 137.60 (d, *J* = 3.8 Hz, C), 135.06 (d, *J* = 2.9 Hz, CH), 135.01 (CH), 134.45 (C), 134.43 (d, *J* = 9.8 Hz, CH), 131.74 (d, *J* = 5.5 Hz, CH), 130.22 (d, *J* = 12.5 Hz, CH), 129.45 (CH), 127.71 (d, *J* = 3.3 Hz, CH), 126.69 (d, *J* = 8.6 Hz, C), 125.34 (CH), 117.75 (d, *J* = 85.8 Hz, C), 114.83 (CH), 83.86 (C), 73.59 (CH), 69.39 (CH_2), 40.82 (CH_2), 31.09 (CH_2), 30.50 (d, *J* = 47.8 Hz, CH_2), 24.93 (CH_3). δ_P {^{1}H} (162 MHz, $CDCl_3$): 23.52 (s). LRMS (ESI^+): 719 (cation, 100%). HRMS: 718.3476, 719.3436 and 720.3461. $C_{47}H_{49}{}^{10}BO_4P$ requires cation, 718.3492, $C_{47}H_{49}{}^{11}BO_4P$ requires cation, 719.3464 and $C_{46}{}^{13}CH_{49}{}^{11}BO_4P$ requires cation 720.3494.

6-(2',4'-Dinitrophenoxy)-6-[4''-(4''',4''',5''',5'''-tetramethyl-1''',3''',2'''-dioxaborolan-2'''-yl)phenyl]hexyltriphenylphosphonium iodide [MitoDNP-SUM(2)] 304

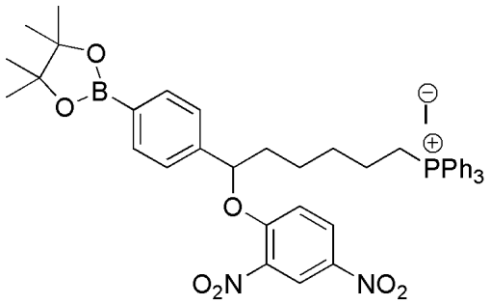

Alkyl iodide **315** (100 mg, 0.17 mmol) and triphenylphosphine (176 mg, 0.67 mmol) were dissolved in Et_2O (0.9 mL) and stirred at 30 °C for 3 d. After concentrating under reduced pressure, crude material was dissolved in minimal $CHCl_3$ and added dropwise to vigourously stirring Et_2O (20 mL). The precipitate was collected by filtration, washed

with Et_2O (10 mL) and dried under reduced pressure to yield phosphonium iodide **304** as a yellow glass. Combined Et_2O was concentrated under reduced pressure and the above isolation procedure was repeated to yield further phosphonium iodide **304** (Combined yield 130.8 mg, 91%). ν_{max} (ATR): 3052 (CH), 2978 (CH), 2925 (CH), 2863 (CH), 1604 (Ar), 1522 (Ar), 1484 (Ar), 1358 (NO_2), 1340 (NO_2) cm^{-1}. δ_H (400 MHz, $CDCl_3$): 8.60 (1H, d, *J* = 2.8 Hz, H-3'), 8.21 (1H, dd, *J* = 9.4 and 2.8 Hz, H-5'), 7.83-7.77 (9H, m, 6 × *o*-H PPh_3 and 3 × *p*-H PPh_3), 7.76 (2H, d, *J* = 8.1 Hz, H-3'' and H-5''), 7.73-7.68 (6H, m, 6 × *m*-H PPh_3), 7.46 (2H, d, *J* = 8.0 Hz, H-2'' and H-6''), 7.38 (1H, d, *J* = 9.5 Hz, H-6'), 5.89 (1H, dd, *J* = 7.9 and 5.0 Hz, H-6), 3.77-3.56 (2H, m, 2 × H-1), 2.09-1.98 (1H, m, H^A-5), 1.91-1.55 (7H, m, 2 × H-2, 2 × H-3, 2 × H-4, and H^B-5), 1.32 (6H, s, 2 × Me), 1.31 (6H, s, 2 × Me). δ_C (100 MHz, $CDCl_3$): 155.88 (C), 142.42 (C), 139.69 (C), 139.14 (C), 135.26 (d, *J* = 23.7 Hz, CH), 135.14 (CH), 133.70 (d, *J* = 9.8 Hz, CH), 130.58 (d, *J* = 12.4 Hz, CH), 129.06 (CH), 125.51 (CH), 121.25 (CH), 118.11 (d, *J* = 86.0 Hz, C), 117.72 (CH), 83.91 (C), 82.33 (CH), 37.28 (CH_2), 29.39 (d, *J* = 16.3 Hz, CH_2), 24.87 (CH_3), 24.85 (CH_3), 24.28 (CH_2), 22.85 (d, *J* = 50.4 Hz, CH_2), 22.17 (d, *J* = 4.2 Hz, CH_2). δ_P {^{1}H} (162 MHz, $CDCl_3$): 24.30 (s). LRMS (ESI^+): 731 (cation, 100%). HRMS: 731.3040 and 730.3081. $C_{42}H_{45}{}^{11}BN_2O_7P$ requires cation, 731.3059 and $C_{42}H_{45}{}^{10}BN_2O_7P$ requires cation, 730.3088. LRMS (ESI^-): 127 (I^-, 100%), 183 (DNP^-, 32).

4,4,5,5-Tetramethyl-2-{4'-[4''-(4''',4''',5''',5'''-tetramethyl-1''',3''',2'''-dioxaborolan-2'''-yl)phenyl]-1,3,2-dioxaborolane 306[199]

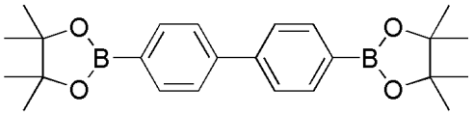

By-product isolated during the attempted synthesis of alkyl bromide **305** using the procedure of Xu *et al.*[160] ^{i}PrMgCl (2.0 M in THF, 0.5 mL, 1.0 mmol) was added dropwise to a stirring solution of aryl iodide **155** (300 mg, 0.9 mmol) and anhydrous $ZnBr_2$ (246 mg, 1.1 mmol) in anhydrous *N*-methylpyrolidinone (1.6 mL) at RT under argon. The solution was stirred at 60 °C for 30 min then at RT for 1 h. Thionyl chloride (1.8 mL, 24.7 mmol) was added to 5-bromovaleric acid (165 mg, 0.9 mmol) at 0 °C and stirred for 5 min. The solution was then stirred at RT for a further 1 h, then concentrated under reduced pressure. $Pd(dppf)Cl_2$ (20 mg, 2.7×10^{-5} mol) and anhydrous *N*-methylpyrolidinone (0.7 mL) were added under argon and this solution added to the initial solution *via* syringe. After stirring at RT for 3 h, H_2O (5 mL) was added and extracts made with Et_2O (3 × 5 mL). Combined organics were dried over $MgSO_4$ and concentrated under reduced pressure. Column chromatography [SiO_2, petroleum ether-EtOAc (1:0) to (4:1)] yielded bis-dioxaborolane

306 as an amorphous solid (93 mg, 36%). R_f [SiO_2, petroleum ether-EtOAc (9:1)]: 0.31. Mp: 240-241 °C. ν_{max} (ATR): 2982 (CH), 2930 (CH), 1605 (Ar), 1501 (Ar) cm^{-1}. δ_H (400 MHz, $CDCl_3$): 7.89 (4H, d, *J* = 8.3 Hz, H-2', H-6', H-3'' and H-5''), 7.64 (4H, d, *J* = 8.3 Hz, H-3', H-5', H-2'' and H-6''), 1.36 (24H, s, 8 × Me). δ_C (100 MHz, $CDCl_3$): 143.60 (C), 135.24 (CH), 126.50 (CH), 83.83 (C), 24.86 (CH_3). δ_B {^{1}H} (128 MHz, $CDCl_3$): 31.25 (s). LRMS (EI$^+$): 406 ($M^{+\bullet}$, 2 × ^{11}B, 100%), 405 ($M^{+\bullet}$, ^{11}B & ^{10}B, 47), 307 (50), 220 (55), 206 (35), 83 (47), 44 (63). HRMS: 406.2493 and 405.2516. $C_{24}H_{32}{}^{11}B_2O_4$ requires $M^{+\bullet}$, 406.2495 and $C_{24}H_{32}{}^{11}B^{10}BO_4$ requires $M^{+\bullet}$, 405.2525. ^{1}H and ^{13}C NMR data agree with literature.[199]

6-(Oxan-2'-yloxy)hexan-1-ol 308[200]

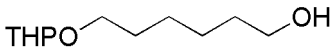

1,6-Hexanediol **307** (40.0 g, 339 mmol) was melted at 60 °C under argon. 2,3-Dihydro-2*H*-pyran (7.1 mL, 78 mmol) was added slowly to the stirring solution. *p*-Toluenesulfonic acid monohydrate (3.2 g, 17 mmol) was added and the resulting solution was stirred for 18 h. After cooling to RT, DCM (100 mL) was added and washed with H_2O (3 × 200 mL). Organics were dried over Na_2SO_4 and concentrated under reduced pressure. Column chromatography [SiO_2, petroleum ether-EtOAc (1:1)] yielded alcohol **308** as an oil (13.97 g, 88%). R_f [SiO_2, petroleum ether-EtOAc (1:1)]: 0.38. δ_H (400 MHz, $CDCl_3$): 4.57 (1H, dd, *J* = 4.5 and 2.7 Hz, H-2'), 3.87 (1H, ddd, *J* = 11.2, 7.5 and 3.6 Hz, H-6'^{AX}), 3.78-3.69 (1H, dt, *J* = 9.6 and 6.8 Hz, H^A-6), 3.61 (2H, t, *J* = 6.6 Hz, 2 × H-1), 3.54-3.46 (1H, m, H-6'^{EQ}), 3.43-3.35 (1H, dt, *J* = 9.6 and 6.6 Hz, H^B-6), 2.56 (1H, broad s, OH), 1.87-1.77 (1H, m, H-4'^{AX}), 1.75-1.67 (1H, m, H-3'^{EQ}), 1.65-1.47 (8H, m, H-3'^{AX}, H-4'^{EQ}, H-5'^{AX}, H-5'^{EQ}, 2 × H-2 and 2 × H-5), 1.45-1.33 (4H, m, 2 × H-3 and 2 × H-4). δ_C (100 MHz, $CDCl_3$): 98.89 (CH), 67.56 (CH_2), 62.68 (CH_2), 62.38 (CH_2), 32.69 (CH_2), 30.77 (CH_2), 29.69 (CH_2), 26.06 (CH_2), 25.61 (CH_2), 25.49 (CH_2), 19.69 (CH_2). LRMS (CI$^+$): 203 [$(M + H)^+$, 20%], 119 (100), 85 ($C_5H_9O^+$, 100). ^{1}H and ^{13}C NMR data agree with literature.[200]

6-(Oxan-2'-yloxy)hexanal 309[200]

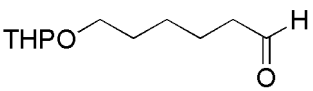

Oxalyl chloride (6.3 mL, 74.1 mmol) was added to anhydrous DCM (250 mL) at –78 °C under argon and stirred for 5 min. Anhydrous DMSO (9.0 mL, 127 mmol) was added and the resulting solution stirred at –78 °C for 30 min. A solution of alcohol **308** (10.71 g, 52.9 mmol) in anhydrous DCM (50 mL) was added slowly. After stirring for 45 min

triethylamine (10.65 mL, 76.4 mmol) was added slowly. After stirring for a further 1 h at –78 °C, the solution was allowed to warm to RT overnight. Organics were washed with H_2O (2 × 100 mL), dried over Na_2SO_4 and concentrated under reduced pressure to yield aldehyde **309** as an pale brown oil that was taken forward without further purification (9.95 g, 94%). δ_H (400 MHz, $CDCl_3$): 9.77 (1H, t, *J* = 1.8 Hz, H-6), 4.57 (1H, dd, *J* = 4.3 and 2.8 Hz, H-2'), 3.86 (1H, ddd, *J* = 11.1, 7.4 and 3.6 Hz, H-6'^{AX}), 3.74 (1H, dt, *J* = 9.6 and 6.7 Hz, H^{A}-6), 3.53-3.46 (1H, m, H-6'^{EQ}), 3.39 (1H, dt, *J* = 9.6 and 6.5 Hz, H^{B}-6), 2.45 (2H, dt, *J* = 1.8 and 7.3 Hz, 2 × H-2), 1.87-1.77 (1H, m, H-4'^{AX}), 1.75-1.48 (9H, m, H-3'^{EQ}, H-3'^{AX}, H-4'^{EQ}, H-5'^{EQ}, H-5'^{AX}, 2 × H-3 and 2 × H-5), 1.47-1.37 (2H, m, 2 × H-4). δ_C (100 MHz, $CDCl_3$): 202.60 (CH), 98.92 (CH), 67.25 (CH_2), 62.38 (CH_2), 43.83 (CH_2), 30.77 (CH_2), 29.51 (CH_2), 25.91 (CH_2), 24.49 (CH_2), 21.93 (CH_2), 19.71 (CH_2). LRMS (CI^+): 201 [$(M + H)^+$, 30%], 183 (70), 117 (100), 99 (100), 85 ($C_5H_9O^+$, 100). ^{1}H and ^{13}C NMR data agree with literature.[200]

6-(Oxan-2'-yloxy)-1-[4''-(4''',4''',5''',5'''-tetramethyl-1''',3''',2'''-dioxaborolan-2'''-yl)phenyl]hexan-1-ol 310

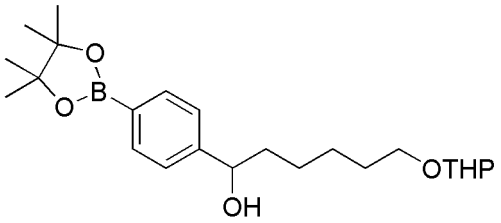

Anhydrous THF (150 mL) was added to a mixture of aryl iodide **155** (9.47 g, 28.7 mmol) and anhydrous LiCl (1.46 g, 34.5 mmol) under argon. The stirring mixture was cooled to –78 °C and ^{i}PrMgCl (2.0 M in THF, 17.2 mL, 34.5 mmol) was added slowly. After stirring for 45 min, aldehyde **309** (5.75 g, 28.7 mmol) in anhydrous THF (30 mL) was added dropwise and the solution allowed to warm to RT overnight. H_2O (25 mL) was added to quench and the mixture was stirred until the precipitate settled before being washed through a pad of Celite with Et_2O. Organics were dried over Na_2SO_4 and concentrated under reduced pressure. Column chromatography [SiO_2, petroleum ether-EtOAc (4:1) to (1:1)] yielded alcohol **310** as an oil in a 1:1 mixture of diastereomers (X and Y) (9.91 g, 85%). R_f [SiO_2, petroleum ether-EtOAc (1:1)]: 0.58. ν_{max} (ATR): 3442 (OH), 2977 (CH), 2938 (CH), 1613 (Ar), 1520 (Ar) cm^{-1}. δ_H (400 MHz, $CDCl_3$): 7.76 (2H, d, *J* = 8.1 Hz, H-3'' and H-5''), 7.31 (2H, d, *J* = 8.0 Hz, H-2'' and H-6''), 4.62 (1H, t, *J* = 6.5 Hz, H-1), 4.52 (1H, dd, *J* = 4.2 and 2.6 Hz, H-2'), 3.80 (1H, ddd, *J* = 11.1, 7.8 and 3.3 Hz, H-6'^{AX}), 3.67 [1H, td, *J* = 9.6 and 6.8 Hz, H^{A}-6-(X)], 3.65 [1H, td, *J* = 9.6 and 6.8 Hz, H^{A}-6-(Y)], 3.48-3.41 (1H, m, H-6'^{EQ}), 3.32 (1H, dt, *J* = 9.6 and 6.5 Hz, H^{B}-2), 2.77 (1H, broad s, OH),

1.83-1.72 (2H, m, H-3'^{EQ} and H-4'^{AX}), 1.71-1.61 (2H, m, 2 × H-2^{A}), 1.59-1.44 (6H, m, H-3'^{AX}, H-4'^{EQ}, H-5'^{EQ}, H-5'^{AX} and 2 × H-5), 1.42-1.26 (4H, m, 2 × H-3 and 2 × H-4), 1.32 (12H, s, 4 × Me). δ_C (100 MHz, $CDCl_3$): 148.33 (C), 134.86 (CH), 125.20 (CH), 98.66 (CH), 83.89 (C), 74.23 (CH), 74.21 (CH), 67.43 (CH_2), 67.39 (CH_2), 62.14 (CH_2), 62.11 (CH_2), 39.05 (CH_2), 30.67 (CH_2), 29.58 (CH_2), 29.56 (CH_2), 26.16 (CH_2), 26.10 (CH_2), 25.52 (CH_2), 25.49 (CH_2), 25.44 (CH_3), 24.83 (CH_2). LRMS (EI^+): 404 ($M^{+\bullet}$, 9%), 319 (83), 233 (100), 99 (63), 85 ($C_5H_9O^+$, 100). HRMS: 404.2733 and 403.2718. $C_{23}H_{37}{}^{11}BO_5$ requires $M^{+\bullet}$, 404.2734 and $C_{23}H_{37}{}^{10}BO_5$ requires $M^{+\bullet}$, 403.2770.

6-(2',4'-Dinitrophenoxy)-6-[4''-(4''',4''',5''',5'''-tetramethyl-1''',3''',2'''-dioxaborolan-2'''-yl)phenyl]hexan-1-ol 311

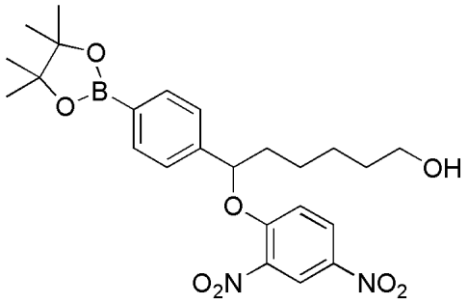

NaH (206 mg, 60% in mineral oil, 5.1 mmol) was added to a stirring solution of alcohol **310** (1.30 g, 3.2 mmol) and 1-fluoro-2,4-dinitrobenzene (1.4 mL, 3.9 mmol) in anhydrous DCM (8 mL) at 0 °C under argon. The solution was allowed to slowly warm to RT. After 5 h, H_2O (10 mL) was added slowly followed by DCM (10 mL). Organics were separated, dried over Na_2SO_4 and concentrated under reduced pressure. The residue was redissolved in DCM (8 mL) and MeOH (8 mL). Concentrated HCl (2.6 mL) was added dropwise to the vigourously stirring solution, which was then stirred at RT for 2 h. H_2O (15 mL) was added and extractions made with DCM (3 × 15 mL). Combined organics were dried over Na_2SO_4 and concentrated under reduced pressure. Column chromatography [SiO_2, petroleum ether-EtOAc (4:1) to (1:1)] yielded alcohol **311** as a viscous yellow oil (950 mg, 61%). R_f [SiO_2, petroleum ether-EtOAc (1:1)]: 0.29. ν_{max} (ATR): 3411 (OH), 2979 (CH), 2936 (CH), 2864 (CH), 1605 (Ar), 1526 (Ar), 1358 (NO_2), 1341 (NO_2) cm^{-1}. δ_H (400 MHz, $CDCl_3$): 8.67 (1H, d, J = 2.8 Hz, H-3'), 8.18 (1H, dd, J = 9.3 and 2.8 Hz, H-5'), 7.81 (1H, d, J = 8.0 Hz, H-3'' and H-5''), 7.35 (1H, d, J = 8.0 Hz, H-2'' and H-6''), 6.97 (1H, d, J = 9.4 Hz, H-6'), 5.38 (1H, dd, J = 7.4 and 5.3 Hz, H-6), 3.62 (2H, t, J = 6.4 Hz, 2 × H-1), 2.19-2.03 (2H, m, H^{B}-5 and OH), 2.00-1.89 (1H, m, H^{A}-5), 1.62-1.51 (3H, m, 2 × H-2 and H^{A}-4), 1.48-1.38 (3H, m, 2 × H-3 and H^{B}-4), 1.331 (6H, s, 2 × Me), 1.327 (6H, s, 2 × Me). δ_C (100 MHz, $CDCl_3$): 155.83 (C), 142.01 (C), 139.83 (C), 139.42 (C), 135.56 (CH),

128.56 (CH), 125.11 (CH), 121.61 (CH), 116.13 (CH), 84.02 (C), 83.39 (CH), 62.58 (CH_2), 38.06 (CH_2), 32.38 (CH_2), 25.38 (CH_2), 25.02 (CH_2), 24.86 (CH_3), 24.82 (CH_3). LRMS (CI^+): 504 [$(M + H)^+$, 55%], 436 (49), 422 (100). HRMS: 504.2509 and 503.2544. $C_{24}H_{35}{}^{11}BN_3O_7$ requires $(M + NH_4)^+$, 504.2516 and $C_{24}H_{35}{}^{10}BN_3O_7$ requires $(M + NH_4)^+$, 503.2548.

1-[4'-(4'',4'',5'',5''-Tetramethyl-1'',3'',2''-dioxaborolan-yl)phenyl]hexane-1,6-diol 312

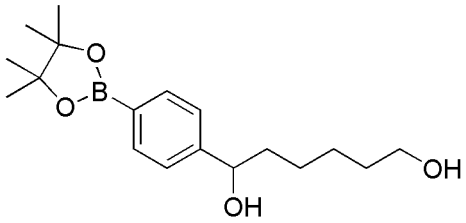

Column chromatography of the mixture that produced alcohol **311** above also gave diol **312** as an oil (122 mg, 12%). R_f [SiO_2, petroleum ether-EtOAc (1:1)]: 0.13. ν_{max} (ATR): 3372 (OH), 2979 (CH), 2934 (CH), 2861 (CH), 1612 (Ar) cm^{-1}. δ_H (400 MHz, $CDCl_3$): 7.79 (2H, d, J = 8.0 Hz, H-3' and H-5'), 7.35 (2H, d, J = 7.8 Hz, H-2' and H-6'), 4.69 (1H, dd, J = 7.2 and 5.9 Hz, H-1), 3.61 (2H, t, J = 6.6 Hz, 2 × H-6), 1.91 (1H, broad s, OH), 1.86-1.76 (1H, m, H^A-2), 1.76-1.66 (1H, m, H^B-2), 1.61 (1H, broad s, OH), 1.59-1.49 (2H, m, 2 × H-5), 1.47-1.27 (4H, m, 2 × H-3 and 2 × H-4) 1.34 (12H, s, 4 × Me). δ_C (100 MHz, $CDCl_3$): 147.21 (C), 133.86 (CH), 124.20 (CH), 82.77 (C), 73.17 (CH), 61.52 (CH_2), 37.95 (CH_2), 31.45 (CH_2), 24.54 (CH_2), 24.40 (CH_2), 23.81 (CH_3). LRMS (CI^+): 343 [$(M+Na)^+$, 36%], 338 [$(M+NH_4)^+$, 100], 320 [$(M+NH_4)^+ - H_2O$, 31], 303 [$(M + H)^+ - H_2O$, 30]. HRMS: 338.2504 and 337.2539. $C_{18}H_{33}{}^{11}BNO_4$ requires $(M + NH_4)^+$, 338.2497 and $C_{18}H_{33}{}^{10}BNO_4$ requires $(M + NH_4)^+$, 337.2533.

6-(2',4'-Dinitrophenoxy)-1-[4''-(4''',4''',5''',5'''-tetramethyl-1''',3''',2'''-dioxaborolan-yl)phenyl]hexane-1,6-diol 313

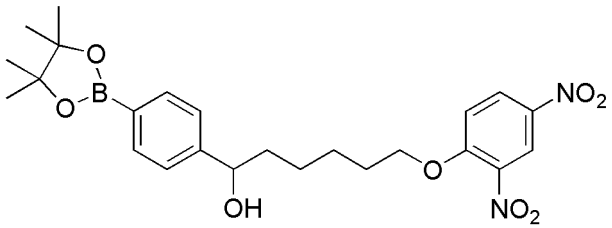

Column chromatography of the mixture that produced alcohol **311** above also gave alcohol **313** as a pale yellow oil (71 mg, 4%). R_f [SiO_2, petroleum ether-EtOAc (1:1)]: 0.37. ν_{max} (ATR): 3428 (OH), 3117 (CH), 3087 (CH), 2979 (CH), 2940 (CH), 2862 (CH), 1608 (Ar),

1526 (Ar), 1357 (NO_2), 1342 (NO_2) cm^{-1}. δ_H (400 MHz, $CDCl_3$): 8.72 (1H, d, *J* = 2.7 Hz, H-3'), 8.40 (1H, dd, *J* = 9.3 and 2.8 Hz, H-5'), 7.77 (2H, d, *J* = 8.0 Hz, H-3'' and H-5''), 7.33 (2H, d, *J* = 8.0 Hz, H-2'' and H-6''), 7.16 (1H, d, *J* = 9.4 Hz, H-6'), 4.70 (1H, broad t, *J* = 6.5 Hz, H-1), 4.19 (2H, t, *J* = 6.3 Hz, 2 × H-6), 2.16 (1H, broad s, OH), 1.92-1.67 (4H, m, 2 × H-2 and 2 × H-5), 1.62-1.41 (4H, m, 2 × H-3 and 2 × H-4), 1.34 (12H, s, 4 × Me). δ_C (100 MHz, $CDCl_3$): 156.87 (C), 147.88 (C), 139.85 (C), 138.88 (C), 134.98 (CH), 129.05 (CH), 125.18 (CH), 121.84 (CH), 114.27 (CH), 83.82 (C), 74.30 (CH), 70.68 (CH_2), 38.74 (CH_2), 28.50 (CH_2), 25.56 (CH_2), 25.12 (CH_3), 24.85 (CH_3). LRMS (CI^+): 504 [$(M + NH_4)^+$, 100%]. HRMS: 504.2510 and 503.2545. $C_{24}H_{35}{}^{11}BN_3O_8$ requires $(M + NH_4)^+$, 504.2516 and $C_{24}H_{35}{}^{10}BN_3O_8$ requires $(M + NH_4)^+$, 503.2548.

2-{4'-[6''-Bromo-1''-(2''',4'''-dinitrophenoxy)hexyl]phenyl}-4,4,5,5-tetramethyl-1,3,2-dioxaborolane 314

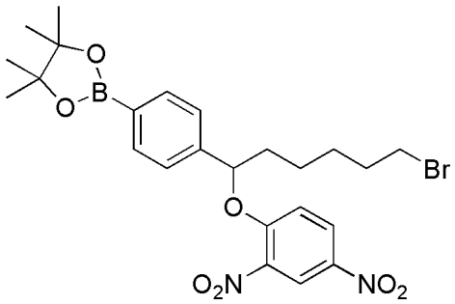

Alcohol **311** (65 mg, 0.13 mmol) and carbon tetrabromide (53 mg, 0.16 mmol) were stirred in anhydrous DCM (0.5 mL) under argon and cooled to 0 °C. A solution of triphenylphosphine in anhydrous DCM (0.5 mL) was added dropwise. After 5 min, the solution was allowed to warm to RT and stir for 16 h. After concentrating under reduced pressure, column chromatography [SiO_2, petroleum ether-EtOAc (2:1) to (1:1)] yielded dioxaborolane **314** as a pale yellow oil (73 mg, 98%). R_f [SiO_2, petroleum ether-EtOAc (1:1)]: 0.76. ν_{max} (ATR): 2978 (CH), 2936 (CH), 2863 (CH), 1604 (Ar), 1527 (Ar), 1359 (NO_2), 1341 (NO_2) cm^{-1}. δ_H (400 MHz, $CDCl_3$): 8.68 (1H, d, *J* = 2.8 Hz, H-3'''), 8.18 (1H, dd, *J* = 9.3 and 2.8 Hz, H-5'''), 7.81 (2H, d, *J* = 8.1 Hz, H-2' and H-6'), 7.35 (2H, d, *J* = 8.0 Hz, H-3' and H-5'), 6.96 (1H, d, *J* = 9.4 Hz, H-6'''), 5.38 (1H, dd, *J* = 7.5 and 5.2 Hz, H-1''), 3.39 (2H, t, *J* = 6.7 Hz, 2 × H-6''), 2.19-2.08 (1H, m, H^A-2''), 2.00-1.90 (1H, m, H^B-2''), 1.90-1.81 (2H, m, 2 × H-5''), 1.60-1.41 (4H, m, 2 × H-3'' and 2 × H-4''), 1.331 (6H, s, 2 × Me), 1.327 (6H, s, 2 × Me). δ_C (100 MHz, $CDCl_3$): 155.75 (C), 141.84 (C), 139.87 (C), 139.41 (C), 135.59 (CH), 128.55 (CH), 125.07 (CH), 121.63 (CH), 116.08 (CH), 84.01 (C), 83.23 (CH), 37.90 (CH_2), 33.66 (CH_2), 32.39 (CH_2), 27.66 (CH_2), 24.86

(CH_3), 24.82 (CH_3), 24.36 (CH_2). MS Analysis was unsuccessful at both the University of Glasgow and the EPSRC Mass Spectometry Centre, University of Swansea.

2-{4'-[6''-Iodo-1''-(2''',4'''-dinitrophenoxy)hexyl]phenyl}-4,4,5,5-tetramethyl-1,3,2-dioxaborolane 315

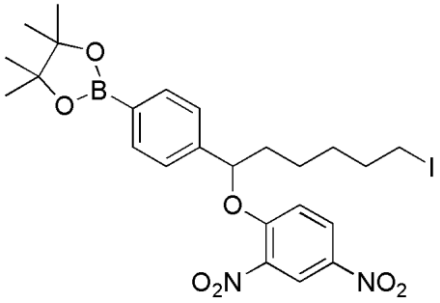

Method A:

Alcohol **311** (229 mg, 0.47 mmol), carbon tetraiodide (392 mg, 0.75 mmol) and triphenylphosphine (198 mg, 0.75 mmol) were dissolved in anhydrous DCM (1.2 mL) under argon and stirred at RT for 18 h. DCM (5 mL) was added washed with aqueous sodium thiosulfate (10%, 4 mL). Organics were separated, dried over Na_2SO_4 and concentrated under reduced pressure. Column chromatography [SiO_2, petroleum ether-EtOAc (1:0) to (1:1)] yielded dioxaborolane **315** as a pale yellow oil (208 mg, 74%). R_f [SiO_2, petroleum ether-EtOAc (1:1)]: 0.86. ν_{max} (ATR): 2976 (CH), 2931 (CH), 2861 (CH), 1605 (Ar), 1527 (Ar), 1485 (Ar), 1358 (NO_2), 1340 (NO_2) cm^{-1}. δ_H (400 MHz, $CDCl_3$): 8.68 (1H, d, J = 2.8 Hz, H-3'''), 8.18 (1H, dd, J = 9.3 and 2.8 Hz, H-5'''), 7.81 (2H, d, J = 8.0 Hz, H-2' and H-6'), 7.34 (2H, d, J = 8.0 Hz, H-3' and H-5'), 6.95 (1H, d, J = 9.3 Hz, H-6'''), 5.37 (1H, dd, J = 7.6 and 5.2 Hz, H-1''), 3.17 (2H, t, J = 6.9 Hz, 2 × H-6''), 2.19-2.07 (1H, m, H^A-2''), 2.00-1.89 (1H, m, H^B-2''), 1.87-1.76 (2H, m, 2 × H-5''), 1.60-1.52 (1H, m, H^A-3''), 1.50-1.40 (3H, m, 2 × H-4'' and H^B-3''), 1.331 (6H, s, 2 × Me), 1.326 (6H, s, 2 × Me). δ_C (100 MHz, $CDCl_3$): 155.76 (C), 141.84 (C), 139.88 (C), 139.42 (C), 135.60 (CH), 128.54 (CH), 125.05 (CH), 121.65 (CH), 116.07 (CH), 84.02 (C), 83.23 (CH), 37.89 (CH_2), 33.07 (CH_2), 29.97 (CH_2), 24.87 (CH_3), 24.83 (CH_3), 24.14 (CH_2), 6.82 (CH_2). LRMS (ESI^+): 1210 [$(2M + NH_4)^+$, 50%], 614 [$(M + NH_4)^+$, 100]. HRMS: 1210.2732, 1209.2758, 614.1531 and 613.1564. $(C_{24}H_{30}{}^{11}BIN_2O_7)_2.NH_4$ requires $(2M + NH_4)^+$, 1210.2735, $(C_{24}H_{30}{}^{10}BIN_2O_7)_2.NH_4$ requires $(2M + NH_4)^+$, 1209.2760, $C_{24}H_{30}{}^{11}BIN_2O_7.NH_4$ requires $(M + NH_4)^+$, 401.1520 and $C_{24}H_{30}{}^{10}BIN_2O_7.NH_4$ requires $(M + NH_4)^+$, 401.1520.

Method B:

Alkyl bromide **314** (215 mg, 0.39 mmol) was dissolved in anhydrous acetone (1.5 mL) under argon. Anhydrous KI (195 mg, 1.17 mmol) was added and the resulting mixture stirred at reflux for 3 h. The mixture was cooled to 0 °C, filtered and the solid washed with a little anhydrous acetone. Concentration under reduced pressure yielded iodide **315** as a pale yellow oil (233 mg, 93%). *Characterisation as previous.*

4-Nitro-3-vinylphenol 336

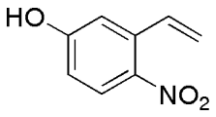

Method A:

A stirring solution of Nysted reagent **341** (3.5 mL, 20% wt. suspension in THF, 1.8 mmol) was cooled to 0 °C under argon, boron trifluoride diethyl etherate (180 μL, 1.4 mmol) added and stirred under argon for 5 min. 5-Hydroxy-2-nitrobenzaldehyde **335** (200 mg, 1.2 mmol) in anhydrous THF (1.4 mL) was cooled to 0 °C and added dropwise. After 5 min the reaction mixture was warmed to RT and stirred for a further 2.25 h. Aqueous HCl (1 M, 6 mL) was added followed by brine (5 mL) and the mixture extracted with DCM (3 × 6 mL). Combined organics were dried over $MgSO_4$ and concentrated under reduced pressure. The crude material was washed through a short pad of silica using petroleum ether-EtOAc (1:1) and concentrated under reduced pressure. The solid was dissolved in $CHCl_3$ and allowed to recrystallise slowly. Solvent traces were removed under reduced pressure yielding alkene **336** as needles (196 mg, 99%). Mp: 90-91 °C ($CHCl_3$). ν_{max} (ATR): 3336 (OH), 3078 (CH), 2924 (CH), 2857 (CH), 2783 (CH), 1601 (Ar), 1576 (Ar), 1316 (NO_2) cm^{-1}. δ_H (400 MHz, $CDCl_3$): 8.03 (1H, d, *J* = 8.9 Hz, H-5), 7.28 (1H, dd, *J* = 17.2 and 10.9 Hz, H-1'), 7.00 (1H, d, *J* = 2.7 Hz, H-2), 6.84 (1H, dd, *J* = 9.0 and 2.8 Hz, H-6), 5.70 (1H, dd, *J* = 17.2 and 0.9 Hz, H-2'-*cis to aryl*), 5.47 (1H, dd, *J* = 10.9 and 0.9 Hz, H-2'-*trans to aryl*). δ_C (100 MHz, $CDCl_3$): 159.99 (C), 140.88 (C), 137.21 (C), 133.47 (CH), 127.70 (CH), 118.89 (CH_2), 115.09 (CH), 115.00 (CH). LRMS (EI^+): 165 ($M^{+\bullet}$, 41%), 148 (58), 136 (44), 120 (37), 107 (41), 84 (55), 77 (100), 65 (78), 63 (49). HRMS: 165.0425. $C_8H_7NO_3$ requires $M^{+\bullet}$, 165.0426.

Method B:

Methyltriphenylphosphonium bromide (941 mg, 2.6 mmol) was stirred in anhydrous THF (6 mL) under argon. The mixture was cooled to –78 °C and ^{n}BuLi (1.64 mL, 2.6 mmol) was added dropwise and the resulting mixture stirred for 30 min. 5-Hydroxy-2-

nitrobenzaldehyde **335** (200 mg, 1.2 mmol) in anhydrous THF (2 mL) was added and the mixture stirred for 1 h before being allowed to warm to RT before stirring at reflux for 2 h. After cooling to RT, saturated aqueous NH_4Cl (15 mL) was added followed by H_2O (15 mL). Extractions were made with DCM (4 × 30 mL). Combined organic extracts were dried over $MgSO_4$ and concentrated under reduced pressure. Column chromatography [SiO_2, petroleum ether-EtOAc (4:1)] yielded alkene **336** as an amorphous solid (85 mg combined mass, 43%). R_f [SiO_2, petroleum ether-EtOAc (4:1)]: 0.21. *Characterisation as previous.*

Method C:

Nysted reagent **341** (3.5 mL, 20% wt. suspension in THF, 1.8 mmol) was added to stirring titanocene dichloride (894 mg, 3.6 mmol) in anhydrous THF (6 mL) under argon and stirred at 40 °C for 30 min. The resulting black/red solution was cooled to –78 °C and a solution of 5-hydroxy-2-nitrobenzaldehyde **335** (200 mg, 1.2 mmol) in anhydrous THF (2 mL) was added dropwise. The solution was stirred for 10 min before being allowed to warm to RT. Saturated aqueous $NaHCO_3$ (25 mL) was added and extractions made with EtOAc (5 × 20 mL). The aqueous layer was acidified using aqueous HCl (3 M) and extracted with DCM (3 × 20 mL). Combined DCM extracts were dried over $MgSO_4$ and concentrated under reduced pressure. Column chromatography [SiO_2, petroleum ether-EtOAc (4:1)] yielded alkene **336** an amorphous solid (77 mg, 39%). R_f [SiO_2, petroleum ether-EtOAc (4:1)]: 0.21. *Characterisation as previous.*

4-Nitro-3-vinylphenyl acetate 342

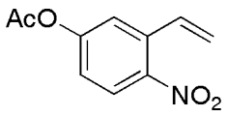

Stirring Nysted reagent **341** (17 mL, 20% wt. suspension in THF, 9 mmol) was cooled to 0 °C and boron trifluoride diethyl etherate (883 µL, 7.2 mmol) added under argon and stirred for 5 min. 5-Hydroxy-2-nitrobenzaldehyde **335** (1.00 g, 6.0 mmol) in anhydrous THF (7 mL) was cooled to 0 °C and added dropwise. After 5 min the reaction mixture was allowed to warm to RT and stir for a further 2 h. Aqueous HCl (1 M, 8 mL) was added followed by brine (8 mL). One extract was made with DCM (15 mL) and residual material washed through a Celite pad with DCM. Combined organics were dried over $MgSO_4$ and concentrated under reduced pressure. The crude material was washed through a short pad of silica using petroleum ether-EtOAc (1:1) and concentrated under reduced pressure. Attempted recrystallisations led to some suspected polymerisation of material upon

warming in $CHCl_3$, forming a black, insoluble oil. The residual yellow material was dissolved in acetic anhydride (7 mL) and AcOH (0.3 mL) was added. The resulting solution was stirred at reflux overnight under argon. Concentration under reduced pressure gave a dark residue. Column chromatography [SiO_2, petroleum ether-EtOAc (95:5) to (4:1)] yielded acetate **342** as needles (863 mg, 70%). R_f [SiO_2, petroleum ether-EtOAc (4:1)]: 0.42. Mp: 85-86 °C. ν_{max} (ATR): 3108 (CH), 3098 (CH), 3081 (CH), 1766 (C=O), 1613 (Ar), 1579 (Ar), 1519 (NO_2), 1343 (NO_2) cm^{-1}. δ_H (400 MHz, $CDCl_3$): 8.02 (1H, d, *J* = 8.9 Hz, H-5), 7.35 (1H, d, *J* = 2.5 Hz, H-2), 7.21 (1H, dd, *J* = 17.2 and 10.9 Hz, H-1'), 7.17 (1H, dd, *J* = 8.9 and 2.5 Hz, H-6), 5.74 (1H, dd, *J* = 17.2 and 0.6 Hz, H-2'-*cis to aryl*), 5.53 (1H, dd, *J* = 11.0 and 0.6 Hz, , H-2'-*trans to aryl*), 2.35 (3H, s, CH_3). δ_C (100 MHz, $CDCl_3$): 168.51 (C), 153.94 (C), 144.78 (C), 135.53 (C), 132.11 (CH), 126.29 (CH), 121.58 (CH), 121.44 (CH), 119.75 (CH_2), 21.06 (CH_3). LRMS (EI^+): 207 ($M^{+\bullet}$, 20%), 165 [$M^{+\bullet} - CH_2CO^{\bullet}$, 23], 148 [$M^{+\bullet} - CH_3CO_2^{\bullet}$, 78], 136 (41), 120 (35), 107 (43), 89 (34), 77 (56), 43 (CH_3CO^+, 100). HRMS: 207.0540. $C_{10}H_9NO_4$ requires $M^{+\bullet}$, 207.0532.

4-Hydroxy-3-methoxy-5-nitrobenzaldehyde 348[201]

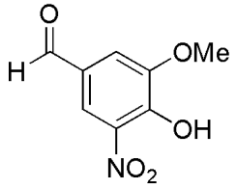

Vanillin **347** (2.50 g, 16.4 mmol) was dissolved in AcOH (35 mL) and cooled to 0 °C before HNO_3 (2.2 mL, 25 mmol, 70%) was added dropwise. After stirring for 5 min at 0 °C and 45 min ant RT, the solution was concentrated under reduced pressure. The resulting solid was recrystallised from acetone to yield aldehyde **348** as a yellow prisms (2.19 g, 68%). Mp: 173-174 °C (acetone) (Lit.[201] 176 °C). ν_{max} (ATR): 3194 (OH), 3078 (CH), 2984 (CH), 2945 (CH), 2878 (CH), 1684 (C=O), 1611 (Ar), 1576 (Ar), 1545 (Ar), 1335 (NO_2) cm^{-1}. δ_H (400 MHz, $CDCl_3$): 11.27 (1H, s, OH), 9.90 (1H, s, CHO), 8.23 (1H, d, *J* = 1.7 Hz, H-6), 7.65 (1H, d, *J* = 1.7 Hz, H-2), 4.03 (3H, s, Me). δ_C (100 MHz, $CDCl_3$): 188.86 (CH), 151.22 (C), 151.08 (C), 133.50 (C), 127.95 (C), 121.34 (CH), 113.52 (CH), 56.98 (CH_3). LRMS (EI^+): 206 ($M^{+\bullet}$, 41%), 180 (21), 122 (20), 86 (63), 84 (100). ^1H NMR data agree with literature.[201]

4-(Benzyloxy)-3-methoxybenzaldehyde 349[202]

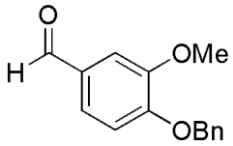

Benzyl bromide (12.3 mL, 104 mmol) was added dropwise to a stirring mixture of vanillin **347** (10.00 g, 65.7 mmol) and K_2CO_3 (4.54 g, 32.8 mmol) in anhydrous acetone (150 mL) under argon. The resulting mixture was stirred at reflux for 16 h. After cooling to RT, H_2O (500 mL) was added and extracted with DCM (3 × 150 mL). Combined organics were dried over Na_2SO_4 and concentrated under reduced pressure. Recrystallisation from hot EtOH yielded aldehyde **349** as plates (11.00 g, 69%). Mp: 60-61 °C (EtOH). ν_{max} (ATR): 3061 (CH), 3034 (CH), 3013 (CH), 2949 (CH), 2839 (CH), 2762 (CH), 1672 (C=O), 1597 (Ar), 1582 (Ar), 1504 (Ar) cm^{-1}. δ_H (500 MHz, $CDCl_3$): 9.84 (1H, s, CHO), 7.46-7.42 (3H, m, 2 × *m*-H Ph and H-2), 7.41-7.36 (3H, m, 2 × *o*-H Ph and *p*-H Ph), 7.35-7.31 (1H, m, H-6), 6.99 (1H, d, J = 8.2 Hz, H-5), 5.25 (2H, s, CH_2), 3.95 (3H, s, Me). δ_C (126 MHz, $CDCl_3$): 190.93 (CH), 153.59 (C), 150.08 (C), 136.00 (C), 130.29 (C), 128.73 (CH), 128.22 (CH), 127.20 (CH), 126.62 (CH), 112.38 (CH), 109.33 (CH), 70.87 (CH_2), 56.07 (CH_3). LRMS (EI^+): 242 ($M^{+\bullet}$, 75%), 91 ($PhCH_2^+$, 100), 84 (75), 65 (56). HRMS: 242.0947. $C_{15}H_{14}O_3$ requires $M^{+\bullet}$, 242.0943. ^1H and ^{13}C NMR data agree with literature.[202]

4-Hydroxy-5-methoxy-2-nitrobenzaldehyde 350[169]

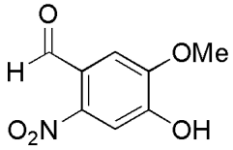

Method A:

Aldehyde **349** (800 mg, 3.3 mmol) was dissolved in AcOH (7 mL) and cooled to 0 °C. Concentrated HNO_3 (0.45 mL) was added dropwise to the stirring solution then warmed to RT after 5 min. After stirring overnight, the solution was concentrated under reduced pressure. Recrystallisation from hot EtOH yielded intermediate 4-(benzyloxy)-5-methoxy-2-nitrobenzaldehyde as a yellow amorphous solid (715 mg). Selected data for intermediate 4-(benzyloxy)-5-methoxy-2-nitrobenzaldehyde: δ_H (400 MHz, $CDCl_3$): 10.43 (1H, s, CHO), 7.67 (1H, s, H-3) 7.49-7.34 (6H, m, Ph and H-6), 5.27 (2H, s, CH_2), 4.02 (3H, s, Me). Crystals were re-dissolved in AcOH (4.5 mL) at 85 °C and HBr (48%, 1.4 mL) was added dropwise to the stirring solution. After 1 h the solution was cooled to RT. The precipitate was collected by filtration, washed with hexane and dried under reduced pressure. Recrystallisation from EtOH yielded phenol **350** as an amorphous yellow solid

(339 mg, 52%). Mp: 208-209 °C (EtOH) [Lit.[169] 208-210 °C (EtOH)]. ν_{max} (ATR): 3129 (OH), 3061 (CH), 2949 (CH), 1670 (C=O), 1582 (Ar), 1510 (NO_2), 1325 (NO_2) cm^{-1}. δ_H (400 MHz, d_6–DMSO): 11.10 (1H, broad s, OH), 10.16 (1H, s, CHO), 7.50 (1H, s, H-3), 7.36 (1H, s, H-6), 3.94 (3H, s, OMe). δ_C (100 MHz, d_6–DMSO): 188.39 (CH), 151.83 (C), 151.03 (C), 143.82 (C), 123.38 (C), 111.05 (CH), 110.65 (CH), 56.36 (CH_3). LRMS (CI^+): 215 [$(M + NH_4)^+$, 26%], 198 [$(M + H)^+$, 100], 168 [$(M + H)^+$ – CHO, 9]. HRMS: 198.0395. $C_8H_8NO_5$ requires $(M + H)^+$, 198.0397. ^1H NMR data broadly agree with literature.[169]

Method B:

Benzyl bromide (19.4 mL, 163 mmol) was added slowly to a stirring mixture of vanillin **347** (20.00 g, 131 mmol) and K_2CO_3 (9.1 g, 138 mmol) in anhydrous acetone (300 mL) under argon. The resultant mixture stirred at relfux overnight. After cooling to RT, H_2O (125 mL) was added and extracted with DCM (3 × 100 mL). Combined organics were dried over Na_2SO_4 and concentrated under reduced pressure. The crude material was dissolved in AcOH (100 mL) at RT and HNO_3 (24 mL) was added slowly to the stirring solution. The resulting mixture was stirred at reflux for 20 h. After cooling to RT, H_2O (80 mL) was added the precipitate collected by filtration. The yellow solid was washed with a little cold H_2O before drying under reduced pressure. The crude was re-dissolved in AcOH (200 mL) at 85 °C and HBr (48%, 75 mL) was added slowly. After 1.75 h the solution was cooled to 0 °C. The precipitate collected by filtration, washed with hexane and dried under reduced pressure. Recystallisation from acetone yielded phenol **350** as an amorphous yellow solid (9.86 g, 38%). *Characterisation as previous.*

4-Hydroxy(4'-iodobutyl)-2-nitro-5-methoxybenzaldehyde 351

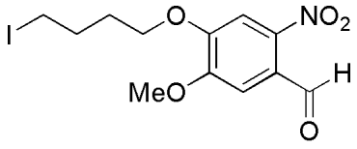

1,4-Diiodobutane **160** (1.6 mL, 12.2 mmol) was added to a stirring mixture of aldehyde **350** (600 mg, 3.0 mmol) and Cs_2CO_3 (2.48 g, 7.6 mmol) in anhydrous MeCN (15 mL) at RT under argon. The resulting mixture was stirred at 80 °C for 16 h with light excluded throughout. After cooling to RT the mixture was filtered and washed through with DCM (20 mL) before concentrating under reduced pressure. Column chromatography [SiO_2, petroleum ether-EtOAc (4:1)] gave aldehyde **351** as a semi-pure pale yellow oil which was taken forward without further purification (677 mg, 59%). R_f [SiO_2, petroleum ether-

EtOAc (4:1)]: 0.26. δ_H (400 MHz, $CDCl_3$): 10.45 (1H, s, CHO), 7.59 (1H, s, H-6), 7.41 (1H, s, H-3), 4.19 (2H, t, *J* = 5.9 Hz, 2 × H-1), 4.01 (3H, s, OMe), 3.29 (2H, t, *J* = 6.5 Hz, 2 × H-4), 2.10-2.01 (4H, m, 2 × H-2 and 2 × H-3). LRMS (CI^+): 380 [$(M + H)^+$, 100%]. HRMS: 379.9981. $C_{12}H_{14}INO_5$ requires $(M + H)^+$, 379.9989.

[4-(4'-Formyl-2'-methoxy-5'-nitrophenoxy)butyl]triphenylphosphonium iodide 352

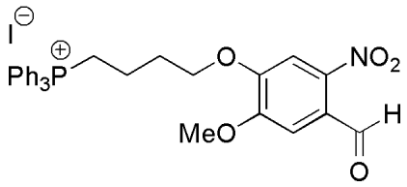

Alkyl iodide **351** (560 mg, 1.5 mmol) and triphenylphosphine (1.16 g, 4.4 mmol) were dissolved in anhydrous MeCN (7 mL) under argon and stirred at 80 °C overnight. After cooling to RT the solution was concentrated under reduced pressure. The residue was dissolved in minimal $CHCl_3$ and added dropwise to vigourously stirring Et_2O (100 mL). The precipitate was collected by filtration, washed with Et_2O and concentrated under reduced pressure. Column chromatography [SiO_2, DCM-EtOH (1:0) to (19:1)] yielded phosphonium iodide **352** as a yellow glass (717 mg, 76%). R_f [SiO_2, DCM-EtOH (19:1)]: 0.29. ν_{max} (ATR): 3053 (CH), 3008 (CH), 2935 (CH), 2866 (CH), 2794 (CH), 1684 (C=O), 1599 (Ar), 1571 (Ar), 1515 (Ar), 1328 (NO_2) cm^{-1}. δ_H (400 MHz, $CDCl_3$): 10.31 (1H, s, CHO), 7.89-7.81 (9H, m, 6 × *o*-H PPh_3 and 3 × *p*-H PPh_3), 7.77-7.70 (6H, m, 6 × *m*-H PPh_3), 7.58 (1H, s, H-6'), 7.32 (1H, s, H-3'), 4.29 (2H, t, *J* = 5.7 Hz, 2 × H-4), 3.88 (3H, s, OMe), 3.87-3.78 (2H, m, 2 × H-1), 2.40-2.30 (2H, m, 2 × H-3), 2.06-1.94 (2H, m, 2 × H-2). δ_C (100 MHz, $CDCl_3$): 187.74 (CH), 153.25 (C), 151.66 (C), 143.81 (C), 135.24 (d, *J* = 2.9 Hz, CH), 133.73 (d, *J* = 10.0 Hz, CH), 130.62 (d, *J* = 12.6 Hz, CH), 125.38 (C), 118.00 (d, *J* = 86.1 Hz, C), 109.91 (CH), 108.49 (CH), 69.12 (CH_2), 56.65 (CH_3), 29.06 (d, *J* = 16.5 Hz, CH_2), 22.74 (d, *J* = 50.9 Hz, CH_2), 19.57 (d, *J* = 3.7 Hz, CH_2). δ_P {^{1}H} (162 MHz, $CDCl_3$): 24.28 (s). LRMS (ESI^+): 546 [(cation + MeOH), 77%), 514 (cation, 100). HRMS: 546.2023 and 514.1767. $C_{31}H_{33}NO_6P$ requires (cation + MeOH), 546.2040 and $C_{30}H_{29}NO_5P$ requires cation, 514.1778. LRMS (ESI^-): 127 (I^-, 100%).

[4-(4'-Formyl-2'-methoxyphenoxy)butyl]triphenylphosphonium iodide 358

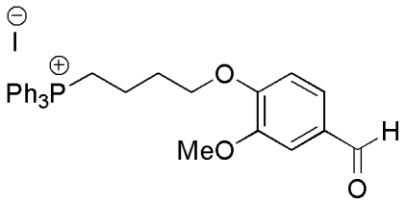

Anhydrous MeCN (10 mL) was added to a stirring mixture of alkyl iodide **161** (1.13 g, 2.0 mmol), vanillin **347** (300 mg, 2.0 mmol) and Cs_2CO_3 (771 mg, 2.4 mmol) under argon. The resulting mixture was stirred at 80 °C for 66 h. After cooling to RT, the mixture was filtered and washed through with $CHCl_3$ before concentrating under reduced pressure. Column chromatography [SiO_2, DCM-EtOH (1:0) to (19:1)] yielded aldehyde **358** as a glass (785 mg, 67%). R_f [SiO_2, DCM-EtOH (19:1)]: 0.41. ν_{max} (ATR): 3057 (CH), 3015 (CH), 2922 (CH), 1678 (C=O), 1585 (Ar), 1508 (Ar) cm^{-1}. δ_H (400 MHz, $CDCl_3$): 9.83 (1H, s, CHO), 7.89-7.79 (9H, m, 6 × *o*-H PPh_3 and 3 × *p*-H PPh_3), 7.76-7.68 (6H, m, 6 × *m*-H PPh_3), 7.47 (1H, dd, *J* = 8.2 and 1.8 Hz, H-5'), 7.37 (1H, d, *J* = 1.8 Hz, H-3'), 7.11 (1H, d, *J* = 8.3 Hz, H-6'), 4.26 (2H, t, *J* = 5.7 Hz, 2 × H-4), 3.89-3.79 (2H, m, 2 × H-1), 3.73 (3H, s, OMe), 2.33-2.24 (2H, m, 2 × H-3), 2.05-1.93 (2H, m, 2 × H-2). δ_C (100 MHz, $CDCl_3$): 190.91 (CH), 153.54 (C), 149.37 (C), 135.19 (d, *J* = 2.6 Hz, CH), 133.53 (d, *J* = 10.0 Hz, CH), 130.55 (d, *J* = 12.5 Hz, CH), 129.87 (C), 126.85 (CH), 117.82 (d, *J* = 86.1 Hz, C), 112.10 (CH), 109.34 (CH), 68.41 (CH_2), 55.90, (CH_3), 28.82 (d, *J* = 16.2 Hz, CH_2), 22.50 (d, *J* = 50.8 Hz, CH_2), 19.70 (d, *J* = 3.4 Hz, CH_2). δ_P {^{1}H} (162 MHz, $CDCl_3$): 23.88 (s). LRMS (ESI^+): 469 (cation, 100%). HRMS: 469.1918. $C_{30}H_{30}O_3P$ requires cation, 469.1927. LRMS (ESI^-): 151 ($C_6H_3(OMe)(CHO)O^-$, 11%), 127 (I^-, 100).

2-Methoxy-5-nitro-4-vinylphenol 362

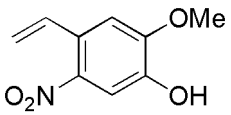

Nysted reagent (3.5 mL, 20% wt. suspension in THF, 1.8 mmol) and boron trifluoride diethyl etherate (190 μL, 1.5 mmol) were stirred under argon for 5 min. A solution of aldehyde **350** (150 mg, 0.76 mmol) in anhydrous THF (1.4 mL) was added dropwise and the resulting mixture stirred for 3 h at RT. Aqueous HCl (1 M, 5 mL) was added dropwise followed by brine (5 mL) and DCM (5 mL). After mixing, the mixture was filtered through a pad of Celite and washed through with DCM. Organics were dried over Na_2SO_4, concentrated under reduced pressure and purificatied by flash column chromatography [SiO_2, petroleum ether-EtOAc (1:1)]. Crystallisation from $CHCl_3$ yielded phenol **362** as yellow needles (120 mg, 81%). R_f [SiO_2, petroleum ether-EtOAc (1:1)]: 0.51. Mp: 89-90

°C. ν_{max} (ATR): 3358 (OH), 3098 (CH), 3078 (CH), 3011 (CH), 2951 (CH), 2849 (CH), 1618 (Ar), 1587 (Ar), 1520 (NO_2), 1331 (NO_2) cm^{-1}. δ_H (400 MHz, $CDCl_3$): 7.60 (1H, s, H-6), 7.24 (1H, dd, *J* = 17.1 and 10.8 Hz, H-1'), 6.96 (1H, s, H-3), 5.89 (1H, broad s, OH), 5.61 (1H, dd, *J* = 17.2 and 0.9 Hz, H-2'-*cis to aryl*), 5.40 (1H, dd, *J* = 10.9 and 0.9 Hz, H-2'-*trans to aryl*), 4.02 (1H, s, OMe). δ_C (100 MHz, $CDCl_3$): 150.58 (C), 145.17 (C), 140.83 (C), 133.48 (CH_2), 127.94 (C), 117.15 (CH), 111.11 (CH), 109.26 (CH), 56.45 (CH_3). LRMS (CI^+): 213 [$(M + NH_4)^+$, 36%], 196 [$(M + H)^+$, 100], 178 [$(M + H)^+ - H_2O$, 11]. HRMS: 196.0602. $C_9H_{10}NO_4$ requires $(M + H)^+$, 196.0604.

Appendices

Appendix 1: Anion exchange chromatography procedure

Amberlite IRA-400 ion exchange resin chloride form (7 g) was packed into a column with H_2O. An aqueous solution of NaOH (10% w/v) was run through the column until the pH of the eluate was 14. The column was then washed with H_2O until the eluate pH was 7 (~6 column volumes). An aqueous solution of $MeSO_3H$ (10% w/v) was washed through the column until the eluate pH was 1 (~2 column volumes) before being washed with H_2O until the eluate pH was 7 (~6 column volumes). The desired mixed anion phosphonium salt was washed through the column in MeOH:H_2O (1:1).

The desired phosphonium methanesulfonate salt was collected either by concentrating the eluate under reduced pressure, or by extracting from the eluate with $CHCl_3$ (3 × 8 mL), drying combined organics over Na_2SO_4, followed by concentration under reduced pressure.

Appendix 2: Buffer solutions

All buffers were adjusted to the desired pH at 37 °C using KOH or HCl. BSA is included in biological testing only.

MAS1 Buffer

Mannitol	220 mM
Sucrose	70 mM
HEPES	1 mM
EGTA	2 mM
KH_2PO_4	10 mM
$MgCl_2$	5 mM
BSA (FA free)	0.2% by weight

SHEP Buffer

Sucrose	290 mM
HEPES	1 mM
EGTA	2 mM
KH_2PO_4	10 mM
BSA (FA free)	0.2% by weight

KHE Buffer

KCl	120 mM
HEPES	5 mM
EGTA	1 mM
KH_2PO_4	5 mM
BSA (FA free)	0.2% by weight

CP1 Buffer – pH 7.4 at 4 °C (approx 9 mL 10 M HCl)

KCl	100 mM
Tris-HCl	50 mM
EGTA	2 mM

CP2 Buffer – pH 7.4 at 4 °C (approx 2.7 mL 10 M HCl)

KCl	100 mM
Tris-HCl	50 mM
EGTA	2 mM
BSA(FA free)	0.5% by weight
$MgCl_2.6H_2O$	5 mM
ATP	1 mM

Protease Type VIII (Sigma P 5380) at 245.7 U 100 mL^{-1}

CP2 can be made the day before use but BSA, ATP and protease must be added on the day of mitochondria isolation. Check pH and adjust if appropriate prior to use. Dissolve solutions completely before adding $MgCl_2.6H_2O$. Adjust to pH 7.1 at RT, put in fridge overnight and check/adjust to pH 7.4 in the morning.

Appendix 3: MitoSUM decomposition time course graphs

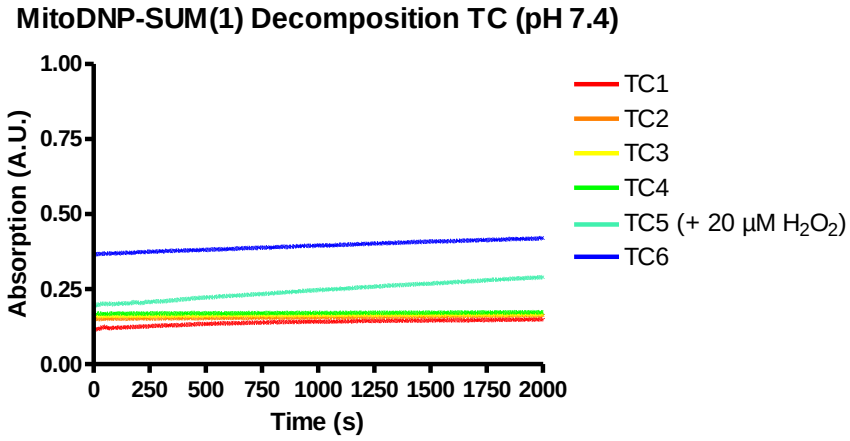

Fig.83: Time course graph showing linearity of MitoDNP-SUM(1) **292** decomposition

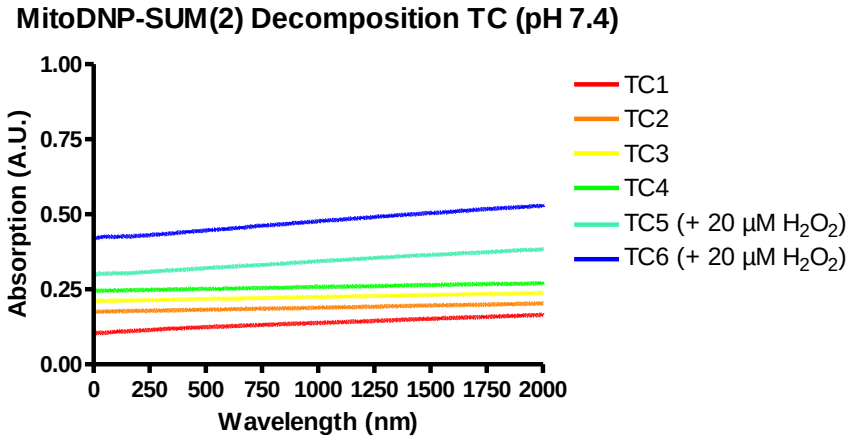

Fig.84: Time course graph showing linearity of MitoDNP-SUM(2) **304** decomposition

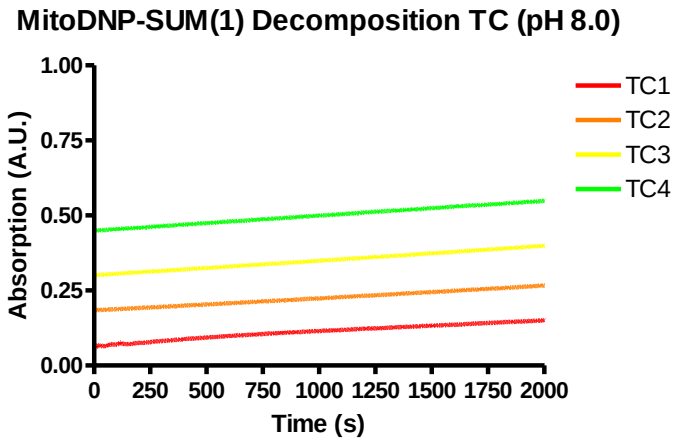

Fig.85: Time course graph showing linearity of MitoDNP-SUM(1) **292** decomposition

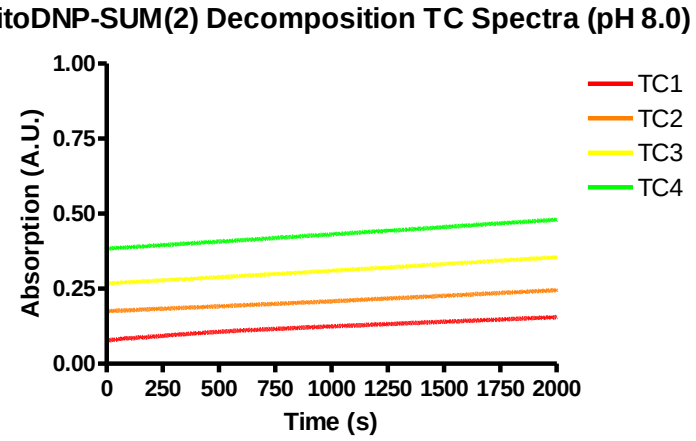

Fig.86: Time course graph showing linearity of MitoDNP-SUM(2) **304** decomposition

Appendix 4: Mitochondria isolation procedure from skeletal muscle tissue

The isolation of the mitochondria was performed in a team each day, with different team members performing different steps in the isolation procedure to split the workload. Changing the steps that individuals complete each day can lead to result variability and so commonly, each person would be involved only in specific steps. Those without animal handling certification can only join the procedure from step 5 onwards. For one rat requires need 1 L of CP1 buffer and 300 mL of CP2 buffer.

Procedure:[203,204,205]

1. Kill the rat by cervical dislocation. Cut around the hind legs with sharp scissors, peel back the skin with a sharp blade and cut out as much skeletal muscle as possible, including some from the back.
2. Place the tissue immediately into CP1 medium on ice.
3. Pour away the medium and weigh the tissue (~15-25 g tissue/rat).
4. Add more CP1 medium immediately to the tissue.
5. Take one piece of tissue at a time, place on a pre-cooled tile and mince with a sharp blade removing as much fat and connective tissue as possible. Once a piece of tissue is minced place it in CP1 medium again.
6. Repeat until all the tissue has been minced in this way.
7. Chop the tissue further with scissors and rinse 4-5 times with CP1.
   Add the tissue to CP2 (with protease & ATP **5**). Use 40 mL of CP2 for every 4-5 g tissue (It is important not to have a higher dilution, as this causes over digestion of the

tissue, resulting in a poor yield of mitochondria). Leave to stir gently in a 250 mL beaker on ice for 5 min (2.5 min for mice).

8. Divide the tissue into 3 or 4 × 100 mL plastic beakers.
9. Polytron the tissue in each beaker separately for 3 × 3 second bursts. (1 × 3 s for mice).

Use the polytron on a slow speed. Remove any fat or connective tissue from head between bursts. Over homogenised tissue results in damaged mitochondria so this step will vary depending on the homogeniser used.

10. Pour the homogenised tissue back into the 250 mL beaker and leave stirring on ice for a further 6 min (3 min for mice).
11. Split the homogenised tissue between 8 × 50 mL plastic centrifuge tubes and spin at 4 °C for 10 min at 500 × g.
12. Filter the supernatant through two layers of muslin into 8 new centrifuge tubes. Fill up the tubes with CP1 if necessary and spin at 4 °C for 10 min at 10,000 × g.
13. Resuspend the pellets in CP1 medium ie. decant off supernatant, remove any white outer layer by gentle swirling of the tube by hand and resuspend the mitochondria with a resuspending stick in a very small volume of medium. At this stage combine two pellets together.
14. Fill up the tubes (4) with CP1 medium and spin at 4 °C for 10 min at 10,000 × g.
15. Resuspend the mitochondria as before and again combine two pellets together.
16. Fill up the tubes with CP1 and spin at 500 × g for 5 min.
17. Transfer the supernatant and spin at 4 °C for 10 min at 10,000 × g.
18. Finally, resuspend and combine the two pellets. Make up to a final volume of approx 1 mL with CP1 medium and determine the protein concentration using a Biuret assay (should be 40-50 mg/mL).

References

1. Hatefi, Y. *Ann. Rev. Biochem.* **1985**, 54, 1015-1069.
2. Smith, R. A. J.; Hartley, R. C.; Cochemé, H. M.; Murphy, M. P. *Trends Pharmacol. Sci.* **2012**, 33, 341-352.
3. http://en.wikipedia.org/wiki/Mitochondria, in *Wikipedia* **2007** 22nd August.
4. Boss, O.; Hagen, T.; Lowell, B. B. *Diabetes* **2000**. 49: p. 143-156.
5. Nicholls, D. G.; Bernson, V. S.; Heaton, G. M. *Experientia. Suppl.* **1978**, 32, 89-93.
6. Halliwell, B.; Gutteridge, J. M. C. *Free Radicals in Biology and Medicine* **1999**, OUP: Oxford
7. Imlay, J. A. *Annu. Rev. Microbiol.* **2003**, 57, 395-418.
8. Brand, M. D.; Affourtit, C.; Esteves, T. C.; Green, K.; Lambert, A. J.; Miwa, S.; Pakay, J. L.; Parker, N. *Free Radic. Biol. Med.* **2004**, 37, 755-767.
9. Kelley, E. E.; Khoo, N. K. H.; Hundley, N. J.; Malik, U. Z.; Freeman, B. A.; Tarpey, M. M. *Free Radic. Biol. Med.* **2010**, 48, 493-498.
10. Galbusera, C.; Orth, P.; Fedida, D.; Spector, T. *Biochem. Pharmacol.* **2006**, 71, 1747-1752.
11. Brioukhanov, A. L.; Netrusov, A. I.; Eggen, R. I. L. *Microbiology* **2006**, 152, 1671-1677.
12. Schriner, S. E.; Linford, N. J.; Martin, G. M.; Treuting, P.; Ogburn, C. E.; Emond, M.; Coskun, P. E.; Ladiges, W.; Wolf, N.; Van Remmen, H.; Wallace, D. C.; Rabinovitch, P. S. *Science* **2005**, 308, 1909-1911.
13. Fenton, H. J. H. *J. Chem. Soc.* **1894**, 65, 899-910.
14. Stohs, S. J.; Bagchi, D. *Free Radic. Biol. Med.* **1995**, 18, 321-336.
15. Yin, H.; Xu, L.; Porter, N. A. *Chem. Rev.* **2011**, 111, 5944-5972.
16. Wiseman, H.; Halliwell, B. *Biochem. J.* **1996**, 313, 17-29.
17. Davies, K. J. A. *J. Biol. Chem.* **1987**, 262, 9895-9901.
18. Davies, K. J. A.; Delsignore, M. E.; Lin, S. W. *J. Biol. Chem.* **1987**, 262, 9902-9907.
19. Davies, K. J. A.; Delsignore, M. E. *J. Biol. Chem.* **1987**, 262, 9908-9913.
20. Satoh, K.; Sakagami, H. *Anticancer Res.* **1997**, 17, 1125-1129.
21. Haenen, G. R. M. M.; Bast, A. *Biochem. Pharmacol.* **1991**, 42, 2244-2246.
22. Rosenberg, H. R.; Culik, R. *Arch. Biochem. Biophys.* **1959**, 80, 86-93.
23. Shay, K. P.; Moreau, R. F.; Smith, E. J.; Hagen, T. M. *IUBMB Life*, **2008**, 60, 362-367.

24. Brown, S. E.; Ross, M. F.; Sanjuan-Pla, A.; Manas, A. B.; Smith, R. A. J.; Murphy, M. P. *Free Radic. Biol. Med.* **2007**, 42, 1766-1780.
25. Kilic, F.; Handelman, G. J.; Serbinova, E.; Packer, L.; Trevithick, J. R. *Biochem. Mol. Biol. Int.* **1995**, 37, 361-370.
26. Shay, K. P.; Moreau, R. F.; Smith, E. J.; Smith, A. R.; Hagen, T. M. *Biochim. Biophys. Acta* **2009**, 1790, 1149-1160.
27. Halliwell, B. *Cardiovasc. Res.* **2007**, 73, 341-347.
28. Hartley, R. C.; Kennedy, M. W. *Trends Ecol. Evol.* **2004**, 19, 353-354.
29. Harman, D. J. *Gerontology* **1956**, 11, 298-300.
30. Lin, M. T.; Beal, M. F. *Nature* **2006**, 443, 787-795.
31. Galindo, M. F.; Ikuta, I.; Zhu, X.; Casadesus, G.; Jordán. J. *J. Neurochem.* **2010**, 144, 933-945.
32. Yoshida, T.; Nakamura, H.; Masutani, H.; Yodoi, J. *Ann. N.Y. Acad. Sci.* **2006**, 1055, 1-12.
33. Sun, J.; Folk, D.; Bradley, T. J.; Tower, J. *Genetics* **2002**, 161, 661-672.
34. Zielonka, J.; Sikora, A.; Joseph, J.; Kalyanaraman, B. *J. Biol. Chem.* **2010**, 285, 14210-14216.
35. Lacza, Z.; Pankotai, E.; Csordis, A.; Geroö, D.; Kiss, L.; Horváth, E. M.; Kollai, M.; Busija, D. W.; Szabó, C. *Nitric Oxide* **2006**, 14, 162-168.
36. Aguirre, E.; López-Bernardo, E.; Cadenas, S. *Mitochondrion* **2012**, 12, 126-131.
37. Coles, S. J.; Easton, P.; Sharrod, H.; Hutson, S. M.; Hancock, J.; Patel, V. B.; Conway, M. E. *Biochemistry* **2009**, 48, 645-656.
38. Cassina, A.; Radi, R. *Arch. Biochem. Biophys.* **1996**, 328, 309-316.
39. Santore, M. T.; McClintock, D. S.; Lee, V. Y.; Budinger, G. R. S.; Chandel, N. S. *Am. J. Physiol. Lung Cell. Mol. Physiol.* **2002**, 282, L727-L734.
40. Novo, E.; Parola, M. *Fibrogenesis & Tissue Repair* **2008**, 1, (5).
41. Ohshima, H.; Tatemichi, M.; Sawa, T. *Arch. Biochem. Biophys.* **2003**, 417, 3-11.
42. Zhang, J.; Jin, B.; Li, L.; Block, E. R.; Patel, J. M. *Am. J. Physiol. Cell Physiol.* **2005**, 288, C840-C849.
43. Prime, T.; Blaikie, F. H.; Evans, C.; Nadtochiy, S. M.; James, A. M.; Dahm, C. C.; Vitturi, D. A.; Patel, R. P.; Hiley, C. R.; Abakumova, I.; Requejo, R.; Chouchani, E. T.; Hurd, T. R.; Garvey, J. F.; Taylor, C. T.; Brookes, P. S.; Smith, R. A. J.; Murphy, M. P. *PNAS* **2009**, 106, 10764-10769.
44. Burwell, L. S.; Nadtochiy, S. M.; Tompkins, A. J.; Young, S.; Brookes, P. S. *Biochem. J.* **2006**, 394, 627-634.

45. MacMillan-Crow, L. A.; Crow, J. P.; Thompson, J. A. *Biochemistry* **1998**, 37, 1613-1622.
46. Borutaité, V.; Brown, G. C. *Biochem. J.* **1996**, 315, 295-299.
47. Brown, G. C.; Borutaite, V. *Cardiovasc. Res.* **2007**, 75, 283-290.
48. Routledge, M. N.; Wink, D. A.; Keefer, L. K.; Dipple, A. *Chem. Res. Toxicol.* **1994**, 7, 628-632.
49. Smith, R. A. J.; Hartley, R. C.; Murphy, M. P.; *Antioxid. Redox Signaling* **2011**, 15, 3021-3038.
50. Murphy, M. P. *Expert Opin. Biol. Ther.* **2001**, 1, 753-764.
51. Ruifrok, P. G. *Biochem. Pharmacol.* **1982**, 31, 1431-1435.
52. Zhao, K.; Zhao, G.; Wu, D.; Soong, Y.; Birk, A. V.; Schiller, P. W.; Szeto, H. H. *J. Biol. Chem.* **2004**, 279, 24682-24690.
53. Yousif, L. F.; Stewart, K. M.; Horton, K. L.; Kelley, S. O. *Chem. Bio. Chem.* **2009**, 10, 2081-2088.
54. Murphy, M. P.; Smith, R. A. J. *Annu. Rev. Pharmacol. Toxicol.* **2007**, 47, 629-656.
55. Smith, R. A. J.; Porteous, C. M.; Gane, A. M.; Murphy, M. P. *PNAS* **2003**, 100, 5407-5412.
56. Snow, B. J.; Rolfe, F. L.; Lockhart, M. M.; Frampton, C. M.; O'Sullivan, J. D.; Fung, V.; Smith, R. A. J.; Murphy, M. P.; Taylor, K. M. *Movement Disord.* **2010**, 25, 1670-1674.
57. Smith, R. A. J.; Adlam, V. J.; Blaikie, F. H.; Manas, A. B.; Porteous, C. M.; James, A. M.; Ross, M. F.; Logan, A.; Cochemé, H. M.; Trnka, J.; Prime, T. A.; Abakumova, I.; Jones, B. A.; Filipovska, A.; Murphy, M. P. *Ann. N.Y. Acad. Sci.* **2008**, 1147, 105-111.
58. Ross, M. F.; Da Ros, T.; Blaikie, F. H.; Prime, T. A.; Porteous, C. M.; Severina, I. I.; Skulachev, V. P.; Kjaergaard, H. G. Smith, R. A. J.; Murphy, M. P. *Biochem. J.* **2006**, 400, 199-208.
59. Smith, R. A. J.; Porteous, C. M.; Coulter, C. V.; Murphy, M. P. *Eur. J. Biochem.* **1999**, 263, 709-716.
60. Asin-Cayuela, J.; Manasb, A. B.; James, A. M.; Smith, R. A. J.; Murphy, M. P. *FEBS Lett.* **2004**, 571, 9-16.
61. Porteous, C. M.; Logan, A.; Evans, C.; Ledgerwood, E. C.; Menon, D. K.; Aigbirhio, F.; Smith, R. A. J.; Murphy, M. P. *Biochem. Biophys. Acta* **2010**, 1800, 1009-1017.
62. Lin, T.; Hughes, G.; Muratovska, A.; Blaikie, F. H.; Brookes, P. S.; Darley-Usmar, V.; Smith, R. A. J.; Murphy, M. P. *J. Biol. Chem.* **2002**, 277, 17048-17056.

63. Fonseca, S. B.; Pereira, M. P.; Mourtada, R.; Gronda, M.; Horton, K. L.; Hurren, R.; Minden, M. D.; Schimmer, A. D.; Kelley, S. O. *Chem. Biol.* **2011**, 18, 445-453.
64. Horton, K. L.; Pereira, M. P.; Stewart, K. M.; Fonseca, S. B.; Kelley, S. O. *Chem. Bio. Chem.* **2012**, 13, 476-485.
65. Horton, K. L.; Stewart, K. M.; Fonseca, S. B.; Guo, Q.; Kelley, S. O. *Chem. Biol.* **2008**, 15, 375-382.
66. Modica-Napolitano, J. S.; Aprille, J. R. *Adv. Drug Deliv. Rev.* **2001**, 49, 63-70.
67. Steliou, K. US 6316652 B1 **2001**
68. El Fangour, S.; Marini, M.; Good, J.; McQuaker, S. J.; Shiels, P. G.; Hartley, R. C. *AGE* **2009**, 31, 269-276.
69. Gallet, P. F.; Maftah, A.; Petit, J.; Denis-Gay, M.; Julien, R. *Eur. J. Biochem.* **1995**, 228, 113-119.
70. Smith, R. A. J.; Murphy, M. P. *Ann. N.Y. Acad. Sci.* **2010**, 1201, 96-103.
71. Filipovska, A.; Kelso, G. F.; Brown, S. E.; Beer, S. M.; Smith, R. A. J.; Murphy, M. P. *J. Biol. Chem.* **2005**, 280, 24113-24126.
72. Zhao, R.; Holmgren, A. *J. Biol. Chem.* **2002**, 277, 39456-39462.
73. Salvemini, D.; Wang, Z.; Zweier, J. L.; Samouilov, A.; Macarthur, H.; Misko, T. P.; Currie, M. G.; Cuzzocrea, S.; Sikorski, J. A.; Riley, D. P. *Science* **1999**, 286, 304-306.
74. Chatterjee, P. K.; Cuzzocrea, S.; Brown, P. A. J.; Zacharowski, K.; Stewart, K. N.; Mota-Filipe, H.; Thiemermann, C. *Kidney Int.* **2000**, 58, 658-673.
75. Krishna, M. C.; Grahame, D. A.; Samuni, A.; Mitchell, J. B.; Russo, A. *Proc. Natl. Acad. Sci. USA* **1992**, 89, 5537-5541.
76. Soule, B. P.; Hyodo, F.; Matsumoto, K.; Simone, N. L.; Cook, J. A.; Krishna, M. C.; Mitchell, J. B. *Free Radic. Biol. Med.* **2007**, 42, 1632-1650.
77. Blinco, J. P.; Hodgson, J. L.; Morrow, B. J.; Walker, J. R.; Will, G. D.; Coote, M. L.; Bottle, S. E. *J. Org. Chem.* **2008**, 73, 6763-6771.
78. Trnka, J.; Blaikie, F. H.; Logan, A.; Smith, R. A. J.; Murphy, M. P. *Free Radic. Res.* **2009**, 43, 4-12.
79. Dhanasekaran, A.; Kotamraju, S.; Karunakaran, C.; Kalivendi, S. V.; Thomas, S.; Joseph, J.; Kalyanaraman, B. *Free Radic. Biol. Med.* **2005**, 39, 567-583.
80. Hardy, M.; Rockenbauer, A.; Vasquez-Vivar, J.; Felix, C.; Lopez, M.; Srinivasan, S.; Avadhani, N.; Tordo, P.; Kalyanaraman, B. *Chem. Res. Toxicol.* **2007**, 20, 1053-1060.
81. Quin, C.; Trnka, J.; Hay, A.; Murphy, M. P.; Hartley, R. C. *Tetrahedron* **2009**, 65, 8154-8160.

82. Murphy, M. P.; Echtay, K. S.; Blaikie, F. H.; Asin-Cayuela, J.; Cochemé, H. M.; Green, K.; Buckingham, J. A.; Taylor, E. R.; Hurrell, F.; Hughes, G.; Miwa, S.; Cooper, C. E.; Svistunenko, D. A.; Smith, R. A. J.; Brand, M. D. *J. Biol. Chem.* **2003**, 278, 48534-48545.
83. Xu, Y.; Kalyanaraman, B. *Free Radic. Res.* **2007**, 41, 1-7.
84. Hardy, M.; Chalier, F.; Ouari, O.; Finet, J. P.; Rockenbauer, A.; Kalyanaraman, B.; Tordo, P. *Chem. Commun.* **2007**, 10, 1083-1085.
85. Lei, W.; Xie, J.; Hou, Y.; Jiang, G.; Zhang, H.; Wang, P.; Wang, X.; Zhang, B. *J. Photochem. PhotoBiol. B: Biol.* **2010**, 98, 167-171.
86. Cuchelkar, V.; Kopečkova, P.; Kopeček, J. *Mol. Pharm.* **2008**, 5, 776-786.
87. Sibrian-Vazquez, M.; Nesterova, I. V.; Jensen, T. J.; Vicente, M. G. H. *Bioconjugate Chem.* **2008**, 19, 705-713.
88. Malouitre, S.; Dube, H.; Selwood, D.; Crompton, M.; *Biochem. J.* **2010**, 425, 137-148.
89. Minamikawa, T.; Sriratana, A.; Williams, D. A.; Bowser, D. N.; Hill, J. S.; Nagley, P. *J. Cell. Sci.* **1999**, 112, 2419-2430.
90. Logan, D. C.; Leaver, C. J. *J. Exp. Bot.* **2000**, 51, 865-871.
91. Dickinson, B. C.; Huynh, C.; Chang, C. J. *J. Am. Chem. Soc.* **2010**, 132, 5906-5915.
92. Brubacher, J. L.; Bols, N. C. *J. Immunol. Methods* **2001**, 251, 81-91.
93. Takanashi, T.; Ogura, Y.; Taguchi, H.; Hashizoe, M.; Honda, Y. *Invest. Ophthalmol. Vis. Sci.* **1997**, 38, 2721-2728.
94. Dikalov, S.; Griendling, K. K.; Harrison, D. G. *Hypertension* **2007**, 49, 717-727.
95. Kuivila, H. G.; Armour, A. G. *J. Am. Chem. Soc.* **1957**, 79, 5659-5662.
96. Brown, H. C.; Mandal, A. K.; Kulkarni, S. U. *J. Org. Chem.* **1977**, 42, 1392-1398.
97. Lo, L.; Chu, C. *Chem. Commun.* **2003**, 2728-2729.
98. Soh, N. *Anal. Bioanal. Chem.* **2006**, 386, 532-543.
99. Saul, S. J.; Sugumaran, M. *J. Biol. Chem.* **1990**, 265, 16992-16999.
100. Srikun, D.; Miller, E. W.; Domaille, D. W.; Chang, C. W. *J. Am. Chem. Soc.* **2008**, 130, 4596-4597.
101. Tanaka, K.; Miura, T.; Umezawa, N.; Urano, Y.; Kikuchi, K.; Higuchi, T.; Nagano, T. *J. Am. Chem. Soc.* **2001**, 123, 2530-2536.
102. Albers, A. E.; Okreglak, V. S.; Chang, C. J. *J. Am. Chem. Soc.* **2006**, 128, 9640-9641.
103. Zielonka, J.; Kalyanaraman, B. *Free Radic. Biol. Med.* **2010**, 48, 983-1001.

104. Robinson, K. M.; Janes, M. S.; Pehar, M.; Monette, J. S.; Ross, M. F.; Hagen, T. M.; Murphy, M. P.; Beckman, J. S. *PNAS* **2006**, 103, 15038-15043.
105. Kalyanaraman, B.; Darley-Usmar, V.; Davies, K. J. A.; Dennery, P. A.; Forman, H. J.; Grisham, M. B.; Mann, G. E.; Moore, K.; Roberts, L. J.; Ischiropoulos, H. *Free Radic. Biol. Med.* **2012**, 52, 1-6.
106. Tsai, C.; Jain, S. C.; Sobell, H. M. *J. Mol. Biol.* **1977**, 114, 301-315.
107. Greenstock, C. L.; Ruddock, G. W. *Chem. Biol. Interact.* **1975**, 11, 441-447.
108. Pluth, M. D.; Tomat, E.; Lippard, S. J. *Annu. Rev. Biochem.* **2011**, 80, 333-355.
109. Kojima, H.; Nakatsubo, N.; Kikuchi, K.; Kawahara, S.; Kirino, Y.; Nagoshi, H.; Nagano, T. *Anal. Chem.* **1998**, 70, 2446-2453.
110. Kojima, H.; Hirotani, M.; Urano, Y.; Kikuchi, K.; Higuchi, T.; Nagano, T. *Tetrahedron* **2000**, 41, 69-72.
111. Gabe, Y.; Ueno, T.; Urano, Y.; Kojima, H.; Nagano, T. *Anal. Bioanal. Chem.* **2006**, 386, 621-626.
112. Zhang, X.; Zhang, H. *Spectrochim. Acta Part A* **2005**, 61, 1045-1049.
113. Lin, L.; Lin, X.; Lin, F.; Wong, K. *Org. Lett.* **2011**, 13, 2216-2219.
114. Lim, M. H.; Lippard, S. J. *Acc. Chem. Res.* **2007**, 40, 41-51.
115. Lim, M. H.; Lippard, S. J. *J. Am. Chem. Soc.* **2005**, 127, 12170-12171.
116. Lim, M. H.; Xu, D.; Lippard, S. J. *Nat. Chem. Biol.* **2006**, 2, 375-380.
117. Pluth, M. D.; McQuade, L. E.; Lippard, S. J. **2010**, 12, 2318-2321.
118. McQuade, L. E.; Pluth, M. D.; Lippard, S. J. *Inorg. Chem.* **2010**, 49, 8025-8033.
119. Ouyang, J.; Hong, H.; Shen, C.; Zhao, Y.; Ouyang, C.; Dong, L.; Zhu, J.; Guo, Z.; Zeng, K.; Chen, J.; Zhang, C.; Zhang, J. *Free Radic. Biol. Med.* **2008**, 45, 1426-1436.
120. Sun, Z.; Wang, H.; Liu, F.; Chen, Y.; Kwong, P.; Tam, H.; Yang, D. *Org. Lett.* **2009**, 11, 1887-1890.
121. Kooy, N. K.; Royall, J. A.; Ischiropoulos, H.; Beckman, J. S. *Free Radic. Biol. Med.* **1994**, 16, 149-156.
122. Possel, H.; Noack, H.; Augustin, W.; Keilhoff, G.; Wolf, G. *FEBS Lett.* **1997**, 416, 175-178.
123. Huang, J.; Li, D.; Diao, J.; Hou, J.; Yuan, J.; Zou, G. *Talanta* **2007**, 72, 1283-1287.
124. Joshi, R.; Adhikari, S.; Patro, B. S.; Chattopadhyay, S.; Mukherjee, T. *Free Radic. Biol. Med.* **2001**, 30, 1390-1399.
125. Ueno, T.; Urano, Y.; Kojima, H.; Nagano, T. *J. Am. Chem. Soc.* **2006**, 128, 10640-10641.

126. Woo, H.; Go, E. P.; Hoang, L.; Trauger, S. A.; Bowen, B.; Siuzdak, G.; Northen, T. R. *Rapid Commun. Mass Spectrom.* **2009**, 23, 1849-1855.
127. Cochemé, H. M.; Quin, C.; McQuaker, S. J.; Cabreiro, F.; Logan, A.; Prime, T. A.; Abakumova, I.; Patel, J. V.; Fearnley, I. M.; James, A. M.; Porteous, C. M.; Smith, R. A. J.; Saeed, S.; Carré, J. E.; Singer, M.; Gems, D.; Hartley, R. C.; Partridge, L.; Murphy, M. P. *Cell Metab.* **2011**, 13, 340-350.
128. Dawson, M. I.; Hobbs, P. D.; Kuhlmann, K.; Fung, V. A.; Helmes, C. T.; Chao, W. *J. Med. Chem.* **1980**, 23, 1013-1022.
129. Cochemé, H. M.; Logan, A.; Prime, T. A.; Abakumova, I.; Quin, C.; McQuaker, S. J.; Patel, J. V.; Fearnley, I. M.; James, A. M.; Porteous, C. M.; Smith, R. A. J.; Hartley, R. C.; Partridge, L.; Murphy, M. P. *Nat. Protoc.* **2012**, 7, 946-958.
130. Cox, A. G.; Peskin, A. V.; Paton, L. N.; Winterbourn, C. C.; Hampton, M. B.; Park, J. H. *Biochemistry* **2009**, 48, 6495-6501.
131. Sikora, A.; Zielonka, J.; Lopez, M.; Joseph, J.; Kalyanaraman, B. *Free Radic. Biol. Med.* **2009**, 47, 1401-1407.
132. Ross, M. F.; Prime, T. A.; Abakumova, I.; James, A. M.; Porteous, C. M.; Smith, R. A. J.; Murphy, M. P. *Biochem. J.* **2008**, 411, 633-645.
133. Magwere, T.; Pamplona, R.; Miwa, S.; Martinez-Diaz, P.; Portero-Otin, M.; Brand, M. D.; Partridge, L. *J. Gerontol. A Biol. Sci. Med. Sci.* **2006**, 62, 136-145.
134. Baron, O.; Knochel, P. *Angew. Chem. Int. Ed.* **2005**, 44, 3133-3135.
135. Knochel, P.; Krasovskiy, A. *Angew. Chem. Int. Ed.* **2004**, 43, 3333-3336.
136. Duca, M.; Dozza, B.; Lucarelli, E.; Santi, S.; Di Giorgioa, A.; Barbarella, G.; *Chem. Commun.* **2010**, 46, 7948-7950.
137. Cho, S.; Chung, J.; Kim, S.; Kweon, D.; Park, K.; Yoon, Y. *J. Heterocycl. Chem.* **1996**, 33, 315-318.
138. Bhunia, A.; Yetra, S. R.; Biju, A. T. *Chem. Soc. Rev.* **2012**, 41, 3140-3152.
139. Ross, S. A.; Pitié, M.; Meunier, B. *J. Chem. Soc.* **2000**, 571-574.
140. Amann, N.; Huber, R.; Wagenknecht, H. *Angew. Chem. Int. Ed.* **2004**, 43, 1845-1847.
141. Huber, R.; Amann, N.; Wagenknecht, H. *J. Org. Chem.* **2004**, 69, 744-751.
142. Lee, M.; Shin, I. *Angew. Chem. Int. Ed.* **2005**, 44, 2881-2884.
143. Brand, M. D.; Pamplona, R.; Portero-Otín, M.; Requena, J. R.; Roebuck, S. J.; Buckingham, J. A.; Clapham, J. C.; Cadenas, S. *Biochem. J.* **2002**, 368, 597-603.
144. Vidal-Puig, A. J.; Grujic, D.; Zhang, C.; Hagen, T.; Boss, O.; Ido, Y.; Szczepanik, A.; Wade, J.; Mootha, V.; Cortright, R.; Muoio, D. M.; Lowell, B. B. *J. Biol. Chem.* **2000**, 275, 16258-16266.

145. Skulachev, V. P. *Biochim. Biophys. Acta* **1998**, 1363, 100-124.
146. Terada, H. *Biochimica et Biophysica Acta* **1981**, 639, 225-242.
147. Tehan, B. G.; Lloyd, E. J.; Wong, M. G.; Pitt, W. R.; Montana, J. G.; Manallack, D. T.; Gancia, E. *Quant. Struct.-Act. Relat.* **2002**, 21, 457-472.
148. Parker, V. H. *Biochem. J.* **1965**, 97, 658-662.
149. Lou, P.; Hansen, B. S.; Olsen, P. H.; Tullin, S.; Murphy, M. P.; Brand, M. D. *Biochem. J.* **2007**, 407, 129-140.
150. Brown, G. C.; Brand, M. D. *Biochimica et Biophysica Acta* **1991**, 1059, 55-62.
151. Nizamani, S. M.; Hollingworth, R. M. *Biochem. Biophys. Res. Commun.* **1980**, 96, 704-710.
152. Kapteijn, G. M.; Grove, D. M.; Kooijman, H.; Smeets, W. J. J.; Spek, A. L.; Van Koten, G. *Inorg. Chem.* **1996**, 35, 526-533.
153. Quin, C.; Robertson, L.; McQuaker, S. J.; Price, N. C.; Brand, M. D.; Hartley, R. C. *Tetrahedron* **2010**, 66, 2384-2389.
154. De Filippis, A.; Morin, C.; Thimon, C. *Synth. Commun.* **2002**, 32, 2669-2676.
155. Li, W.; Burgess, K. *Tetrahedron* **1999**, 40, 6527-6530.
156. Pennington, T. E.; Kardiman, C.; Hutton, C. A. *Tetrahedron* **2004**, 45, 6657-6660.
157. Whiting, D. A.; Pilling, R. J. *J. Chem. Soc.* **1999**, 15, 2077-2086.
158. Breton, G. W. *J. Org. Chem.* **1997**, 62, 8952-8954.
159. Kim, S. G.; Kim, I. S.; Park, Y. H.; Park, J. H. *Synlett.* **1991**, 1, 183-184.
160. Xu, H.; Ekoue-Kovi, K.; Wolf, C. *J. Org. Chem.* **2008**, 73, 7638-7650.
161. Appel, R. *Angew. Chem. Int. Ed.* **1975**, 14, 801-811.
162. Gagnon, D.; Spino, C. *J. Org. Chem.* **2009**, 74, 6035-6041.
163. Firouzabadi, H.; Iranpoor, N.; Jafarpour, M. *Tetrahedron* **2004**, 45, 7451-7454.
164. Chen, L. B. *Ann. Rev. Cell Biol.* **1988**, 4, 155-181.
165. Zhu, A.; Romero, R.; Petty, H. R. *Anal. Biochem.* **2010**, 403, 123-125.
166. Murphy, M. P. *Biochem. J.* **2009**, 417, 1-13.
167. Chalmers, S.; Caldwell, S. T.; Quin, C.; Prime, T. A.; James, A. M.; Cairns, A. G.; Murphy, M. P.; McCarron, J. G.; Hartley, R. C. *J. Am. Chem. Soc.* **2012**, 134, 758-761.
168. Mayer, G.; Heckel, A. *Angew. Chem. Int. Ed.* **2006**, 45, 4900-4921.
169. Tsai, S.; Klinman, J. P. *Bioorg. Chem.* **2003**, 31, 172-190.
170. Aujard, I.; Benbrahim, C.; Gouget, M.; Ruel, O.; Baudin, J.; Neveu, P.; Jullien, L. *Chem. Eur. J.* **2006**, 12, 6865-6879.
171. Pelliccioli, A. P.; Wirz, J. *Photochem. Photobiol. Sci.* **2002**, 1, 441-458.

172. Furata, T.; Wang, S. S.; Dantzker, J. L.; Dore, T. M.; Bybee, W. J.; Callaway, E. M.; Denk, W.; Tsien, R. Y. *Proc. Natl. Acad. Sci. USA* **1999**, 96, 1193-1200.
173. Furuta, T.; Watanabe, T.; Tanabe, S.; Sakyo, J.; Matsuba, C. *J. Org. Chem.* **2007**, 9, 4717-4720.
174. Pillai, V. N. R. *Synthesis* **1980**, 1, 1-26.
175. Kaplan, J. H.; Forbush, B. III.; Hoffman, J. F. *Biochemistry* **1978**, 17, 1929-1935.
176. Parma, L.; Omenetto, N. *Chem. Phys. Lett.* **1978**, 54, 541-543.
177. Helmchen, F.; Denk, W. *Nat. Methods* **2005**, 2, 932-940.
178. Chen, Q.; Hoppel, C. L.; Lesnefsky, E. J. *J. Pharmacol. Exp. Ther.* **2006**, 316, 200-207.
179. Scallet, A. C.; Haley, R. L.; Scallet, D. M.; Duhart, H. M.; Binienda, Z. K. *Annu. N. Y. Acad. Sci.* **2003**, 993, 305-312.
180. Hébert, J.; Gravel, D. *Can. J . Chem.* **1974**, 52, 187-189.
181. Gravel, D.; Hébert, J.; Thoraval, D. *Can. J. Chem.* **1983**, 61, 400-410.
182. Haahr, A.; Rankovic, Z.; Hartley, R. C. *Tetrahedron* **2011**, 52, 3020-3022.
183. Fűrstner, A.; Aïssa, C.; Riveiros, R.; Ragot, J. *Angew. Chem. Int. Ed.* **2002**, 41, 4763-4766.
184. Abraham, R. J.; Warne, M. A.; Griffiths, L. *J. Chem. Soc.* **1997**, 8, 1751-1757.
185. Knappe,W. R. *Chem. Ber.* **1975**, 108, 2422-2438.
186. Wolan, A.; Zaidlewicz, M. *Org. Biomol. Chem.* **2003**, 1, 3274-3276.
187. Bergman, N. A.; Jansson, M.; Chiang, Y.; Kresge, A. J.; Yin, Y. *J. Org. Chem.* **1987**, 52, 4449-4453.
188. Chhen, A.; Vaultier, M.; Carrié, R. *Tetrahedron* **1989**, 30, 4953-4956.
189. Knight, J. D.; Sauer, S. J. Coltart, D. M. *Org. Lett.* **2011**, 13, 3118-3121.
190. Bernardon, J.; Nedoncelle, P. US 6649612 **2003**.
191. Serra, S.; Fuganti, C.; Moro, A. *J. Org. Chem.* **2001**, 66, 7883-7888.
192. Winkle, M. R.; Ronald, R. C. *J. Org. Chem.* **1982**, 47, 2101-2108.
193. Perkins, M. V.; Kitching, W.; Drew, R. A. I.; Moore, C. J.; König, W. A. *J. Chem. Soc.* **1990**, 1111-1117.
194. Harmata, M.; Calkins, N. L.; Baughman, R. G.; Barnes, G. L. *J. Org. Chem.* **2006**, 71, 3650-3652.
195. Nugent, B. M.; Williams, A. L.; Prabhakaran, E. N.; Johnston, J. N. *Tetrahedron* **2003**, 59, 8877-8888.
196. Sauerberg, P.; Olsen, G. S.; Jeppesen, L.; Mogensen, J. P.; Pettersson, I.; Jeppesen, C. B.; Daugaard, J. R.; Galsgaard, E. D.; Ynddal, L.; Fleckner, J.; Panajotova, V.;

Polivka, Z.; Pihera, P.; Havranek, M.; Wulff, E. M. *J. Med. Chem.* **2007**, 50, 1495-1503.

197. Molina, P.; Fresneda, P. M.; Sanz, M. A. *J. Org. Chem.* **1999**, 64, 2540-2544.
198. Hori, M.; Janda, K. D. *J. Org. Chem.* **1998**, 63, 889-894.
199. Mo, F.; Jiang, Y.; Qiu, D.; Zhang, Y.; Wang, J. *Angew. Chem. Int. Ed.* **2010**, 49, 1846-1849.
200. Hayashi, Y.; Gotoh, H.; Tamura, T.; Yamaguchi, H.; Masui, R.; Shoji, M. *J. Am. Chem. Soc.* **2005**, 127, 16028-16029.
201. Grenier, J. L.; Cotelle, N.; Catteau, J. P.; Cotelle, P. *J. Phys. Org. Chem.* **2000**, 13, 511-517.
202. Qin, H.; Xu, Z.; Cui, Y.; Jia, Y. *Angew. Chem. Int. Ed.* **2011**, 50, 4447-4449.
203. Ernster, L.; Nordenbrand, K. *Method Enzymol.* **1967**, 10, 86-94.
204. Ashour, B.; Hansford, R. G. *Biochem. J.* **1983**, 214, 725-736.
205. Letellier, T.; Malgat, M.; Mazat, J. *Biochim. Biophys. Acta* **1993**, 1141, 58-64.